Yoshimi Ito (Editor)

Leading-edge Perspectives for Theory and Suppression of Chatter in Machine Tools

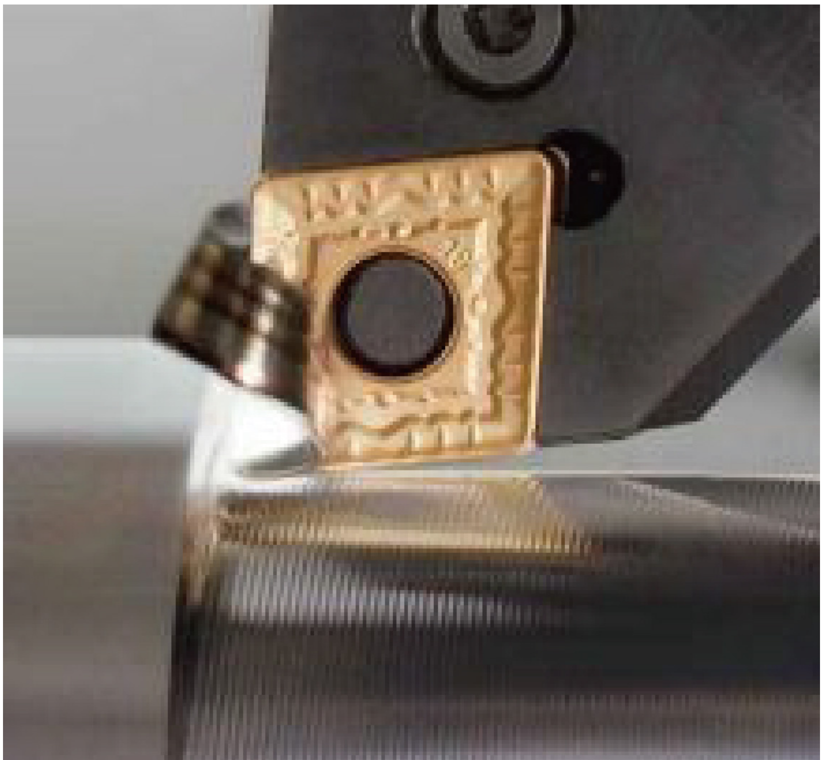

March 2019
Machine Tool Engineering Foundation

MTEF Research Guide Series No. 02
Yoshimi Ito (Editor)

Leading-edge Perspectives for Theory and Suppression of Chatter in Machine Tools

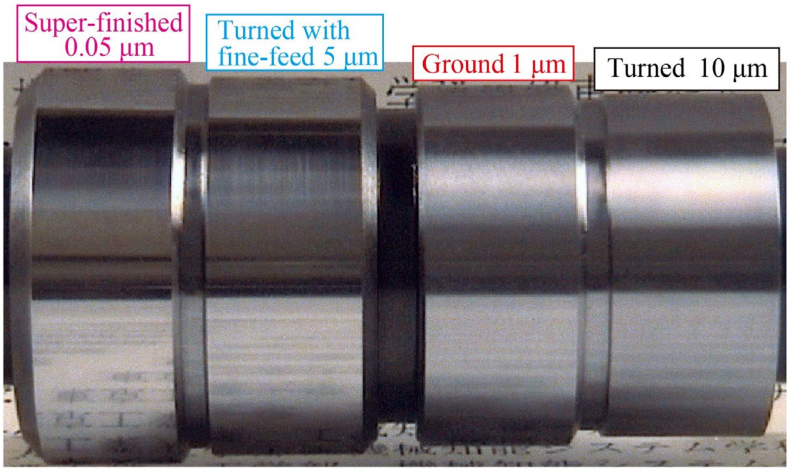

Various finished surface without chatter mark

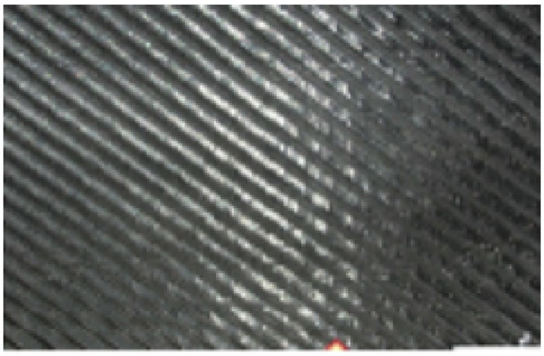

Finished surface with chatter mark

Electronic compiled by
Machine Tool Engineering Foundation in March, 2019

ISBN 978-4-909859-01-3

Photographs in front cover: By courtesy of Tungaloy

Preface

Within the machine tool engineering context, there are the four core technologies, i.e. light-weighted rigid design for the structural body with larger damping capacity, enhancement of anti-chatter capability, reduction of thermal deformation and development of innovative NC (Numerical Control) technology. In viewing from another standing point, the machine tool technologies consist of those for the "Manufacture (Design and Production)" and "Utilization", and the "Utilization" technology depends upon the skill and qualification of the user to a large extent. Even when we can purchase the machine tool with the best performance, we cannot run it efficiently and effectively without having the mature technician.

Of these core technologies mentioned above, the "Anti-chatter Capability" is closely related to both the manufacturing and the utilization, and thus has been since 1930s and being investigated vigorously in both the academia and the industry. Of course, the chatter suppression is at burning issue on the strength of the chatter vibration theory established in the 1960s, i.e. *Traditional Chatter Theory*.

In retrospect, Arnold of University College of Swansea publicized an interesting report in 1945 and importantly he suggested that Shizuo Doi of Ryojyun (Lshun) Institute of Technology conducted firstly an academic research into the chatter vibration in 1937 (1946). After then, many researchers and engineers involved in R & D (Research and Engineering Development) activities on the chatter vibration in metal cutting and grinding, and in the 1960s, Tobias, Tlusty and Merritt contributed to a large extent to establish the theory of the self-excited chatter vibration of regenerative type, i.e. major part of the *Traditional Chatter Theory*.

As well known, this traditional chatter theory consists of the three basic expressions, i.e. "*Uncut Chip Thickness, Cutting Process and Structural Expressions*". In fact, this theory can facilitate considerably the contrivance and establishment of a handful of valuable remedies for the chatter suppression. One of such outstanding remedies is the "*Milling Cutter of Irregular Tooth Pitch Type and with Differing Helix Angle (Variable Helix Angle of Flute)*", and at present such milling cutters become very popular while carrying out the heavy-duty cutting.

With the growing importance of a kind of the heavy-duty cutting, e.g. heavy machining per unit time for the aircraft component made of Al alloy, however, we can observe a considerable number of the evidences, which suggest implicitly the limitation in the application of the traditional chatter theory so far used to some facing problems. Paraphrasing, we rely on the traditional chatter theory, where the main spindle speed was 2, 000 rev/min in maximum; however, it is, in general, more than 5,000 rev/min and up to 40,000 rev/min at present. As a result, the chatter vibration induces unexpected phenomena far beyond from those in the 1960s, and thus, it is natural to reinvestigate to what extent the traditional chatter vibration theory is applicable, and also what is the necessary modification to the traditional chatter vibration theory in order to be compatible it with the facing problem.

As can be seen from practice at factory floor, furthermore, even now we face often the unknown chatter vibration problem, even when the machine tool available is in the best quality. In certain cases, we face certain difficulties in the chatter suppression, even when the mature engineer and technician endeavor to solve it. Such present perspectives imply also the capability limitation of the traditional chatter theory and concerns.

In contrast and in due course, we can observe recently some interesting symptoms through a relatively few noteworthy and challenging research activities of time- and manpower-consumption. Importantly, such symptoms range from the meticulous observation of chatter vibration, through modification of the chatter theory, to further engineering development for skillful chatter suppression. Of course, such a challenging research includes a considerable number of the controversial points; however, people in the traditional chatter vibration sphere seem not to have paid any attentions to these new waves. More specifically, they eye only the machining point, and do not pay any attention to its surrounding environments, i.e. machining system, although the chatter vibration is closely related to the machine-attachment-tool-work system.

Concretely saying, we must discuss to what extent the stability chart applicable, in which the parameters of the machine-attachment-tool-work system are measured while the system is in still-stand and also assumed as to be linear characteristic. For example, a handful of researchers have already suggested the poor applicability of the stability chart in the higher-speed milling for Al alloy in the aircraft component. On the strength of valuable and innovative findings within some challenging researches, and also in full consideration of changes in machining environments, thus, it is natural to reinvestigate and reconsider the traditional chatter theory having been relied on, and we must deploy to a new horizon. In the most desirable case, these new waves may provide us with a clue for unveiling the further essential features of the chatter vibration and also some tools to contrive an innovative remedy for the chatter suppression.

This book consists of two parts, and Part I describes first the fundamentals of the chatter vibration theory and suppression technology by especially placing the stress on the self-excited chatter vibration of "*Regenerative Type*". Then, Part I proposes "*A Concept for Advanced Chatter Theory*" to modify the traditional chatter theory to be compatible with the machining environments at present together with suggesting the leading-edge issues to be discussed. In nearly all technical papers, reports and books, the chatter vibration deals with in fact only eying the machining point, although these publications state nominally the necessity of considering the machine-attachment-too-work system. Against this context, Part I can be characterized by its wider scope, which ranges from the machining point, through the machining space, to the structural body.

Following Part I, Part II displays first the present perspective of the research into the chatter vibration and then shows interesting behavior in the chatter vibration at present, when machining the component with higher-speed cutting. It is, in principle, noteworthy that the two representative leading-edge researches are demonstrated to understand what are facing issues in consideration of a modified block diagram of chatter loop. Such a block diagram of chatter loop is, of course, produced by referring to the traditional one, but integrates satisfactorily symptoms, which imply the necessity to enhance the traditional chatter theory. In this context, the Editor gives especially a quick note for the dynamic behavior of the main spindle with higher-rotational speed, which is one of the fatal issues when discussing the applicability of the stability chart.

Importantly, thought-provoking quick notes are furthermore publicized for the chatter vibration in metal grinding in consideration of inactive research activities during these several decades. In fact, we cannot find any valuable and noteworthy research papers in metal grinding field, and thus the chatter vibration theory for metal grinding remains its states as that in 1960s.

Eventually, Part II in this book is in the form of "Omnibus-like Style" to provide related people with a map maneuver-like meeting spot in order to exchange various differing proposals, suggestions and discourses, through which we may approach to the authentic and reliable information. To this end, the Editor is very proud of the valuableness of the book in the practice, and extremely the role of the book facilitating the guide for leading-edge research for young people in the academia.

Arnold R N. (1946) *The Mechanism of Tool Vibration in the Cutting of Steel, Cutting Tools Research*: Report of Subcommittee on Carbide Tools. Proc. I Mech E., 261-284.

Professors Drs. Cornel-Mihai NICOLESCU Andreas ARCHENTI
KTH Royal Institute of Technology, Chapter 5

Professor Dr. Tony SCHMITZ
UNC Charlotte, Chapter 6

Professor Dr. Hwa-Soo LEE
Nihon University, Chapter 8

Editor Yoshimi ITO, Tokyo Institute of Technology
Professor Emeritus Dr., Part I Chapters 4 and 7

Contents

Preface

Chapter 5 Statistical Dynamics - Analysis of Machining Systems Operational Conditions
(by Professors Andreas Archenti and Cornel-Mihai Nicolescu: KTH Royal Institute of Technology)

PART I FUNDAMENTALS OF CHATTER VIBRATION THEORY AND SUPPRESSION TECHNOLOGY

Headnotes

In Chapter 1, we describe first the fundamental knowledge about the chatter in turning together with the three burning issues, i.e. (1) *Lower-speed Stability*, (2) *Rational Determination of Chatter Onset in Experiment* and (3) *Influences of Attachment on Chatter Stability*. Of these, the lower-speed stability is one of the well-known research subjects and has been investigated vigorously without considering its essential features, which will be suggested within Item 1.1.1. For the latter two of three, we have been aware of their great importance; however, it is regrettable that people in chatter concerns are not interested in such research subjects. In fact, we can observe several forerunning researches at present as exemplified in Items 1.1.2 and 1.1.3.

On the strength of the chatter theory in turning, then, we describe the chatter vibration theories in drilling, milling and grinding in Section 1.2 by extremely revealing their characteristic and differing features as compared with those in turning. Importantly, the grinding mechanism may be regarded as one of the variants of milling; however, we can observe the very differing behavior of the chatter vibration in grinding. Such differing behavior are derived, for example, from the non-uniform elasticity of the grinding wheel, grain with negative rake angle and grain self-edging function. In consequence, we discuss the self-excited chatter of regenerative type in grinding in Section 1.3 and suggest that the chatter theory for grinding does not progress since 1960s. More specifically, we can suggest what are at burning and facing issues for the chatter vibration in metal cutting, whereas we cannot unveil such issues in grinding, because of not conducting any forerunning and challenging researches so far. Thus, the Editor suggests finally some representative research subjects like "Determination for Contact Stiffness of Grinding Wheel in Consideration of Grain Self-Edging Function".

On the strength of the block diagram of chatter loop, we classify first the remedies for the chatter suppression, and give some quick notes for each representative remedy in Chapter 2. In addition, we show a first-hand view for R & D activities in the form of "Puttick Grid", which may play the role of seeking a forerunning research subject. Of course, there have been a considerable number of remedies for the chatter suppression, which ranges from the contrivance of the cutting edge, through the employment of the damper, to the application of the vibration-proof material. Of these, the utmost excellent remedies are credited to both the milling cutter of irregular tooth pitch type with differing helix angle, and the elastic grinding wheel. Thus, the theory and practice of such milling cutters and grinding wheel describe also in Chapter 2. Importantly, we clarify the differing aspects in the effectiveness of the chatter suppression between those of irregular tooth pitch type and differing helix angle. In Chapter 2, we give furthermore some quick notes for the positive use of the machine tool joint to increase the damping capacity in the machine-attachment-tool-work system together with suggesting the difficulty to measure correctly the damping capacity within this system.

As can be readily seen from some controversial points suggested in Chapters 1 and 2, the dire necessity is to conduct the further research into the chatter from an innovative viewpoint, so that we may clarify the newer essential feature of the chatter than ever before. On that occasion, we must be first aware what are at burning issues to be the traditional chatter theory applicable to the machining state at present. Paraphrasing, a crucial issue is to establish an advanced chatter theory, which is fully available for the higher rotational speed of the main spindle at present, and which can be facilitated the chatter including the forced excitation caused by the cutting mechanism itself. Thus, Chapter 3 deals first with the influence of the forced excitation on the stability chart, and then discuss the major issues in the three basic expressions for the chatter theory after proposing a modified block diagram of chatter loop. In the latter case, it is extremely notified that we must measure the coefficients of the structural equation while the main spindle rotates more than 2,000 rev/min, if possible 5,000 rev/min and beyond together with considering the effects of the joint like those between main spindle and collet chuck, and between collet chuck and end mill.

Chapter 1 Basic Mathematical Model, Three Basic Expressions and Stability Chart

In machining, the chatter vibration (hereafter call it "*Chatter*" only) is at facing issue to increase the productivity and to ensure the part quality. Although we have had the long history in R and D (Research and Engineering Development) for the chatter since 1930s, we cannot suppress the chatter completely in certain machining cases even now. A root cause of its difficulties lies in the complex and synergistic behavior of the chatter. In fact, we must deal with the chatter from the viewpoint of the dynamic behavior in the machine-attachment-tool-work system. More specifically, R and D for the chatter ranges from the clarification of essential features of the chatter, through the establishment of the chatter theory, to the contrivance of various suppression remedies. Obviously, we may observe influences of each entity's own, and in certain cases the synergistic influences of some entities in the above-mentioned system on the chatter.

Reportedly, we have, in nearly all cases, conducted the research into the self-excited chatter of regenerative type so far, although there are a considerable number of the unknown types in the chatter (refer to Chapter 3). It is furthermore worth suggesting that the chatter while milling and drilling have recently been investigated vigorously because of their enchanting features from academic research point of view, e.g. influences by the continuous change of the wedge angle and thinning of chisel point on chatter in drilling. In fact, we need to discuss the sophisticated mathematical model in such machining methods as will be discussed in Section 1.2, and the advanced simulation software and dynamic information processing available at present can facilitate considerably to solve such a complex model.

As will be clear from the above, we must first understand the utmost simplest case in the chatter, i.e. regenerative type in turning, and as widely known, Tobias (1961), Merritt (1965) and Tlusty (1970) contributed to the establishment of the corresponding chatter theory to a large extent as will be described in Section 1.1 (hereafter call it “*Traditional Chatter Theory*”). Importantly, nearly all researchers and engineers rely on this traditional chatter theory, although there remain still some engineering problems, e.g. “Lower-speed Stability”, “Rational Determination of Chatter Onset (Commencement) in Experiment“ and “Effects of Attachment on Chatter“.

Of special note, we must be aware that the chatter in metal cutting has been so far investigated to a large extent as compared with that in metal grinding. In addition, it is notable that the leading objective is the chatter for bending mode, but not for torsional mode. In general, we may assume that the chatter in torsional mode activates at the higher rotational speed of main spindle as compared with that for bending mode, and thus for the time being, such a chatter is not crucial issue in metal cutting. In contrast, Entwistle and Stone (2013) have suggested a preferable effect of the torsional movement in the grinding wheel on the chatter.

1.1 Basic Knowledge about Self-excited Chatter Vibration of Regenerative Type in Metal Cutting

In many respects, it is, in general, very convenient for the ease of understanding to use the “*Block Diagram of Chatter Loop*” shown in Fig. 1.1. As widely known, Merritt first proposed it in the 1960s based on the three basic expressions so far established by Tobias and Tlusty. We can benefit considerably from the block diagram of chatter loop especially when estimating the stability limit for the chatter by relying on the automatic control theory. In addition, the chatter suppression technology has so far been developed on the strength of the block diagram of chatter loop to a large extent as typically exemplified by the milling cutter of irregular tooth pitch type and with differing helix angle.

For the simplified model of the machine-attachment-tool-work system shown together in Fig. 1.1, the three basic expressions can be written as

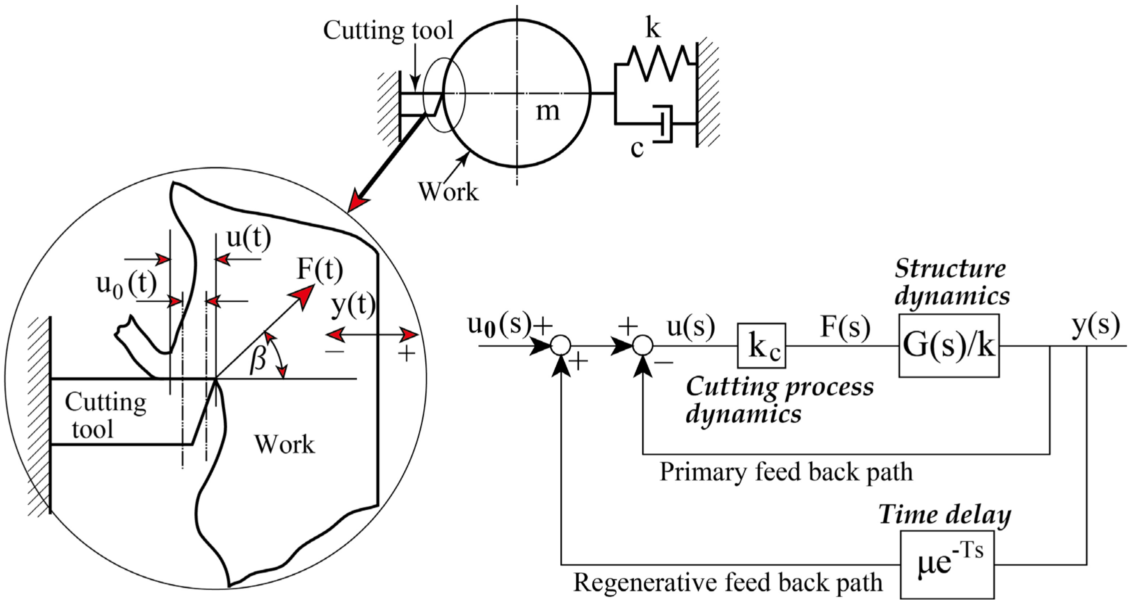

Fig. 1.1 Mathematical model and block diagram of chatter loop for self-excited chatter vibration of regenerative type (by Merritt)

"Uncut Chip Thickness Equation"

$$u(t) = u_0(t) - y(t) + \mu y(t\text{-}T) \text{ ----------- } (1.1)$$

"Cutting Process Equation"

$$F(t) = k_c u(t) \text{ --------------------}(1.2)$$

"Structural Equation"

$$F(t)\cos\beta = m\frac{d^2y(t)}{dt^2} + c\frac{dy(t)}{dt} + ky(t) \text{ ----------- } (1.3)$$

where,

c = Damping coefficient

F(t) = Resultant cutting force or vector force exciting structure

k_c = Specific cutting force (Static cutting stiffness)

k = Spring constant of structure

m = Equivalent mass of structure

N = Spindle speed

T = Delay time (1/N for lathe)

t = Time

u(t) = Instantaneous uncut chip thickness

u_0(t) = Steady-state (initial) uncut chip thickness

$y(t)$ = Relative displacement between tool and work

μ= Overlap factor

To produce the block diagram of chatter loop, then, we should convert these expressions into the following by using the Laplace transformation.

$$u(s) = u_0(s) - y(s) + \mu e^{-Ts} y(s) \text{ ----- } (1.4)$$

$$F(s) = k_c u(s) \text{ ---------------------- } (1.5)$$

$$y(s)/F(s) = (1/k)G(s) \text{ ------------------- } (1.6)$$

where,

G = Normalized dynamic compliance of structure

s = Laplace operator

From the three basic expressions, we can first determine the "Characteristic Equation (Transfer Function)", and then produce the stability chart as shown in Fig. 1.2, where a representative index is either "Limit Depth of Cut or Limit Width of Cut" in the vertical axis. In producing the stability chart, we must assume the utmost critical condition, i.e. μ = unity.

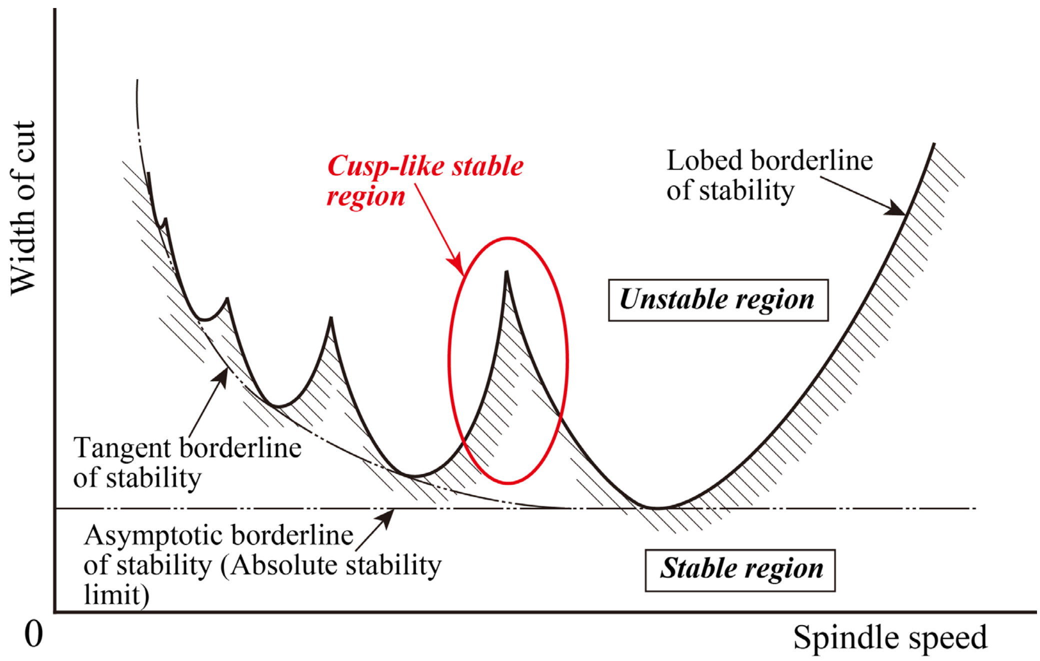

Fig. 1.2 Typical stability chart (by Merritt)

Within the allowable magnitude of this index, i.e. less magnitudes than absolute stability limit, we have not any chatter across the whole spindle speed. To ease of use, we define the three borderlines as shown together in Fig. 1.2, i.e. asymptotic, tangent and lobed borderlines [1].

As can be readily seen, the asymptotic borderline indicates the absolute stability limit, under which no chatter occurs across the whole spindle speed. Reportedly, it is desirable to machine the component by using the spindle speed, which corresponds with the "Cusp-like Region" of lobed borderline, and duly such a remedy is being prevailed as exemplified by some merchandized software.

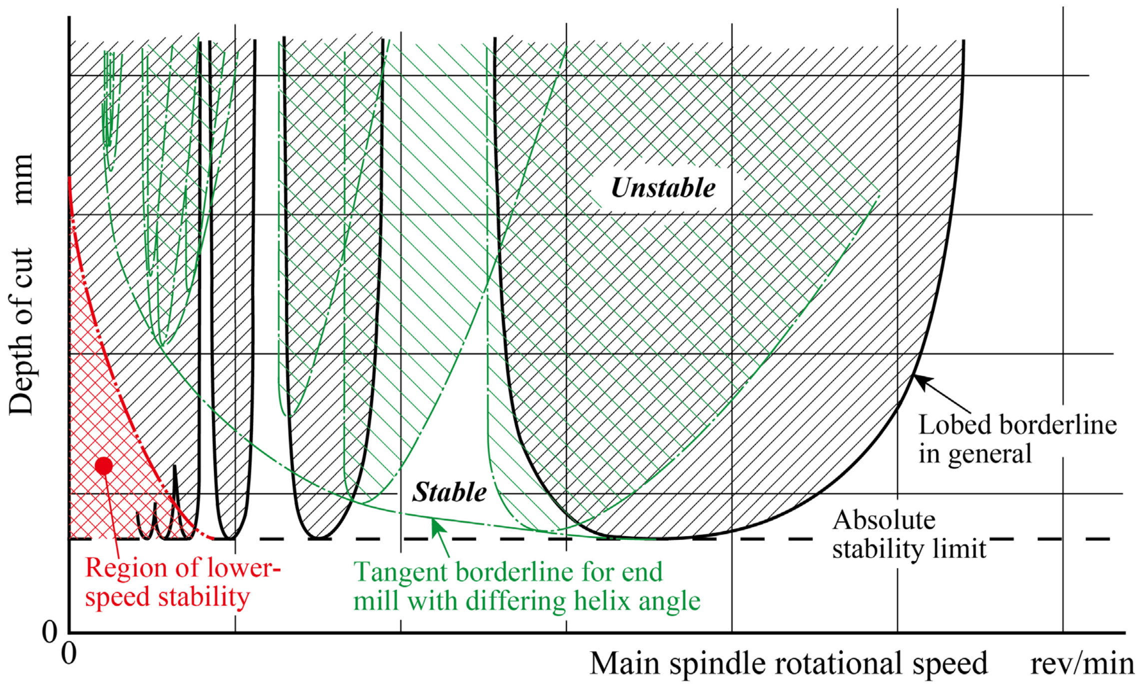

Fig. 1.3 Stability chart in general, lower-speed stability and effect of end mill with differing helix angle

Obviously, the stability chart can facilitate the prediction of the chatter onset, whereas we have two fundamental problems to be solved since 1960s: one is the existence of "*Lower-speed Stability*", and another is the

---

[1] In the stability chart, we employ often some indexes equivalent to either the limit depth of cut or the limit width of cut. For example, Tobias employed the "Vibration amplitude enlargement coefficient Q", which is given by Q = 1/(2D), where D is the ratio of equivalent damping coefficient to critical damping coefficient. In addition, Tlusty and Merritt employed "Ratio of chip width to limited chip width" and "Ratio of cutting stiffness to machine stiffness", respectively.

"*Rational Determination of Chatter Onset in Experiment*".
For the sake of further understanding, Fig. 1.3 illustrates the ranges of the lower-speed stability and the stability limit obtainable from the milling cutter with differing helix angle, which is very beneficial especially in the lower-speed range by enlarging the stability limit.

1.1.1 Lower-speed Stability

As widely known, there is a discrepancy between the theoretical and experimental stability charts at the lower-speed range as already shown in Fig. 1.3. More specifically, the limit depth of cut increases considerably at the lower-speed range in practice, although the chatter should occur at the same speed range in accordance with the chatter theory. This is the "*Lower-speed Stability*", and in general the heavy-duty cutting is carried out in such speed ranges, where we face considerable danger of chatter onset, and thus, the turner welcomes the lower-speed stability. As suggested by Tobias, the lower-speed stability is derived from the interaction between the relief angle (flank) in the cutting tool and the work, i.e. "*Penetration Effect*", which can facilitate the increase of damping. In fact, Tobias verified theoretically the validity of the lower-speed stability by including the penetration effect in the (nominal) dynamic cutting force. Of special note, now we use the term, "*Process Damping*" instead of the penetration effect, and importantly such a hypothesis of the process damping has been, with no doubt, accepted as the utmost leading causality for the lower-speed stability by nearly all people in chatter concerns.
From the empirical point of view, such an interpretation is acceptable. In fact, the turner increases often the contact between the relief face of cutting tool and the work as a factory floor-based remedy to suppress the chatter [2].
Of note, we can also suppress the chatter with higher frequency by placing the structural component with large damping, e.g. tool slide made of

---

[2] Following the proposal of Tobias, Kegg conducted a series of experiments for the lower-speed stability in 1969, and he verified the validity of the penetration effect. In the experiment, he carried out cylindrical turning, parting-off and milling for the workpieces made of cast iron, steel, Al alloy and plastics.
Kegg R L. (1969) Chatter Behaviour at Low Cutting Speeds. Annals of CIRP; 17: 97-106.

concrete, as close to the cutting point as possible.

In this context, Sellmeier and Denkena (2010) conducted recently an interesting research into milling of the Al alloy. Fig. 1.4 reproduces the experimental data, and as can be readily seen, they reported the amazing increase of the depth of cut without the chatter by increasing the chamfer length of cutting edge. In fact, the depth of cut increases around four times and three times in the lower and higher speed ranges, respectively. Importantly, they assert that the chamfer of the cutting edge can increase process damping, and that process damping is effective even in the higher spindle speed range.

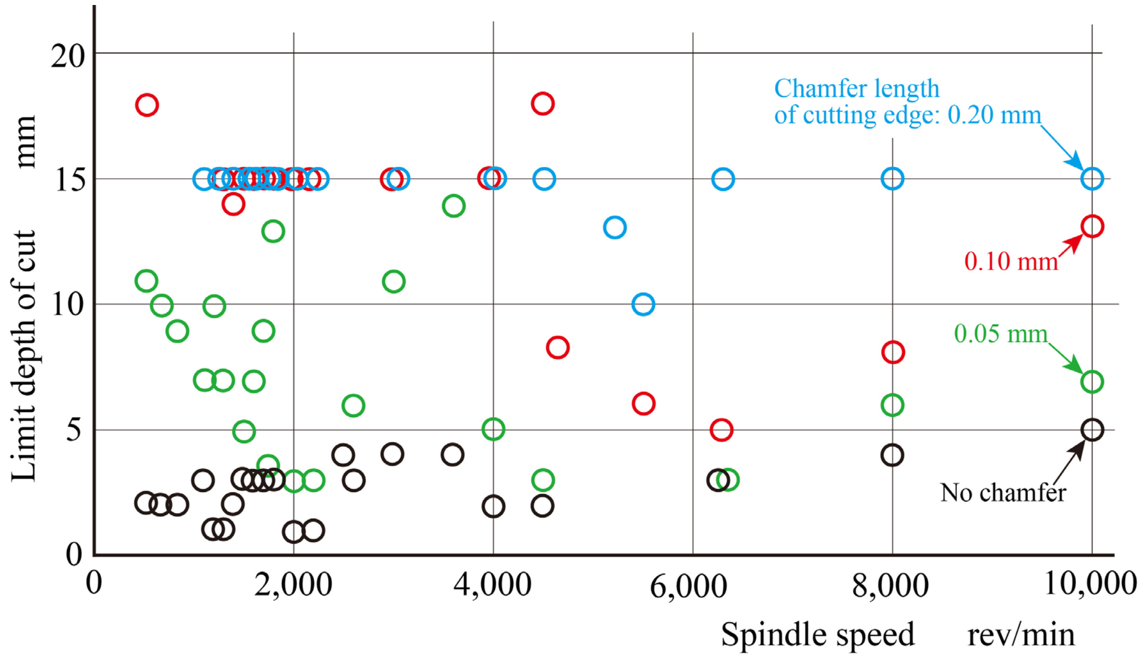

Fig. 1.4 Changes of stability limit for various chamfer length
(by courtesy of Denkena, 2015)

In consideration of the average magnitude of damping capacity in the machine tool as a whole, is it possible to be attributed such an amazing increase of the depth of cut to only the process damping? Although not denying the effectiveness of the factory floor-based remedies, we must eye other sources of damping possible within the machine-attachment-tool-work system. In fact, we have not verified obviously so far that damping at the cutting point is dominant in the determination of the damping coefficient within the “Structural Equation”. More specifically, process damping has not been experimentally and quantitatively verified its validity; however, some researchers and engineers assert the following.

(1) Process damping is derived from the elastic and plastic deformation of the interference volume at the joint between the flank of cutting tool and the wavy surface of the work. In short, the plowing force causes process damping.
(2) Process damping is subjected to the “Frictional Energy Loss” and viscous-like.

Even admitting that the plowing force is one of the leading causalities of process damping, a burning issue is the “*Strain Rate*”, when the interference volume deforms elastically and plastically. In general, we can compute such deformation by using the material constants, which can be obtained by the material testing. As well known, the strain rate at the material testing is less than 10^{-3}/s, whereas the strain rate at the rake face while machining is more than 10^{3}/s. Although the concrete data for the strain rate at the flank is not clarified as yet, at least, we must be aware of differing features of deformation mechanism between at the flank and at the material testing.

It can be furthermore suggested the necessities for conducting the corresponding research with much wider scope as follows (Ito, 2014).

(1) In accordance with the knowledge in the tribology and machine tool joint, viscous damping appears at the dry joint, provided that the “*Tangential Force Ratio*”, i.e. microscopic coefficient of friction, regulates the sliding condition to large extent, but not the “*Coulomb’s Friction*”. We must thus investigate once the availability of the tangential force ratio at the cutting point.
(2) The tangential force ratio varies with the magnitude of sliding length, i.e. “*Displacement-dependence Characteristics*”. In general, the shorter the sliding length, the more effectiveness of the tangential force ratio.

In this context, Ito and Matsumura (2017) suggested that the contact between the relief angle of cutting tool and the work is one of the machine tool joints, and they asserted a doubt for the effectiveness of process damping from viewpoint of its magnitude, i.e. process damping being too small to suppress the vibration [3]. In addition, they suggested the difficulty for measuring correctly process damping, although some researchers publicized the measured value of process damping. Of special note, the damping capacity of tooling with HSK (in German; der Hohle Schaft Kegel, in English; Hollow Shank Taper) is 0.01 ~ 0.03 in logarithmic damping decrement in accordance with the private information from professor Tsutsumi of Tokyo Agricultural University.

More specifically, Saljé and Isensee (1976) measured, for example, the damping capacity of the center by exciting the mid-way of the slender work, which was supported at both the ends by centers. In many respects, the damping capacity of surrounding components could include in the measured values, and of course, it is very difficult to eliminate such unfavorable noises without using, at least, the equivalent monolithic center system. Thus, Saljé and Isensee reported some comparative damping capacity, but not the real one. Of these measured values, the damping capacity for the axial force of 1,000 kgf is 0.005 in damping rate, which is equivalent to 0.03 in logarithmic damping decrement by the simple conversion. This magnitude is only several times of the material damping of cast iron. It is thus natural to estimate relatively small damping force at the cutting edge.

Against to this context, someone asserts that the contact condition of cutting point differs from the machine tool joint; however, it may be said that the sliding condition at the tool flank is not severe as compared with that at the rake face, where the apparent contact area seems to be the same as the real contact area.

---

[3] Jochem et al suggest that process damping increases with lowering the speed, where the pitch of wavy surface generated by the chatter is shorter, resulting in the density contact at the relief face of the cutting tool. From the viewpoint of the joint stiffness and damping capacity in machine tools, this suggestion is incredible and seems to be wrong. In fact, this suggestion is completely in reverse to the fundamental knowledge about the joint characteristics, where the density contact results in more rigid and less damping capacity.
Jochem C, Roukema, Altintas Y. (2006) Time domain simulation of torsional-axial vibrations in drilling. Inter. Jour. of Machine Tools & Manufacture; 46: 2073-2085.

Of special note, we must eye furthermore the excitation energy aspect in the chatter, and for example, Sato (1973) conducted an interesting research into the mechanical impedance for the turning machine-tool-work system. In this experiment, the system was excited by the small-sized hydraulic vibrator, which was placed between the tool slide and the work and input the cutting force-related signal, while the work is still stand. He showed an obvious difference of the mechanical impedance in the lower frequency from that in higher frequency as shown in Fig. 1.5.

In short, the system cannot be excited in the lower frequency range less than 60 Hz, because of shortage of excitation energy, and intuitively, this implies another causality of the lower-speed stability.

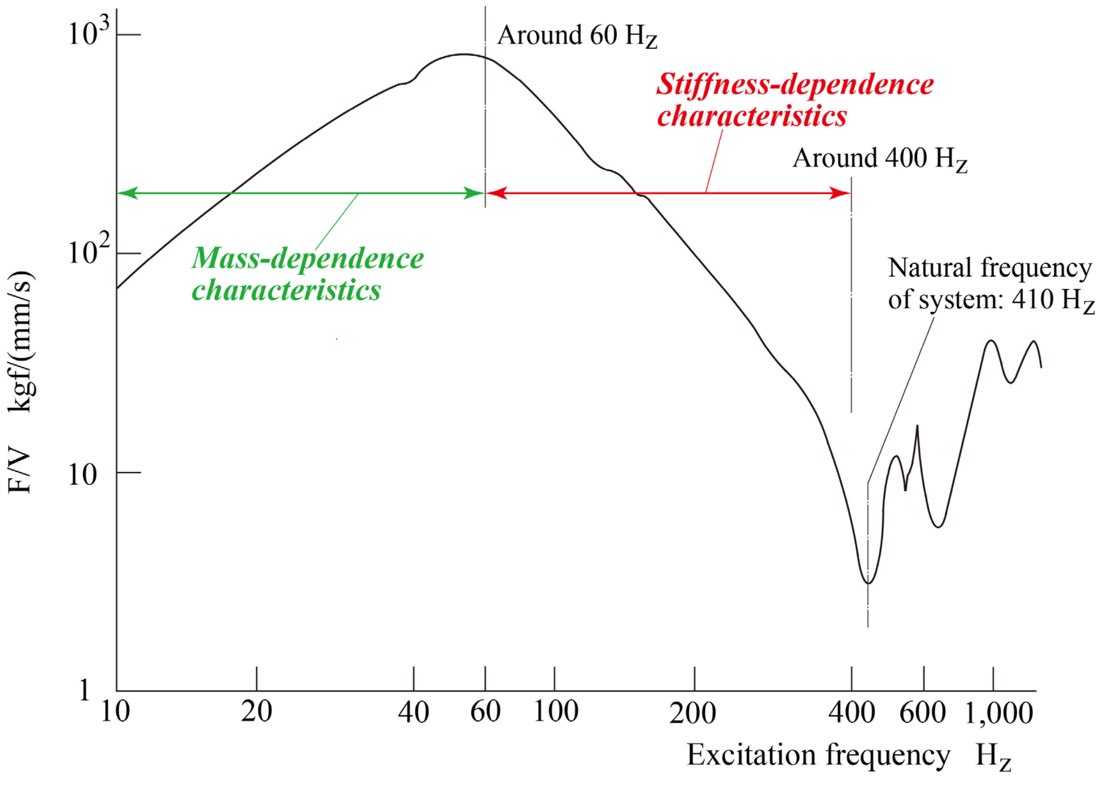

Fig. 1.5 Change of mechanical impedance in turning machine-tool-work system (by courtesy of Sato)

Summarizing, process damping has been theoretically investigated by assuming some damping sources at the contact between the relief face of cutting tool and the work in nearly all research reports. A “Must” at present is the verification of such an assumption so far employed, and thus it is necessary to visualize such contact conditions. In this context, people assert the difficulty for the visualization; however, Itoh et al (1991) tried an in-process measurement of the tool wear by using the ultrasonic waves. Fig. 1.6 reproduces the single-point cutting tool integrated the ultrasonic transducer, and they publicized some fruitful results.

More specifically, prior that of Itoh et al, Spur and Leonard (1975) once tried an in-process measurement of the flank wear also by means of ultrasonic waves. Spur and Leonard measured the flank wear by using the response time of ultrasonic waves, whereas Itoh et al used the change of the sound pressure, i.e. echo height on CRT (Cathode Ray Tube), to improve the measuring accuracy by eliminating the thermal elongation of the tool shank. As will be clear from the above, we will be able to verify experimentally that the lower-speed stability increases when the contact area of flank face becomes larger.

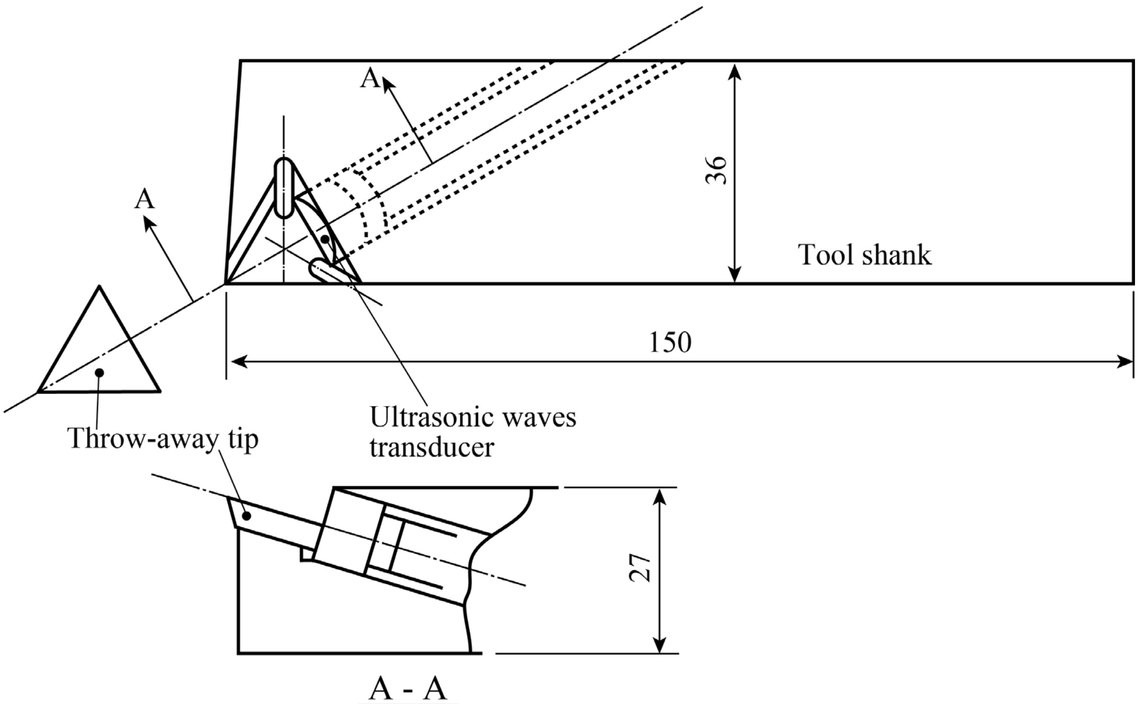

Fig. 1.6 In-process sensor of built-in type for flank wear measurement by ultrasonic waves

1.1.2 Rational Determination of Chatter Onset in Experiment

With respect to the "*Rational Determination of Chatter Onset*", the Editor publicized already a position paper, and suggested duly that nearly all research papers and technical reports so far publicized did not pay any attentions to the identification of the chatter onset in the experiment (Ito, 2013). Apparently, these publications believe that the chatter onset can be automatically and absolutely determined without any problems from the experimental data. It is however necessary to pay the special attention to the arbitrary behavior for the output signal obtainable from the chatter. In addition, we must be aware that the machining space is very bad environments for the sensor, and often very noisy. As a result, a root cause of difficulties lies in the selection of the robust sensor and suitable signal processing to detect the reliable output signal.

In retrospect, Braun of Israel Institute of Technology (1975) suggested already the difficulty in identifying correctly the chatter onset without processing properly the signal and proposed an index for the absolute threshold to determine the transition from stable to unstable states. Following that of Braun, Nakazawa et al (1979), Higuchi et al (1986) and Nicolescu (1991) conducted similar researches and reported some valuable results. For example, Higuchi et al detected sound signal with time-series analysis and observed that the chatter onset decided by the sound signal is earlier than that decided by the human sensory. In fact, Rahman and Ito reported already such an interesting suggestion as will be stated in detail below.

Rahman and Ito (1979) once suggested that the determination of chatter onset depends considerably upon what is the characteristic index, and how to detect such an index. In fact, they detected independently (1) the vibrational amplitude, (2) cutting force, (3) work displacement, and (4) surface roughness of the finished work as shown, for example, in Fig. 1.7. Importantly, they employed the tapered workpiece, which was proposed by The Machine Tool Industry Research Association, England.

From Fig. 1.7, we can understand the considerable difficulties in the identification of the chatter onset in the experiment as follows.

(1) A characteristic behavior can be observed in the work displacement in horizontal direction (depth of cut direction) at the chatter onset. More specifically, the horizontal displacement of the work launches out to reduce at a certain point (as marked with “a” in Fig. 1.7), although the depth of cut increases continuously.

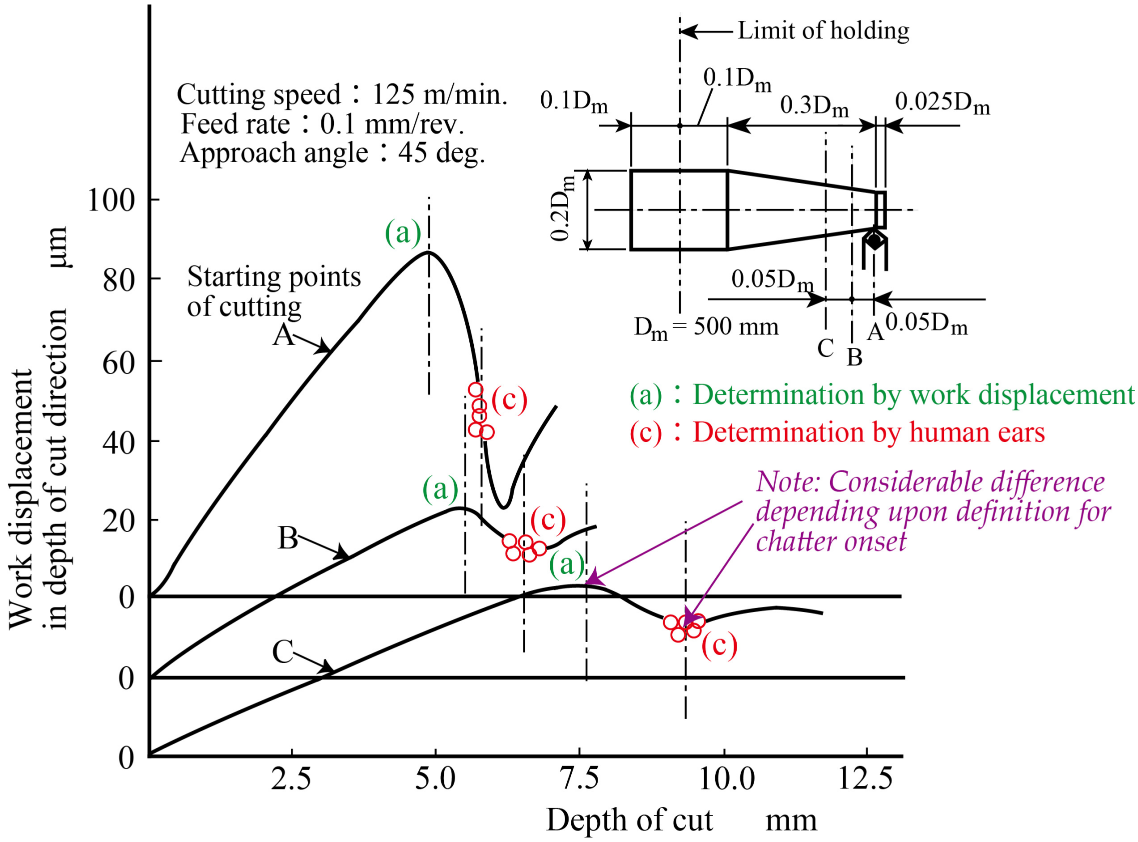

Fig. 1.7 Determination for onset of self-excited chatter using characteristic behavior in displacement of work

(2) The point, where the horizontal displacement of the work is about to decrease, is identical to the point, where the surface finish of the work starts to be worse. In contrast, the vibrational amplitude shows any marked changes at this point.

(3) The detection of the chatter onset by human ears (as marked with “c” in Fig. 1.7) is later than that by the horizontal displacement of the

work. For example, we can recognize about 2.5 mm different between both the depths of cuts.

In 2010, Denkena et al (2010) have quickly stated that they determined the chatter onset in end milling by totally using the information obtained from the visual inspection, surface roughness of finished work, sound and vibration while machining, and deflection of tool holder. This implies that even now we have not had any reliable tools to determine experimentally the chatter onset, and thus we must be duly aware of the following.

(1) As exemplified in Fig. II.1 (a) in the headnote of Part II, there have been a considerable number of the reports regarding the identification of the chatter; however, it is even now difficult to determine rationally the chatter onset in practice.

(2) We can detect the chatter by various sensors and methods, e.g. human ears, microphone, accelerometer, cutting force, surface roughness and so on. There are however no guides indicating a suitable and reliable detection method of the chatter onset.

Of special note, Nicolescu (1991) investigated the chatter onset by using similar methods to that of Braun by detecting the mean-square value of vibrational amplitude. In addition, Yeh et al (1992) proposed a method, in which signal processing is based on the average value of vibrational amplitude together with using the two-tiered threshold. By it, the detection accuracy becomes better than other methods.

As will be clear from the above, it is incredible that some researchers assert the good agreement between the theoretical and experimental stability charts without clearly stating the determination method of the chatter onset in the experiment. It is again emphasized that one of crucial issues in the self-excited chatter is to define rationally and to determine correctly the chatter onset in the experiment. In this context, we must be furthermore aware that the machine-attachment-tool-work system is of multiple-degree of freedom with directional orientation in vibrational parameters. Conceptually, we must produce a stability chart, in which the stability lobe should have certain allowances, i.e. stability chart depicting with band-like lobe, even when using the simplified mathematical model. Then, we must compare the agreement between the theoretical and experimental stability limits.

1.1.3 Influences of Attachment on Chatter Stability

We used to state a stereotyped introduction in the research paper, i.e. chatter being dynamic behavior within the machine-attachment- tool-work system. On the contrary, nearly all research papers assert the good agreement between the theoretical and experimental stability charts without stating anything about the work and tool holding devices. In general, such

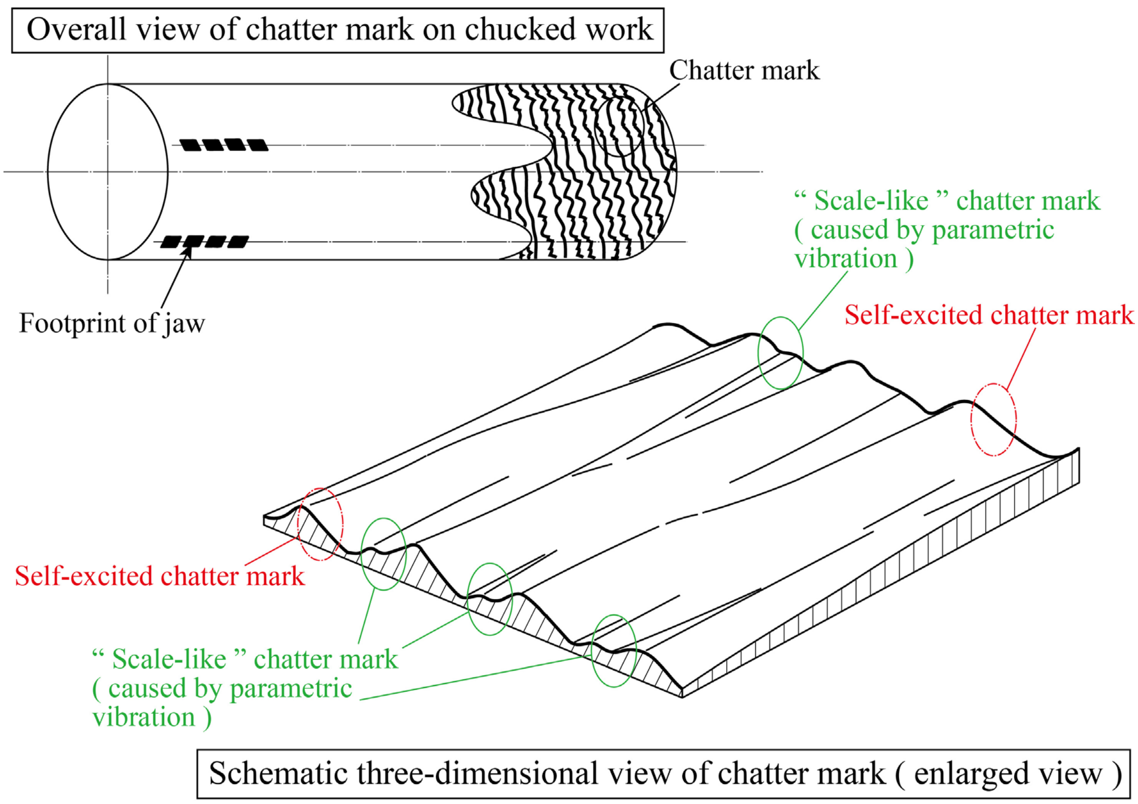

Fig. 1.8 Superimposing "Scale-like Mark" on self-excited chatter mark

work and tool holding devices are non-linear characteristic in their joint rigidities and affect considerably the magnitude of the spring constant in the "Structural Equation" (Ito, 2017). In accordance with Editor's long-standing experience in the factory floor, the stability chart varies considerably by the work holding condition. For example, the work held by the chuck with knurled gripping surface increases much more the stability limit in turning than that with finish-turned.

Typically, M. Doi et al (1982) revealed that the three-jaw chuck induces the parametric vibration mingling within the self-excited chatter of regenerative type as will be discussed herein. As reported elsewhere, the work holding stiffness of the three-jaw chuck varies three times every one rotation of the main spindle, resulting in the directional orientation effect of the work stiffness [4]. As a result, the chatter onset differs from each other depending upon the jaw position as shown in Fig. 1.8. Eventually, we must investigate the regenerative type in consideration of mingling the parametric vibration caused by such a directional orientation by solving the "Mathieu Differential Equation".

More specifically, they showed apparently an evidence, i.e. superimposing partly "Scale-like" mark caused by the parametric vibration on the self-excited chatter mark as shown together in Fig. 1.8 with enlarged view for the three-dimensional surface roughness. In fact, we can observe obviously the "Scale-like" mark at the slope of the self-excited chatter mark.

Figure 1.9 demonstrates a comparison of the theoretical asymptotic borderline of stability for work held by the three-jaw scroll chuck with that by four-jaw independent chuck. Of note, the chatter stability is evaluated by the index k_c/k_w, where k_c and k_w are the cutting stiffness and average stiffness of chuck-work system, respectively, and the experimental value of stability limit is also shown in Fig. 1.9.

From Fig. 1.9, we can observe the very interesting behavior as follows.

(1) In the case of three-jaw scroll chuck, the experimental values are plotted far lower at lower spindle speed and higher at the higher spin-

[4] In retrospect, Tlusty suggested already the directional orientation in the rigidity of the tailstock and also certain influences of the live center on the stability limit.
Tlusty J. (1970) 4.3 Centre lathe. In: Koenigsberger F, Tlusty J (eds) Machine Tool Structures, Pergamon Press, pp. 243-265.

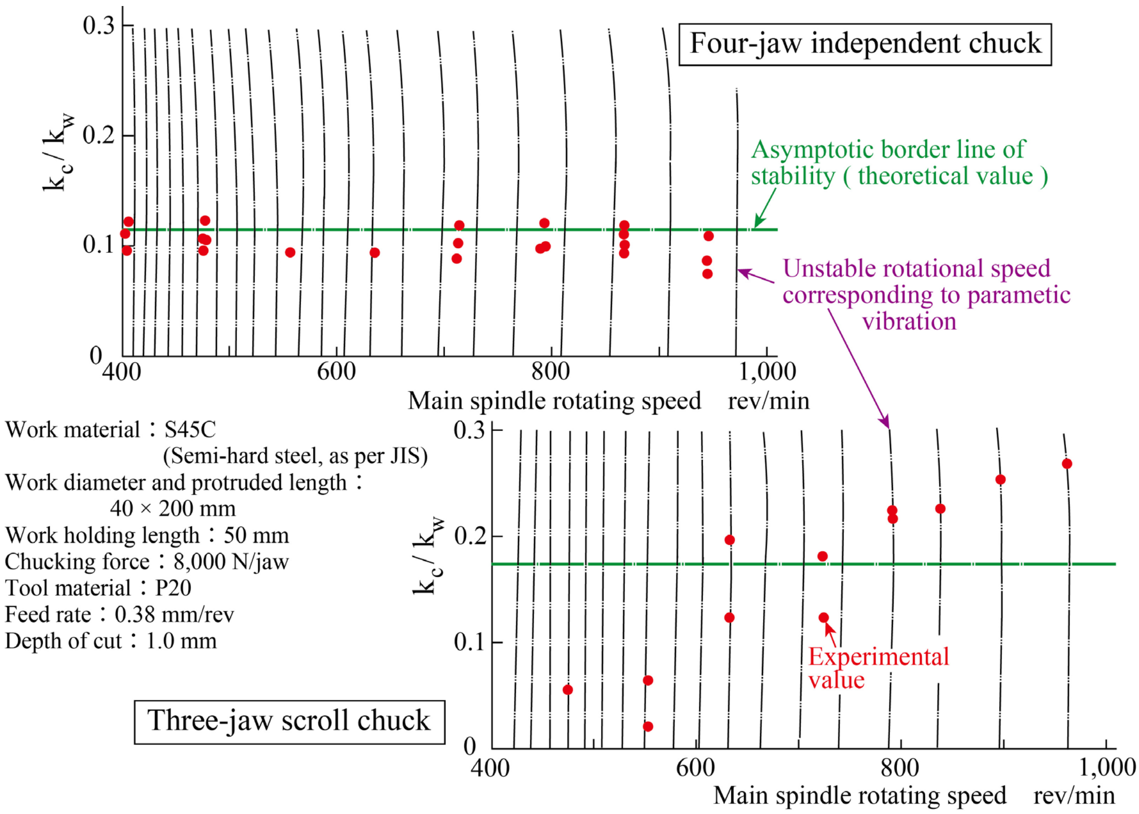

Fig. 1.9 Decrease of stability limit by mingling with parametric vibration

dle speed than the theoretical asymptotic borderline, respectively. The experimental value at higher spindle speed corresponds well with that of parametric vibration.

(2) In the case of four-jaw independent chuck, all the experimental values can be plotted to be closer to the theoretical asymptotic borderline, and thus it may be concluded that there are no influences of the parametric vibration. Importantly, we can observe such a parametric vibration even in light cutting as shown also in Fig. 1.9.

In addition, M. Doi et al (1985, 1990) suggested the larger influence of jaw traveling mechanism on the chatter stability by comparing the four-jaw independent chuck with that of scroll type.

After long interval, Monnin (2013) has recently measured the frequency response in the first bending mode of the main spindle-holding device-milling cutter system in still stand as shown in Fig. 1.10 and Table

1.1. In addition, Monnin identified the specific cutting force for each milling cutter.

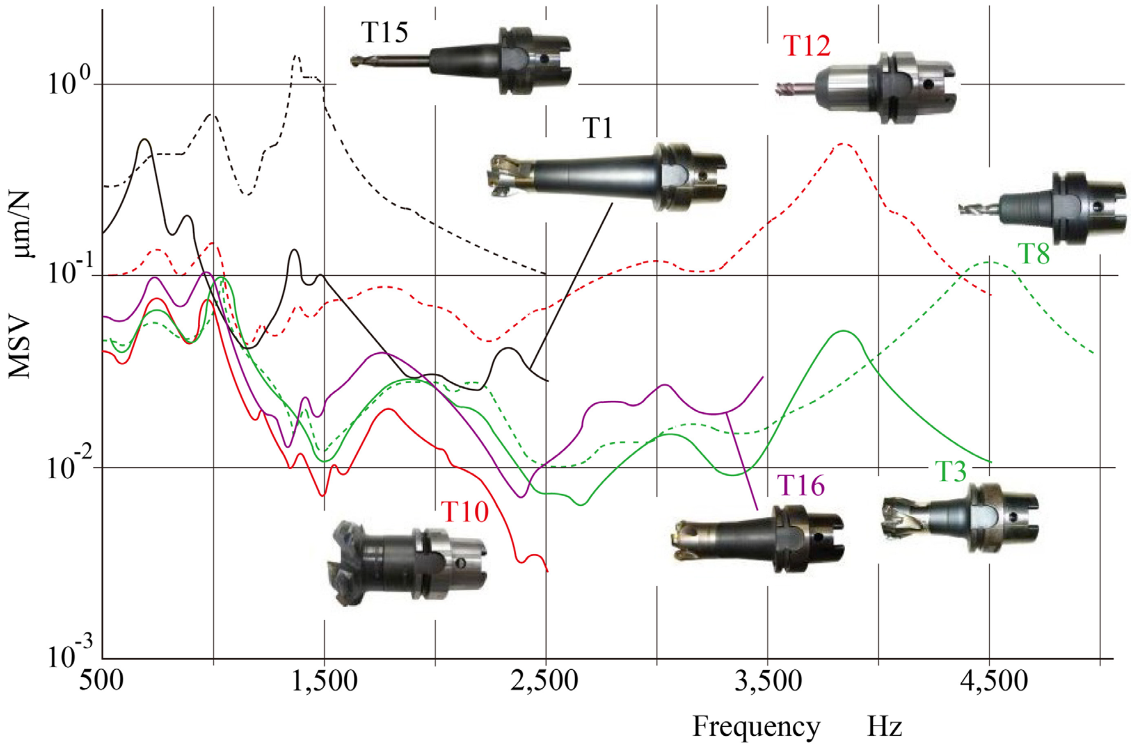

Fig. 1.10 Receptance functions at tool tip for various tool-holder assemblies (by Monnin)

Tool-holder assemblies	Type	Diameter mm	Free length mm	Number of teeth	Helix angle deg.	Engaging angle deg.
T1 T3	Insert end mill	40	175 100	5	10	+90
T8	End mill (sintered carbide)	10	103	2	30	
T10	Face mill	63	90	5	20	+45
T12 T15	End mill (sintered carbide)	16 12	124 171	4 2	40	+90
T16	Round insert end mill	40	116	5	4	—

Table 1.1 Dimensional specifications of milling cutters (by Monnin)

Monnin conducted the experiment by using the quinaxial-controlled MC

(Mikron Agie Charmilles-brand; Type HPM), and the frequency response was measured by impulse excitation. In the experiment, furthermore, the corresponding signal was detected with the accelerometer, and the maximum singular value (MSV) is an index to represent the maximum amplitude of receptance function. As can be readily seen, we can observe the remarkable differing feature when varying the milling cutter and its holding device.

To this end, it emphasizes again, as exemplified these forerunning research works, that the chatter should be dealt with from the system point of view; however, we are not so keen to do so.

1.2 Characteristic Facets of Drilling, Milling and Grinding in Analyses of Chatter

In the year 2000 and beyond, we have placed the main stress on the research into the chatter for milling and drilling instead of turning. Of course, the research has been carried out on the strength of the traditional chatter theory for turning; however, it is necessary and inevitable to pay the special attention to the differing features in cutting mechanisms among turning, milling, drilling, and furthermore grinding.

For example, a root cause of difficulties in drilling lies in the uncertainty derived from the damping capacity of the chisel point. Fig. 1.11 sows the typical triangular-like shape of the hole, which is generated in the very beginning of the drill engagement to the work (Abele et al., 2007). Such a behavior is well known from the past, and Shiozaki and Furukawa (1974) proposed already a simple qualitative analysis regarding why the triangular-like hole is generated as shown in Fig. 1.12.

In the left-hand side of Fig. 1.12, the simple mathematical model is shown in consideration of the geometrical deviation of both the cutting edges in the chatter.

From Fig. 1.12, the instantaneous relationships between the drill diameter and waviness of drilled hole can be written as

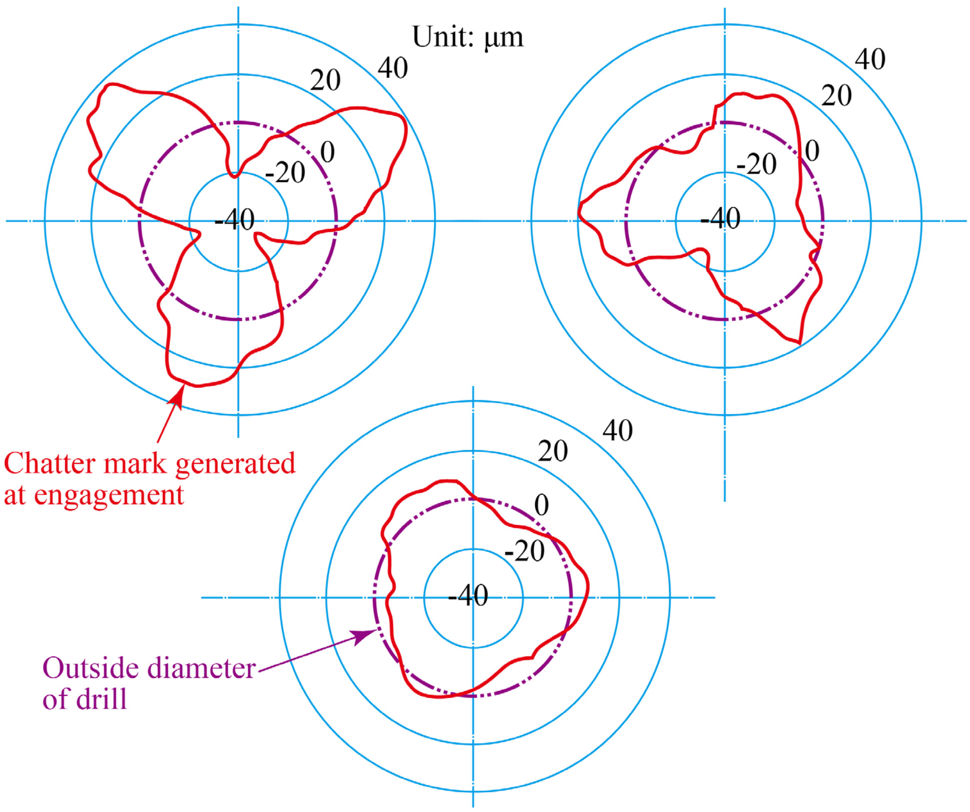

Fig. 1.11 Triangular-like hole shaped by chatter of self-excited type
(by courtesy of Abele et al., 2018)

$$[\ r_w(\varphi_c) + r_{w0}\ ] + [\ r_w(\varphi_c - \pi) + r_{w0}\ ] = d_0 + y(\varphi_c) \text{ --------- } (1.7)$$

where, $d_0 = 2r_{w0}$, and $r_w(\varphi_c) + r_w(\varphi_c - \pi) = y(\varphi_c)$

Thus, we should first convert φ_c in Eq. (1.7) by the Laplace transformation, and then the operator "s" is replaced by "jn". Consequently, the transfer function between Y(s) and R_w(s) yields to

$$[\ R_w(jn)/Y(jn)\ ] = 1/[\ 1+ e^{-\pi jn}\ ] \text{ --------- } (1.8)$$

The gain of this transfer function is in maximum when n is odd number as shown in right-hand side of Fig. 1.12. In general, the vibration amplitude becomes larger at the lower odd number, and thus we can observe the chatter mark of triangular-like shape. It is however regrettable that they did not analyze quantitatively, because of difficulty to estimate the damping capacity at the chisel point. It seems that Abele et al faced also the same problem.

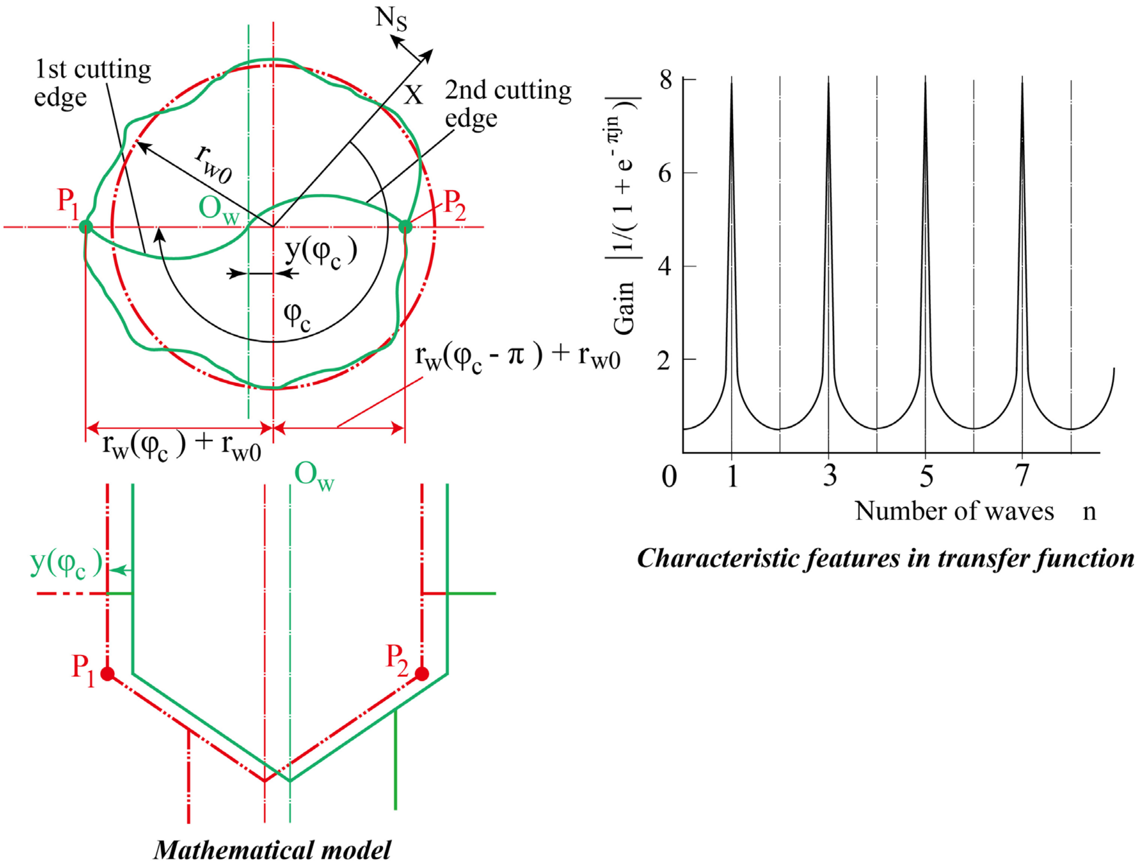

Fig. 1.12 Mechanism for generating “Odd-shaped” hole in drilling (by Shiozaki and Furukawa)

In the following, thus, some quick notes will be given with respect to the differing features in drilling, milling and grinding as compared with turning by single-point cutting tool, which is closely related to the “Cutting Process Equation”.

Figure 1.13 shows the characteristic features in twist drill, i.e. existence of chisel point and changing wedge angle (equivalent rake angle) along cutting edge. More specifically, the chisel point has certain thickness (web) and acts like rotating dull chisel resulting in the poor cutting performance, whereas it may facilitate higher damping to be in realty. Importantly, the equivalent rake angle increases with the distance from the drill center as shown in the right-hand side of Fig. 1.13 [5]. In short, the specific cutting force changes along with the cutting edge (in radial direction).

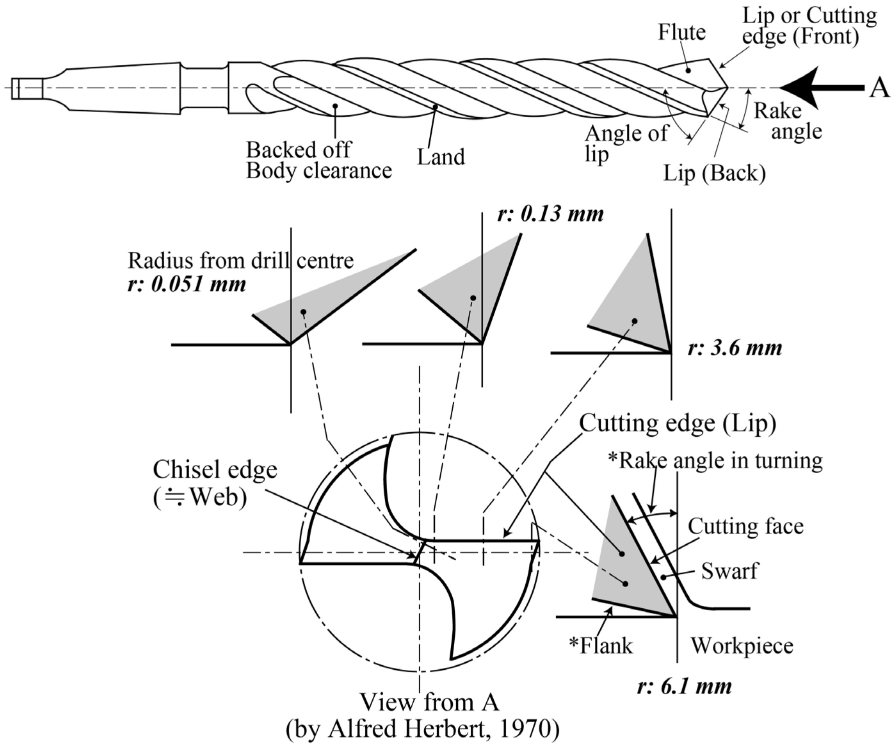

Fig. 1.13 Changes of cutting edges from dull to sharp wedges in twist drill

More importantly, we often employ the thinning of the drill point to reduce the thrust component of the cutting force and to improve the cutting performance as shown in the right-hand side of Fig. 1.14. In drilling for larger hole, we used to pre-machine the small hole to eliminate the unfavorable influence of the chisel point as shown in the left-hand side of Fig. 1.14. As can be readily seen, such a drilling method can be replaced by turning with twin-cutting edge of continuously changing rake angles. In addition, the re-ground drill shows certain deviations from the symmetry in both the cutting edges, i.e. lips of different lengths, without carefully re-grinding, which results in the unevenness in the radial component of the cutting force in practice. Obviously, such an incremental radial component

[5] To ease of understanding, the cutting edge is schematically illustrated as like as that of single-point cutting tool in turning, and thus we call it "Equivalent Rake Angle". In fact, the rake angle of the twist drill is indicated in the top of Fig. 1.13.

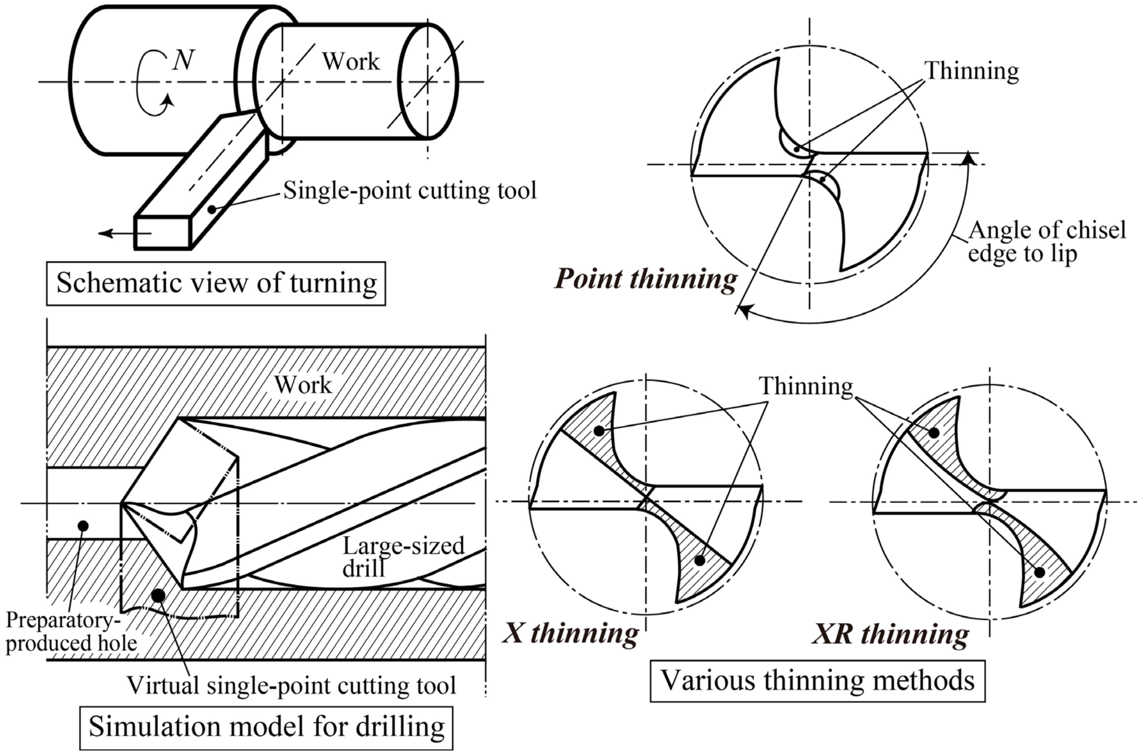

Fig. 1.14 Various thinning methods and preparatory-produced hole to eliminate unfavorable influences of chisel point in twist drilling

may cause either unfavorable, or advantageous influences on the chatter stability, although the twist drill has the body clearance. It is thus recommendable to investigate the chatter when using the re-ground drill in consideration of its quality.

Reportedly, the research into the chatter in milling has recently been carried out vigorously, because of its attractive features as mentioned beforehand. For example, we need to discuss the sophisticated mathematical model, whereas we can apply the advanced simulation software and dynamic information processing to solve the chatter, which can facilitate the ease of analytical and experimental activities to a large extent.

The milling cutter rotates and traveling simultaneously, and thus the cutting edge generates the trajectory represented by *Trochoidal* curve as shown in Fig. 1.15. In consequence, the uncut chip thickness is given by the area, which is surrounded by both the tooth being engaged and the preceding tooth. In many respects, the characteristic features in milling are thus derived from the following three factors.

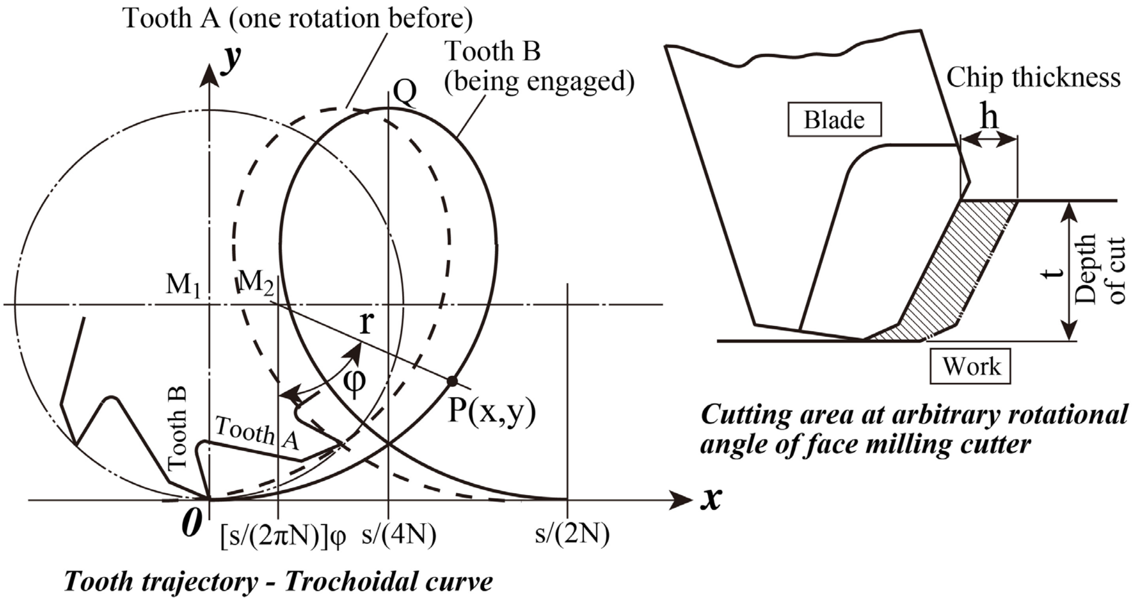

Fig. 1.15 Tooth trajectory and uncut chip thickness in milling

(1) The uncut chip thickness is approximately proportional to the feed rate per tooth and simultaneously the rotational angle of tooth.
(2) The cutting force depends upon the number of cutting teeth being engaged in the work.
(3) The impact load acts on the work when the tooth engages in the work, and thus there are considerable differences in the cutting mechanism between up-cut and down-cut modes.

Now let us determine the (x, y) co-ordinate by taking the deepest position of the tooth as an origin, and the tooth is now in the position P after rotating φ as shown in Fig. 1.15, the co-ordinate P can be written as

$$\left.\begin{aligned} x &= M_1 M_2 + r \sin\varphi \\ y &= r - r\cos\varphi \end{aligned}\right\} \text{-------------- (1.9)}$$

$$M_1 M_2 = s\frac{\varphi}{\omega} = \frac{s}{2\pi N}\varphi \text{ -------- (1.10)}$$

where, r = Radius of milling cutter, s = Feed speed of table

N = Rotational speed of milling cutter,

ω = Angular velocity of milling cutter.

By substituting Eq. (1.10) to Eq. (1.9),

$$\left.\begin{aligned} x &= \frac{s}{2\pi N}\varphi + r\sin\varphi \\ y &= r(1-\cos\varphi) \end{aligned}\right\} \text{--------- (1.11)}$$

The cutter trajectory for one revolution before is given by

$$\left.\begin{aligned} x &= \frac{s}{2\pi N}(\varphi - \varphi_Z) + r\sin\varphi \\ y &= r(1-\cos\varphi) \end{aligned}\right\} \text{--------- (1.12)}$$

where,

$$\varphi_Z = \frac{2\pi}{Z}$$

Because the *Trochoidal* curve is one of the transcendental functions, it is difficult to calculate analytically the distance between two adjacent curves, and thus after carrying out the approximation method, the uncut chip thickness yields to

$$h = s_z \sin\varphi \text{ ------------------- (1.13)}$$

where,

$$s_Z = \frac{s}{Nz}$$

In short, the chip thickness changes continuously with the rotation of the milling cutter, and thus the specific cutting force is not constant, but varies while the milling cutter rotates. Importantly, we must be aware that the chatter theory becomes complex in the order of turning, drilling, milling and grinding as will be clear in the following.

Figure 1.16 illustrates the grinding wheel mounted on the wheel flange, and furthermore three core components consisting of the grinding wheel, i.e. grain, binder and pore.

In grinding, a grain behaves like the tooth (cutting edge) in milling, i.e. trajectory for form-movement being represented by the *Trochoidal* curve, and in due course, grinding can be classified into the up-cut and down-cut modes. In general, the down-cut mode is dominant and eventually, we can observe other characteristic features as follows.

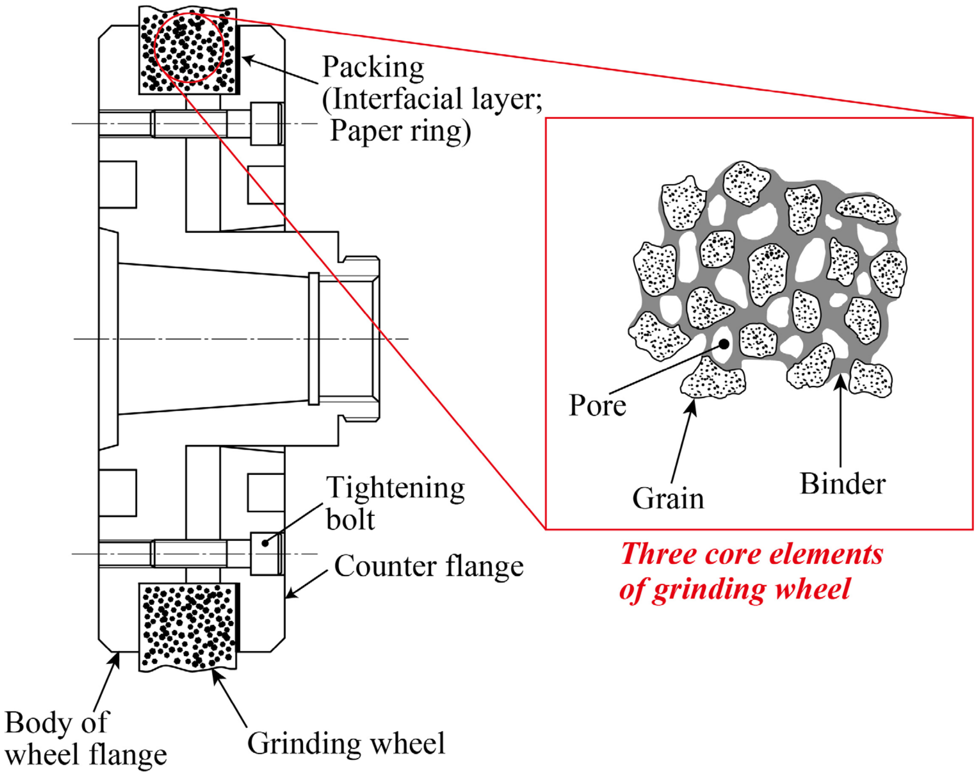

Fig. 1.16 Three core elements of grinding wheel and flange for wheel mounting

(1) A grinding wheel is very elastic as compared with the cutter body and tool shank in the milling cutter.

(2) In the case of the vitrified grinding wheel, its rigidity is not uniform across the whole circumference, resulting in the directional orientation of rigidity. Thus, we must consider the danger of mingling the

parametric vibration like that caused by the jaw chuck in turning as will be discussed in Section 1.3. In contrast, with the advance of the production technology for the grinding wheel, we may guess that such a rigidity deviation becomes less, although we have not had the publicized data since the late 1960s.

(3) A grain seems as to be a tooth with negative rake angle, and the uncountable number of grains engages in the work, resulting in a problem for the quantification of "*Grain Distribution*", which is, in general, very difficult.

(4) The grain distribution is very unstable, which is caused by the "*Grain Self-Edging Function (Grain self-regeneration effects, Autogenous edge-generation effects)*". In short, the worn grain cannot stand the grinding force, and then drops out from the grinding wheel. In due course, a new grain joins within grinding instead of the worn one.

As a result, we must, at least, consider (1) the "Contact Stiffness of Grinding Wheel", (2) "Grinding Stiffness and Damping", and (3) "Anti-wear Stiffness of Grinding Wheel" in the block diagram of chatter loop for grinding as will be discussed in Section 1.3. Importantly, the grinding wheel may generate the wavy surface on the work, when the grinding stiffness is higher than its anti-wear stiffness, and it may be interpreted that such waviness induces either the forced vibration or chatter of regenerative type.

Based on our long-standing experiences, furthermore, we must pay the special attention to the flange structure for mounting the grinding wheel. As can be seen from Fig. 1.16, the wheel flange consists of various interfaces, which give rise certain damping capacity, and eventually, the paper ring is somewhat helpful to increase the damping capacity effective for suppressing the chatter vibration with higher frequency.

In addition, it is better to consider that the radial component (axial component in turning) of the grinding force is larger than the tangential component (principal component in turning), which is definitely in reverse relation to turning.

To this end, thus, it emphasizes that the chatter in grinding is much more complex than those in metal cutting, and this is one of the obstacles regarding the poor research achievement for the chatter in grinding.

1.3 Basic Knowledge about Self-excited Chatter of Regenerative Type in Metal Grinding

In discussing both the chatters of regenerative types in metal cutting and grinding, it is first better to understand the differing features in the chatter onset with machining time.

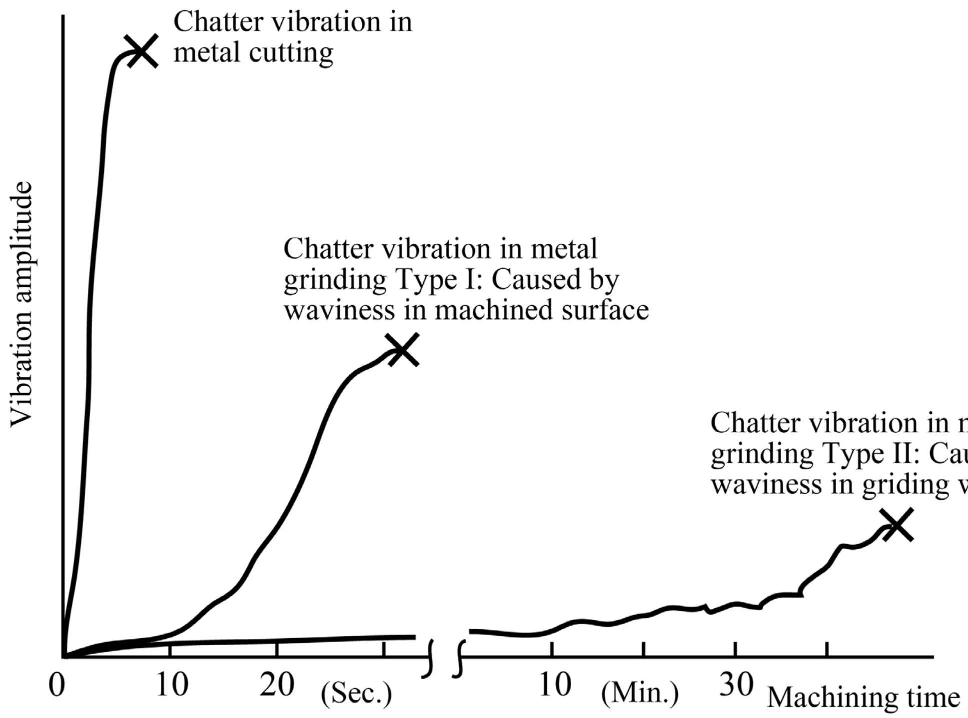

Fig. 1.17 Representative behavior of chatter vibration of regenerative type in metal cutting and grinding in general (by Furukawa)

Fig. 1.17 shows the general behavior, and as can be seen, the chatter in metal cutting occurs at the very short time lapse after the start of cutting and rapidly increases its amplitude. In contrast, the chatter vibration in metal grinding occurs after relatively long time lapse, and the amplitude is not so large. It is also interesting that we can identify two differing causalities for the chatter in metal grinding as shown together in Fig. 1.17. In fact, there are two types: “Type I” is caused by the waviness of machined surface, and its frequency is either closer to the resonance state of the grinding wheel-work system, or a little bit higher than the resonance frequency. In contrast, “Type II” is caused by the waviness of the grinding wheel being in contact with the work, and in general, its frequency is much higher than that of Type I.

Importantly, we can observe the chatter onset with increasing the depth of cut in metal cutting, whereas the chatter onset in metal grinding occurs with decreasing the depth of cut.

1.3.1 Theory for Chatter of Regenerative Type

Now let us discuss the three basic expressions on the strength of those for turning with single-point cutting tool [6].

Figure 1.18 illustrates the correlation between the initial depth of cut $u_0(t)$ and the instantaneous depth of cut u(t), and as can be readily seen, the instantaneous depth of cut is given by

$$u(t) = u_0(t) + r_{wout} - r_{win} \text{ -------- } (1.14)$$

In the cylindrical and internal grinding methods, and furthermore surface grinding with rotary table type, the period per one revolution of the work T_w is constant, and thus by substituting $r_w(t)$ into r_{win},

$$r_{wout} = r_w(t - T_w) \text{ -------- } (1.15)$$

Thus,

$$u(t) = u_0(t) + r_w(t - T_w) - r_w(t) \text{ -------- } (1.16)$$

By applying the Laplace transformation, the “Uncut-chip Thickness Equation” yields to

---

[6] Because of ease of understanding, the theoretical analysis in Section 1.3 is based on that of Furukawa. Furukawa Y. (June 1975) Chatter Vibration in Grinding and Its Suppression. Handouts in No. 411 Seminar for “Fundamental Technologies in Machining”.

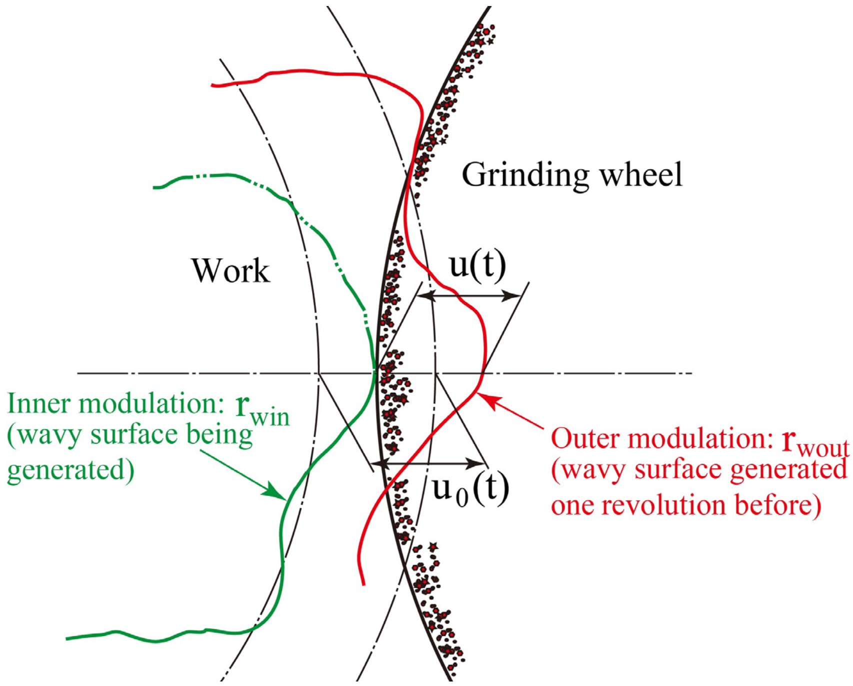

Fig. 1.18 Relationships between initial and instantaneous depths of cuts (by Furukawa)

$$u(s) = u_0(s) - (1 - e^{-T_w s})r_w(s) \text{ ---------- } (1.17)$$

Obviously, Eq. (1.17) represents the regenerative effect, and in due course applicable also to the chatter of Type II.

In grinding, we must consider the damping force, because the grinding area depends upon not only the specific grinding force, but also the relative approaching speed of grinding wheel to the work. Thus, the "Grinding Process Equation" can be written as

$$P_n(t) = k_g u(t) + c_g \frac{dx_r(t)}{dt} \text{ -------- } (1.18)$$

where, P_n = Radial component of grinding force, k_g = Specific grinding force (grinding stiffness), c_g = Grinding damping.

By applying the Laplace transformation, Eq. (1.18) yields to

$$P_n(s) = k_g u(s) + c_g s x_r(s) \text{ --------- } (1.19)$$

In both the above expressions, k_g and c_g are given by

$$\left.\begin{array}{l} k_g = (\kappa B v)/(V + v) \\ c_g = [(\kappa B)/(V + v)]\sqrt{[(2Rr)/(R + r)]u_0(t)} \end{array}\right\} \text{------- (1.20)}$$

$$\kappa = (\tan^{-1}\beta)\,\sigma_s$$

where, B = Grinding width, V = Rotational speed of grinding wheel, v = Rotational speed of work, R = Radius of grinding wheel, r = Work radius, β = Angle between wheel approaching axis and acting direction of radial component of grinding force, and σ_s = Specific grinding force.

Because of the considerable elasticity of the grinding wheel, its contact deflection to the work cannot ignore in discussing the dynamic characteristics of the machine-attachment-work-tool system in grinding. When x_n is the deflection along the direction of the radial component P_n, in due course the "Structural Equation" (total dynamic receptance) yields to

$$\frac{x_n}{P_n(s)} = \frac{G_m(s)}{k_m} + \frac{1}{k_{con}} \text{ --------- (1.21)}$$

where, k_{con} is the contact stiffness of the grinding wheel, which is the ratio of the radial component of grinding force to the due wheel deflection.

It is said that the contact stiffness shows the non-linear spring characteristics, i.e. hard spring, depends upon the grain size, hardness and so on, and can be estimated on the strength of Herz theory. From the viewpoint of the machine tool joint, however, it is doubtful that the contact stiffness of the grinding wheel can be estimated by Hertz theory as will be discussed in Item 1.3.2.

In discussing the chatter in metal grinding, another primary concern is the wear of the grinding wheel, i.e. increasing wear of grinding wheel with machining time. Thus, we must consider the "*Wear Stiffness of Grinding Wheel*", which is the ratio k_a of the radial component of the grinding force to the wear thickness of the grinding wheel as follows.

$$k_a = k_g q \frac{V}{v} \text{ --------- } (1.22)$$

where, q is the grinding ratio [7].

In addition, we must eye that the waviness of ground surface r_w is not identical to the vibration amplitude x_n between the grinding wheel and the work in radial direction, and these two are interrelated by

$$g = \left| \frac{r_w}{2x_n} \right| = \begin{cases} \frac{1}{2}(1 - \cos \frac{\omega_{cr}}{\omega} \pi) \text{ ------- } \frac{\omega_{cr}}{\omega} < 1 \\ 1 \text{ ---------- } \frac{\omega_{cr}}{\omega} \geqq 1 \end{cases} \text{ -------- } (1.23)$$

where, ω_{cr} is the critical angular frequency and given by

$$\omega_{cr} = v \Big/ \sqrt{\frac{2rR}{r \pm R} x_n}$$

(+ sign is for cylindrical and surface grinding, and – sign is for internal grinding)

From Equations (1.17), (1.19), and (1.21) ~ (1.23), we can produce the block diagram of chatter loop as shown in Fig. 1.19, which consists of two loops corresponding with Types I and II as already mentioned beforehand (see Fig. 1.17) [8]. In fact, we can discriminate these two clearly without any trouble. For example, we can observe a cycle of chatter onset-growth-saturation for every work in Type I, whereas Type II disappears by dressing the grinding wheel whenever.

---

[7] In the past, q was more than 20 and V/v was between 50 and 100 in carbon steel grinding with standard grinding conditions, an thus

$$1{,}000 < k_a / k_g < 2{,}000$$

In short, the "Wear Stiffness" was more than 1,000 larger than the "Grinding Stiffness".

[8] In Eq. (1.23), the interference effect is larger when ω_{cr} is smaller than the chatter frequency ω, resulting in the smaller r_w. In general, the interference effect becomes larger in the order of cylindrical, surface and internal grinding, and along with in the lower rotational speed of the work.

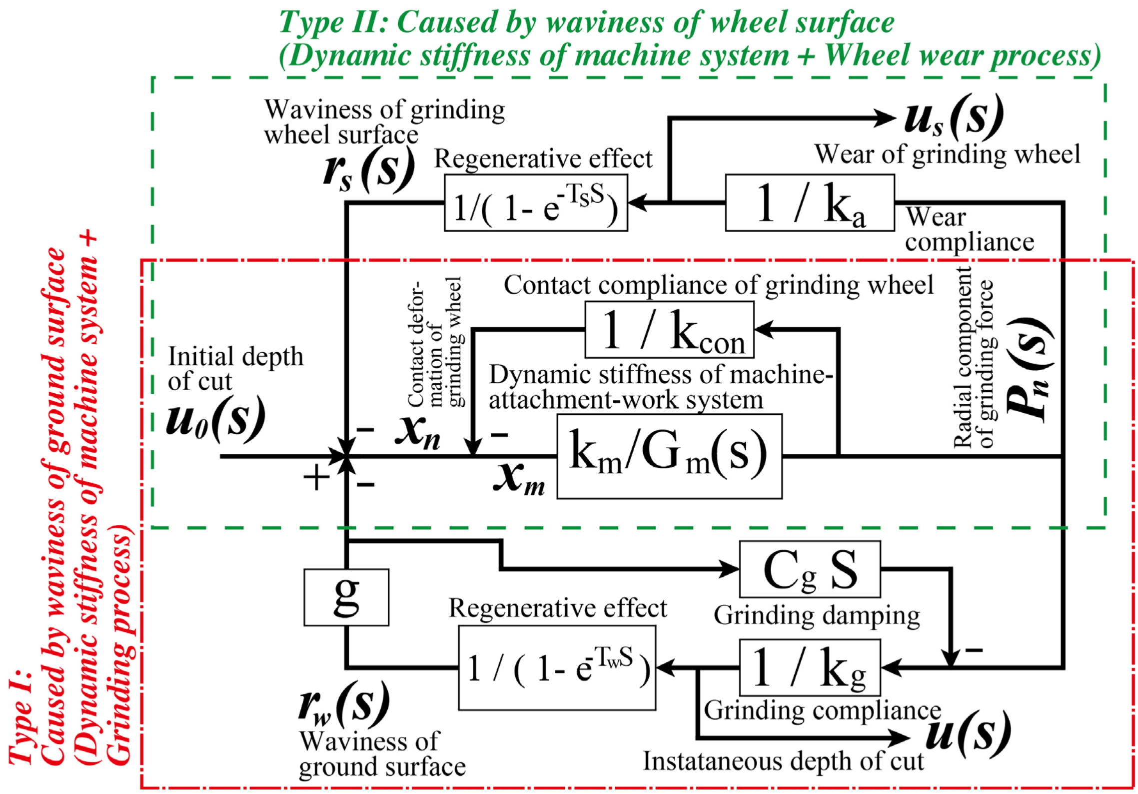

Fig. 1.19 Block diagram of self-excited chatter loop for regenerative type (by Furukawa)

In general, at issue in grinding chatter is to suppress the onset of Type I, which is caused by the waviness of the machined surface, and thus we may suggest several guides as follows.

(1) Ease of chatter onset in cylindrical and center-less grinding, and furthermore in surface grinding with rotary table and horizontal main spindle.

(2) Plunge grinding is the utmost dangerous to chatter onset.

(3) High anti-chatter capability in internal grinding.

(4) The lower hardness of a grinding wheel, the more anti-chatter capability is its property. In general, the elastic grinding wheel is recommendable to suppress the chatter.

For the sake of further understanding, Fig. 1.20 shows the block diagram of chatter loop for cylindrical grinding of plunge type (g = unity), and from this diagram, the "Characteristic Equation (Transfer Function)" can be written as

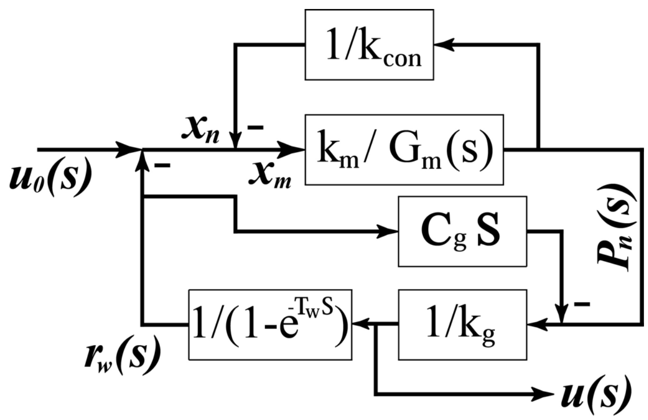

Fig. 1.20 Block diagram for self-excited chatter caused by waviness of machined surface

$$1 + \{G_m(s)/k_m + 1/k_{con}\}\{ C_g S + k_g(1- e^{-T_w S})\} = 0$$

By solving the above expression, we can determine the stability limit, and thus the characteristic equation for the chatter of Type II is also shown below.

$$G_m(s)/k_m + 1/k_{con} + 1/k_g = -1/k_a(1- e^{-T_s S})$$

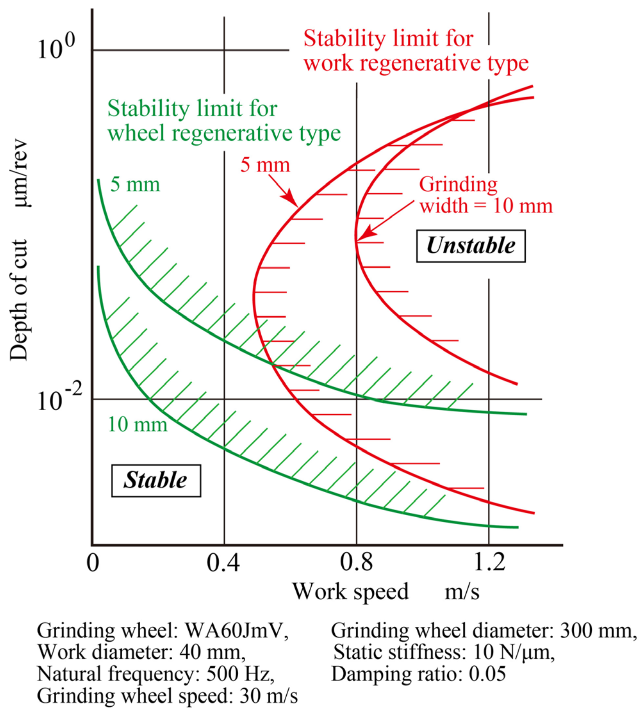

Fig. 1.21 Stability charts for plunge grinding (by Inasaki)

Figure 1.21 shows simultaneously two stability charts for Types I and II in plunge grinding together with varying the grinding width (Inasaki, 1977). As can be readily seen, there are apparently different behavior between the Types I and II. More specifically, Type I does not occur at the lower work speed, i.e. larger absolute stability limit nearly all grinding conditions, whereas Type II occurs easily across the whole grinding conditions.

1.3.2 Research and Engineering Development Subjects

As will be clear from the above, there are even now a handful of fatal problems being unsolved, which are in closer tie with the grinding wheel's own characteristic features. Such features are obstacle to establish much more reliable chatter theory for grinding than ever before, and in contrast result in some hindrances for the inactive research into the chatter behavior in metal grinding.

Having in mind the achievements so far reported and fatal problems to be investigated hereafter, the Editor suggests first the necessity of the meticulous observation of the chatter behavior again. In the observation, primary concern is the discrimination of the torsional chatter as suggested by that of Entwistle and Stone (2013). Obviously, we must reinvestigate duly the availability of the chatter theory so far established for grinding and concerns at present as same as the traditional chatter theory for metal cutting.

Paraphrasing, we must mind why we cannot find the stability chart recently publicized instead of that of Fig. 1.21, which was produced in the 1970s. In fact, this evidence indicates the complexity in the chatter of regenerative type in metal grinding. After conducting the research into the availability of the chatter theory from total and wider scopes, we must thus delve into the individual R & D subject, for which some quick notes will be given in the following. Of course, it is desirable to discuss in detail what are necessary to establish an advanced chatter theory as same as that for metal cutting; however, we have not had enough reference materials to do so (see Chapter 3).

Contact stiffness of grinding wheel

As reported elsewhere, some researchers assert that the contact stiffness of the grinding wheel can be estimated by Hertz theory. In short, Hertz theory is available for the two-surface in contact problem, where both the surfaces are perfect planes without any roughness and waviness; however, the grinding wheel has the very rough surface. Importantly, it is common sense now that the contact between the grinding wheel and the work is one of the machine tool joints, where we can apply Hertz theory in very special cases, i.e. joint consisting of nearly perfect surfaces.

In fact, the contact stiffness depends strongly upon the "*3-Dimensional Distribution of Grains*", and thus changes almost every second while grinding. In consequence, we need now to establish an innovative method for determining the contact stiffness in real time; however, as well known, primary concern in grinding mechanism is to measure and visualize the 3-dimensional grain distribution at present.

Grinding Damping

As can be readily seen from Eq. (1.20), "*Grinding Damping*" is calculated by only considering the geometrical relationship while the grinding wheel approaches to the work. Is this assumption acceptable, when we discuss the vibration problem?

Supposedly, the theoretical analysis is good agreement with the experimental result by considering the grinding damping, which plays similar roles of the process damping in metal cutting, i.e. wider absolute stability limit in lower rotational speed. Against to this context, we have not clarified yet what is the essential feature of the grinding damping including its causality. It seems that the binder behaves like a viscous damper; however, we have not had any evidences to support such an assertion yet.

Regenerative Chatter Mingling with Parametric Vibration

The grinding wheel of vitrified type seems to show certain fluctuation in its contact stiffness around the wheel, and such a fluctuation induces a parametric vibration as similar as that shown in Fig. 1.8. In fact, Hahn and Price (1969) measured the variation of the resonance frequency when the grinding wheel contacts with the cantilever, i.e. one of the equivalent indexes for the rigidity.

As shown in Fig. 1.22, we can see a considerable variation in the resonance frequency, and other researchers also suggested such an interesting behavior on that occasion. In short, the contact stiffness can be calculated from the resonance frequency, and we can understand that the vibrational amplitude becomes larger with large deviation of the contact stiffness.

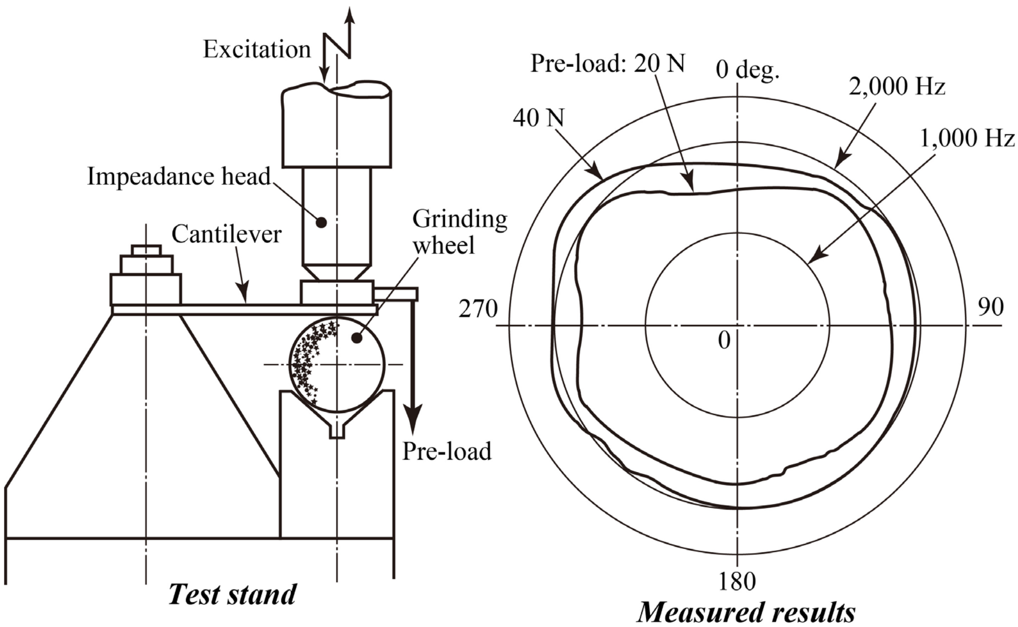

Fig. 1.22 Directional orientation in rigidity of grinding wheel - Measurement of contact resonance frequency (by Hahn and Price)

It is regrettable that we have not had such valuable data since then, and thus a facing problem is to investigate the present state in the unequal of the contact stiffness of the grinding wheel. In addition, we must examine the magnitude of such an unequal is enough to excite the parametric vibration. In general, we may believe that the grinding wheel shows uniform contact stiffness with the advance of the related technology, whereas the directional orientation in the contact stiffness could affect something definite with enhancement of the finished quality of the work.

References

Abele E, Tschannerl M, Kulok M. (2007) *Produktivitätsfaktor Bohrungsqulität: Dreieckige Bohrungen Entstehung, Identifikation, Parametereinfluss*. ZwF; 102-6: 340-344.

Braun S. (1975) *Signal Processing for the Determination of Chatter Threshold*. Annals of CIRP; 24/1: 315-320.

Denkena B, De Leon L, Grove T. (2010) *Prozessstabilität eines kordelierten Schaftfräsers*, ZwF, 105/1/2, 37- 41.

Doi M, Masuko M, Ito Y. (1982) *Re-observation of the Chatter Vibration in Chuck Works - Effects of Jaw Number on the Appearance of a Scale-like Chatter Mark*. In: Proc. of 10th NAMRI of SME, 409-416.

Doi M, et al. (1985) *Study on Parametric Vibration in Chuck Work*. Trans. of JSME (C); 51-463: 649-655.

Doi M, Muroya Y. (1990) *Development of Dynamic Performance Test for Lathe*. Trans. of JSME (C); 56-529: 2521-2526.

Entwistle R, Stone B. (2013) *Position Paper - Fundamental Issues in Self-excited Chatter in Grinding*. Jour. of Machine Eng.; 13-3: 26-50.

Hahn and Price (1969) ASTME Technical Paper.

Higuchi M, et al. (1986) *Study on Determination of Chatter Commencement in Turning*. Trans. of JSME (C); 52-477: 1697-1700.

Inasaki I. (1977) *Regenerative Chatter in Grinding*. Proc. of 18th MTDR Conf., p. 423-429.

Ito Y. (2013) *Position Paper – Fundamental Issues in Self-excited Chatter in Turning*. Jour. of Machine Eng.; 13-3: 7-25.

Ito Y. (2014) *Chapter 1 Tangential Force Ratio and Its Applications to Industrial Technologies: Anti-Vibration Steel Plate for Refrigerator and Derailment of Rolling Stock*. In: Ito. Y (ed) Thought-Evoking Approaches in Engineering Problems, Springer.

Ito Y (2017) *Chapter 7 Concept of "Platform", Its Application and Modular Tooling System*. In: Ito Y, Matsumura T (eds) Theory and Practice in Machining Systems, Springer Nature.

Itoh S et al. (1991) *Ultrasonic Waves Method for Tool Wear Sensing - In-process and Built-in Type*. In: Proc. of Inter. Mech. Engg. Congress, Sydney, pp. 83-87.

Merritt H E. (Nov. 1965) *Theory of Self-Excited Machine-Tool Chatter, Contribution to Machine-Tool Chatter Research-1*, Trans. of ASME Jour. of Engg. for Industry, 447-454.

Monnin J. (2013) *Active Structural Methods for Chatter Mitigation in Milling Process*. Dissertation of ETH Zürich.

Nakazawa H, et al. (1979) *Detection of Stability Limit – 1st report Detection software*. Jour. Precision Eng.; 45-11: 1353-1358.

Nicolescu C M. (1991) *Analysis, Identification and Prediction of Chatter in Turning*. Doctoral Thesis No. 18, Department of Production Engineering, Royal Institute of Technology, Stockholm.

Rahman M, Ito Y. (1979) *A Method to Determine the Chatter Threshold*. In: Proc. of 19th Inter. MTFR Conf., MacMillan, 191-196.

Saljé E, Isensee U. (1976) *Dynamische Verhalten schlanker Werkstücke bei unterschiedlichen Einspannbedingungen in Spitzen*. ZwF; 71/8: 340-343.

Sato H. (1973) *Research perspective for Machine Tool Vibration*. Jour. of JSME; 76-658: 1105-1113.

Sellmeier V, Denkena B. (2010) *High Speed Process Damping in Milling*. Proc. of 4th CIRP Inter. Conf. on High Performance Cutting.

Shiozaki S, Furukawa Y. (1974) *Vibration in Drilling Machine*. In: Reports of Research Unit for Rigidity and Cutting Performance Improvement in Machine Tools. JSME, p.249.

Spur G, Leonards F. (1975) *Sensoren zur Erfassung von Prozesskenngrößen bei der Drehbearbeitung*. Annals of CIRP; 24/1: 349-354.

Tlusty J. (1970) *Chapter 2 The Theory of Chatter and Stability Analysis*. In: Koenigsberger F, Tlusty J (eds) Machine Tool Structure Vol. 1, Pergamon Press, 133-177.

Tobias S A. (1961) *Schwingungen an Werkzeugmaschinen*. Carl Hanser

Verlag, München.
Yeh L J, Lai G L, Ito Y. (July 1992) *A Study to Develop a Chatter Vibration Monitoring and Suppression System While Turning Slender Workpieces*. In: Proc. of 2nd Inter. Conf. on Automation Tech. Vol. 2, 337-343, Taipei.

Chapter 2 First-hand View for Chatter Suppression Technology

Along with the establishment of the chatter theory, we have endeavored to develop various remedies to suppress the chatter since 1930s. Fig. 2.1 exemplifies some leading remedies so far widely used, which range from the technician's contrivance at the factory floor, through engineering knowledge-based method like the damper and end mill with differing helix angle, to the development of the new vibration-proof material.

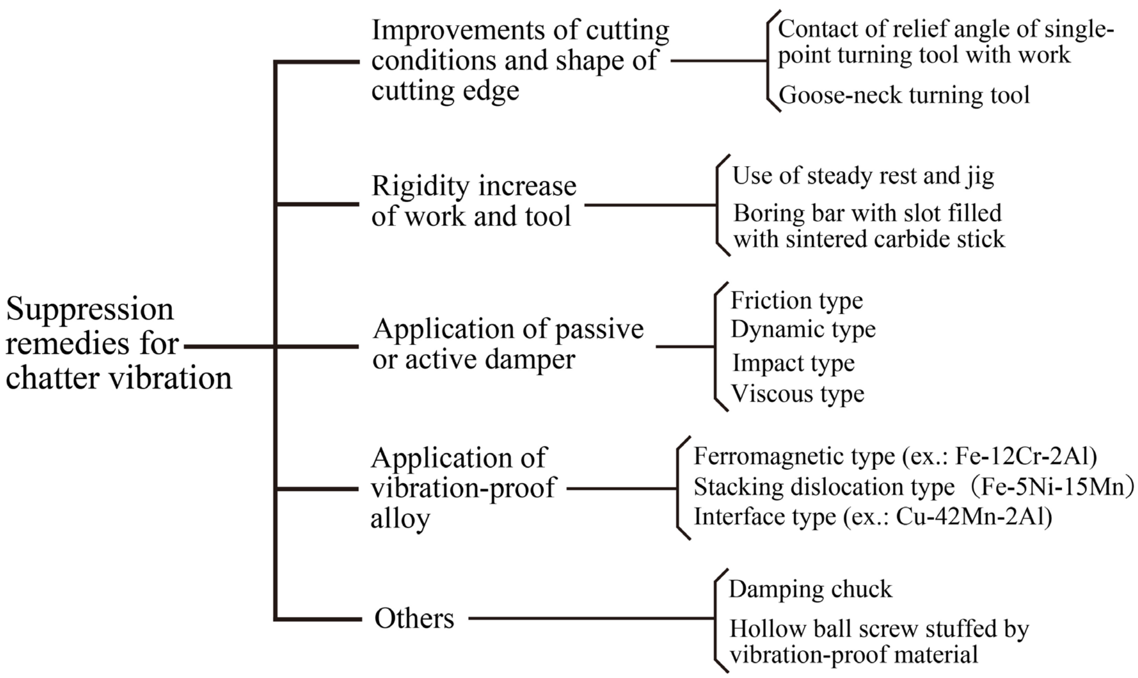

Fig. 2.1 First-hand view of remedies for chatter suppression in general

The vibration suppression and absorption are one of the conventional technologies across the whole engineering field, and thus the damper and vibration-proof material shown in Fig. 2.1 are specified to be applicable to the machine tool sphere. More specifically, we have so far contrived a myriad of passive dampers, e.g. ball screw stuffing with damping material, damping chuck, milling cuck stuffing with damping material such as a

TRIBOS (see Fig. 2. 19) and also active dampers to suppress the chatter; however, nobody claims systematically the facing limitation in their capabilities for the chatter suppression and also the involved engineering problems.

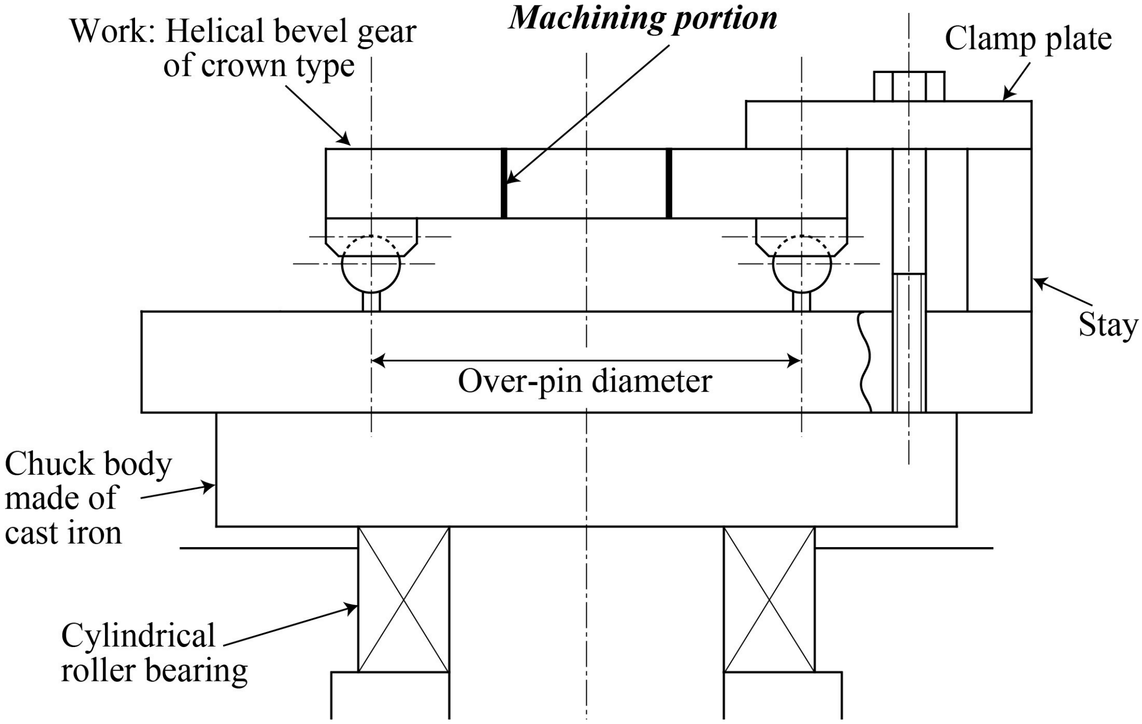

Fig. 2.2 Gear chuck body made of cast iron to decay chatter with higher frequency

Importantly, the vibration-proof material has not been applied to the machine tool so far, apart from the mounting device for the main motor, whereas we can reduce the chatter with higher frequency by placing the unit or component with larger damping near the cutting point, e.g. chuck body made of cast iron in crown gear cutting as shown in Fig. 2.2, tool post made of concrete in turning and quick changing cutting head with buttress thread in milling (see Fig. 2.16). In fact, the blur-like chatter mark can be disappeared by replacing the chuck body made of steel to that made of cast iron in Fig. 2.2. Consequently, we must be aware of the increasing necessities to investigate, with wider scope, the application of the materials with higher internal damping.

More importantly, Fig.2.1 is one of the traditional classification systems, and against this context, the purpose and aims of this chapter are to suggest and discuss the remedies being used and possible to contrive on the strength of the block diagram of chatter loop shown already in Fig. 1.1. As can be readily seen from Fig. 1.1, we can suppress the chatter of regenerative type by the following three remedies.

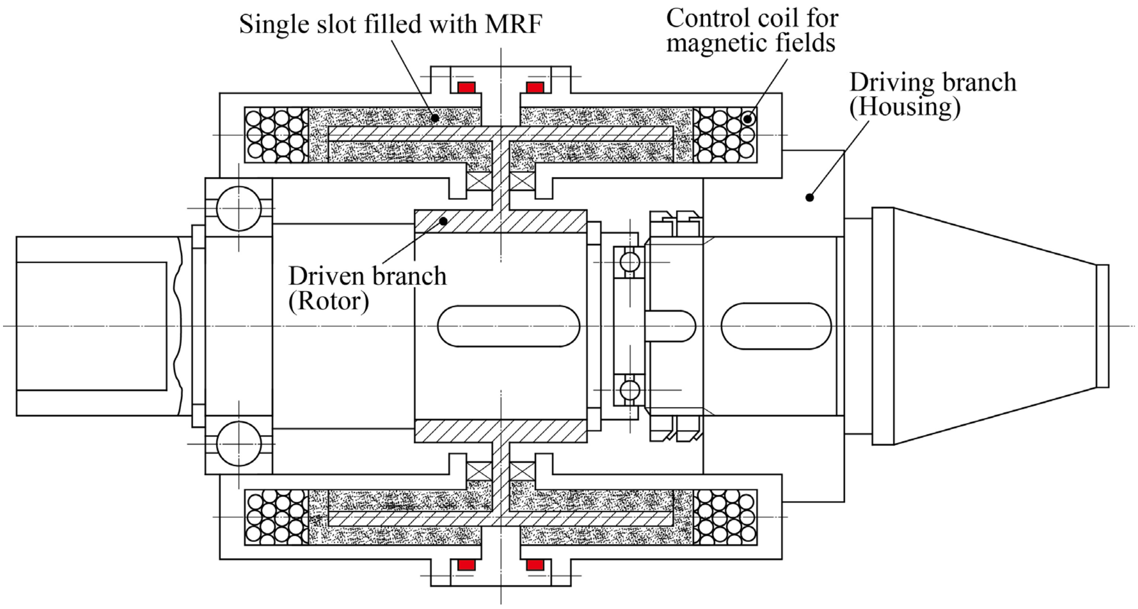

Fig. 2.3 An example of active damper - Adaptive tool holder
(by Weinert and Kersting, and courtesy of Carl Hanser)

(1) Control of "Cutting Process Dynamics", i.e. specific cutting force (cutting stiffness): the end mill with serrated-tooth is one of the representatives, and this end mill can simultaneously control the "Time Delay".
(2) Control of "Structural Dynamics", i.e. dynamic compliance of machine-attachment-tool-work system: as well known, nearly all prevailed remedies are to increase damping capacity within the system, and obviously the damper is the utmost representative. For example, Fig. 2.3 reproduces one of the active dampers for gun drilling with single cutting edge, in which the gun drill is mounted on the rotor and the rotor is driven through MRF (Magnetic Rheology Fluid) coupling.

More specifically, the chatter suppression can be facilitated by the control of the magnetic fields (Weinert and Kersting, 2005).

(3) Control of "Time Delay": this remedy is exemplified by the milling cutter of irregular tooth pitch type and with differing helix angle as will be discussed in Section 2.1. In the case of turning by single-point cutting tool, we may use this idea by means of the main spindle with variable speed.

In consideration that the block diagram of chatter loop yields to the stability chart, it is furthermore notable that we can use the stability chart when investigating the synthetic suppression remedy to the chatter of regenerative type as follows.

(a) Increase of the "Absolute stability limit".

(b) Positive use of the "Cusp-like region" within lobed borderline of stability.

Of these two, the latter remedy is preferable to be the heavy-duty cutting in realty, provided that the stability chart is fully reliable, and in fact, the corresponding software has been merchandized. It is however difficult to get the reliable stability chart over wider cutting conditions (see Section 3.3.3), and in general, the stability limit should be indicated by band-width way, because of considering uncertainties while producing the stability chart. For example, the thin-walled work changes its dynamic characteristic drastically with the progress of cutting.

Figure 2.4 is a first-hand view for R & D activities in the form of "Puttick Grid", simultaneously indicating a time series-like development history for the remedies with respect to the time delay control. More specifically, the remedies are for turning and milling, and having in mind these achievements, we have recently established some new remedies, e.g. variable speed broaching and broaching with irregular tooth pitch type. As will be clear from Fig. 2.4, an expectable remedy will be the "Turn-Milling with Differing (Variable) Helix Angle". In many respects, we may recommend the use of the milling cutter of irregular tooth pitch type and with differing helix angle on the basis of the practical achievement.

In the case of turning, we must use the variable speed method as will be clear from the above; however, in such a remedy, the spindle speed should be fluctuated around 100 rev/min, while the average speed maintains at 305 rev/min as reported elsewhere. These values imply the difficulty of the practical application of the variable speed method.

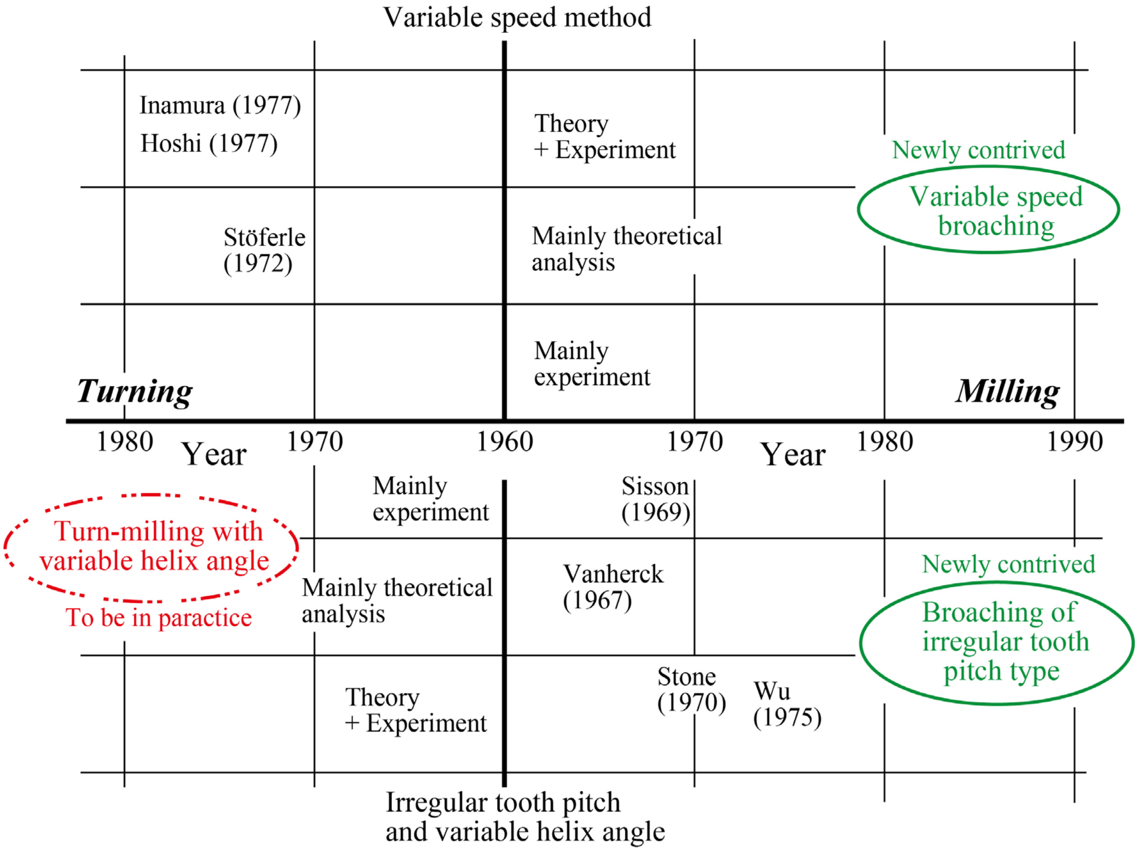

Fig. 2.4 First-hand view of R & D in chatter suppression based on Time-Delay Control

2.1 Milling Cutter of Irregular Tooth Pitch Type and with Differing Helix Angle

As can be seen from the headnotes in Part II, nearly all researchers place the stress on the self-excited chatter of regenerative type in their works. Importantly, they rely on even now the chatter theory established in the 1960s (*traditional chatter theory*), although a handful of the questioned points have been suggested elsewhere. In contrast, it is very interesting that such a theory is very effective even now to contrive some outstanding remedies for the chatter suppression as exemplified by the end mill of either irregular tooth pitch type or with differing helix angle. We will thus delve into its past and present perspectives in the following.

In this context, we must first be aware that both the milling cutters of irregular tooth pitch type and with differing helix angle are effective at the higher-speed range in practice, where the main spindle rotates more than 2,000 and up to 40,000 rev/min.

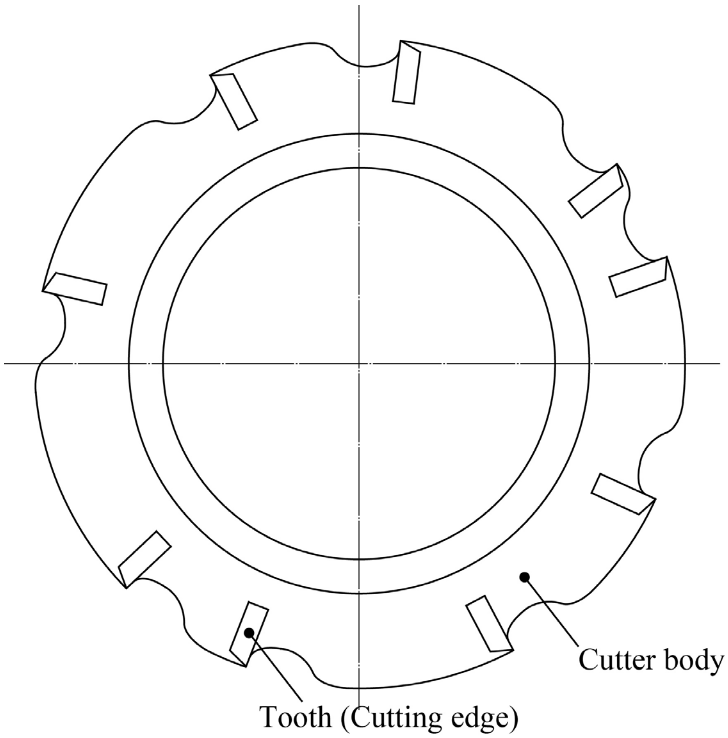

Fig. 2.5 Example of face milling cutter of irregular tooth pitch type (by Sisson)

As reported elsewhere, Slavíček (1966), Opitz et al (1967) and Sisson (1969) investigated the milling cutter of irregular tooth pitch type, and Vanherk (1968) and Stone (1970) investigated the milling cutter with differing helix angle in the past. Of these, Sisson investigated such a milling cutter shown in Fig. 2.5 and suggested that the chatter can be suppressed when the succeeding cutting edge is shifted (1/4) λ (λ: wave length of chatter mark). Importantly, Sisson suggested already on that occasion that the irregular tooth allocation could first facilitate the relaxation of the impact load caused by the engagement of cutting tooth.

It is extremely notable that we clarified already the essential differing effects of the irregular tooth pitch type from those with the differing helix angle in the 1960s. In short, the former is effective within limited spindle speed range as will be shown in Fig. 2. 10. In contrast, the latter is very effective across the whole lower spindle speed range. These characteristic features maintain even now as exemplified by the merchandized product as will be shown in Fig. 2.6 and in that of Denkena et al (2010). We must thus credit these outstanding theoretical analyses and experiments to the forerunning researchers, for example, Opitz et al and Stone. Eventually, we must reinvestigate why the theories established by Opitz et al and Stone are applicable to the machining conditions with the higher-spindle speed at present, which is far beyond expectation of the researcher in the era of 1960s.

Figure 2.6 shows first the merchandized end mill of irregular tooth pitch type and with differing helix angle, and then the marked effect of the differing helix angle type on the critical depth of cut. At present, both types are applied furthermore to (1) the band and metal saws, (2) hole saw, (3) side milling cutter, and (4) broach in practice.

In the academia, Denkena et al (2010) investigated the critical depth of cut

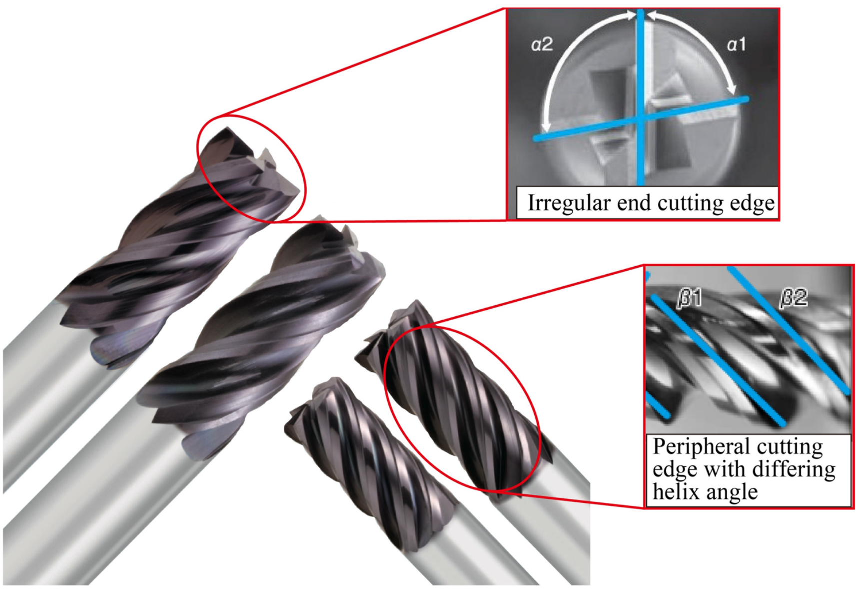

(a) Schematic view of cutting edge

Diameter (mm)	10
Number of cutting edges	4
Tool material	Micro-grain sintered carbide with TiAlN coating
Machining type	Slotting
Feed per tooth	0.05 mm/tooth
Helix angles	36/39 deg.
Coolant	Water soluble (5 %)
Work material	Ti-6Al-4V
Machine tool	Vertical MC (BT 40)

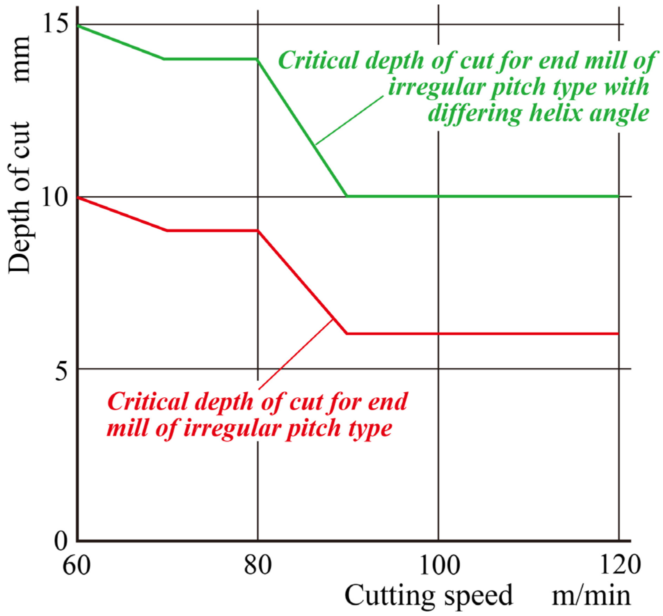

(b) Increase of critical depth of cut by end mill with differing helix angle
Fig. 2.6 End mill with cutting edges of irregular pitch type and with differing helix angle (by courtesy of OSG, 2018)

of 3-flute end mill, which is of irregular tooth pitch along the flute, and with nicked cutting edge (serration type), but the constant lead angle, while machining the monolithic complex component for the aircraft made of Al alloy [1]. In due course, such an end mill improves considerably its anti-chatter capability as shown in Fig. 2.7. In fact, the chip removal volume per unit time is up to 8.85 l/min at 27,000 rev/min in main spindle rotational speed, which is around 50 % larger than that removed by the conventional end mill. Importantly, Denkena et al suggested that the nicked cutting edge contributes furthermore the reduction of the depth of cut, resulting in the superimposing effect on the chatter suppression. Of special note, we can observe the remarkable anti-chatter capability at certain speed ranges only in Fig. 2.7. As already stated, this evidence can be reconfirmed the essential feature of the milling cutter of irregular tooth pitch type.

As a matter of course, we can find another trial in this field, and Fig. 2.8

[1] The research was carried out in corporation with Heller, MAG, Waldrich Coburg and Walter.

reproduces a patented idea (US 2005/0084341 A1, 2005), which can be

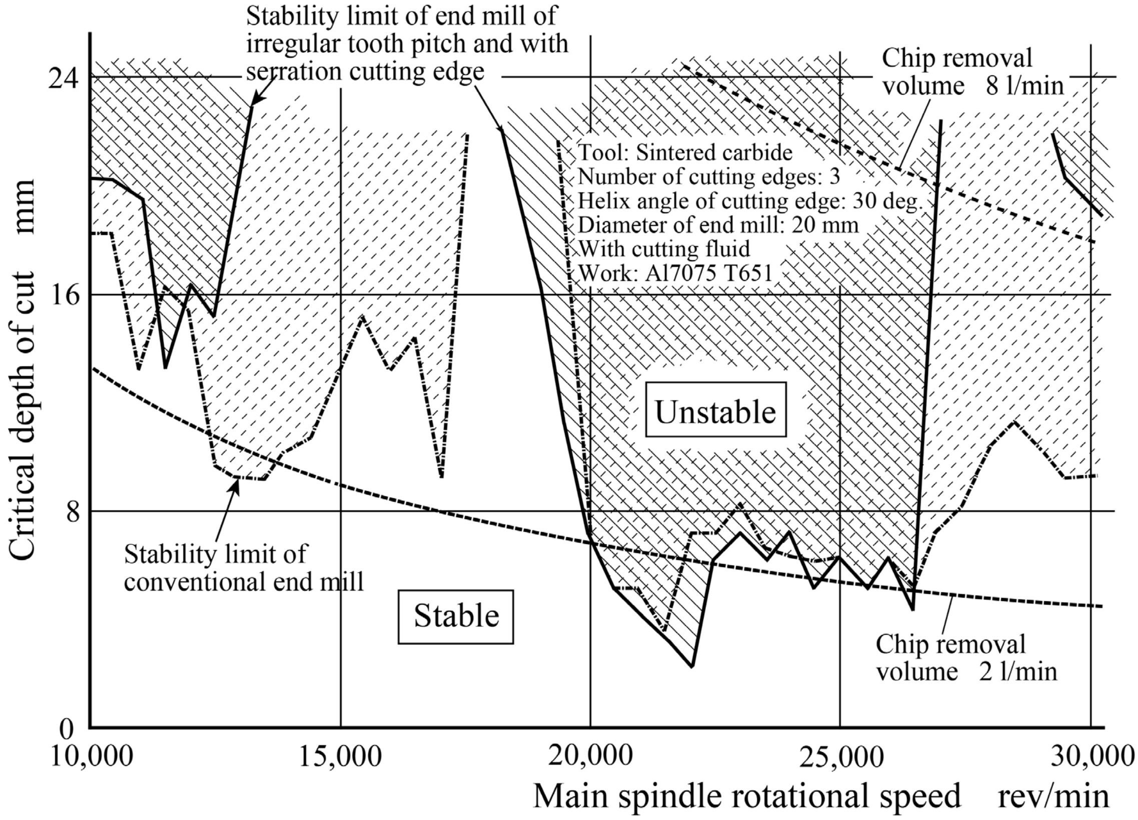

Note: To avoid complexity, origainal illustarion is simplified

Fig. 2.7 Anti-chatter capability of end mill of irregular tooth pitch type and with serrated cutting edge while slotting (by courtesy of Denkena)

characterized by integrating either two or three spacing irregularities within a whole cutter body. More specifically, three irregularities are as follows.

(1) In the first irregularity, the columns of pockets typically associated with flutes are staggered circumferentially, and in preferable case, the cutter body has three flutes with different dividing angles.
(2) In the second irregularity, at least, some pockets are arranged at different radial rake angles.
(3) In the third irregularity, at least, some pockets are arranged at different axial rake angles.

In consideration of the better applicability of the milling cutter of “Time Delay Control” type to the practice even now as mentioned above, we will note quickly its theoretical background and concerns based on those of

Opitz et al and Stone in the following.

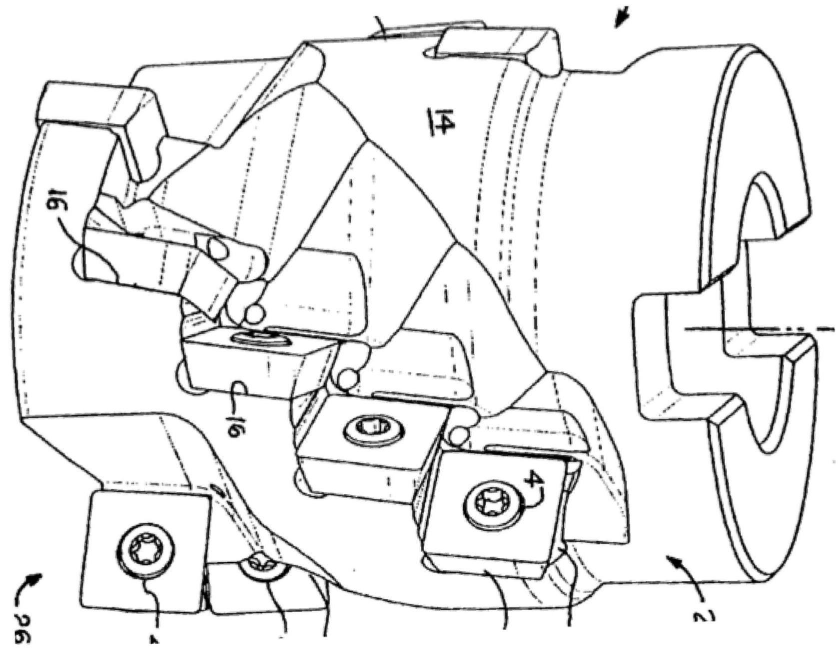

Fig. 2.8 A further development of milling cutter of irregular tooth pitch type (US Patent, US 2005/0084341 A1, 2005)

2.1.1 Milling Cutter of Irregular Tooth Pitch Type

Opitz et al (1967) aimed at the analysis of face milling and employed a mathematical model shown in Fig. 2.9, where the cutter has a couple of the different teeth pitches, and both the trajectories (*Trochoidal curves*) of teeth are replaced by the concentric double circles for simplicity. More specifically, such an irregular tooth pitch can facilitate the relaxation for the superimposing effect of the cutting force by the succeeding tooth as already mentioned. Obviously, such a phase shift in cutting force is effective to suppress the chatter.

By modifying the three basic expressions in the case of turning to be compatible with milling, the cutting force F_x for instantaneous uncut chip thickness u(t) can be written as

$$F_x = - k_1 [(R_1 + R_2)\, x(t) - R_1\, x(t - aT) - R_2\, x(t - bT)] \text{ ------(2.1)}$$

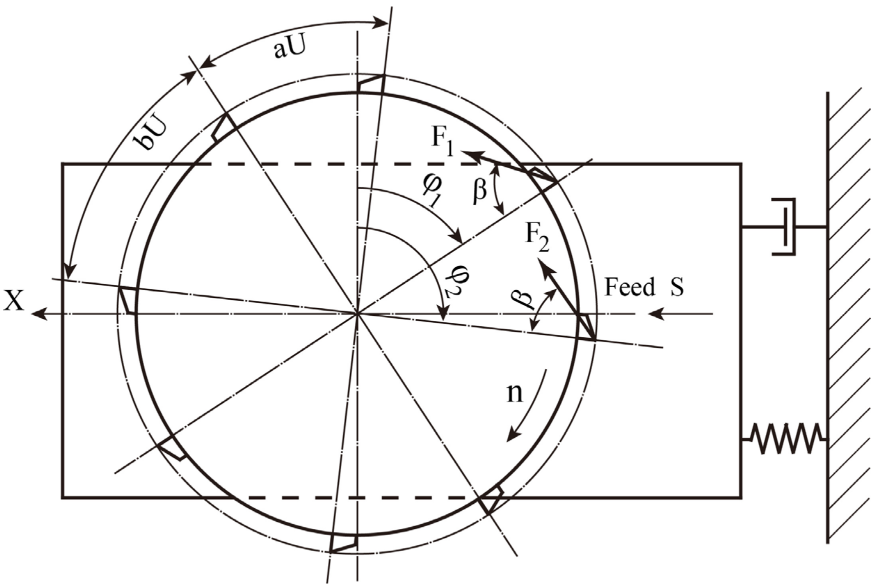

Fig. 2.9 Mathematical model for face milling cutter of irregular tooth pitch type (by Opitz et al)

$$\left.\begin{aligned} R_1 &= \sum_i \sin(\varphi_i - \varepsilon)\sin(\varphi_i - \varepsilon + \beta) \\ R_2 &= \sum_i \sin(\varphi_{i+1} - \varepsilon)\sin(\varphi_{i+1} - \varepsilon + \beta) \end{aligned}\right\} \text{------(2.2)}$$

where, k_1: Specific cutting force,

$x(t)$: Vibration amplitude of work at time t,

T: Time for one revolution,

U: Circular length of cutting teeth,

z: Total number of cutting teeth,

ε: Angle between leading direction of vibration and feed direction, and in case of Fig. 2.9, $\varepsilon = 0$.

i = 1, 3, 5---z-1.

By substituting the cutting force into the structural equation, and carrying out the discrimination of the chatter onset, the stability charts are duly produced as shown, for example, in Fig. 2.10 (because of difficulties in the analytical calculation, they used the analog computer). In Fig. 2.10, experimental values are not plotted for the simplification and it is noticeable that Opitz et al asserted that the theoretical stability limit is in good agreement with that obtained by the experiment.

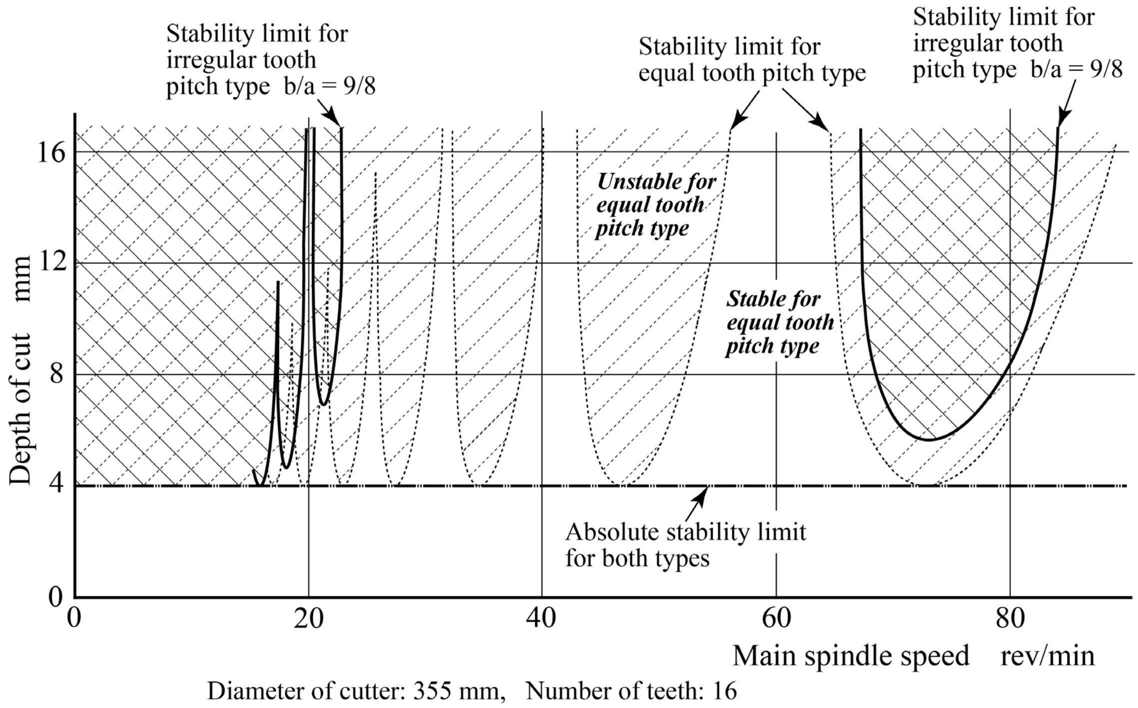

Fig. 2.10 Effects of face milling cutter of irregular tooth pitch type
(by Opitz et al)

Importantly, the stability limit increases considerably by employing the face mill of irregular tooth pitch type, provided that the speed range is limited between 20 and 70 rev/min as can be seen from Fig. 2.10. In addition, it is interesting that the absolute stability limits are equal in both the face milling cutters.

After conducting a series of investigations, they provided us duly with the simplified formula to select the preferable pitch ratio as follows.

$$\frac{b}{a} = \frac{240(f_0/z) + n}{240(f_0/z) - n} \quad \text{------}(2.3)$$

where, f_0 (cps) and n (rev/min) are the natural frequency of system and main spindle speed, respectively.

In short, they suggested that the limitation of the milling cutter of irregular tooth pitch type depends upon the natural frequency of the system.

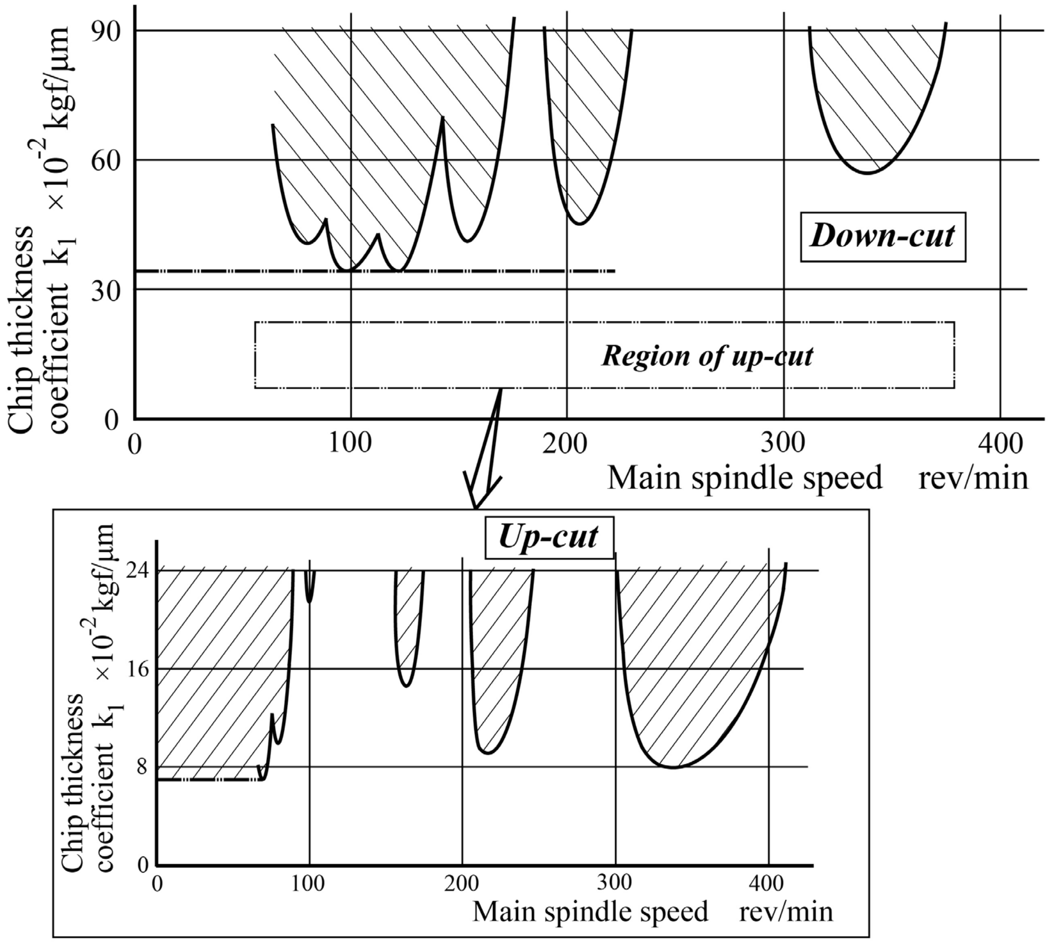

Note: Modified original drawing by Opitz et al

Fig. 2.11 Differences in stability charts depending upon cutting modes
- In face milling with cutter of irregular tooth pitch type

Importantly, they investigated furthermore the difference of the stability charts between for up-cut milling and for down-cut milling from both the theoretical and experimental aspects. Fig. 2.11 reproduces the theoretical comparison, where the evaluation index of the chatter onset is the "Chip Thickness Coefficient k_1". In the experiment, the evaluation index is the width of cut; however, both the stability charts are qualitatively in good agreement, and thus it is very interesting that the stability limit for down-cut milling increases drastically as compared with that for up-cut milling, although the shock load is considerably large in down-cut milling. This interesting behavior is caused by the differing relationships among φ, ε and β in Eq. (2.2) while either down-cut milling or up-cut milling.

2.1.2 Milling Cutter with Differing Helix Angle

This milling cutter was first developed to improve the shortcoming in the face mill of irregular tooth pitch type and aimed at the application to the circular (cylindrical, plain, or slab) mill. Thus, this cutter seems as to increase the number of the adjacency teeth up to infinity and also vary the tooth pitch continuously along the cutting edge (flute).

Stone (1970 a and b) employed the mathematical model, which is a developed plan view of cutter with successive teeth at different approach angles, as shown in Fig. 2.12. Of course, he applied his theory to broaching and obtained the fruitful result.

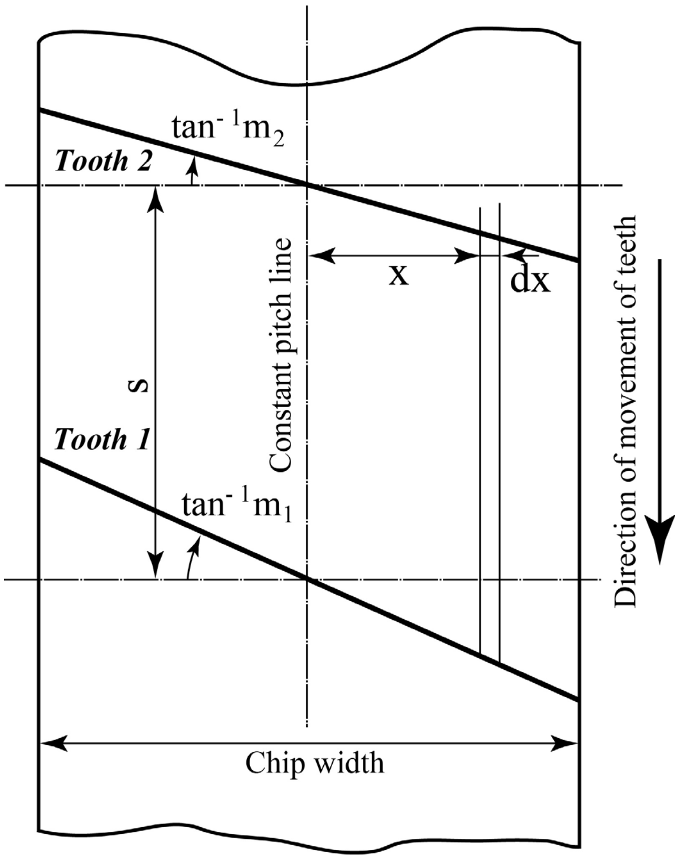

Fig. 2.12 Developed plan view of cylindrical milling cutter with differing helix angle (by Stone)

When assuming the original point of x axis at the constant pitch line, and considering an element of width dx at distance x, the cutting force dP acting on the element dx yields to

$$dP = - K[y_0 \sin\omega t - y_0 \sin\omega t(t-\tau)]dx \text{ ------(2.4)}$$

where, k = Specific cutting force

y_0 = Vibration amplitude

ω = Frequency of vibration

t = Time variable

τ = Time interval between successive teeth

Obviously, the second term in Eq. (2.4) expresses the regenerative effect. Then, in consideration of the time interval for one revolution of the cutter T, $\tau = T/z$ on the constant pitch line, where z is the total number of teeth on circular cutter.

Thus, τ at x can be written as

$$\tau = (T/z)\{[(m_1 - m_2)x + s]/s\} \text{ ------(2.5)}$$

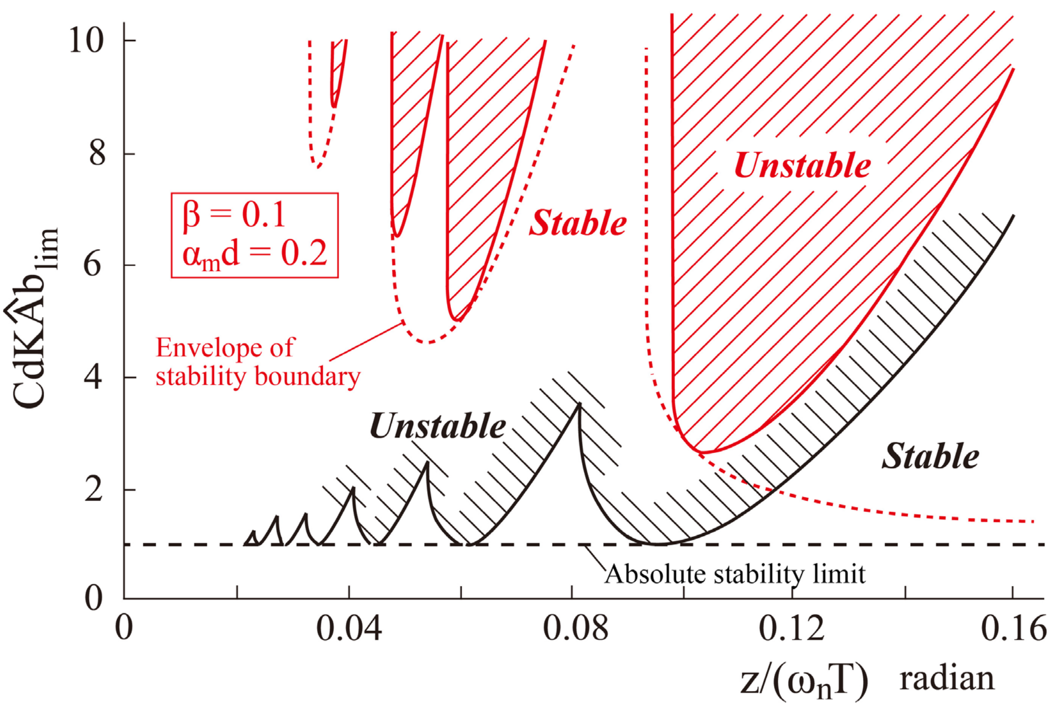

Fig. 2.13 Stability charts for circular milling cutters without and with differing helix angle (by Stone)

In short, we can control continuously the regenerative effect along the whole cutting edge by the difference between m_1 and m_2. In short, the characteristic index $\alpha_m d$ is given by

$$\alpha_m = [(1/m_1 - 1/m_2)m]/(2s) \text{ -------(2.6)}$$

where, d = Length of arc of cut

$\tan^{-1}m$ = Mean helix angle

As can be readily seen, we can substitute Eq. (2.4) into the structural equation, and duly obtain the stability chart, in which the vertical and horizontal axes indicate the indexes equivalent to the limit width of cut and main spindle speed, respectively. Fig. 2.13 shows the extreme effectiveness of the circular milling cutter with differing helix angle on the chatter suppression, where β is “Damping Ratio”.

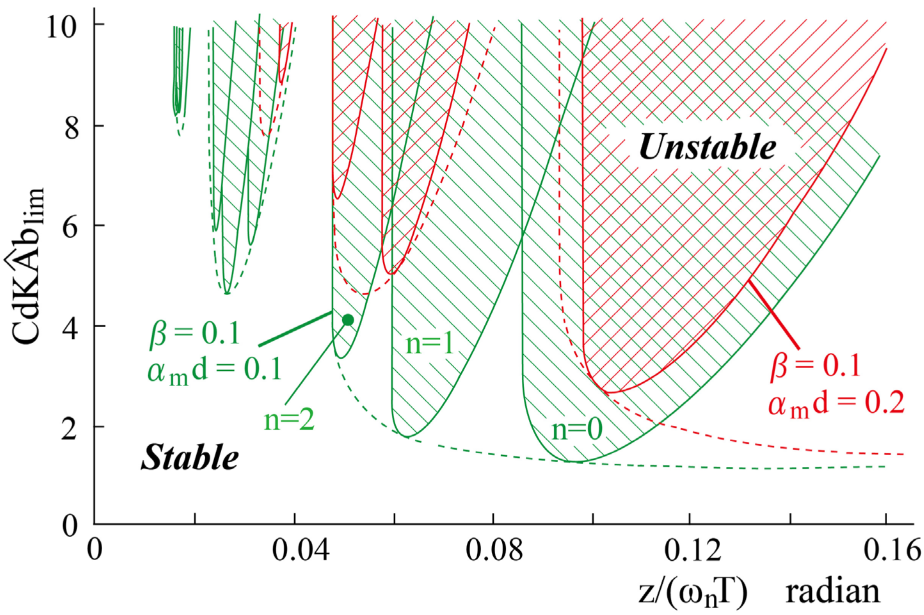

C: Constant relating width of cut and mean number of teeth in contact

d: Length of arc of cut

K: Coefficient relating cutting force to chip cross section

Â: Maximum amplitude of response to unit force

b_{lim} : Limiting workpiece width

z: Total number of teeth on circular cutter

T: Time interval for one revolution of cutter

ω_n: Natural frequency of simple system = $\sqrt{k/M}$

Fig. 2.14 Stability charts for milling with successive teeth at different angles (by Stone)

More specifically, the milling cutter with differing helix angle shows larger stability limit in the lower spindle speed range than that in the higher spindle speed range, which seems the lower-speed stability-like behavior, and which differs absolutely from that for the milling cutter of irregular tooth pitch type. In due course, we can benefit considerably in practice, and as a result, the end mill with differing helix angle has been mushroomed as already shown in Fig. 2.6.

Figure 2.14 shows the effect of characteristic index $\alpha_m d$, and as expected the stability chart depends upon it to a large extent. Importantly, Stone conducted a series of experiments to clarify the effect of the helix angle on the limit width of cut by using the tapered testpiece as shown in Fig. 2.15 and suggested some valuable design data as follows (in case of 122 rev/min, data are not shown).

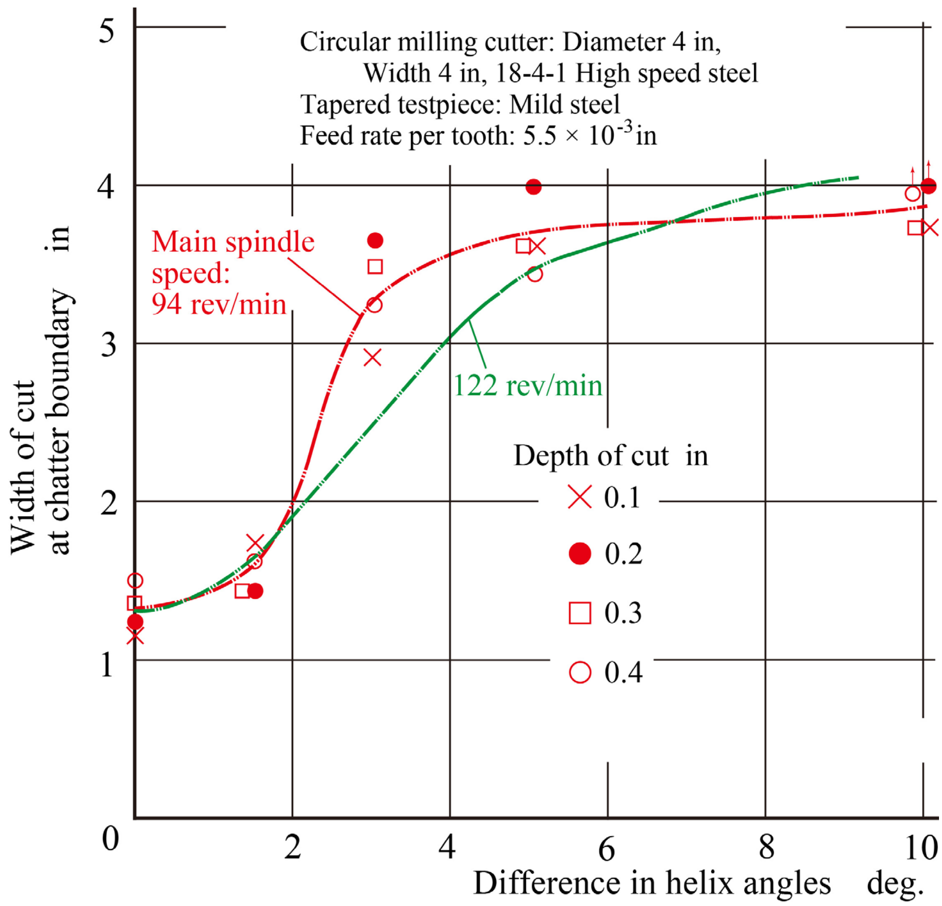

Fig. 2.15 Widths of cut at stability boundary for various differences in helix angle (by Stone)

(1) The chatter suppression capability increases with the helix angle, and it is extremely improved when the helix angles are between 2 ~ 4 deg.
(2) Similar chatter suppression effect can be obtained when the helix angle varies continuously within a tooth [2].

To this end, it emphasizes that Opitz et al and Stone proposed the valuable theories for the milling cutter of irregular tooth pitch type and with differing helix angle, respectively, and their validities have been verified by a considerable number of the merchandized milling cutters. In this context, we must reinvestigate to what extent in the main spindle speed those of Opitz et al and Stone are applicable at present.

2.2 A New Horizon - Integrating Damping Entities within Machine Bodies, Machine Elements, Attachments and Tools

With prevailing the machining function-integrated kind like "Mill-turn", both the modular-designed chuck and the cutting tool become gradually popular. In the sphere of machine tool joint, it is common knowledge that the jointed body shows higher damping capacity, but lower rigidity as compared with those in the monolithic body component.

Typically, we may expect the preferable capability of chatter suppression in modular tooling, in which the cutting-edge module is jointed with the tool shank module by the thread of buttress type as shown, for example, in Fig. 2.16. The buttress thread has a saw tooth-like shape, and thus ease of tightening, but hard for loosening. It emphasizes again that the joint placed closer to the cutting point can facilitate the suppression of the chatter mark with the higher frequency (see Fig. 2.2). Of course, we cannot expect the higher damping capacity when the joint is in the node of the vibration mode.

As will be clear from the above, it is preferable to suppress the chatter

---

[2] $\beta = h/k$, where h is "Hysteretic Damping Coefficient" showing the viscous damping-like effect when its magnitude is small, and k is "Spring Stiffness".

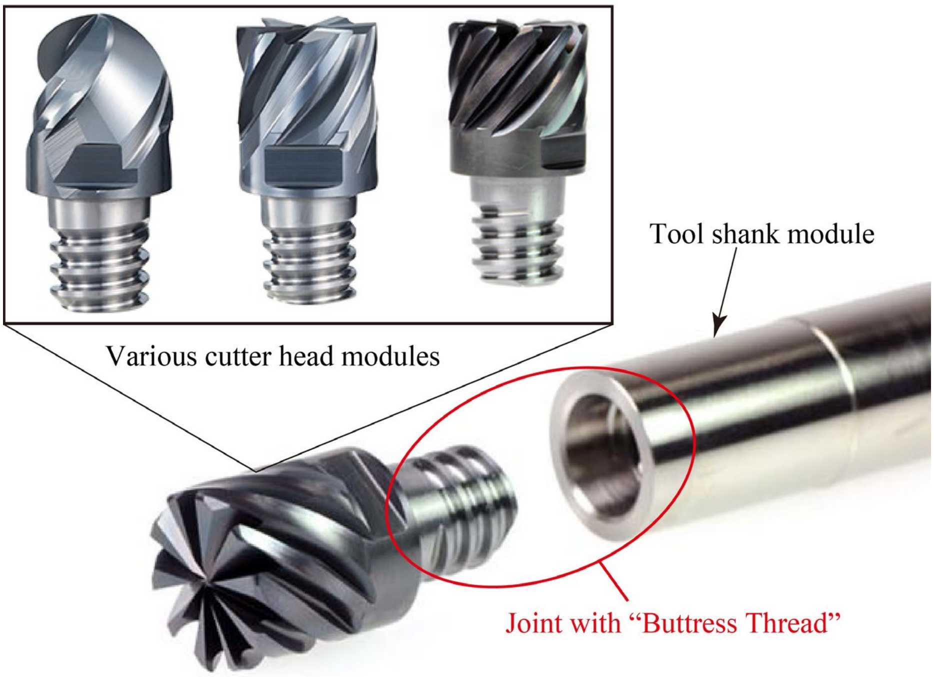

Fig. 2.16 End mill of modular tooling system (Type PXM, by courtesy of OSG, 2018)

without using the additional device like the damper. Conceptually, we must develop an innovative remedy either capable of integrating within the machine body, attachment and tool compactly, or by contriving the structural constitution of the machine body itself. In fact, the modular tool is one of the representatives of the former, and regarding the latter, for example, Watanabe and Sato (1988) clarified the effects of the fitting tolerance in the bearing, i.e. non-linearity in the spring constant, on the dynamic characteristics of the main spindle. More specifically, they employed NLBBA (Nonlinear Building Block Approach) to obtain the frequency response of the main spindle. Importantly, we can see the considerably large real number in the loci of the spindle compliance on the complex plane, when the exciting force and bearing clearance are 25 N and 1.0 μm, respectively. Conceptually, the bearing clearance is large in this case from the viewpoint of the structural design; however, that of Watanabe and Sato suggests the importance for the positive use of the non-linearity in the structural design to suppress the chatter.

As will be clear from the above, it is desirable that the structural body component itself is either with higher damping capacity together with acceptable rigidity, or integrates compactly the higher damping element. It is however regrettable that we have not had such engineering design data, apart from a very few reports. In fact, we have not measured the damping capacity of the main bearing while rotating since 1980, because of extreme difficulty in the measurement of the damping capacity (for detail, refer to Chapter 8 of Ito, 2008).

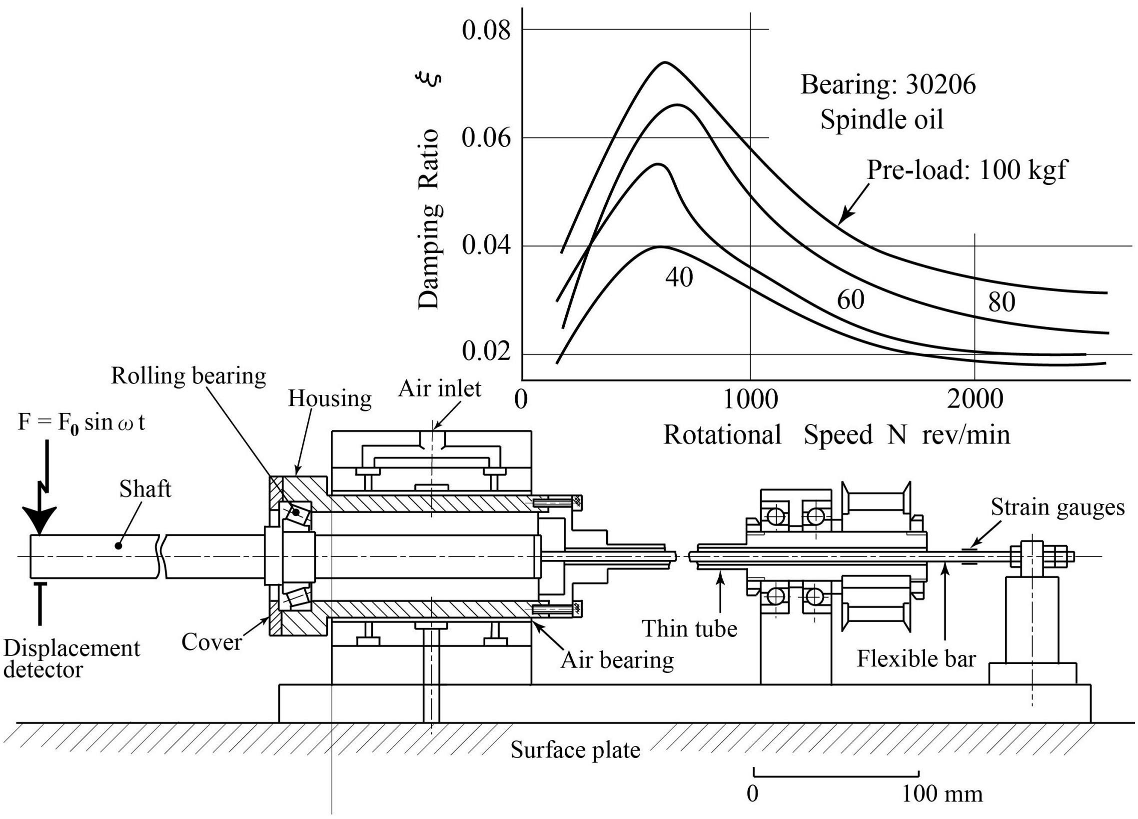

Fig. 2.17 Experimental set-up to measure damping of bearing while rotating (by courtesy of Tsutsumi)

Figure 2.17 reproduces the well-contrived test rig and some damping ratios for the tapered roller bearing while rotating the outer ring, which were measured from the magnification factor in second vibration mode (Tsutsumi et al, 1980). Importantly, damping of the tapered roller bearing is in strong dependence upon the pre-load and rotational speed,

simultaneously showing the maximum value at certain rotational speed.
It is notable that the measurement of the damping capacity is very difficult work as exemplified the test rig shown already in Fig. 2.17. To carry out the accurate measurement, Tsutsumi et al were very keen to eliminate the disturbance from the driving system and to avoid the unfavorable disturbance from surroundings. In fact, the shaft is fixed using a flexible bar, the bearing housing is supported by the air bearing to minimize the influence of damping of surroundings, and the housing is driven by the motor through the gear-toothed belt and thin tube. In addition, the bearing and its surroundings are cooled by the air and oil bath lubrication, so that the temperature of the shaft-bearing system is to be in constant.

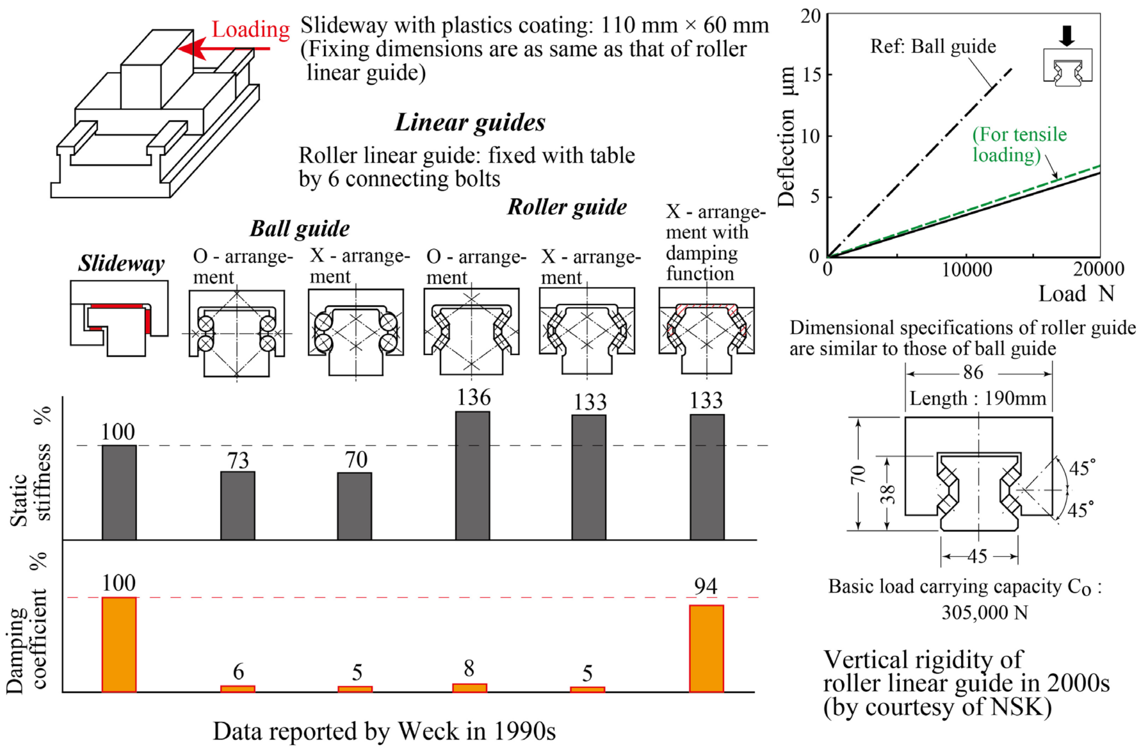

Fig. 2.18 Examples of engineering data of linear guide (by Weck and NSK)

It is furthermore notable that TH (Technische Hochschule) Aachen (Weck, 1993) and NSK publicized some valuable data for the linear guide as shown in Fig. 2.18. At present, the linear guide is a core machine element for the conventional TC and MC, which have prevailed across the whole world market. Importantly, the machine tool joint shows, in general, non-linear characteristic, apart from that under the lower interface pressure. It is thus very interesting that the linear guide of NSK-brand shows the linear relation between the applied load and the deflection [3].

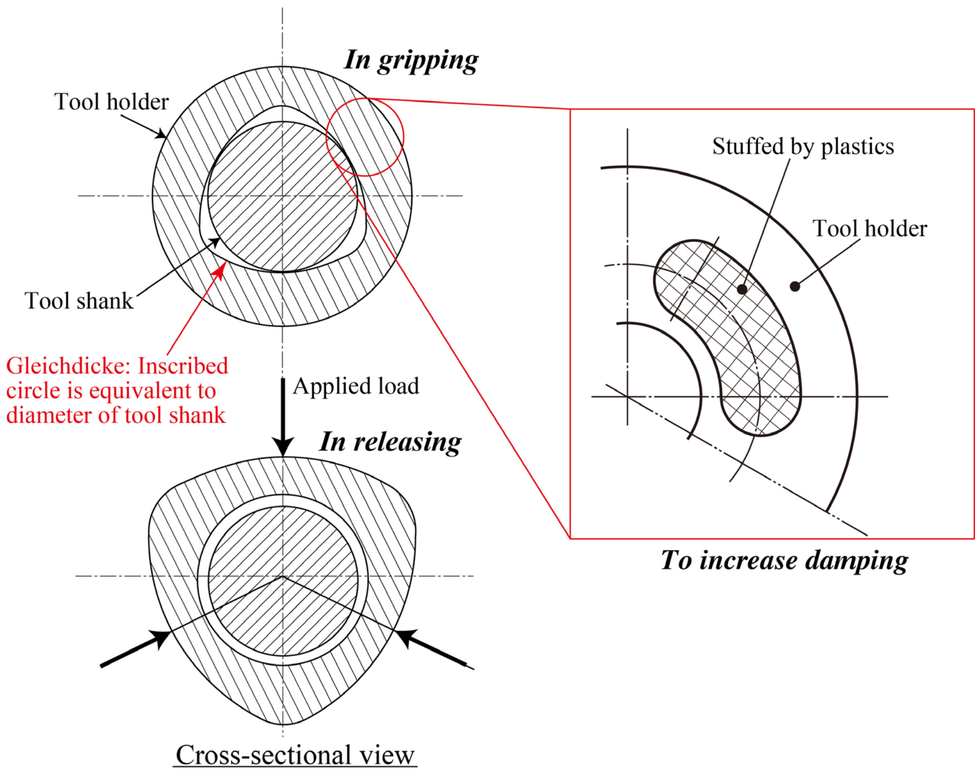

Fig. 2.19 Damping tool holder of "Gleichdicke" type called TRIBOS, 2001 (by courtesy of Schunk)

Figure 2.19 shows a tool holder with higher damping capacity by stuffing plastics within the tool holder without excessing holder's dimension. The same idea was also applied to the hollow ball screw by THK around 2005. In fact, the free decay vibration continues up to 1 sec. in the case of the conventional ball screw, whereas the hollow ball screw stuffed damping material can decay the vibration within 0.25 sec., while rotating with 3,000 rev/min

[3] Professor Weck publicized these data in 1993 in part; however, the detail is not publicized as yet, because of company's confidentiality in accordance with the message from Dipl.-Ing. Brockmann in 2013. Refer to the following dissertation. Müni Hakan Ispaylar. (1996) Betriebseigenschaften von Profil-Wälzfürungen. Compu TEAM, Würzburg.

To this end, we must be aware again that a crucial shortage in the engineering data is the rigidity and damping capacity of the rolling bearing while rotating more than 2,000 rev/min.

2.3 Elastic Grinding Wheel and Others

Within the context of chatter suppression in metal grinding, we may talk a similar story to that in metal cutting. Typically, we must reinvestigate the validity for using the term "Forced Chatter" caused by, for example, the unbalance of the grinding wheel, which is not a due exciting source inhabiting within the grinding mechanism.

Obviously, we may have various ideas for the remedy of the regenerative chatter suppression from the block diagram of chatter loop. For example, there are two typical remedies: one is to control the regenerative effect, e.g. variable rotational speed in either work or grinding wheel, and the other is to decrease the contact stiffness of the grinding wheel, e.g. elastic grinding wheel.

In the former, the variation rate should be at least ± 10% of the grinding wheel speed in constant, and thus this remedy is only applicable to rough grinding as reported elsewhere. Regarding the latter, Inasaki et al (2001) introduced an idea proposed by Bzymek et al in 1994, in which both the sides of wheel body can be facilitated by a considerable number of the holes and grooves with various shapes. Although aiming at the reduction of the thermal deformation, Naxos Union once developed a grinding wheel with a considerable number of the grooves placed radially at both the wheel side faces as shown in Fig. 2.20 (beginning of 1980s). In accordance with the Editor's experience, such a grinding wheel is very noisy by wind shearing.

Within the systematic contrivance for the chatter suppression, Folkerts (1993) proposed a notable guide as shown in Fig. 2.21, which can be obtained from the frequency response analysis for the cylindrical grinding machine while plunge grinding.

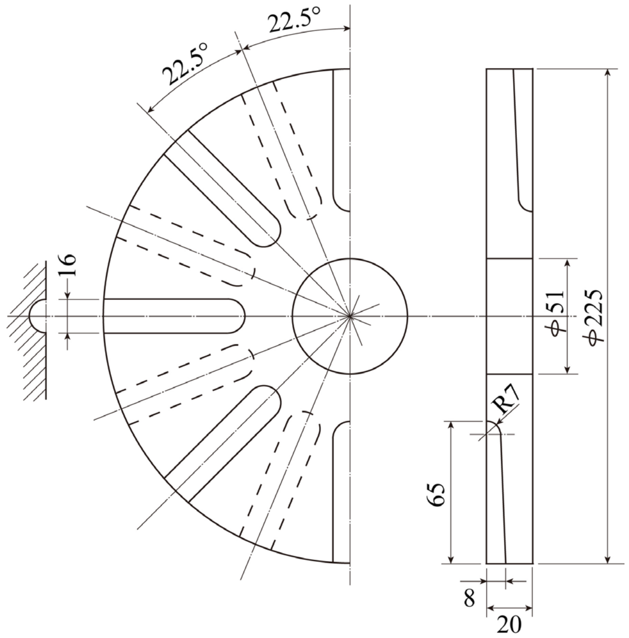

Fig. 2.20 Special-purpose grinding wheel developed by Naxos Union

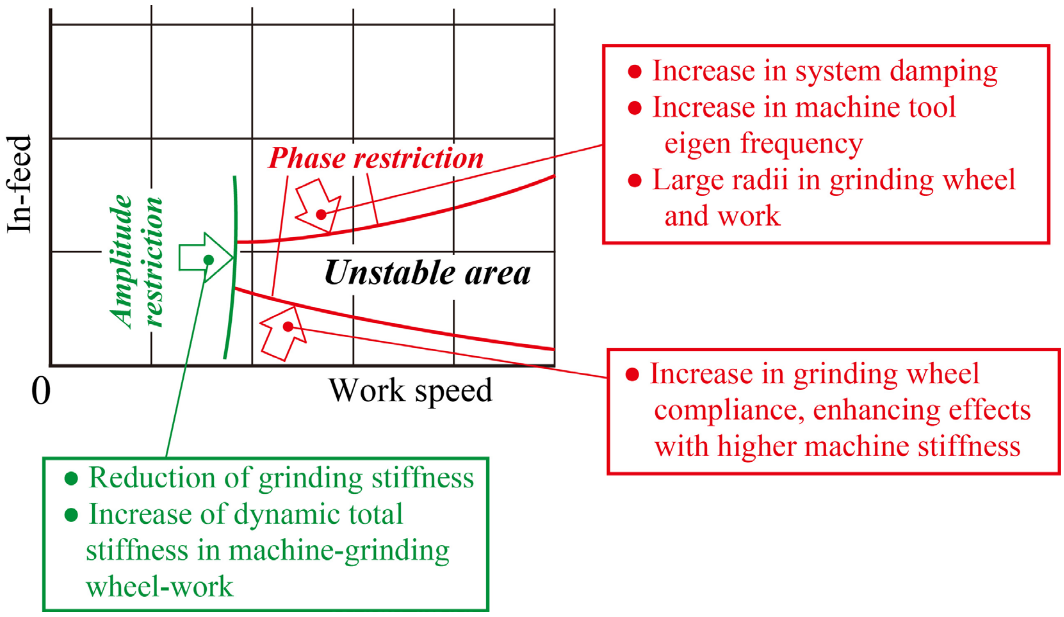

Fig. 2.21 First-hand view of remedies to increase grinding stability (by Folkerts)

More specifically, Folkerts eyes the compliance and phase shift in the frequency response and suggests that the unstable conditions can be determined by the three stability restriction curves, i.e. vertical amplitude restriction, upper and lower phase restriction curves, resulting in the "Stability Field". Importantly, Folkerts summarizes systematically each remedy so far known by using the stability field as shown also in Fig. 2.21. Within those shown in Fig. 2.21, it is very interesting that the chatter can be suppressed by employing the larger work diameter, and importantly, this remedy implies similar effects to that proposed by Entwistle and Stone (2013). Accidentally, they suggested that the torsional vibration of the work could result in the improvement of the chatter stability.

Although the idea of stability field is very valuable, the stability field depends upon (1) the grinding machine, (2) grinding condition, and (3) grinding wheel to a large extent, and thus obviously it is very difficult to select a suitable remedy in accordance with each grinding requirement.

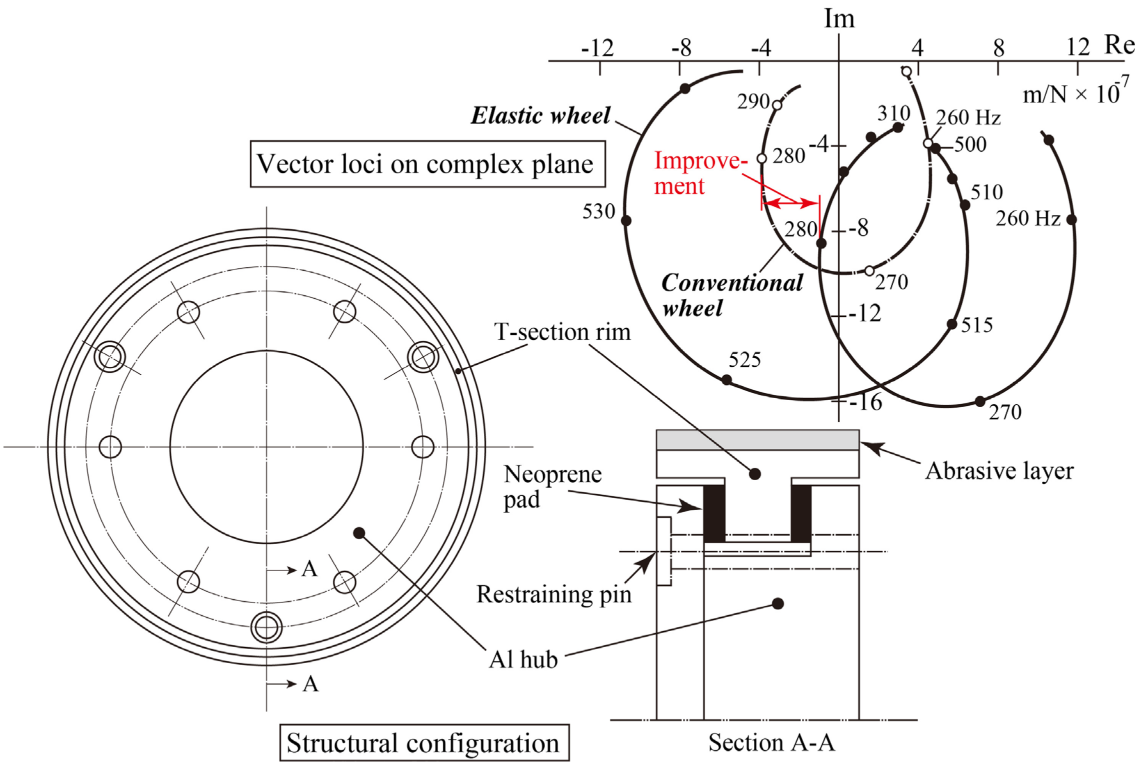

Fig. 2.22 A cBN elastic grinding wheel and its vector locus on complex plane (by Sexton et al)

Having in mind such difficulties, it is recommendable to develop furthermore the elastic grinding wheel in consideration of the success story for the milling cutter of irregular tooth pitch type and with differing helix angle. Fig. 2.22 reproduces thus a cBN elastic grinding wheel proposed by Sexton et al. (1982). Of note, this grinding wheel is for cylindrical grinding of hardened CrMo steel (EN 31 as per BS), can be characterized by fixing the T-section rim with abrasive layer through 40 pads made of neoprene, and in due course shows fruitful results.

More specifically, the control of the contact stiffness is equivalent to the "Shift of Harmonic Locus" on the complex plane, and as shown also in Fig. 2.22, we can credit such an effect clearly. Conceptually, the design principle of this elastic grinding wheel is as same as that of single-point cutting tool of gooseneck type. Importantly, Sexton et al. (1981) tried beforehand a cBN elastic grinding wheel for HSS (High Speed Steel) work by the surface grinder, the hub of which was made of Ni porous material together with realizing about 1.4×10^6 N/m per mm in radial rigidity.

References

Denkena B, de Leon L, Grove T. (2010) *Prozessstabilität eines kordelierten Schaftfräsers*. ZwF; 105-1/2: 37- 41.

Entwistle R, Stone B. (2013) *Position Paper - Fundamental Issues in Self-excited Chatter in Grinding*. Jour. of Machine Eng.; 13-3: 26-50.

Folkerts W. (1993) *Dynamische Prozeßkennwerte des Schleifens und deren Einfluß auf das Prozeßverhalten*. Dr. Thesis, RWTH Aachen.

Inasaki I, et al. (2001) *Grinding Chatter - Origin and Suppression*. Annals of CIRP; 50-2: 515-534.

Ito Y. (2008) *Chapter 8 Design Guides, Practices, and Firsthand View of Engineering Developments - Sliding Joints*. In: Modular Design for Machine Tools, McGraw Hill.

Opitz H, et al. (1967) *Improvement of the Dynamic Stability of the Milling Process by Irregular Tooth Pitch*. Proc. of 7th Inter MTDR Conf. p.

213-227, Pergamon Press.
Sexton J S, Stone B J. (1981) *The Development of an Ultrahard Abrasive Grinding Wheel Which Suppresses Chatter*. Annals of CIRP; 30-1: 215-218.
Sexton J S, Howes T D, Stone B J. (1982) *The Use of Increased Wheel Flexibility to Improve Chatter Performance in Grinding*. IMechE Proceedings; 196-25: 291-300.
Sisson T R. (1969) ASTME Technical Paper. MR 69-245.
Slavíček J. (1966) In: Proc. of 6th Inter. MTDR Conf., p. 15, Pergamon.
Stone B J. (1970 a) *The Effect on the Chatter Behaviour of Machine Tools of Cutter with Different Helix Angles on Adjacent Teeth*. In: Proc. of 11th Inter. MTDR Conf., Vol. A; p. 169-180, Pergamon Press.
Stone B J. (1970 b) *The effect, on the regenerative chatter behaviour of machine tools, of cutters with different approach angles on adjacent teeth*. Research Report No. 34, The MTIRA (Distributed only for members).
Tsutsumi M, Nabeta N, Nishiwaki N. (1980) *Damping in Single-row Rolling Bearings*. In: Proc. of the 4th ICPE, p. 374-379, JSPE and JSTP, Tokyo.
Vanherck P. (1968) In: Proc. of 8th Inter. MTDR Conf., p. 947, Pergamon.
Watanabe K. Sato H. (1988) *Development of Nonlinear Building Block Approach*. Trans. of ASME, Jour. of Vibration, Acoustic Stress, and Reliability in Design; 110: 36-41.
Weck M. (1993) *Trends of Manufacturing Technology Looking Towards the 21st Century*. Industrial Technical Seminar, Kobe, May 19th.
Weinert K, Kersting M. (2005) *Konzeptionelle Entwicklung eines adaptiven Werkzeughalters*. ZwF; 100-6:352-354.

Chapter 3 Symptoms of Needs to Advanced Chatter Theory

Although carrying out the uncountable activities, even now the chatter is still at burning issue in the academia and industries as mentioned in Chapters 1 and 2. These evidences imply the capability limitation of the chatter theory, which is based on those of Tobias, Tlusty and Merritt, i.e. "*Traditional Chatter Theory*". In contrast, with the advance of the traditional chatter theory, experimental techniques, chatter suppression technology and engineering knowledge, we can have a considerable number of new findings and proposals, and furthermore conduct challenging trials such as shown in the "Headnotes in Part II".

In consideration of both the critical issues and the valuable findings so far obtained, we must pave the way to a new horizon in the chatter theory and concerns, i.e. "*Establishment of Advanced Chatter Theory*" and innovative technologies for the chatter suppression. In this context, there are the three leading driving factors, i.e. (1) reinvestigation of essential features of "*Forced Chatter Vibration*", (2) improvement for applicability of block diagram of chatter loop to higher rotational speed of main spindle, and (3) validity verification of self-excited chatter derived from "*Drooping Characteristics in Cutting Force*".

Thus, the Editor proposes first a new classification of the chatter and a modified block diagram of chatter loop in consideration of these driving factors. In short, the proposed classification can be characterized by disregarding the forced chatter vibration, which is not caused by the cutting mechanism itself and by incorporating the new vital factors with the increasing main spindle speed.

Following these proposals together with some quick notes, the Editor will then reveal something underpinning these proposals, and discuss duly the corresponding matters in three basic expressions for the chatter of regenerative type. Of special note, the Editor does not deal with the advanced chatter theory for metal grinding, because of not enough achievements available for such discussion as compared with those for metal cutting (see Section 1.3). Against this context, Professor Lee of Nihon University will first review in detail the past and present perspectives for the chatter in metal grinding and then suggest a handful of issues in Chapter 8. Such issues are related to the contact stiffness and damping of the grinding wheel and concerns, and necessary to paving the way to the establishment of the advance chatter theory for metal grinding.

3.1 A New Proposal for Classification of Chatter - Reinvestigation into Validity of "*Forced Chatter*"

In the classification of the chatter having been prevailed, there are two leading types, i.e. "*Forced Chatter*" and "*Self-excited Chatter*". Importantly, primary concern is the "*Regenerative Type*" within the self-excited chatter in practice. This classification is somewhat helpful to conduct R & D (Research and Engineering Development); however, we must now modify it in consideration of the fundamental definition, some new findings recently obtained and the changes in machining conditions, e.g. prevalence of heavy-duty machining per unit time by using higher-cutting speed.
In the modification, we must first recall the following definition of the self-excited chatter, which is based on our long-standing experience. More specifically, we know now that primary concern is the chatter of regenerative type; however, we cannot deny the occurrence of the other chatter, which is caused by the "*Drooping Characteristics in Cutting Force*". In addition, it is common sense that the forced vibration disappears completely by eliminating the external and internal excitation sources.

"The machine-attachment-tool-work system vibrates considerably even when not existing any internal and external excitation sources within the system".

Secondly, we must reconsider the validity of using the term, "Forced

Chatter", as will be discussed later. For example, it has been said that we can observe the "Saw Tooth-like Chip" in Ti alloy turning, which affects the stability limit, because of inducing a vibration with frequency close to the generated pitch of the saw teeth. Some researchers assert to include such chatter within the regenerative type and to call it "Material Property-related Type". Conceptually, the chip generation seems as one of the excitation sources; however, we cannot eliminate it in certain cases, because the chip generation is a part of cutting mechanism itself.

Thirdly, we must investigate the role of some new excitation sources, which are actualized within the machine-attachment-tool-work system with the advance of the higher-speed machining. For example, M. Doi et al (1982) reported already the differing behavior in chatter between the works held by the three-jaw scroll chuck and by the four-jaw independent chuck. In fact, the work holding stiffness of the three-jaw scroll chuck varies three times every one rotation of the main spindle, resulting in the directional orientation effect of the work stiffness. Consequently, such an influencing factor could act considerably with increasing the main spindle speed. Eventually, we must investigate the regenerative type in consideration of mingling the parametric vibration caused by such a directional orientation (see Section 1.1.3).

In consideration all the controversial points mentioned above, Fig.3.1 shows a new proposal for the classification of the chatter, and as can be readily seen, this classification may be characterized by regarding the forced excitation source as a disturbance in the self-excited chatter. We will thus discuss its characteristic features in the following, and obviously, these will give us some guides to advance and enhance the chatter theory.

With respect to a new classification for the chatter, we must furthermore continue the meticulous observation for the chatter mark and concerns to unveil the essential features in some uncertain chatter vibrations. In fact, we face much more unfavorable chatter, the mark of which is microscopic "Blur-like", in grinding even now. In addition, a machine tool manufacturer has an experience, in which the blur-like chatter mark or micro-beat-like chatter mark can be clearly observed while wet-machining Al alloy with 3-flute end mill, i.e. full side cutting mode and cutting speed being more than 11,000 rev/min. Although we have not verified the validities of these findings yet, some researchers already observed similar chatter in higher-speed machining of the Al alloy, and asserted that this chatter may be classified into the "*Friction-based Excitation Type*". In the friction-based excitation type, it is said that the chatter frequency is more than the order of kHz.

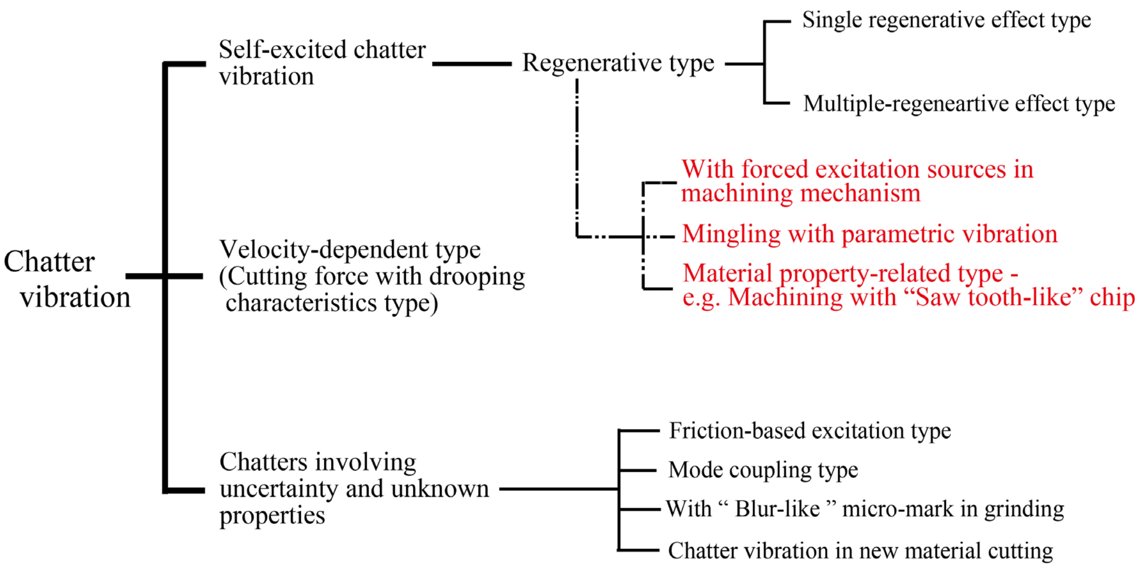

Fig. 3.1 A new proposal for classification of chatter

Although the forced chatter in the past sounds "Out-of-place" term, it is inevitable that the cutting mechanism itself includes often the excitation sources. Obviously, we cannot eliminate such sources, and thus now let us discuss the detail for the self-excited chatter with forced excitation.

In accordance with the definition so far used, the forced chatter involves those caused by, for example, the unbalance within the work, rotating tool and chuck, intermittent cutting and the meshing ratio of the driving gear system of the machine tool. Correctly, such a forced chatter should be regarded as one of the forced vibrations, because we can suppress easily it by eliminating the corresponding excitation source. In contrast, even when considering that the forced vibration decays rapidly, we must discuss a problem, where the excitation source inhabits within the cutting mechanism itself like shock loading in down-cut milling and saw-like chip generation in turning of Ti alloy. For example, the shock load acts frequently at the engagement of cutting tooth to the work in down-cut milling before decaying the previous forced vibration. Obviously, such excitation sources cannot eliminate, and thus we may guess its certain influences on the self-excited chatter.

With the growing importance of the higher-speed cutting for the aircraft component made of Al alloy, we can observe another excitation source, i.e. run-out (whirling) of end mill, which can be called the "*Excitation by Forced Deviation*". Even when we can set the rotating tool to the main spindle without run-out in the preparatory work, the rotating tool shows a considerable run-out, while running higher-speed. In due course, we face a

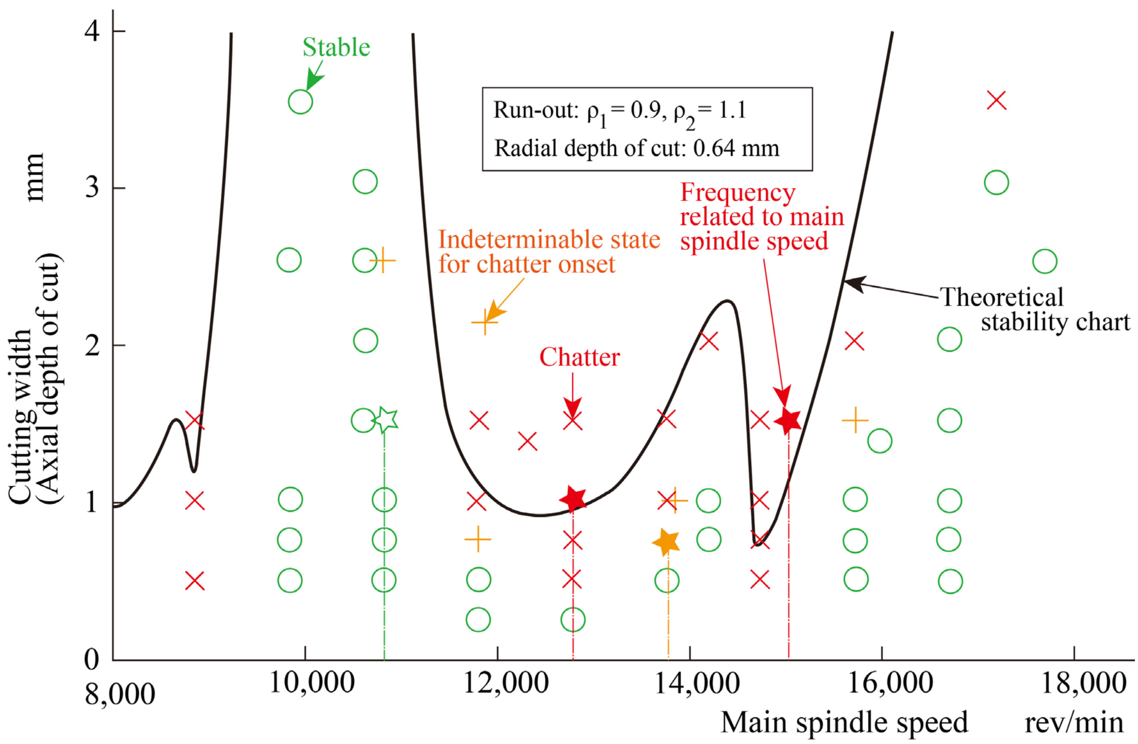

Fig. 3.2 Changes in stability chart by run-out of end mill while machining (by courtesy of Insperger, 2015)

new problem, i.e. influence of run-out caused by centrifugal force on

chatter stability, and thus we will scrutinize it in the following.
In this context, Insperger et al (2008) reported already an interesting behavior in down-cut milling of Al alloy with two-flute end mill (slot drill). They show a theoretical stability chart together with experimental values as shown in Fig. 3.2, where $\rho_1=\rho_2$ means no run-out, and $\rho_1=0.9$ and $\rho_2=1.1$ mean that the first edge cuts 10 % less than and the second edge cuts 10 % larger than those without run-out, respectively.
Importantly, Insperger et al reported that the stability limit does not depend upon the run-out, and that the experimental values are not in good agreement so much with theoretical ones, because of difficulty in correct estimation of the cutting stiffness. In contrast, we can observe an interesting behavior at 13,000 and 15,000 rev/min in the rotational speed of the main spindle. In short, the unstable state is amplified around these rotational speeds, and thus we may guess the implicit influence of the run-out on the stability limit.

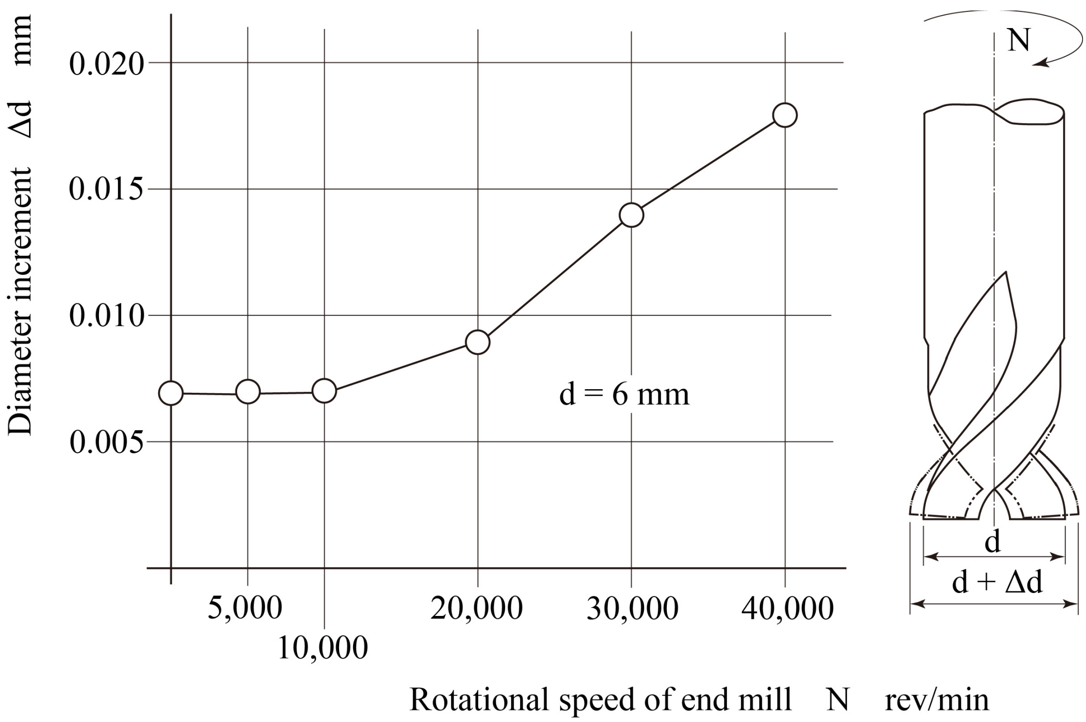

Fig. 3.3 Actual diameter of two-flute end mill while rotating higher-speed (by Rall et al., 1998)

In retrospect, Rall et al (1998) suggested already the change of the actual diameter of the end mill with the increase of the rotational speed as shown in Fig. 3.3. They conducted a research from viewpoint of the in-process measurement of the cutting tool. In addition, Opitz et al (1967) reported the differing effects on the chatter stability while up-cut and down-cut milling by the face mill with irregular pitch tooth type as already shown in Fig. 2.11. Importantly, they suggest that such an interesting behavior is caused by the milling mechanism itself, i.e. time-dependent direction coefficient, which can evaluate the influence of the cutting tooth position on the vibration direction (see Section 2.1).

To this end, it is thus worth suggesting that we must conduct a research into the influence of forced excitation, which is derived from the cutting mechanism itself, on the self-excited chatter.

3.2 A Proposal for "Modified Block Diagram of Chatter Loop"

Along with a proposal for the classification of the chatter, the Editor asserts the necessities to establish an advanced chatter theory. In fact, we can observe some further evidences to support such an assertion in addition to the symptoms, which necessitate the revision of the classification of the chatter.

Thus, Fig. 3.4 shows a new block diagram of chatter loop by modifying the traditional one. More specifically, the Editor indicates the corresponding modifications by the red letter, which include the (1) influences of the forced deviation and periodic excitation inhabiting the cutting mechanism, (2) estimation of the real dynamic specific cutting force, (3) reinvestigation into the dynamic compliance while machining with the higher rotational speed more than 2,000 rev/min, and (4) influence of the multiple-regenerative effect on the stability chart.

To deepen our understanding to such a modification, let us discuss herein the discrepancy between both the stability charts obtained theoretically and experimentally in the higher rotational speed as shown in Fig. 3.5. Van Dijk et al (2008) reported valuable results together with specifying neatly the

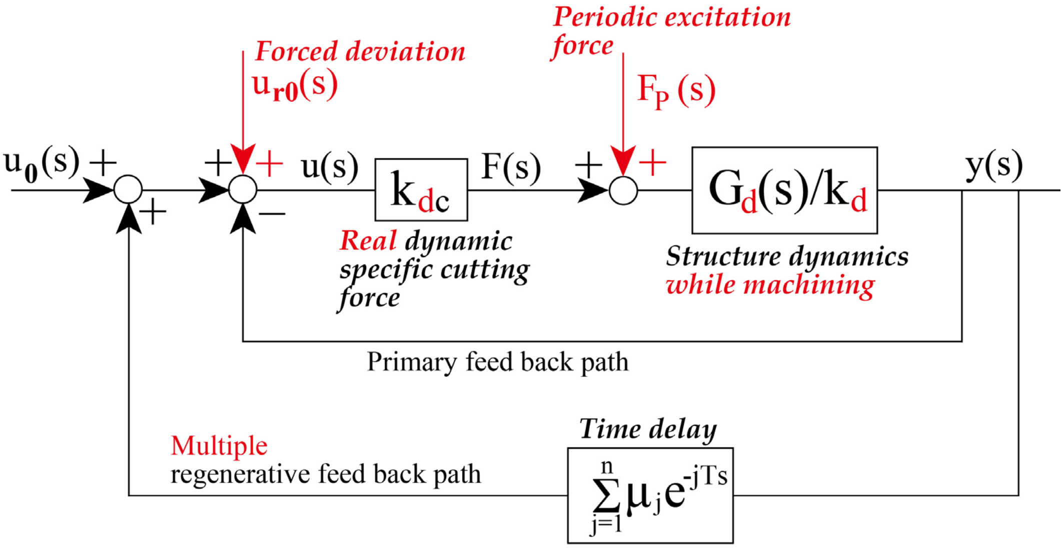

Fig. 3.4 A proposal for modified block diagram of chatter loop

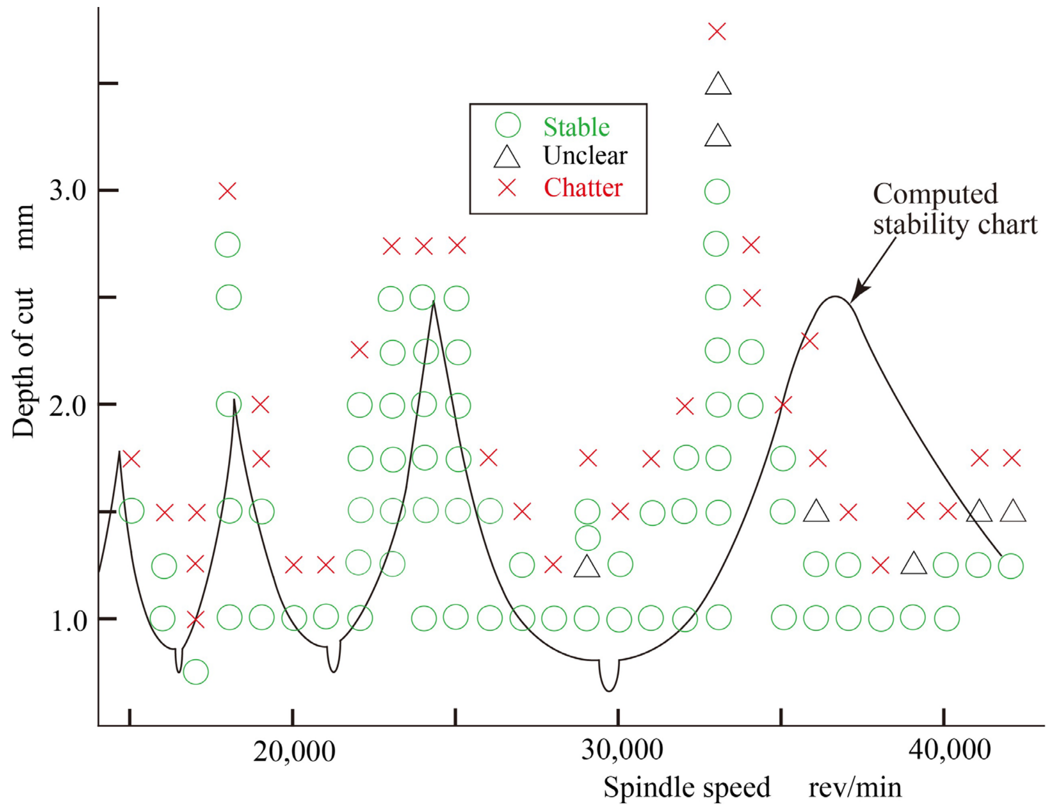

Fig. 3.5 Comparison between computed stability chart and experimental values (by van Dijk et al)

experimental conditions as follows.

The theoretical stability chart was computed for the milling machine of Mikron-brand (Type HSM700) with the two-flute end mill (10 mm in diameter and 57 mm in length), which was held by shrink-fitting. Of note, the necessary data for computing the stability chart were obtained by the impulse hammer method, and the cutting test was carried out for Al alloy 7075 with mode of slot (full circular) milling.
It is very interesting that the computed stability chart differs considerably from the experimental one at the higher-speed range of the main spindle, i.e. up to 27,000 rev/min. They suggested that this behavior is caused by the speed-dependence of the spindle dynamics [1]. In addition, they suggested that the acceleration sensor is preferable to detect the chatter in its earlier stage of onset as compared with the force and sound sensors, although not clearly stating how to define the chatter onset (commencement). Thus, it seems that such a discrepancy is, in part, caused by the uncertainty in the determination of the chatter onset.
Importantly, Schmitz et al (2004) publicized already a similar theoretical result as shown in Fig. 3.6, where the stability chart for non-rotating main spindle is compared with that for rotating [2]. More specifically, they measured the frequency response function by using impact testing, while the main spindle was either still stand or rotating, and consequently produced both the stability charts shown in Fig. 3.6. In due course, they verified the validity of these stability charts by slot cutting for the work made of 6061-T6 Aluminum with the end mill. As can be also seen, there is considerable difference between both the stability charts, and they suggested the certain influence of gyroscopic and centrifugal effects in both the front and rear bearings in the main spindle system on the chatter stability. Apparently, we can observe such an interesting behavior when the

---

[1] The spindle dynamics depend upon considerably the kinds of main bearings and their arrangement including the magnitude of pre-load; however, the stiffness and damping capacity of the rolling bearing at higher rotational speed is not investigated as yet even in the sphere of the machine tool joint. In fact, we have a few design data as exemplified in Fig. 2.18 for the case of linear guide (see Chapter 7).

[2] In end milling, recently the terms “Axial Depth of Cut” and “Radial Depth of Cut” are prevailed, but these should be used in accordance with the traditional way, i.e. former and latter being “Width of Cut” and “Depth of Cut”, respectively, apart from the very special cases, so that the analogy to other machining methods is to be guaranteed.

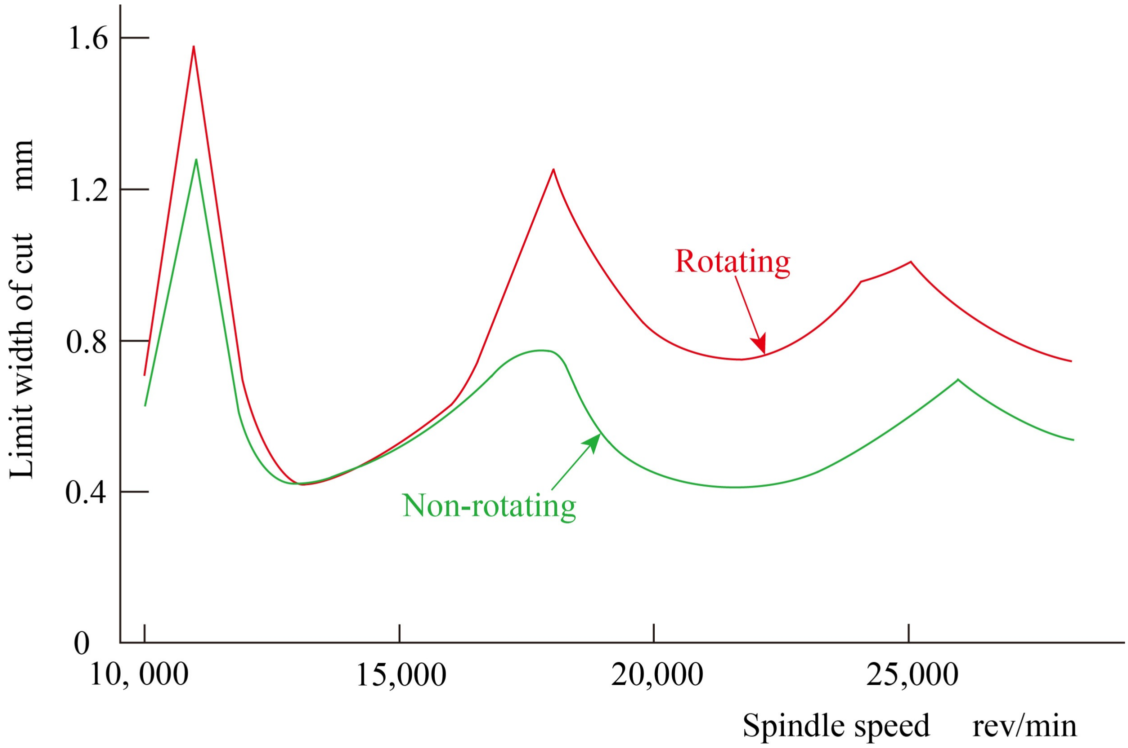

Fig. 3.6 Differing phase in stability chart either non-rotating or rotating main spindle (by courtesy of Schmitz, 2015)

rotating speed is more than 17,000 rev/min. In consequence, we must be aware the dire necessity for investigating the rigidity and damping capacity of the main spindle system while its higher-speed rotating states; however, as already mentioned in Section 2. 2, we have not had any corresponding engineering data even now (see Figs. 2. 17, 2.18 and Chapter 7).

As exemplified these evidences, the facing problems in the chatter are far beyond from those observed in the 1960s with the continuous increase of the spindle speed. On the strength of findings within some challenging researches, it is thus natural to reconsider the chatter theory having been relied on, and we must deploy to new horizons, so that we will be able to seek the essential features of the chatter than ever before.

3.3 Some Representative Issues within Three Basic Expressions

In accordance with the indications within Fig. 3.4, we will discuss some fundamental issues within the three basic expressions for the chatter of regenerative type. More specifically, we must place the main stress on the following issues.

(1) Although dealing with the vibration problem, the specific cutting force in the "*Cutting Process Equation*" has so far been estimated, in nearly all cases, on the basis of the orthogonal (two-dimensional) static or quasi-static cutting model.

(2) As same as above, the dynamic characteristics in the "*Structural Equation*" have been measured while the machine-attachment-tool-work system is still stand or non-loading condition. Intuitively, the dynamic characteristics in cutting differ from those for still stand and non-loading.

3.3.1 Issues in Uncut Chip Thickness Equation

The "*Uncut Chip Thickness Equation*" is of great importance to understand the characteristic features of the self-excited chatter of regenerative type; however, it is better to discuss something related to this expression together with the "*Cutting Process Equation*", because these two are in mutual closer relationship.

In retrospect, we used to consider only the regenerative feedback path as already shown in Fig. 1.1, which corresponds with the wavy surface generated by the cutting tool at one revolution before. Against to this context, Kondo, Sato et al (1980) were first aware of the noteworthy regenerative effects of the wavy surfaces generated at two and further revolutions before as shown in Fig. 3.7.

Reportedly, they call it "*Multiple-regenerative Effect*", and skillfully revealed why the vibrational amplitude is constant after the chatter onset by taking this effect into consideration. Following that of Kondo et al., Tlusty and Ismail (1981) applied this idea to milling, and nowadays the multiple-regenerative effect becomes one of the leading factors in the chatter analysis (Sato, 2013). For example, Jemielniak and Wypysinski (2013) suggested again the importance of the multiple regenerative effects, although not showing the detail, and thus it is desirable to quantify the changing phase in the stability chart in consideration of the multiple-regenerative effect. Against this context, it is said elsewhere that the multiple-regenerative effect does not influence on the stability limit, although such an assertion is not verified yet.

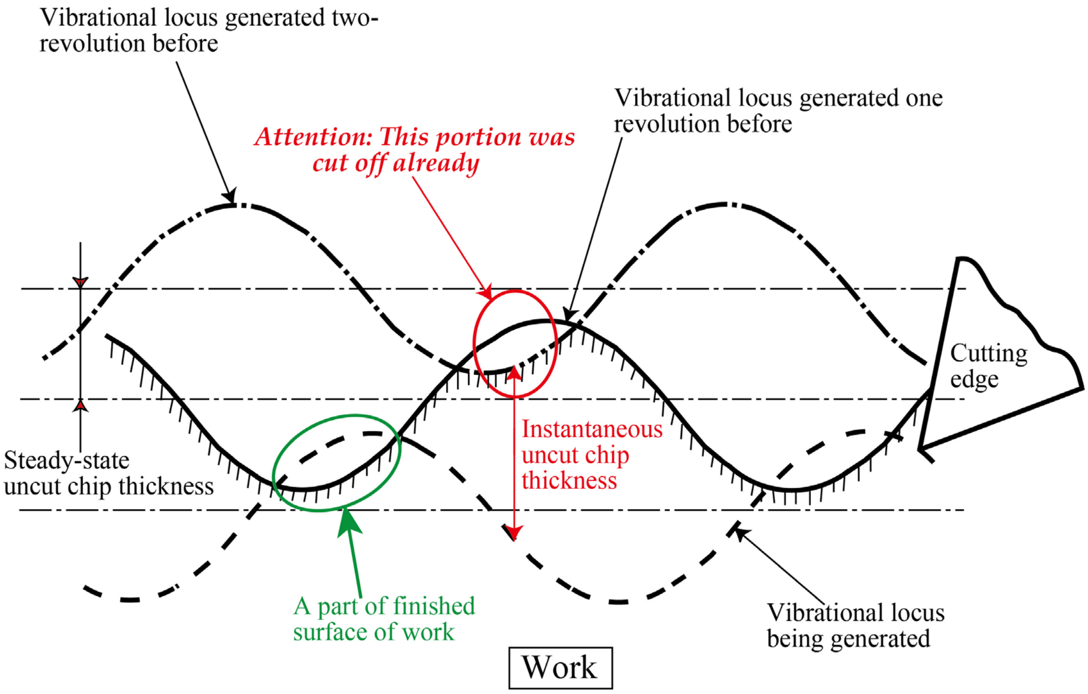

Fig. 3.7 Concept of "Multiple-regenerative Effect" in self-excited chatter (by courtesy of H. Sato)

As a minimum requirement, the uncut chip thickness equation should be revised in consideration of the "Primary Multiple-regenerative Effect" as follows.

$$u(t) = u_0(t) - y(t) + \mu_1 y(t\text{-}T) + \mu_2 y(t\text{-}2T) \text{ -------(3.1)}$$

Admitting that, within the uncut chip thickness equation context, another issue is to consider the run-out of the rotating cutting tool as shown already in Fig. 3.2, we believe that the uncut chip thickness equation has not further problems in general concerns. Dare to say, the Editor asserts the necessity of a reinvestigation into what is the "*Real Uncut Chip Thickness*" corresponding with the "*Real Dynamic Cutting Component in Cutting Force*" (see Section 3.4).

3.3.2 Issues in Cutting Process Equation

As already shown in Fig. 2.7, Denkena et al verified the excellent anti-chatter capability of the nicked cutting edge in the end mill, and they suggested that such a capability is derived from the preferable control of the specific cutting force. Obviously, the specific cutting force (cutting force coefficient, cutting stiffness) is of great importance in the analysis of the chatter, and thus it is desirable to determine theoretically the specific cutting force on the strength of the cutting mechanism model. As widely known, we have used often the orthogonal cutting model with single shear plane without any doubt; however, we must first recall the major assumptions within this model as follows.

(1) The shear angle can be estimated by various ways depending upon the yield criterion of the engineering material. In fact, we have various criteria, e.g. hypotheses of maximum main stress, maximum shear stress and octahedral shear stress; however, even now there are uncertainties in the applicability of each criterion when the engineering material is specified.

(2) In practice, we can observe the side flow on the rake face of the tool while cutting; however, the cutting mechanism model does not consider it.

In addition, the specific cutting force varies with the depth of cut and feed rate. As a result, it is difficult to estimate the specific cutting force by using such a cutting mechanism model, and in general, we can estimate the specific cutting force by measuring the cutting force itself.

In this context, we must be aware that in all the research and engineering reports so far publicized, the specific cutting force is, without exception, determined by measuring the average value of the cutting force, i.e. static component in cutting force. As well-known from the past, the static cutting force is closely related to the dimensional accuracy of the finished component, whereas the dynamic cutting force generates, in general, the surface roughness of the finished component [3].

The chatter is, as literally shown, one of the dynamic phenomena in the engineering problem, and eventually we must consider something discrepancy in the identification of the specific cutting force so far employed.

Nevertheless, people in the chatter sphere used to determine the specific cutting force from the measurement of the static cutting force. It seems that they have followed the theory and practical technology established in the 1960s without any doubt. In retrospect, we were able to measure only the static component of the cutting force when the traditional self-excited chatter theory was established.

With the advance of the related technologies, of course, we have endeavored to improve the shortcomings in such traditional ways. Of note, Altintas et al (2008) publicized some measured results of the dynamic specific cutting force and process damping while turning with grooving tool (hereafter to avoid unnecessary confusion, we call it "*Nominal Dynamic Specific Cutting Force*"). They employed the test rig consisting of the tool holder with piezo-actuator-driven fast tool servo and load cell, and furthermore of laser displacement sensor. The former is for control the vibration frequency and amplitude of the cutting tool, and the latter can facilitate the measurement of cutting tool displacement. Following that of Altintas et al., Sellmeier et al (2009) conducted a similar investigation into the measurement of the process damping by using the milling machine of traveling spindle type. In this case, the spindle is supported by electromagnetic guide and driven by the linear motor. In the experiment, the spindle was under the sinusoidal excitation with amplitude control, and the cutting force was measured by the dynamometer of Kistler-brand while end milling.

In fact, these are very challenging trials; however, the Editor asserts that

---

[3] Some researchers conduct machining the work with wavy surface and measure the average value of the cutting force. After then, they determine the specific cutting force, and duly call it "Dynamic Specific Cutting Force". Thus, there are confusions to certain extent.

those of Altintas et al and Sellmeier et al measured the specific cutting force for fluctuation component, i.e. nominal value, but not real dynamic one, as will be discussed in Section 3.4. Consequently, we have some doubt regarding whether the measured values are reliable or not, and in addition, both the test rigs appear as to be not suitable for the measurement of the real dynamic specific cutting force. In short, these are for the investigation into ultrasonic machining with phase control itself, and supposedly we may not guarantee the one-to-one relation between the measured result by these test rigs and that in the chatter in practice. Conceptually, the dynamic waviness should be, at least, estimated from the chatter mark left on the finished surface, and then such a signal should be input to the oscillator.

Admitting that we have benefited by applying the nominal dynamic specific cutting force so far used to some extent as will be stated later, on the contrary, we must reconsider the applicability limit of such a nominal dynamic specific cutting force. This is because we can now measure the real dynamic specific cutting force as will be stated in Section 3.4.

In the case of composite material, Kecik et al (2012) determined the nominal specific cutting force and suggested an interesting behavior. Importantly, they clarified that the nominal specific cutting force changes depending upon the fiber orientation as shown in Fig. 3.8 (a), even when the fiber direction is constant. This results from the relative position change of the fiber with the rotational cutting edge. Eventually, they can formulate both the nominal specific cutting force for tangential and radial components by using the regression model as follows [4].

$$K_{n,\ t} = a_p^n(a_0 + a_1\theta + a_2\theta^2 + a_3\theta^3 + a_4\theta^4 + a_5\theta^5) \text{ ------(3.2)}$$

where, θ is in radians.

[4] In accordance with the information from Kecik, Fig. 3.8 (a) is based on that of Sheikh-Ahmad J Y. (Machining of Polymer Composite. Springer-Verlag, 2009).

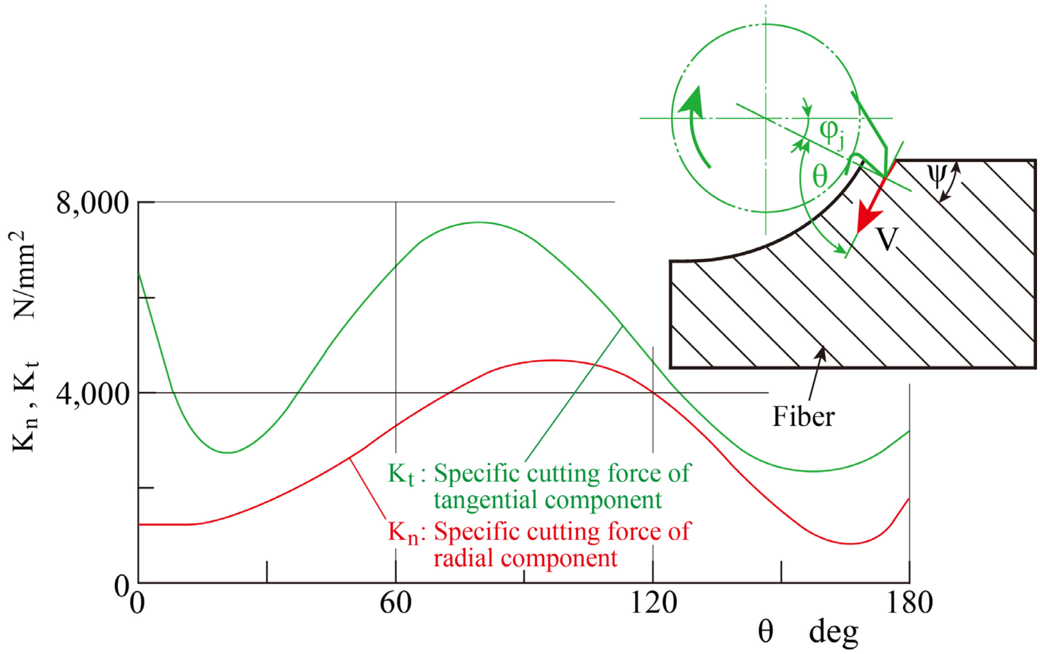

(a) Variation of specific cutting force with fiber orientation and tooth position (ϕ = 45 deg.)

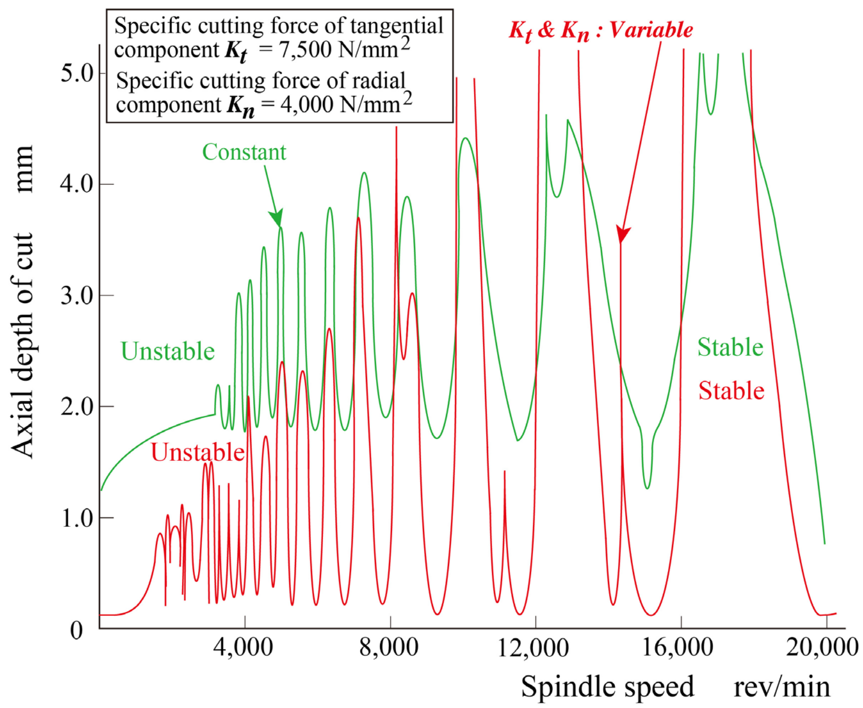

(b) Comparison of stability charts for constant K_n and K_t with those variable

Fig. 3.8 Stability charts for composite material (by courtesy of Kecik)

As can be readily seen, the stability chart shows some differing features as shown in Fig. 3.8 (b), when the nominal specific cutting force varies with the rotational angle of the end mill. The stability charts were produced for milling with one-flute PCD (Poly Crystalline Diamond) end mill of 12 mm in diameter, 6 mm in (radial) depth of cut, and 0.03 mm/tooth in feed, where the chip thickness coefficient κ is 0.9 [4]. In addition, the dynamic characteristics of CNC (Computerized Numerical Control) milling machine were obtained by the modal analysis, i.e. m = 0.8 kg, c = 57.3 Ns/m and k = 2.22×10^{7} N/m.

To this end, it is worth suggesting that the cutting process equation should be modified as follows, when we will estimate the deterioration magnitude of the chatter stability by the inevitable disturbance like the impact force while milling.

$$F(t) = k_c u(t) + f_0 \sin\omega t \text{ (forced vibration)}, \quad t = 2\pi/\omega \text{ ---(3.3)}$$

3.3.3 Issues in Structural Equation

Within the "*Structural Equation*" context, there are three leading issues, i.e. (1) measurement of dynamic characteristics, m, c and k shown already in Fig. 1.1, (2) clarification for distribution diagram with respect to the rigidity and damping coefficient within a whole system, and (3) effect or influence of non-linearity in structural body component on chatter.

Of these, the item (1) is at burning issue and vital, and thus we will discuss it in the following. For the item (2), we have not enough engineering data at present; however, even in the discussion about process damping, it is better to refer to the "*Damping Distribution Diagram*" as well as the "*Deflection (Rigidity) Distribution Diagram*" of the machine-attachment-tool-work system as a whole, so that we can clarify quantitatively the validity of process damping in consideration of its relative damping capacity within a whole system.

The idea of the distribution diagram is one of the auxiliary design methodologies having been used since 1960s, and a deflection distribution diagram for the planomiller of portal type is reproduced in Fig. 3.9 (Geiger, 1965). Regarding the item (3), we must be aware of the very importance of fitting tolerance design in both the structural body components. In fact, the anti-chatter capability can be improved by designing a suitable fitting tolerance; however, such an outstanding structural design is not fruition yet (see Section 2.2).

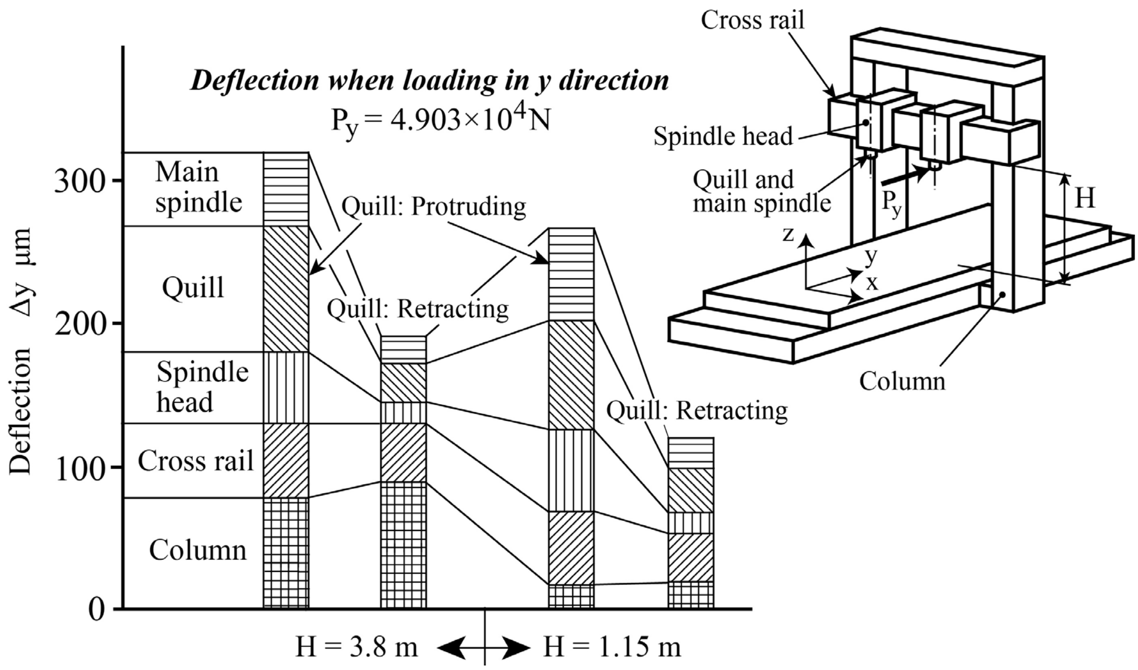

Fig. 3.9 Deflection distribution diagram for planomiller of portal type (by Geiger)

Conceptually, the machine-attachment-tool-work system is, in principle, of multiple-degree of freedom, and thus we employ the equivalent mass, damping coefficient and spring constant in the utmost simplified structural equation for one-degree of freedom system. We can however suggest the following problems even in the simplified structural equation.

(1) With the advance of FEM (Finite Element Method) analysis for the structure, we can compute the dynamic behavior of the machine-attachment-tool-work system to some extent; however, the availability of the computed values is limited because of including uncertainties, e.g.

damping capacity at the joint.

(2) In the case of thin-walled work, the dynamic behavior changes continuously with machining, and thus we need to get the structural equation with real-time adaptability.

(3) We used to measure experimentally these coefficients, for example, by the impact hammer method; however, it is difficult to measure them in consideration of all the directional orientations in the dynamic behavior correctly.

(4) In general, the measurement of the coefficients is carried out in the still stand of the system; however, we need those in the machining condition. More specifically, the dynamic characteristics have been measured while the machine-attachment-too-work system is in the still stand or non-loading operation so far. As can be easily imagined, such measured values could be far from those in actual machining states at present, and it is thus natural to discuss the availability of the stability chart.

(5) Extremely regarding the damping coefficient, its reliable measuring method is not established yet, because of the great difficulty in the quantified measurement of the damping capacity as already stated in Chapter 2, and also revealed in the sphere of machine tool joints (Ito, 2008).

Now let us discuss furthermore the measurement of dynamic characteristics while machining. In this context, we must also reinvestigate, up to how much spindle speed, the dynamic characteristics, i.e. m, c and k, measured in still stand are available. In the 1960s, there could be non-influential deviations between those for 2,000 rev/min in rotational speed and still stand of the spindle state, and thus the measured characteristics were within allowable values when applying them in practice.

Figure 3.10 reproduces some measured values for m, c, k and due frequency by the impulse excitation, while end milling (Matsumura and Haibara, 2002). Although not stating the differences between those for still

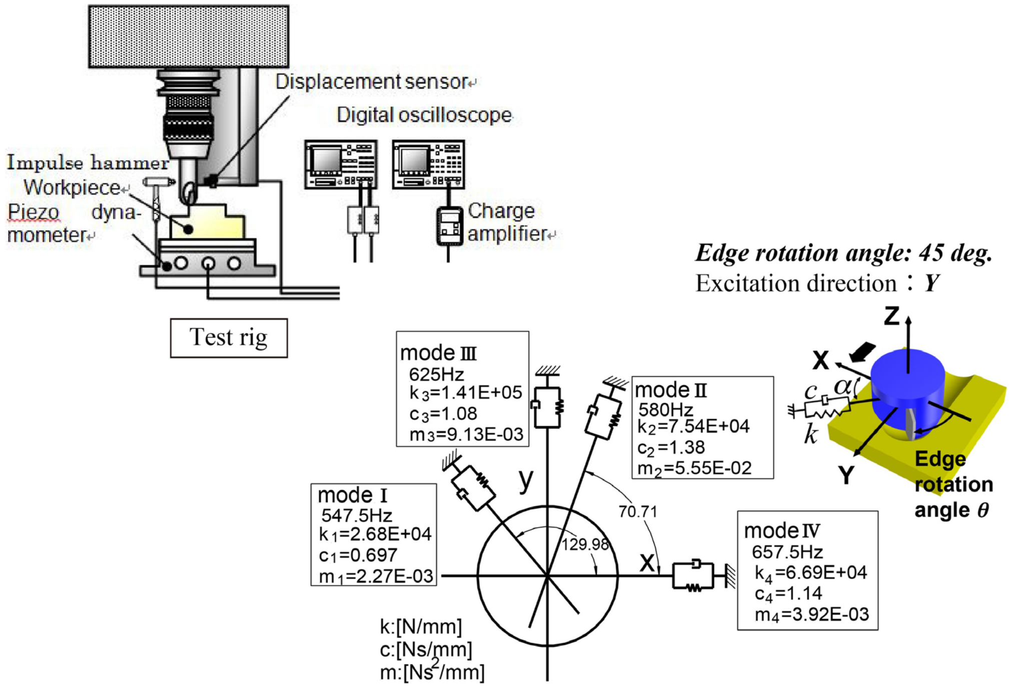

Fig. 3.10 Measured values for m, c, and k while end milling in 2002 (by courtesy of Matsumura, 2014)

stand and in milling, as can be readily seen, the measured values vary considerably depending upon the rotational angle of the cutting edge. Conceptually, the milling process is of vibrational phenomena with multiple-degree of freedom and, considering it, that of Matusmura and Haibara may suggest the necessity of identifying the dynamic characteristics in the structural equation while actual cutting, but not being in still stand.

Of special note, Nicolescu and Archenti (2013) investigated the dynamic characteristics while turning the cylindrical work supported at both the ends with centers. More specifically, they detected first both the vibrational signals, i.e. those for stable turning and with chatter, by the microphone. Then, they conducted the simulation for the “Motion of Equation” excited by the white noise, and then by comparing the simulated result to the output signal of the microphone, the damping coefficient and spring constant are identified.

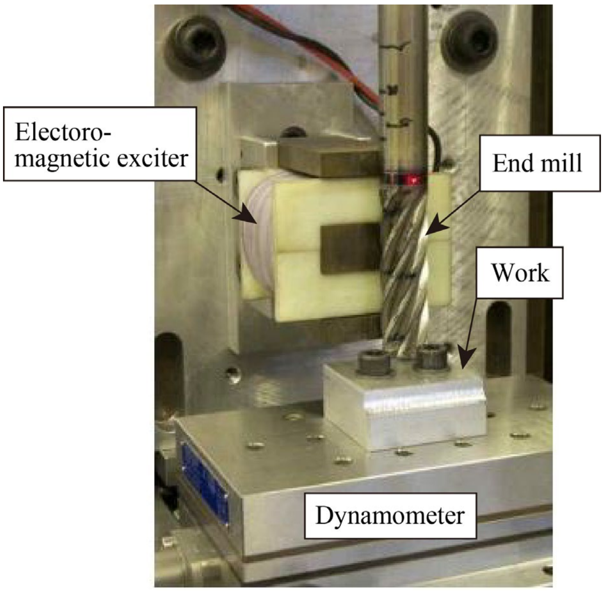

Fig. 3.11 Test rig for measurement of dynamic characteristics while end milling (by courtesy of Sims, University of Sheffield, 2015)

Following these, the Dynamic Research Group of University of Sheffield has launched out an investigation to measure the dynamic characteristics while the aerospace component is finished with higher-speed milling. Fig. 3.11 reproduces the test rig, which is being used under the aegis of EPSRC (GR/S49858/01). Importantly, the frequency response of the milling cutter and concerns shows the non-linearity, which could be caused by the joint between the tool holder and main spindle. In this case, we must be furthermore aware of the counter-effect of the electromagnetic exciter, which plays in turn a role of damper so far suggested elsewhere, although the Group seems not pay any special attention to it.

For the ease of further discussion, the logarithmic damping decrement is approximately calculated from the dynamic characteristics so far measured as shown in Tables 3.1 (a) and (b). In this case, we assume that the machine-attachment-too-work system is one-degree of freedom with decay vibration, and that the logarithmic damping decrement δ can be written as

$$\delta = 2\pi c/c_c = \pi c/\sqrt{mk} \text{ --------- } (3.4)$$

where, m: Mass, k: Spring constant, c: Damping coefficient

c_c: Critical damping coefficient

Sources	Machine tool kinds	Machine tool Types/Manu-facturer	Cutting tool	Measuring method	Dynamic chracteristics m Ns^2/mm	c Ns/mm	k N/mm	Equivalent loga-rithmic damping decrement (around)
Matsumura 2002	MC		Ball end mill	Impulse hammer	3.92×10^{-3}	1.14	6.69×10^{4}	0.21
					9.13×10^{-3}	1.08	1.41×10^{5}	0.09
					9.13×10^{-3}	1.08	1.41×10^{5}	0.06
					At three different tooth positions			

(a) While cutting

(b)

Sources	Machine tool kinds	Machine tool Types/ Manu-facturer	Cutting tool	Measuring method	Dynamic chracteristics m kg	c Ns/m	k N/m	Equivalent loga-rithmic damping decrement (around)
Kecik 2012	CNC milling machine	Blue Bird MG6037 PKK	One-flute end mill	Modal analysis	0.8	57.3	2.22×10^{7}	0.003
Ahmadi 2011	3-axis controlled milling machine		Work held by spindle / Parting-off tool fixed on table	Curve fitting for FRF	3.8	731.5	2.2×10^{7}	0.73
Insperger 2008	5-axis controlled MC - Ingersol		End mill		0.046	4.32	9.57×10^{5}	0.02
Sellmeier 2010	4-axis controlled MC	MCi 16 Heller	End mill with HSK 63	Impulse hammer - Genetic algorithm to FRF	22.20	11336.70	149.49×10^{5}	0.57
					(at first natural frequency)			
					0.86	314.21	456.38×10^{5}	0.014
					(at the highest natural frequency)			
Altintas 2008	CNC lathe		Grooving tool		1.742	1.768	7.92×10^{6}	0.001

FRF: Frequency Response Function

(b) While in still-stand or non-loading operation

Table 3.1 Conversion of measured m, c and k into equivalent logarithmic damping decrement

From the magnitudes of the equivalent logarithmic damping decrement shown in Table 3.1, we may understand first the difficulty in the measurement of the damping capacity, because of their widely scattered values. Then, we must scrutinize the reasons regarding why we observe the incredible magnitudes as exemplified by those of Ahmadi and Sellmeier. In case of that of Sellmeier, the equivalent logarithmic damping decrement is larger at the first natural frequency of the system than that for the highest natural frequency. Apparently, we may expect the effect of the

“Lower-speed Stability”; however, the equivalent logarithmic damping decrement itself is too large as compared with that in the mechanical vibration system. In addition, we may find certain uncertainties in the measured values regarding whether the damping coefficient is of directional-orientation and frequency-dependent characteristics or not by nature.

Importantly, it has been said that the total damping capacity of a machine tool as a whole is less than 0.3 in logarithmic damping decrement, and that the machine-attachment-too-work system does not occur any chatter vibration when its logarithmic damping decrement is more than 0.6. More importantly, the machine tool joint can facilitate the sources of the larger damping capacity, provided that the joint is not located at the node in the vibration mode.

To this end, it is also worth suggesting that the structural equation should be further generalized by incorporating, for example the “Directional Orientation in Chucking Stiffness”, and “Non-linearity in Stiffness of Structural Body Component”. In the case of work holding by the three-jaw chuck, the structural equation yields to

$$F(t)\cos\beta = m(d^2/dt^2)y(t) + c(d/dt)y(t) + (k + k_w \sin 3\omega t)y(t) \quad \text{----(3.5)}$$

where, k_w = Average stiffness of chuck-work system

In addition, the Editor emphasizes furthermore that we have so far discussed the necessity of *the measurement of dynamic characteristics, m, c and k, for example, in the main spindle branch of MC only. In contrast, we have not paid any attentions to those belonging to the table-fixture-work system, i.e. table branch. This is because we assume that the table branch is dynamically stiffer than that of the main spindle branch*; however, in certain cases, we must combine the dynamic characteristics of both the branches, although such a research is about to launch out (see Chapter 5).

3.4 Drooping Characteristics in Real Dynamic Component of Cutting Force and Self-excited Chatter

In the measurement of the cutting force, Kistler AG contrived an innovative force sensor of piezoelectric type in the late 1960s, and in consequence, we can measure accurately the cutting force. Importantly, we can discriminate three components, i.e. static, fluctuation and dynamic components, as shown schematically in Fig. 3.12. In this case, the fluctuation component is caused by the change of the number of cutting teeth in simultaneously engaging to the work.

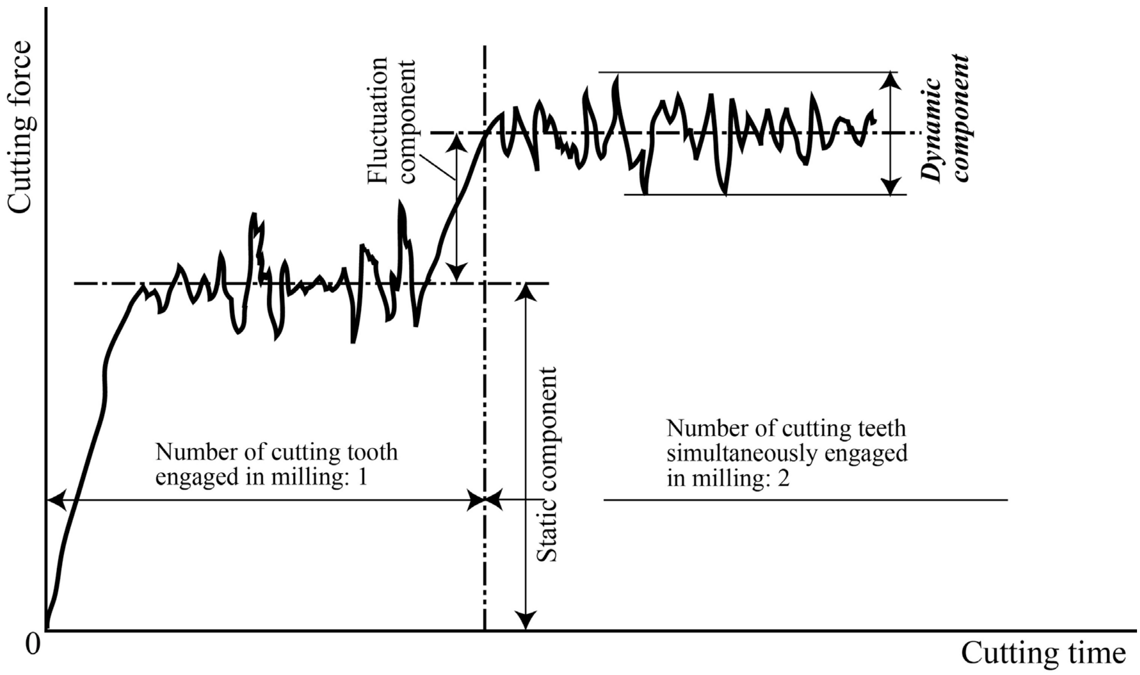

Fig. 3.12 Static, fluctuation and dynamic components in cutting force

More importantly, Opitz et al (1970) and Langhammer (1972) revealed, especially in Dr. Thesis of Langhammer, the characteristic features of the dynamic component in cutting force, as shown, for example, in Fig. 3.13. As can be readily seen, there are apparent differences in the behavior of the dynamic component from static one together with their magnitudes. It may thus worth suggesting that we must eye a new direction in the determination of the "*Real Dynamic Specific Cutting Force*" as follows.

(1) The nominal dynamic specific cutting force has been so far determined by measuring the average value of the cutting force, i.e. static component in Fig. 3.12. Is such a nominal dynamic specific cutting force reliable and applicable to the analysis of the chatter vibration?

(2) What is the role of the dynamic component in the cutting force unveiled by Langhammer in the analysis of the chatter? Must we determine the real dynamic specific cutting force by using the dynamic component?

Supposedly, there have been no publications related to these controversial issues, and thus for the sake of further research activities, some quick notes will be given in the following.

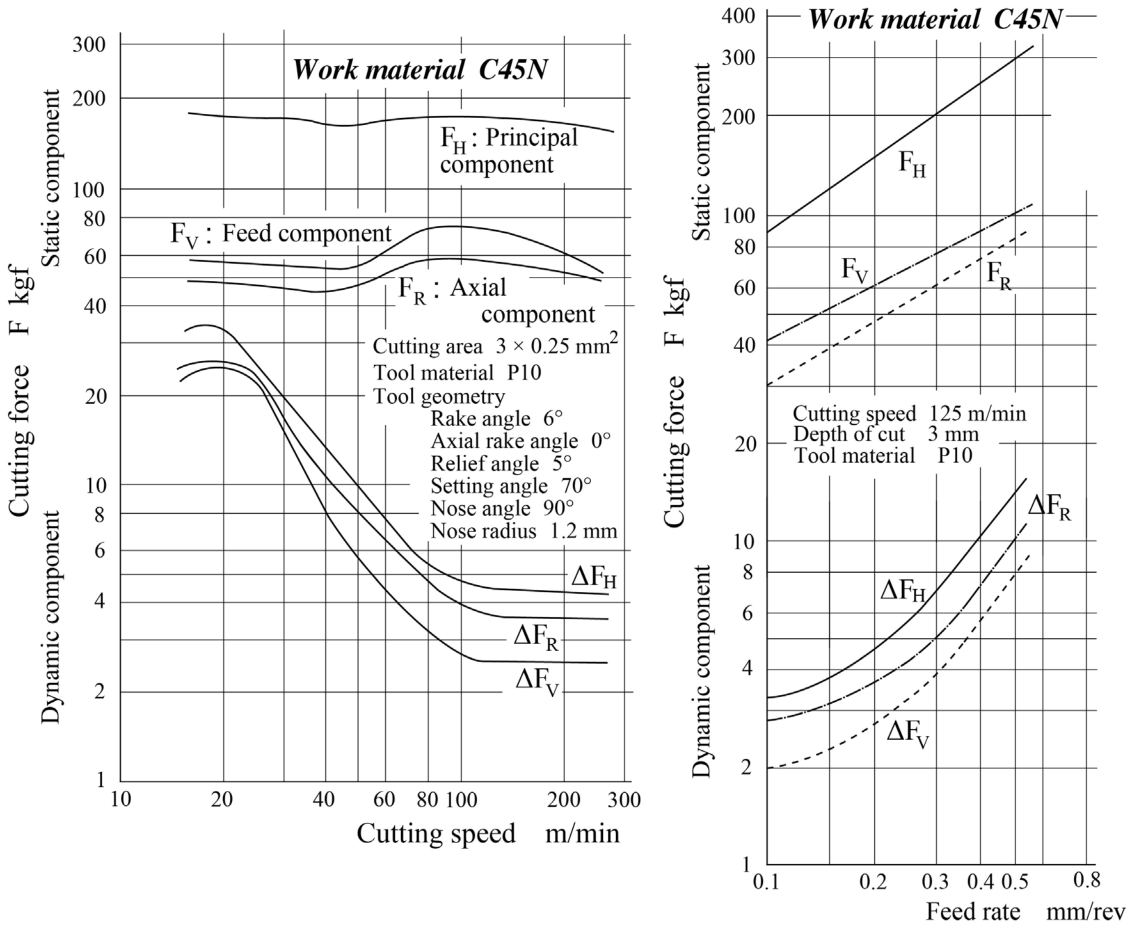

Fig. 3.13 Static and dynamic components of cutting force in carbon steel turning (by Langhammer)

As can be readily seen from Fig. 3.13, the static component in the cutting force is in nearly constant with increase of the cutting speed, whereas the dynamic component shows the typical "*Drooping Characteristics*", i.e. dynamic component reducing with cutting speed, in turning of the work made of carbon steel. In fact, Langhammer obtained a similar result when turning the work made of alloy steel (DIN 16MnCr5G).

As already suggested by Arnold in the past and again resurged recently by Entwistle and Stone (2013), the drooping characteristics in the cutting force may induce the self-excited chatter without any regenerative effects (Arnold, 1946), provided that the dynamic component is larger enough. Thus, Fig. 3.14 illustrates the mechanism of such a chatter type.

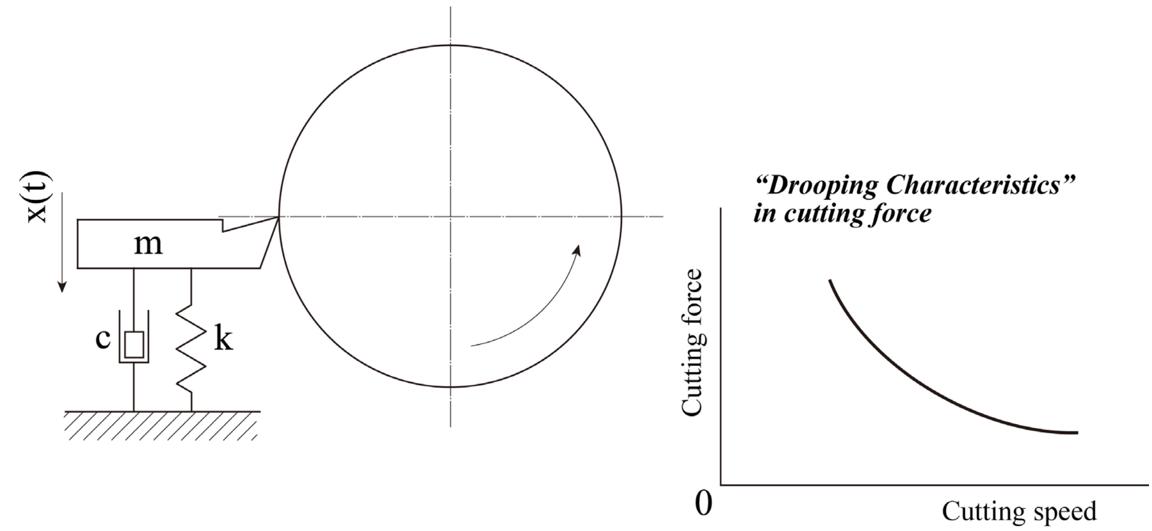

Fig. 3.14 Theoretical model for self-excited chatter vibration derived from "Drooping Characteristics" in cutting force

If x(t) represents the displacement of the tool in the direction of the force, the principal component of the cutting force is given by

$$F = -\, bu_0(R_0 - \beta \frac{dx(t)}{dt}) \text{ ------- } (3.6)$$

Thus, the equation of motion for one degree-of-freedom yields to

$$m\frac{d^2x(t)}{dt^2} + (\, c - bu_0\, \beta\,)\frac{dx(t)}{dt} + kx(t) = 0 \text{ -----}(3.7)$$

where, b = Cutting width, u_0 = Depth of cut, R_0 and α = Positive coefficient determined by work material, cutting conditions, shape and size of cutting edge and so on.

When the coefficient for velocity is negative, the system becomes unstable, and thus the chatter onset can be regulated by

$$(c - bu_0\beta) \leqq 0 \text{ ----(3.8)}$$

Intuitively, another facing issue is whether the nominal dynamic cutting force proposed by Tobias is identical to the real dynamic cutting force measured by Langhammer, and thus we must, at least, conduct the following research.

(1) Measurement of the dynamic plowing force in both the stable and the self-excited chatter, which can be regarded as an evaluation factor of process damping when verifying the hypothesis suggested by Tobias. The plowing force can be obtained by applying the extrapolation method to the "Cutting Force - Feed Rate or Depth of Cut" chart. The force corresponding to the nil in depth of cut or feed rate axis is the plowing force. For example, from Fig. 3.13, we can obtain the static plowing force as to be 70 kgf in the case of the principal component of 300 kgf in full range.
(2) To unveil the correlation of the dynamic cutting force with the corresponding instantaneous uncut chip thickness.

Langhammer publicized furthermore another interesting results, which were obtained when turning the work made of heat resistant steel. As reported elsewhere, the heat resistant steel is prone to generate the saw-like chip, and thus Fig. 3.15 shows also such information. In fact, the dynamic component is larger at the cutting speed, where the saw-like chip can be observed. On the strength of those shown by Langhammer, we could expect that the dynamic component of the cutting force is a clue for unveiling the essential features of the self-excited chatter.

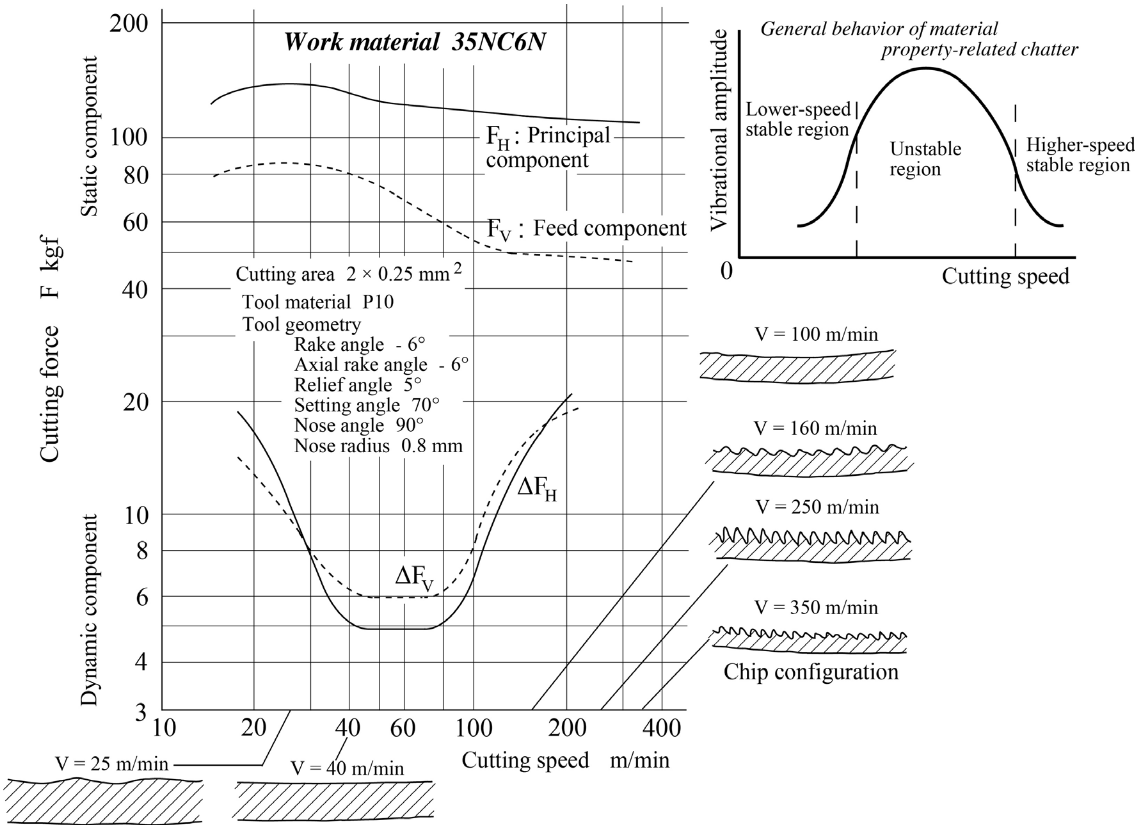

Fig. 3.15 Static and dynamic components in cutting force when machining heat-resistant steel (by Langhammer)

Summarizing, it is necessary to investigate to what extent the dynamic component contributes to the self-excited chatter. In such an investigation, we must be aware that the cutting stiffness has been evaluated by using the average value (static component) of the measured cutting force, and thus a newly arisen problem is to verify the validity of the determination method for the cutting stiffness so far used.

References

Altintas Y, Eynian M, Onozuka H. (2008) *Identification of dynamic cutting force coefficients and chatter stability with process damping*. CIRP Annals - Manufacturing Technology; 57: 371-374.

Arnold R N. (1946) *The Mechanism of Tool Vibration in the Cutting of Steel, Cutting Tools Research: Report of Subcommittee on Carbide Tools*.

Proc. I Mech E: 261-284.
Doi M, Masuko M, Ito Y. (1982) *Re-observation of the Chatter Vibration in Chuck Works - Effects of Jaw Number on the Appearance of a Scale-like Chatter Mark*. In: Proc. of 10th NAMRI of SME, 409-416.
Entwistle R, Stone B. (2013) *Position Paper - Fundamental Issues in Self-excited Chatter in Grinding*. Jour. of Machine Eng.; 13-3: 26-50.
Geiger H G. (1965) *Statische und dynamische Untersuchungen an Schwerwerkzeugmaschinen*. Dissertation, TH Aachen, 1965.
Insperger T. et al. (2008) *On the chatter frequencies of milling processes with runout*. Inter. Jour. of Machine Tools & Manufacture; 48: 1081-1089.
Ito Y. (2008) *Modular Design for Machine Tools*. McGraw-Hill.
Jemielniak K, Wypysinski R. (2013) *Review of Potential Advantages and Pitfalls of Numerical Simulation of Self-excited Vibrations*. Jour. of Machine Engineering; 13-1: 77-90.
Kecik K, et al. (2012) *Chatter control in the milling process of composite materials*. Jour. of Physica: Conference Series 382: 012012.
Langhammer K. (1972) *Die Zerspankraftkomponenten als Kenngroßen zur Verschleißbestimmung an Hartmetall-Drehwerkzeugen*. Dissertation der RWTH Aachen.
Kondo Y. et al. (1980) *Behaviour of self-excited chatter due to multiple regenerative effect*. Trans. of JSME(C); 46-409:1024-1032.
Matsumura T, Haibara T. (2002) *Simulation of Dynamic Cutting Process in Milling Operation*. Preprint of Assembly of Manufacturing & Machine Tool Division, JSME.
Nicolescu M, Archenti A. (2013) *Dynamic Parameter Identification in Nonlinear Machining Systems*. Jour. of Machine Engineering; 13-3: 91-116.
Opitz H, Dregger E U, Röse H. (1967) *Improvement of the Dynamic Stability of the Milling Process by Irregular Tooth Pitch*. In: Proc. of 7th Inter. MTDR Conf., Pergamon, p. 213 - 227.
Opitz H. et al. (1970) *Statische und dynamische Schnittkräfte beim Drehen und ihre Bedeutung für den Bearbeitungsprozess*. Forschungsberichte des

lands Nordrhein-westfalen, Nr. 2144, Westdeutscher Verlag.
Rall K et al. (1998) *Vermessung rotierender Werkzeuge in HSC-Fräsemaschinen*. ZwF; 93-4: 127.
Sato H. (2013) *Multiple Regenerative Effect Governing Chatter Behaviour After Onset*. Jour. of Machine Engineering; 13-3: 51-76.
Schmitz T L, Ziegert J C, Stainslaus C. (2004) *A Method for Predicting Chatter Stability for System with Speed-dependent Spindle Dynamics*. Trans. North American Manufacturing Research Institution of SME; 32: 17-24.
Sellmeier V, Hackeloeer B, Denkena B. (2009) *Process Damping in Milling - Measurement of Process Damping Forces for Chamfered Tools by Means of an Electromagnetically Guided Spindle*. 12th CIRP Conf. on Modelling of Machine Operations, San Sebastian.
Tlusty J, Ismail F. (1981) *Basic non-linearity in machining chatter*. CIRP Annals; 30-1: 299-304.
Van Dijk N J M. et al. (Oct. 2008) *Real-Time Detection and Control of Machine Tool Chatter in High Speed Milling*. 2nd Inter. Conf. "Innovative Cutting Processes & Smart Machining", Cluny.

PART II LEADING-EDGE RESEARCH AND ENGINEERING DEVELOPMENT WITHIN ADVANCED CHATTER VIBRATION THEORY

Headnotes

In Part I, we describe first the fundamental knowledge about the chatter, and in due course note quickly the leading remedies for the chatter suppression like the milling cutter with irregular pitch and differing helix angle in cutting teeth. Importantly, on the strength of the achievements obtained from a handful of forerunning and challenging researches, we suggest a considerable number of the issues in Chapter 3, which cannot regulate by the chatter theory at present. Such issues may give us certain clues to advance the theory and suppression remedies of the chatter, i.e. further research guides into the chatter.

Following Part I, we display quickly a first-hand view for the research and engineering development conducted in the year 2005 and beyond herein. Along with the first-hand view, we display the interesting observation in the chatter while higher-speed machining the aircraft component at present in Chapter 4. Obviously, these ascertain the dire necessity for conducting the research into the issues suggested in Chapter 3.

Figure II.1 illustrates such a first-hand view for the research objectives by classifying them into the following three categories.

(1) The long-standing traditional subjects like “Chatter Suppression” and “Lower-speed Stability and Process Damping”, which are based on those of Tobias, Tlusty and Merritt. Obviously, these are dominant even now.

(2) Trial and challenging subjects like “*Influence of Run-out in End Mill on Stability Chart*” and “*Identification of Coefficients in Structural Equation While Cutting*”, which intend to modify the regenerative chatter theory to be compatible with the higher rotational speed of the main spindle at present.

(3) Interesting subjects like “*Chatter in Consideration of Joint Stiffness of*

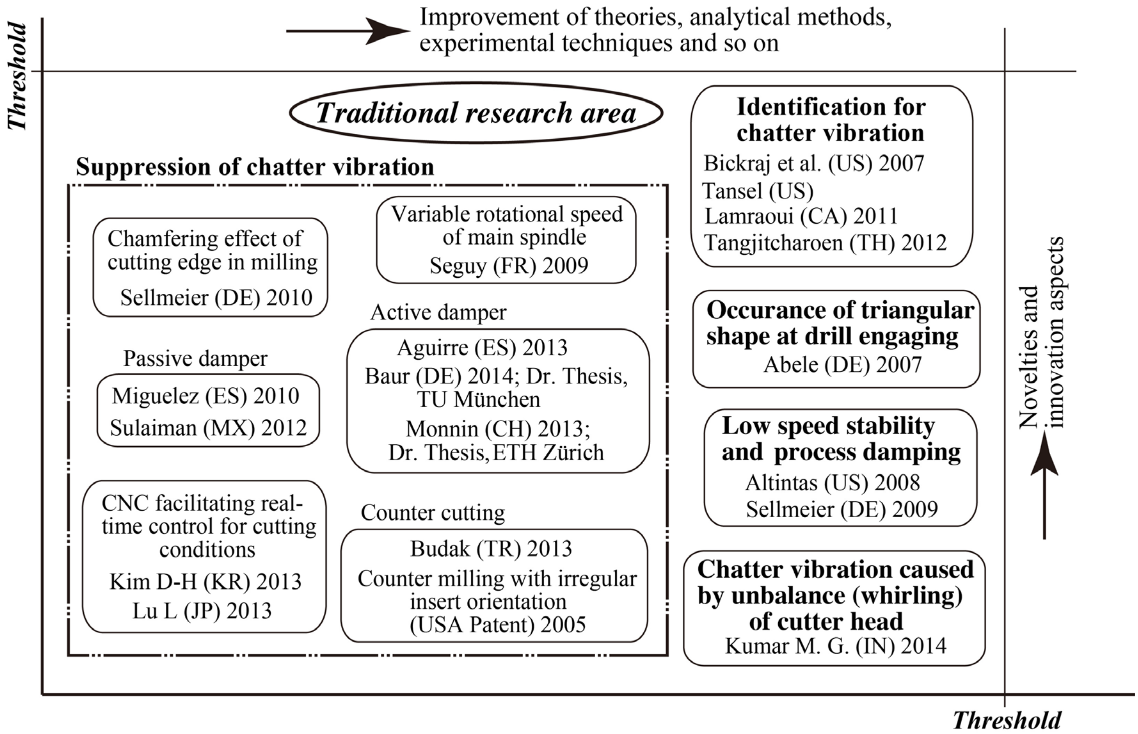

(a) Traditional research area

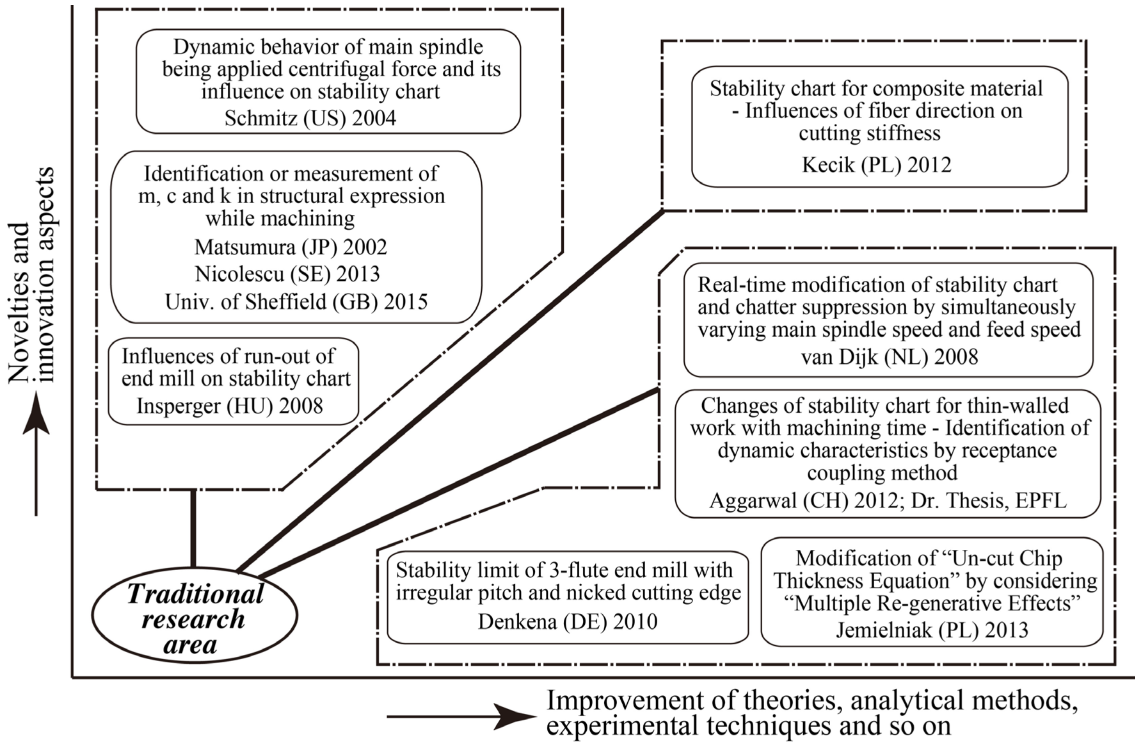

(b) Challenging and innovative research to unveil essentials

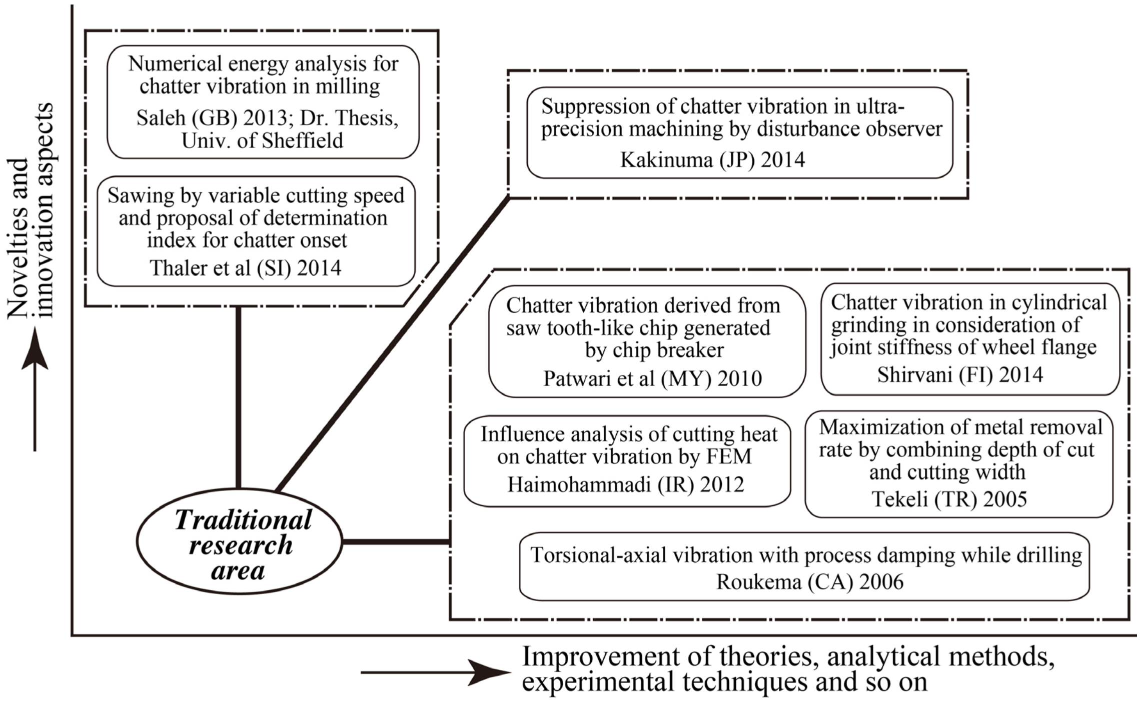

(c) Interesting research although including uncertainties and controversial points

Fig. II.1 Present perspectives for research into chatter between 2005 and 2014 (Country Codes as per ISO 3166)

Wheel Flange While Cylindrical Grinding", although including something uncertainty and controversial points.

In short, Fig. II.1 is produced by the literature survey and concerns, where the objectives are around 40 papers including the Dr. thesis, to unveil some symptoms for the new research direction within the chatter. In this context, the list of references in Chapters 5 and 6 is somewhat valuable to understand the past and present perspectives for the research into the chatter.

With growing importance of milling to machine the aircraft component and molding die, it is thus natural that nearly all researches aim at milling. Milling is, in principle, complicated and difficult to clarify its mechanism by the analytical method. This is because the cutter path trajectory can be represented by the Trochoidal curve, and the chip thickness is given by both the curves. In contrast, we can apply the advanced simulation software and dynamic information processing to overcoming such difficulties, and these tools can facilitate the ease of work to a large extent.

We can observe similar difficulties in drilling and grinding; however, the computational simulation can facilitate considerably to solve such complicated mechanisms at present. In contrast, a considerable number of the research papers deal with the computation only and don't pay any attentions to the essential feature in the facing problem.

As will be clear from Part I, importantly one of the crucial issues at present is to discriminate the chatter pattern because we can observe various complex chatters including unknown ones having not been experienced so far with increasing the machining speed. Eventually, such various chatters are caused by the self-excitation of regenerative type; however, it is very rare case to observe the pure regenerative type at present. In contrast, each chatter pattern includes more or less the influences of forced excitation derived from the cutting mechanism itself and also the non-linearity in the machine-attachment-tool-work system. Thus, a trouble shooting method is furthermore proposed in Chapter 4 after investigating the chatter mark so far observed. In the proposed method, the chatter pattern may be identified from the sample (reference) chatter mark together with suggesting some recommendable tools to suppress the corresponding chatter.

In due course, in Part II we publicize the two contribution papers from the potential researchers, which deal with some leading issues mentioned above, to deepen the understanding for the essential feature in the chatter (see Section 3.3.3 and Fig. 3.6). As widely known, we used to detect various signals related to the chatter, e.g. sound, vibration acceleration, cutting force and so on, with various transducers; however, we have used such signals to identify only the chatter onset so far. Against this context, these contributions suggest further importance of signal processing in detail by exemplifying concretely that signals at chatter onset and immediately before onset involves the valuable information to unveil the essential features of the chatter.

More specifically, Professors Archenti and Nicolescu of KTH Royal

Institute of Technology introduced the concepts of statistical dynamics for the identification of the dynamic parameters of the machining system, in actual machining operations, by using both the non-parametric and the parametric computational models in Chapter 5. Importantly, these proposed procedures can be characterized by real time estimation of the operational dynamic parameters of the machining system, represented by the interaction of the two subsystems, machine tool elastic structure and cutting process. More importantly, they suggest the importance of chemistry between the real-time identification of dynamics in the machining system with the statistical signal processing as exemplified by the application of "*Markov Process Representation*". Chapter 5 can play furthermore the role of a "Position Paper" with respect to the output signal processing when discriminating the properties of the chatter.

Professor Schmitz of UNC Charlotte conducts a numerical and experimental investigation in Chapter 6 to accurately predict both stable and unstable milling conditions. He uses the well-known "Poincaré Map" (a phase map between displacement and velocity) to study the self-excited vibrations due to the regenerative effect (called "*Secondary Hopf*") as well as instabilities that result in behavior that repeats every second, third, fourth, and so on tooth period (called "*Period-n bifurcations*"), rather than each tooth period ("*Forced vibrations*").

In consideration that a crucial issue at present is to improve the applicability of the stability chart while carrying out higher-speed machining, furthermore, a quick note is given for the present and near future perspectives with respect to the dynamic behavior of the main spindle in Chapter 7. In short, it is notable that the dynamic behavior of the main spindle is not clarified as yet while rotating more than 2,000 rev/min, and this is one of the major obstacles to establish the stability chart, which is available for the machining condition with higher-cutting speed. Dare to say, people in chatter concerns are not familiar to the characteristics of the main spindle in detail and its influences on the chatter, although they are interested in such subjects. Thus, the Editor suggests some leading research subjects to be investigated hereafter. Paraphrasing, we cannot apply the stability chart to the machining condition with the higher-cutting speed, where we face certain difficulties to determine the parameters of the "Structural Expression" in the chatter theory. As can be easily imagined, one of the determinants in this case is the rigidity and damping capacity of the main spindle.

In accordance with the aims and purpose of this book, Chapter 8 provides us with the though-provoking quick notes for the research guide to the chatter in metal grinding. As well and widely known, the research into the chatter in metal grinding has been inactive since 1970s, and thus the Editor suggest roughly that we have no systematic remedies for the facing problems, which could be derived from the contact stiffness, grinding stiffness, grinding damping and so on. In Chapter 8, these influencing factors to be in current issues are detailed following the quick notes in Section 1.3. It is extremely noteworthy to clarify the influence of the "*Unbalance of Grain Distribution*" in the grinding wheel on the chatter.

Chapter 4 Observation for Various Chatter Marks and a Proposal of Trouble Shooting for Identification of Chatter Patterns

With continuing requirements for the product innovation, we need to enhance machining requirements for the part of the product, and thus the machine tool user is often suffered from the chatter. In due course, the machine tool manufacturer must solve such trouble in accordance with the user's claims. Obviously, such claims are very valuable to understand the facing chatter problems; however, because of fierce competition among machine tool manufacturers, in general, we cannot obtain their details. In this context, we must be aware that the chatter mark is one of the dominant clues to solve such chatter problems.

As reported elsewhere, we can observe at present the chatter with more complicated pattern (type) ever than before with prevailing the higher-speed machining, and often we face certain difficulty to identify its causality. In such cases, the chatter mark may also provide us with useful information.

In this chapter, thus, we discuss first the characteristic features in the chatter mark accidentally obtained from some case studies on machining by MC at present, and then in consideration of the discussion in Chapter 3, we suggest a troubleshooting method to identify the chatter pattern from the chatter mark. In addition, we suggest how to seek the recommendable cutting tool when we can identify the chatter pattern.

4.1 Case Studies on Observation of Chatter Marks

As can be readily understood from Part I, we can observe various chatter patterns at present with prevailing the higher-speed machining. In certain cases, we can observe a chatter pattern, which is unfamiliar and far beyond our knowledge resulting in the difficulty of identifying its causality.

As already mentioned in the headnote, the chatter mark gives us with some clues to identify the chatter pattern and in the simplest case, the chatter of regenerative type generates the micro-inclined ridge-like mark along the feed direction of the cutter as shown in the “Title Page”. In grinding, at the burning issue is to finish the surface without any “Blur-like” texture, and in this case, we can identify, whether it is derived from the “Forced Vibration, e.g. that caused by the unbalance of the grinding wheel” or “Regenerative Effect”, by polishing the surface with the oilstone (*Arkansas stone*). More specifically, the former seems the micro-ridge with “Beat wave-like”, which is perpendicular to feed direction of the grinding wheel, whereas the latter is an inclined micro-ridge to feed direction of the grinding wheel, i.e. that of typical regenerative type.

Admitting the effectiveness of the chatter mark in identifying the chatter pattern, however, we face often certain difficulties to obtain the obvious and reliable information for the chatter mark, because of the company’s

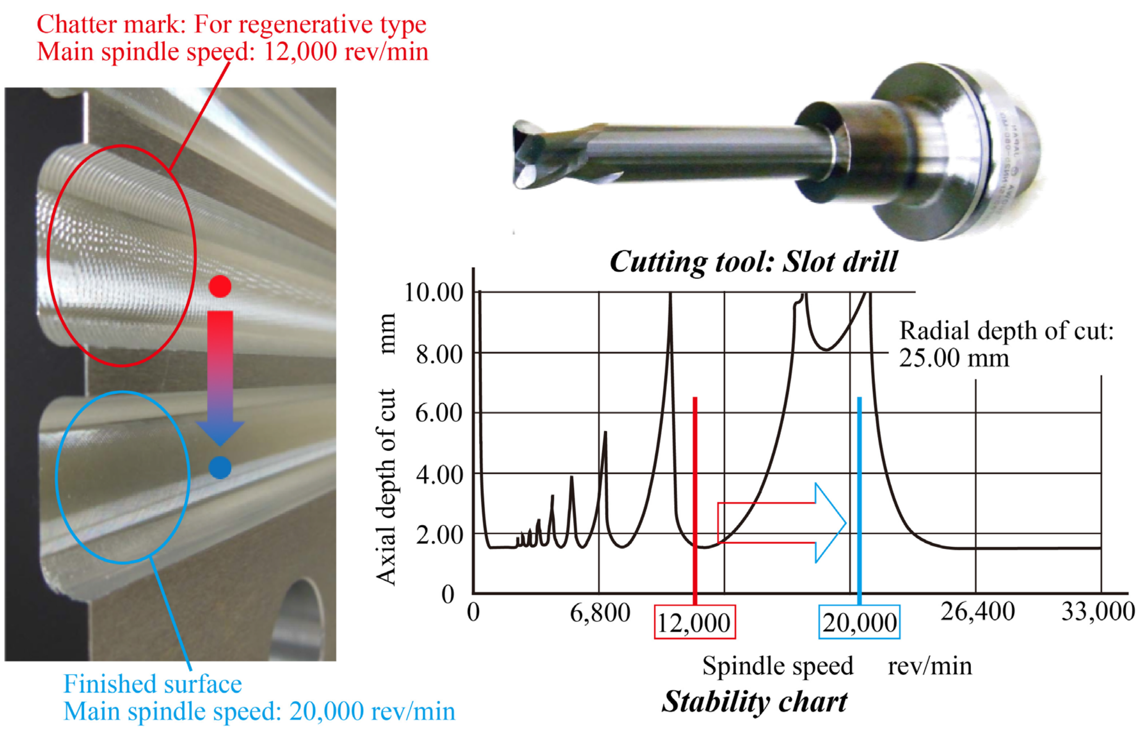

Fig. 4.1 Representative chatter mark for regenerative type

confidentiality. Against this context, the Editor can obtain fortunately some examples of the chatter marks from the publicized material as follows, although being not enough information, but rough ones to discuss something necessary.

Figure 4.1 shows a typical chatter mark caused by the regenerative effect when the spindle speed is 12,000 rev/min. As can be readily seen from the stability chart shown in the bottom right of Fig. 4.1, we can suppress it by shifting the spindle speed from 12,000 rev/min to 20,000 rev/min (see left of Fig. 4.1).

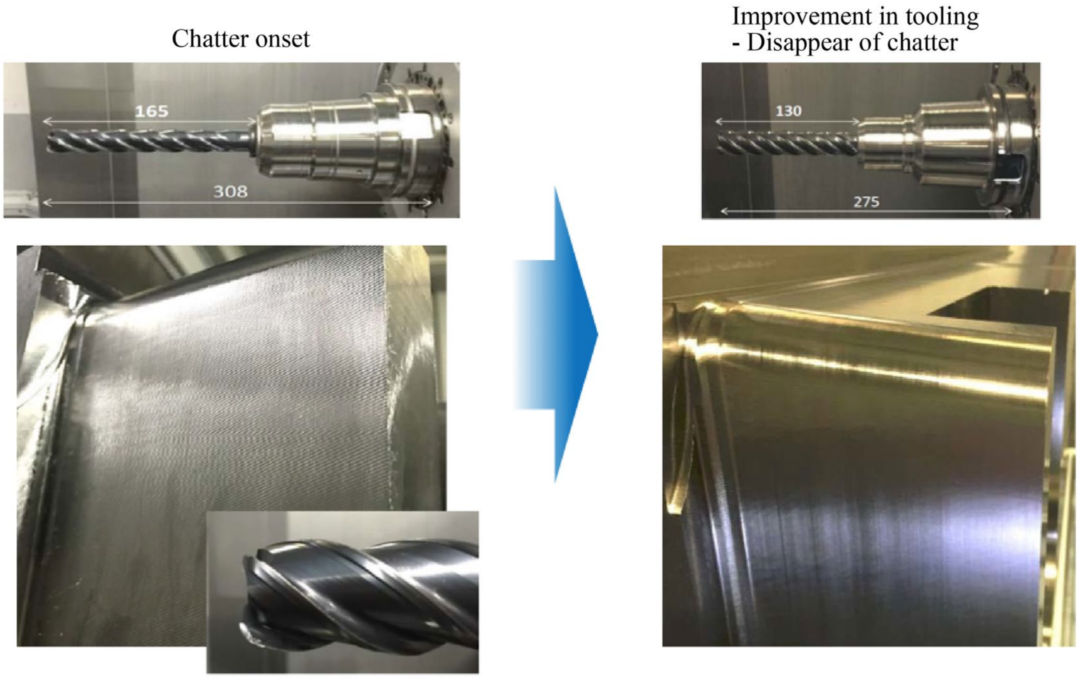

Fig. 4.2 Regenerative chatter mark mingling with beat-like cutter mark and its suppression

Figure 4.2 shows an interesting chatter mark, which may be regarded as a regenerative type mingling with the beat-like mark at certain interval in feed direction. Could be, such a chatter is derived from the influence of the excitation factor within the cutting mechanism, e.g. run-out of end mill, as implied by cutting tooth chipping. This suggestion may be supported by the fact: we can suppress such a chatter mark by changing only the cutting tool-tool holder system as shown also in Fig. 4.2.

Figure 4.3 shows a chatter mark observed in thread milling and its suppression by changing the cutting tool. More specifically, in the left of Fig. 4.3, we can observe the chatter mark, which is generated by a synergy of the torsional and bending vibrations, and in which the crown-pleat-like mark may correspond with the torsional chatter as similar as that generated by the cutting edge while twist-drilling the pocket hole (Roukema and Altintas, 2006). In contrast, in the right of Fig. 4.3, we can observe the suppression of the torsional chatter, but still the aftermath of the bending chatter, although reducing the vibration amplitude.

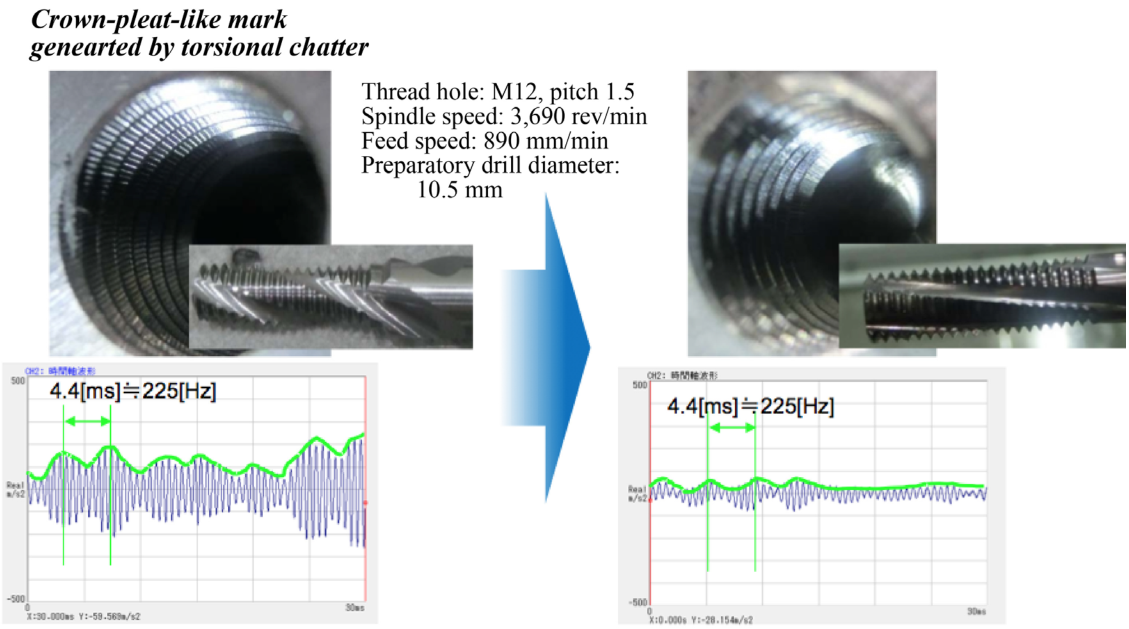

Reduction of bending chatter: Frequency 225 Hz

Natural frequencies of main spindle-tool system: 1,750 and 1975 Hz

Fig. 4.3 Chatter mark generated by synergy of torsional and bending vibration

Admitting that we can identify, in certain cases, the chatter pattern from the chatter mark, we can observe, in contrast, unfamiliar chatter mark with prevailing the higher-speed machining and also growing demands for machining of difficult-to-machine material like heat-resistance steel. Fig. 4.4 shows such a chatter mark, which consists of blur-like and beat-like marks along with large burr at disengagement of the end mill and the beat-like mark appears at certain interval as indirectly proven by the fluctuation of the cutting force. Importantly, there are no apparent chatter marks indicating that related to the regenerative type.

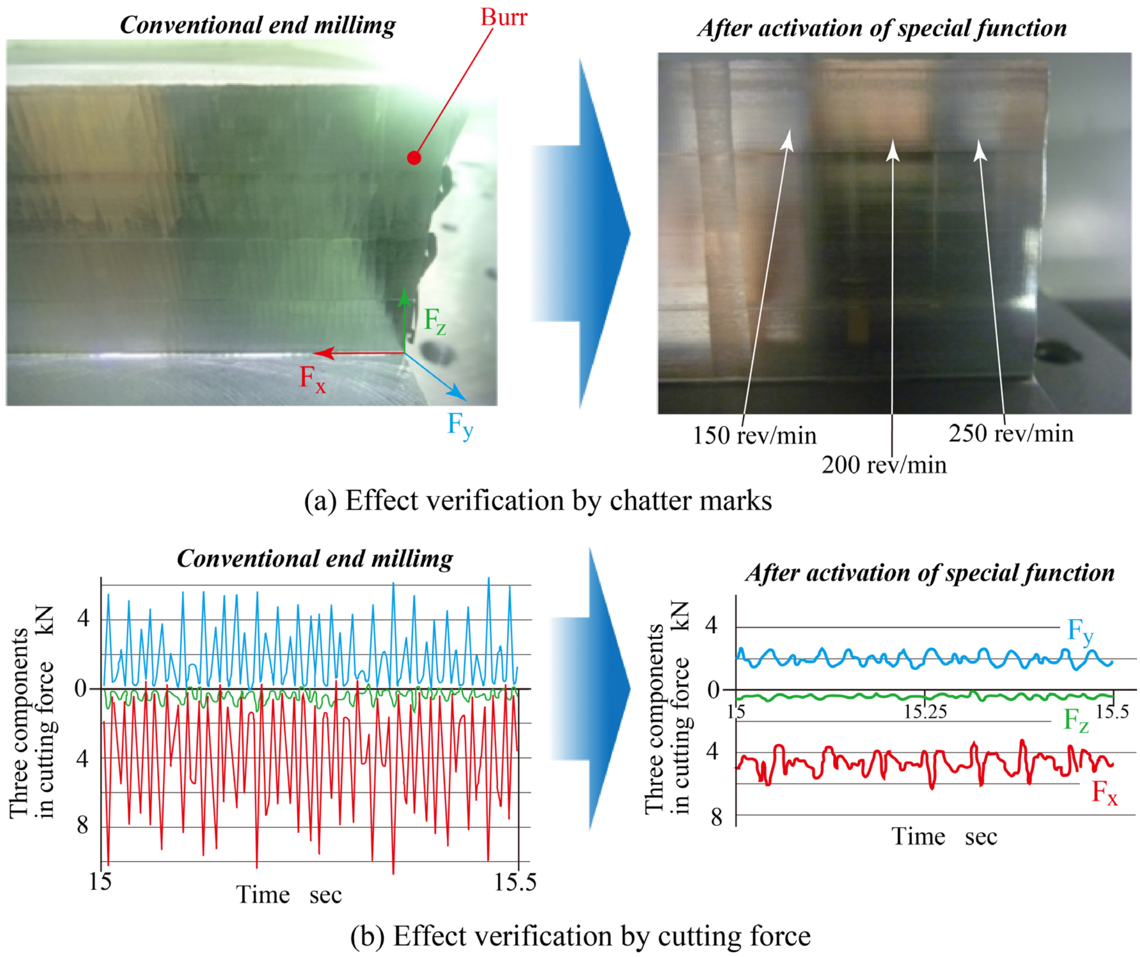

End mill: 5-flute and 80 mm in diameter with sintered carbide insert

Fig. 4.4 Effect of special function for chatter suppression while end milling

More importantly, the chatter can be suppressed by a special function integrated within a machine tool itself (no information because of company's confidentiality): however, it seems that there remains the disturbance in the cutter mark and the small fluctuation of the cutting force. Thus, it is necessary to investigate what is the essential feature of the fluctuation of the cutting force, e.g. either dynamic component of the cutting force in stable milling (see Fig. 3.12) or cutting force corresponding with the blur-like chatter mark.

4.2 A Proposal for Troubleshooting to Identify Chatter Patterns

Figure 4.5 demonstrates one of the typical evidences in the chatter suppression remedy at the factory floor. As can be seen from it, we try, in general, the chatter suppression by relying only the qualitative and simple data, e.g. vibration amplitude, and also employing a simple remedy with the cheaper cost, e.g. change of the cutting tool. In fact, the chatter can be suppressed by only changing the slot drill of two-flute type to that of three-flute type, and the engineer and technician in concern don't conduct any further activities.

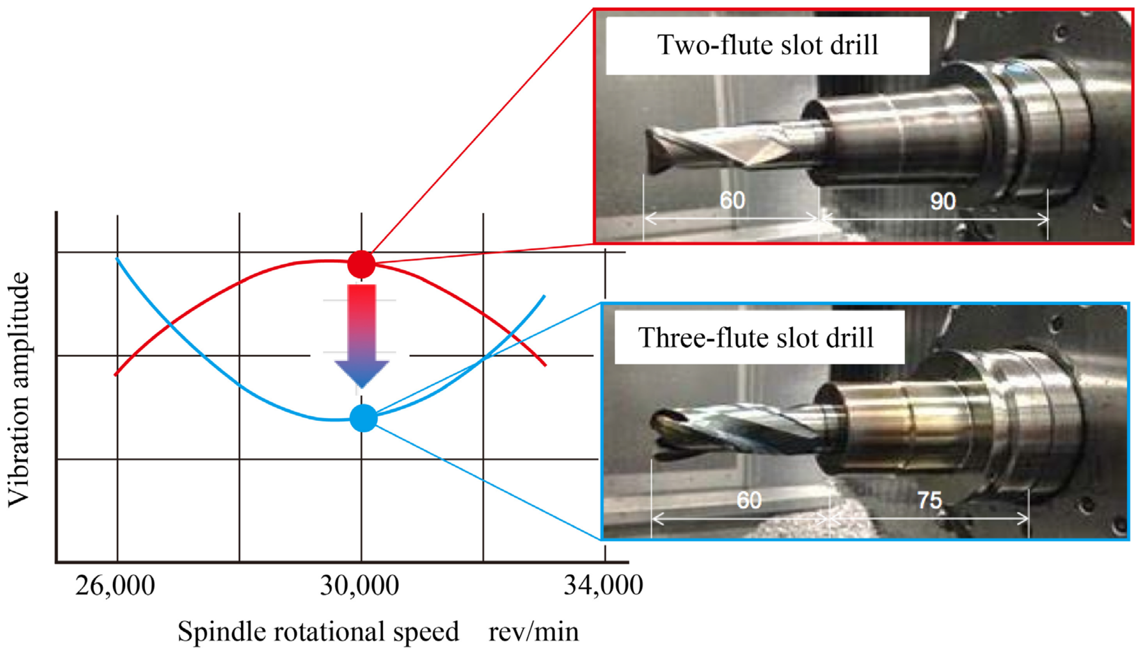

Fig. 4.5 A suppression remedy by changing cutting tool

It is however recommendable to pursuit the causality of the chatter together with identifying its pattern. On such an occasion, it is very useful to use the trouble shooting method by referring the chatter mark being observed to the model pattern (reference chatter mark).

In this context, it is furthermore desirable that we will be able to indicate a correlation between the chatter mark and the cutting tool preferably facilitating the chatter suppression in practice; however, nearly all the cutting tool manufacturers advertise, in general, only the effectiveness of their products to suppress the chatter without any guidance for the corresponding chatter pattern. Of course, in the case of the milling cutter of irregular tooth pitch type and with differing helix angle, we can identify such a correlation without any problems.

Now let us discuss this issue by taking some sample cutting tools demonstrated at JIMTOF (Japan International Machine Tool Fair) 2018. In the discussion, it is better to use a linkage diagram, which can delineate the close tie among the cutting tool, its characteristic features, and chatter pattern possible to suppress together with the suppression principle to certain extent.

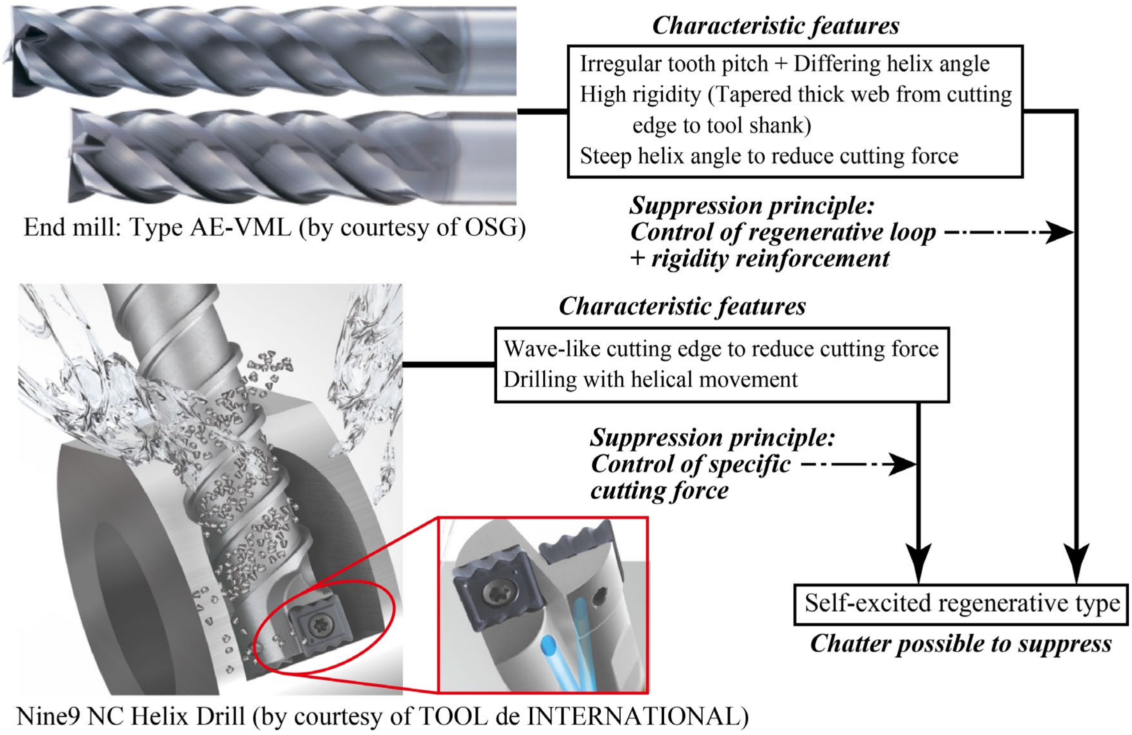

Fig. 4.6 Linkage diagram for visualizing close tie among cutting tool, its characteristic features and chatter pattern possible to suppress (1)

Figure 4.6 shows a representative case study on the end mill and slot drill, and as can be seen from Fig. 4.6, these cutters can facilitate the chatter suppression in accordance with the self-excited chatter theory of regenerative type. More specifically, the former controls the regenerative effect together with rigidity reinforcement, whereas the latter controls the specific cutting force by the wave-like cutting edge as similar as that shown in Fig. 2.7. It is furthermore notable that we may expect the reduction of the run-out in the end mill by the tapered web while rotating higher-speed, although the manufacturer does not pay any attention to it.

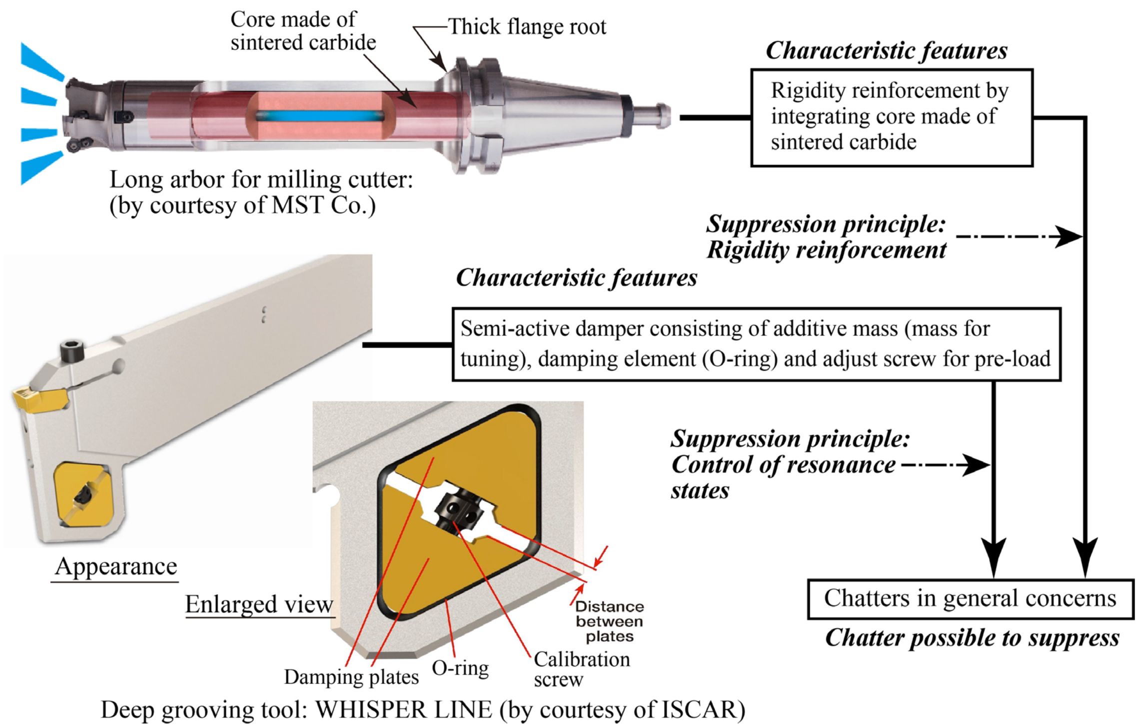

Fig. 4.7 Linkage diagram for visualizing close tie among cutting tool, its characteristic features and chatter pattern possible to suppress (2)

In contrast, Fig. 4.7 shows two cutting tools, which are for generalized remedies to chatter, and thus it is difficult to identify their utmost effective chatter pattern. More specifically, the long arbor can increase its rigidity by integrating the core made of sintered carbide and shaping the thick flange root, and thus is expectable to suppress the vibration in general. At present, the long arbor is for the milling cutters of 50 ~ 100 mm in diameter. In retrospect, Giddings & Lewis employed once the boring bar inserted partly the sintered carbide as shown in Fig. 2.1 in the 1960s, and obtained the fruitful result, although such a boring bar was very expensive on that occasion.

As similar as the long arbor of MST-brand, the deep grooving tool with semi-active damper is one of the very popular remedies for the chatter suppression. In this case, it is very interesting that we can adjust the damping capacity on-site by controlling the pre-load between the O-ring and the "Damping plates (mass for tuning)" by the calibration screw (adjust screw) as can be seen from the bottom left of Fig. 4.7. In deep grooving tool, furthermore, we must be aware of its extreme effectiveness for suppressing the vibration with higher frequency as suggested elsewhere; however, the manufacturer does not care about it nevertheless one of the valuable information for advertisement.

Admitting that the tool manufacturer has often contrived the innovative tool for the chatter suppression, as exemplified above, the manufacturer does not delve into the potential function and performance of the developed tool and may lose the obtainable benefits. For example, Walter has contrived a new drill made of sintered carbide (Type Advance DC 160), in which the main stresses are placed on (1) a new thinning method, i.e. could be a variant of XR type, (2) the double-margin for better guiding, (3) the innovative two-layered coating by TiSiAlCrN and AlTiNi and (4) 140 degree in point angle. As a result, the cutting force reduces considerably and the drill guiding accuracy is improved to some extent, resulting in the better hole-location accuracy.

Intuitively, we may, as will be clear from above, expect the reduction of the specific cutting force duly resulting in the suppression of the torsional chatter, which was shown, for example, in Fig. 4.3, together with less bending chatter. We must thus examine whether such suppression is functioned or not.

Now let us discuss what is a desirable trouble shooting method. As will be clear from Figs. 4.1 ~ 4.4, a method enables first the chatter pattern to be identified from the chatter mark, and then as shown for example in Fig. 4.6, one of the recommendable cutting tools should be selected by using the reverse flow in Fig. 4.6.

Caused by only regenerative effects
Regenerative effects + Forced excitation within machining mechanism (run-out of tool at higher-rotational speed, impact at tool engagement, generation of saw-like chip)
Regenerative effects + Parametric vibration, e.g. work held by three-jaw chuck, cutting with two-flute slot drill (directional orientation in stiffness)
Blur-like mark or/and beat-like mark
Difficult-to-identify mark or unknown marks

Table 4.1 Various chatter marks possible to observe in 2010s

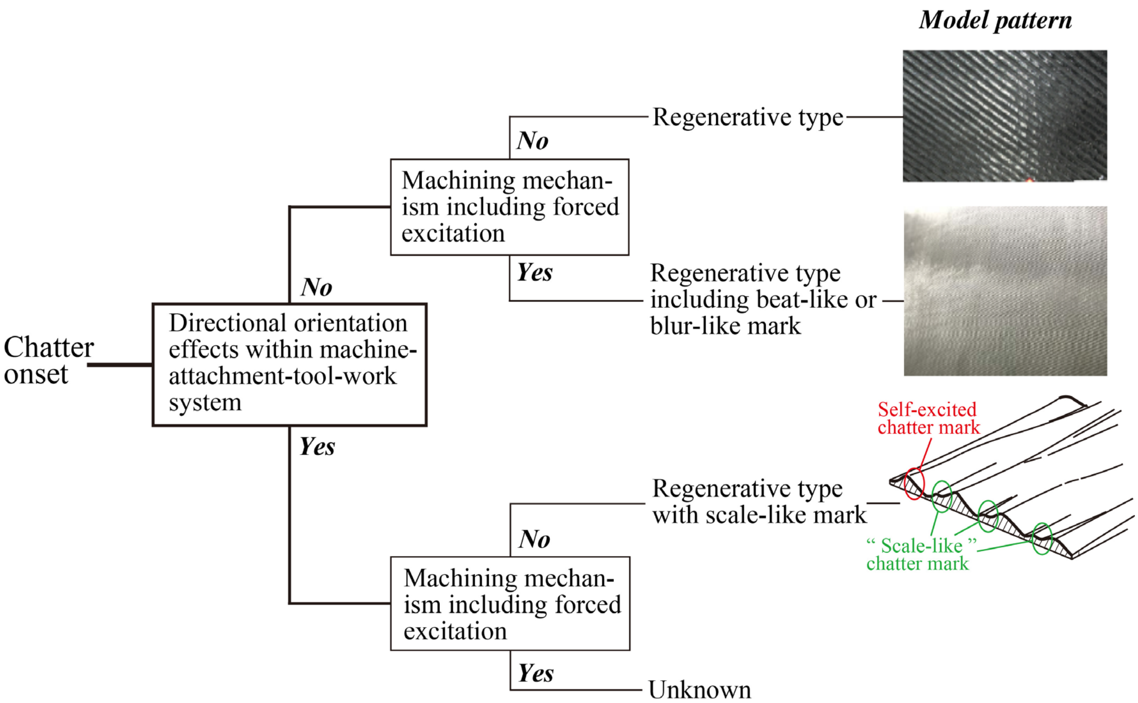

Fig. 4.8 A proposal for trouble shooting of chatter in metal cutting

More specifically, we may classify the chatter pattern on the strength of the factory floor experience as shown in Table 4.1, which can be also deduced from Part I, and simultaneously we can propose a flow of trouble shooting as shown in Fig. 4.8, although it is far from completion. Paraphrasing, at burning and crucial issue at present is to establish such a trouble shooting method by accumulating further knowledge about the correlation between the chatter mark and its causality.

To this end, the Editor suggest an attractive research into the observation of *the chatter mark generated around the chatter onset while face milling with full cutter width*. As can be readily seen from Fig. 2.11, it is very interesting to observe what is differing feature in the chatter mark while up-cut and down-cut modes within one revolution of the cutter.

References

Roukema J C, Altintas Y. (2006) *Time domain simulation of torsional-axial vibrations in drilling*. Inter. Jour. of machine Tools and Manufacture; 46: 2073-2085.

Chapter 5 Statistical Dynamics - Analysis of Machining Systems Operational Conditions

In this chapter the subject of statistical dynamics are discussed and non-parametric and parametric models for machining system identification are derived. The common characteristic for all discussed models is that they may be used for computing the operational dynamic parameters (ODP) of the closed loop machining system. Though the input to these models originates from the machining operations, not all models can be implemented for real-time identification. Generally, non-parametric models may be used solely for off-line identification, i.e., first recording the vibration signal from machining operations and then analysing the signal and identifying the nature of the excitation. Parametric models implemented in recursive algorithms are used for real-time identification of machining systems dynamic characteristics.

The main objectives of the chapter are: (i) the development of parametric and non-parametric models based on identification techniques with the purpose of integrating into a single step within the estimation of dynamic parameters characterising the machining system, (ii) in non-parametric identification, implementing techniques for ODPs and random excitation estimation, (iii) in parametric identification, the development of the recursive computational model of the machining system based on the data obtained during the actual operational regime. Through these contributions, a step is taken beyond the classical approach to analyse the dynamics of a machining system by separately identifying the structural and process parameters. In the proposed process, the two substructures, tool/toolholder and workpiece/fixture, are coupled, in addition to the open loop (elastic structure of the machine tool), by a feedback loop closing the energy loop, through the thermoplastic chip formation mechanism. The machining system can only be completely analysed only in closed loop i.e. in operational conditions since specially designed off-line experiments with controlled input, such as modal testing, give the response from only the open loop.

5.1 Introduction

In the modern manufacturing environment, high productivity and quality are key requirements for competitive production. As the metal removal rates and the quality of machined surfaces are impaired by vibrations, a critical issue in the art and science of machining technology is to control the machining system dynamics.

Even if the technology of virtual manufacturing is steadily growing in the production environment, experimental investigations of dynamic systems still play a key role because they provide valuable information to production engineers concerning the influence of process modification on the system's performance, the prediction of failures in the system and support for the maintenance of the production systems.

Generally, a machining system represents a closed-loop system with the machine tool's mechanical structure in the main loop and the machining process dynamics in the feedback loop. From dynamics point of view, the machining system can be characterized by the modal characteristics of the joint system. We denote these modal parameters by operational dynamic parameters (ODPs), as they represent the parameters of the joint machine tool structure and cutting process, respectively (Archenti and Nicolescu, 2009 and Archenti, 2011. The modal parameters in this respect are the operational frequency and damping and corresponding terms of operational mass and stiffness.

The most important scientific issue considered in machining dynamics is probably the analysis of self-excited vibrations or chatter. This topic has attracted the scholars' attention for over 100 years. Taylor stated in 1907 that chatter is the "most obscure and delicate of all problems facing the machinist" (F.W. Taylor, 1907). Even though the machining process should always be run free of chatter, the analysis of chatter as a non-linear phenomenon is considered essential in the theory of machining system dynamics. The interest resides especially in studying the intricate interaction of the internal parameters of the machining system and a comprehensive understanding of their motion regulation is beneficial for optimising the design of machining systems. Many analytical, numerical and experimental methods were developed in this field (e.g. Tlusty [1954], Tobias [1965], Tlusty [1983], Rahman and Ito [1986], Altintas and Budak [1995], Insperger and Stepan [2002], Budak and Tunc, [2010], Quintana [2011]).

The theory of self-excited vibrations, and consequently of machining system chatter, has experienced significant progress in the last decades. H. Poincare founded in the 19th century the nonlinear dynamics theory that has greatly advanced with the rapid development of the calculation technique and the important contributions of many scientists as the Hopf bifurcation theory that is extensively used to analyse various self-excited vibrations (Wenjing Ding, 2010).

Chatter in machining has detrimental effects on the quality of the parts and on the safety of the operations; parts incused even slightly by chatter marks have to be discarded. In other fields of physics, though undesirable, self-excited vibrations are tolerated within certain limits as for instance in aeromechanical systems (flutter, aircraft flight dynamics) and aerothermodynamics (flame instability), in fluid dynamics, – known as Kármán vortices, in dry friction in many mechanical situations, and so on. The core part of the theory of chatter is concerned with methods of predicting the stability of equilibrium and deducing stability criteria.

The motivation of the study presented in this chapter is the development of methods for real time analysis of the dynamics of machining systems, i.e. the computation of the operational dynamic parameters. The focus is on the theoretical and practical aspects of the parameter identification of the closed loop machining systems. Generally, the parameter identification of dynamic systems belongs to the field of statistical dynamics. As we will later demonstrate, the benefit of parameter identification is twofold: (i) it gives an efficient method to represent, by a synthetic model, the machining system in operational conditions and (ii) it offers a robust stability criterion that is inferred from the equivalent physical model. By this approach, cumbersome estimation of system stability by independently studying the machining system's constituent parts is avoided. In addition, the parameter identification method provides means to separate the sources of vibration, which supports implementation of robust technologies for vibration suppression. The identification of the machining system considered in this chapter is based on both non-parametric and parametric models (autoregressive-moving average, ARMA). Therefore, a central part in this chapter is the relation of this Markovian representation of a stationary stochastic process to the autoregressive moving average (ARMA) models.

The chapter is organised in three parts. In the first section, in the view of statistical dynamics, a linear Langevin equation for a stationary stochastic process is derived under the assumption of the Gaussian Markov process with the whiteness of random force excitation. The transition probability density function is demonstrated to be a solution of the Fokker-Planck-Kolmogorov (FKP) equation. The transition probability density function is used to construct a criterion for the discrimination between forced and self-excited vibrations, i.e. detection of the stability border. This forms the nonparametric representation of the stability criterion. In the second section, for parametric identification, the stochastic process of the system is constructed and described by an ARMA (autoregressive moving average) model. Practical implementation of the discrimination algorithm in mechatronic systems for machining operation milling and turning are exemplified through this chapter. The chapter presents a unified theory originating from the Markov processes for both nonparametric and parametric approaches. The structure of the chapter is illustrated in Fig. 5.1.

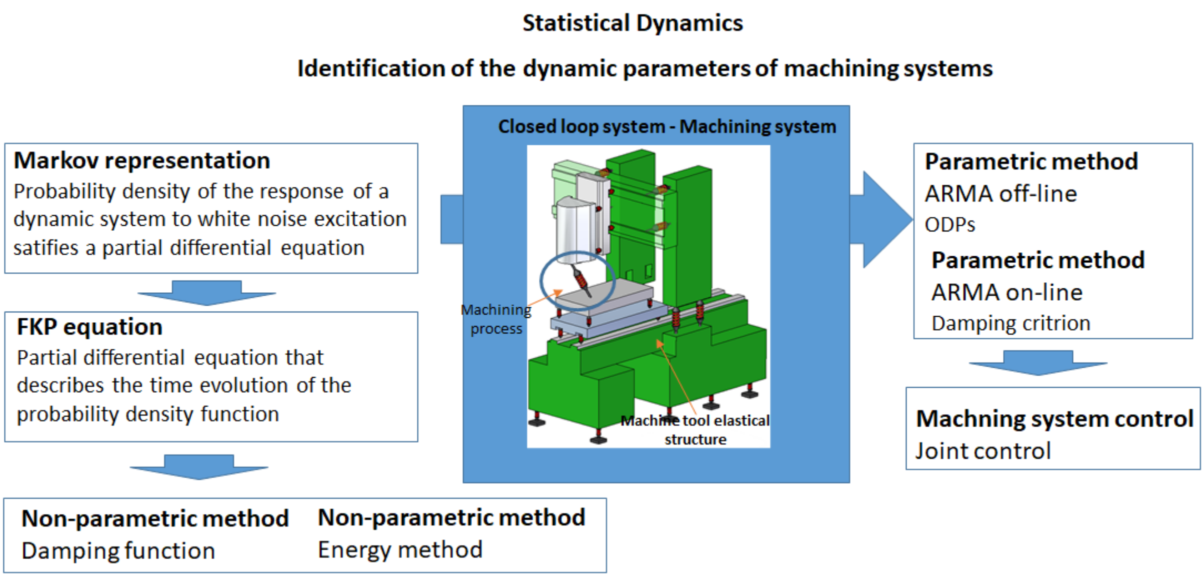

Fig. 5.1 Structure of the chapter

5.2 Statistical Dynamics

The excitations that occur in many dynamic systems are of a random nature and cannot be described adequately by the deterministic function of time (Nicolescu, 1996). An adequate description of excitation, and therefore of the response of the system to such excitation has to be developed within the framework of the statistical dynamics theory. Statistical methods are widely used for the analysis of the dynamic phenomena. Statistical dynamics as a general discipline examines various random phenomena in dynamic systems. The use of statistical models opens the possibility to extend the analysis to the real response of the dynamic systems. There are three main groups of problems where statistical dynamics find applications (Svetlitsky, 2003):

i. The first group consist of problems in which the scope is to estimate the response level of a system exposed to random excitation, and to study the dependence of the response level on different parameters.

ii. The second group of problems belongs to the reliability theory with a typical example of “the first-passage time”, which deals with prediction of the probability that during a given time interval (response of a dynamic systems) will stay within a given admissible domain.
iii. The third field of applications of statistical dynamics is concerned with the identification of dynamic systems. In machining systems, the parameters of the system cannot be precisely estimated from off-line experiments. In the case of a machine tool structure interacting with the cutting process, the correct model of the system can solely be based on the data from real machining tests.

When applying identification methods for modelling dynamic machining systems, the input itself is not measurable (observable) and only the response to a random input can be measured. The field of application of statistical dynamics that is the focus in this chapter is related to two concepts: (i) identification and (ii) classification of the response of dynamic systems.

The term identification refers to the formulation of a mathematical model of the dynamic system based upon on-line signal measurements of system response, and belongs to a class of inverse dynamic problems encountered in various technological fields (Ljung, 2006). The classification term aims to determine, from the model, a function to characterise the nature of the system’s response, i.e., whether $x(t)$ represents a forced/free vibration response or if it is a self-excited vibration. The problem of identification and classification of a system’s response to find the border between the random forced vibration and self-excited vibration is the key issue for the evaluation of the stability boundary in operational conditions. The response of the system to a broadband random force will be a nonzero steady-state signal both in stable and in unstable state.

Special problems of so-called qualitatively and semi-qualitative identification are of special importance in studying dynamic stability of machining systems. The qualitatively identification implies that the discrimination between different types of dynamic systems is based on the statistical analysis of measured response. The solution to this problem should precede the estimation of system parameters, i.e. quantitative identification. The results of a qualitative identification may be of direct practical importance, for instance for developing of methods for the analysis and control of self-excited vibrations (e.g. chatter in machining, flutter in aerodynamics and Kármán vortex in fluid dynamics). The term semi qualitative identification is used for those problems in which only few key parameters are sought. The results from qualitative identification can be used to detect chatter vibrations of machining systems from its measured random response. Algorithms for chatter detection may be used for selection of machining parameters to avoid instabilities of chatter type (Archenti, 2011).

From the dynamics of a machining system point of view, there are two main objectives, (i) the identification of the system's response and (ii) the prediction of the stability limit. With respect to the first issue, the lack of qualitative criteria for evaluation of a machining system´s dynamical behaviour led to extensive use of Fast Fourier Transform (FFT) analysis for a relative comparison of signals recorded during machining. Quantitative analyses are then performed to detect whether or not chatter occurs. As these analyses are based on the signal's amplitude measurement at certain characteristic frequencies, they are relative in their nature and consequently lead to subjective decisions. The problem of discrimination between random forced vibrations and self-excited vibrations is a key issue for the evaluation of the system's stability boundary in operational conditions. The response of a dynamic system to a broadband random excitation will be a nonzero steady-state signal both in stable and in unstable state. In case of self-excited vibrations, the excitation persists even in the absence of the random excitation (Blankenship, 1978). This is an important issue in computing the border separating the self-excited and forced vibration in operational conditions because this determines the control strategy that may be implemented to reduce or cancel the vibration. Following this methodology, control algorithms can be directly implemented in mechatronic devices for identification and control of system stability.

Regarding the second problem, the main techniques used today are related to a judicial (limits are not absolute) use of "stability lobes" to find relatively stable operating regimes (Rivin, 2002). The traditional evaluation of machining system's dynamic behaviour has invariably been approached in the following steps (Brecher, 2009 and see Fig. 5.2):

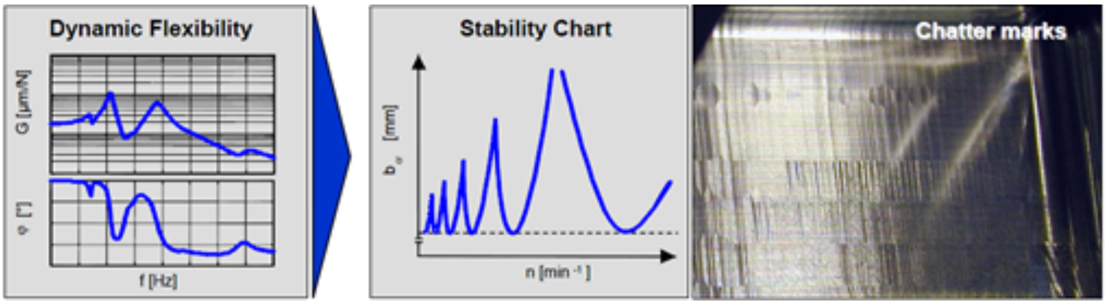

(a) (b) (c)

Fig. 5.2 Analysis of the dynamic behaviour of the machining system: (a) Extraction of dynamic parameters of the elastic structure, (b) Stability charts, (c) Chatter marks as a result of dynamically unstable machining

1. Identification of the dynamic properties of the elastic structure of machine tools. Generally, this step is done experimentally often using experimental modal analysis (EMA).
2. Identification of the characteristics of the cutting process, i.e. the dynamic parameters describing the transfer function of the subsystem represented by cutting process dynamics
3. Evaluation of the stability lobe diagram of the machining system from step 1 and step 2.

Because the evaluation of dynamic stability and of modal parameters, carried out following the above approach, does not take into consideration the actual operational conditions, the results have limited applicability.

Take for instance a 5-axis milling machine, in which the tool follows a complex 3D trajectory, and where the modal direction of the machine tool depends upon the relative orientation of the cutting tool and the workpiece. This situation is difficult to adequately capture with traditional EMA techniques, as the receptance is customarily measured in two orthogonal directions. Furthermore, the classical methodology described above makes use of external forces that are of a different nature than cutting forces. The separation into the two subsystems does not take into consideration the mutual interaction between the two subsystems in real operations. In order to do this, it is necessary to monitor and analyse the real system in full operation. Design and measured data could then be put together to make a realistic digital model of a physical machine system individual, that could be used as input in machining simulation software to find the root causes of stability problems. Also, in the classical methodology, straight paths of the cutting tool have to be adopted since the stability limit is detected by gradually increasing the depth of cut. This makes it in many situations inapplicable in the case of workpieces with complex shapes.

From a dynamics point of view, a machining system (MS) is formed by two interacting subsystems; the mechanical structure of the machine tool and the cutting process. In the absence of the process, the MS represents the structural open loop between two substructures, tool/toolholder and workpiece/fixture, through the machine tool structure, e.g. columns, bed, movable and fixed parts, see Fig. 5.3 (a). With the process considered, the two substructures, tool/toolholder and workpiece/fixture, are coupled, in addition to the open loop, by a feedback loop closing the energy loop, through the plastic chip formation mechanism, see Fig. 5.3 (b). As the operational behaviour of the system is described by the interaction between process and machine, the system can be complete analysed only in closed-loop since specially designed off-line experiments with controlled input, such as modal testing, give the response from only open-loop.

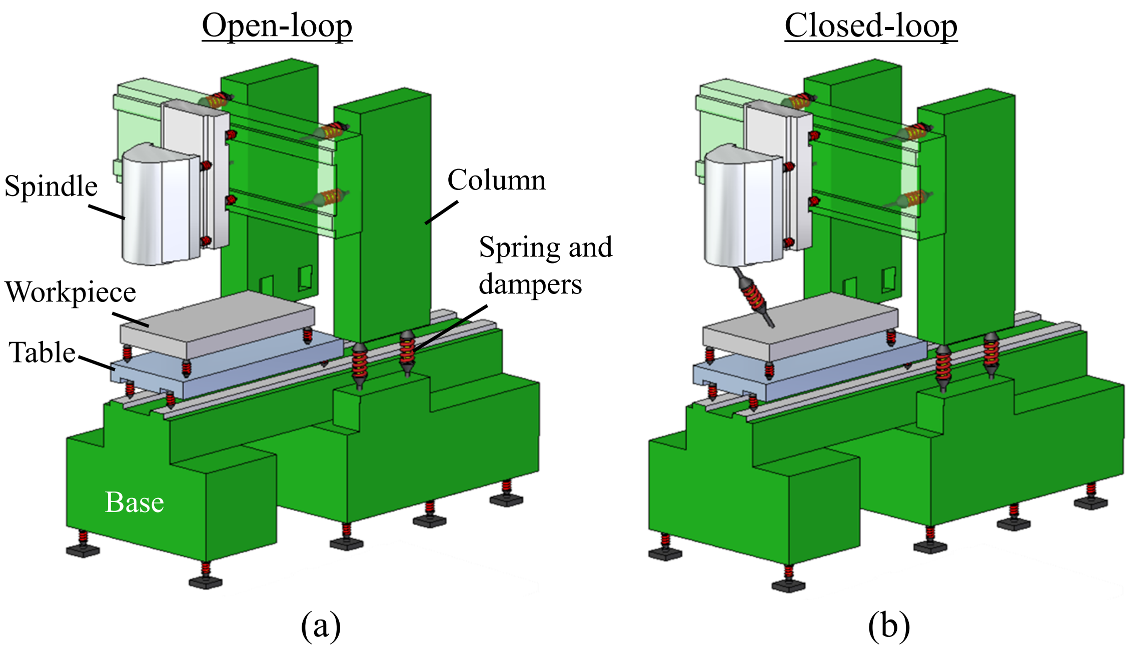

Fig. 5.3 Machine tool represented as an open-loop system (a), and closed-loop system (b)

5.3 Random Processes

Problems are only considered in this chapter where the systems response to a random excitation can be observed. This may be a case of the machine tool structure interacting with the cutting process. In this case the input excitation is not measurable. A force sensor does not measure the input excitation but some complex response that is transmitted through the structural path from the tool – workpiece interface to the sensor location. This signal is partly attenuated on this path and partly amplified by the local structural resonances resulting in signal behaviour of a random nature (Archenti, 2010). In machining, there are many mechanisms that contribute to the random excitation, among others the dynamic variation of the contact workpiece – cutting edge and the intermittent engagement of the multi-tooth cutter of impulse nature. This, in combination with the dynamic variations of the material flow on the cutting edge, leads to a broadband frequency excitation of the machine tool structure.

Real dynamic systems that possess some inertia may respond only to a limited range of excitation frequencies, with very high input frequencies having practically no influence on the response. Therefore, if the excitation is broadband, with its spectral density close to a constant value within the bandwidth of the system (within the range of those excitation frequencies to which the system may respond significantly), then the response of the system will be the same as to white-noise excitation.

An adequate description of random excitation, and therefore of the response of the machining system to such excitation, must be developed within the framework of the random process theory (Dimentberg, 2004). The adaptation of such a probabilistic point of view implies that some statistical characteristics of both the random excitation and the system's response to this excitation are considered.

The problem of identifiability of an autoregressive moving average process is demonstrated to be a complete solution of the Markovian representation of the process.

5.4 Markov Process

A function or process X(t) is called random if its values are random variable (Chua, 2005). The argument t is considered to be deterministic and it is interpreted as time. It is well known that a basic characteristic of a random variable X is its cumulative probability function

$$F(x) = P(x < X) \qquad (5.1)$$

where P(x<X) denotes the probability of the event (x>X) or the probability density function

$$p(x) = \frac{dF}{dx} \qquad (5.2)$$

For a random function or process such a representation will not be complete in general. The complete description of a random process X(t) is available through the infinite-dimensional probability density $p(x_1, x_2, ..., x_n)$, where n tends to infinite. Since this complete representation is not possible it is important to develop various models for the random process, which permit the expression of the infinite-dimensional joint probability density (or its corresponding joint cumulative function) in terms of a finite series of functions. One such model that is of practical importance to our approach is the Markov random process.

Among other methods such as Statistical linearization (Kazakov [1954, 1955], Sawaragi [1962], Nogouchi [1985], Harrison and Hammond [1984]), Equivalent non-linear equation (Caughey [1986], Cai and Lin [1988]), Perturbation and functional series (Crandall [1963], Manning [1975], Roy and Spanos [1990]), it has been demonstrated that the response of dynamic system to broadband random excitation can be accurately represented in terms of Markov processes. The state transition probability density function for such processes is governed by the Fokker-Planck-Kolmogorov (FPK) equation known as the forward diffusion equation (Mohanty [1986], Gardner [1994]). A continuous Markov process is defined in terms of conditional probability density functions

$$p(x_n, t_n \,|\, \mathrm{x}_{\text{n-1}}, t_{n-1} ... x_{1,} t_1) = p_x(x_n, .t_n \,|\, x_{n-1}, t_{n-1}); t_n > t_{n-1} > ... > t_1 \qquad (5.3)$$

Assuming that $t_2 > t > t_1$ and x(t) is a stationary Markov process, then, the transition probability density function satisfies the Chapman-Kolmogorov-Smoluchowski equation (Sun Jian-Qiao, 2006; Stochastic Dynamics and Control, Elsevier)

$$p_X(x_2, t_2 \,|\, \mathrm{x}_1, t_1) = \int_R p_X(x_2, t_2 \,|\, \mathrm{x}, t) p_X(x, t \,|\, \mathrm{x}_1, t_1) dx \qquad (5.4)$$

For a random Markov stationary process which is both wide-sense Markovian and weakly stationary the correlation coefficient function

$$\rho_{\mathrm{XX}}(t-s) = \rho_{XX}(t-u)\rho_{XX}(u-s); t \le u \le s \qquad (5.5)$$

or

$$\rho_{\mathrm{XX}}(\tau) = \rho_{XX}(\varphi)\rho_{XX}(\tau - \varphi) \qquad (5.6)$$

Taking derivatives with respect to τ

$$\dot{\rho}_{XX}(\tau)=\rho_{XX}(\varphi)\dot{\rho}_{XX}(\tau-\varphi) \tag{5.7}$$

and upon setting τ = ϕ

$$\dot{\rho}_{XX}(\tau)=\rho_{XX}(\tau)\dot{\rho}_{XX}(0)=-\beta\rho_{XX}(\tau) \tag{5.8}$$

which, taking into account that $\rho_{XX}(0) = 1$, has the unique solution

$$\rho_{XX}(\tau)=\exp(-\beta\tau);\beta>0 \tag{5.9}$$

From expression (5.9) the auto-correlation function of the Markov process can be evaluated

$$R_{XX}(\tau)=\sigma_X^2\exp(-\beta|\tau|) \tag{5.10}$$

The Fourier transform of Eq. (5.10) gives the power spectra density with the variance σ^2 and the time constant β^{-1}.

$$S_{XX}(\omega)=\frac{\beta\sigma_X^2}{\pi(\beta^2+\omega^2)} \tag{5.11}$$

A Markov process, x(t), may be generated by the following stochastic differential equation (Polidori, 2000).

$$dx(t) = A(x(t))dt + B(x(t))L(t) \tag{5.12}$$

In the above equation, L(t) is assumed to be a Gaussian random force with zero mean and with δ-correlated noise

$$\langle L(t)\rangle=0;\quad \langle L(t)L(t')\rangle=q\delta(t-t') \tag{5.13}$$

where q is the intensity factor of the excitation and the angle brackets denote averaging. Eq. (5.12) is a first order Langevin equation (Mohanty,1986) and for B(x(t)) constant the equation is called Langevin equation with additive noise force

$$dx(t) = A(x(t))dt + \sigma L(t) \tag{5.14}$$

In the context of Brownian motion, x(t) is interpreted as the velocity of a particle moving in one dimension, and the Ornstein-Uhlenbeck, Beck (1987) theory introduces the damping force $A = -\alpha x(t)$, $\alpha > 0$

Because L(t) is a stochastic quantity, it follows that x(t) is a stochastic quantity too. Then, the essential problem is to find the probability distribution p(x). One way to describe the evolution of the probability distribution is by means of the Fokker-Planck-Kolmogorov (FPK) equation that, for one variable, can be represented in the following form (Risken, 1996).

$$\frac{\partial}{\partial t}p(x,t)=\left[-\frac{\partial}{\partial x}D^{(1)}(x(t))+\frac{\partial^2}{\partial x^2}D^{(2)}(x(t))-...\frac{\partial}{\partial x^n}D^{(n)}(x(t))\right]p(x,t) \tag{5.15}$$

where $D^{(1)}$ and $D^{(2)}$ are the drift and diffusion coefficients, respectively. The drift and diffusion coefficients can be calculated using Kramers-Moyal expansion (Van Kampen [1981], Ghasemi [2007]).

$$D^{(n)}(x,t)=\frac{1}{n!}\lim_{\tau\to 0}\frac{1}{\tau}\left\langle\left[x(t-\tau)-x(t)\right]^n\right\rangle \tag{5.16}$$

When the process x(t) satisfies an Langevin differential equation driven by a white noise excitation, the right hand side of Eq. (5.15) retains only the first two terms. In this case, the state transition probability density $p_X(x,t;y,s)$, $s < t$, of a Markov process satisfies the FKP equation

$$\frac{\partial}{\partial t}p_X(x,t|y,s)=-\frac{\partial}{\partial x}\left[A(x,t)p_X\right]+\frac{\partial^2}{\partial x^2}\left[\frac{B(x,t)}{2!}p_X\right] \tag{5.17}$$

The first term containing A(x, t) on the right hand side of Eq. (5.17) is again the drift term associated with the deterministic behaviour of the system, while the second term containing B(x, t) is the diffusion term due to the stochasticity of the excitation. Stationary solutions are obtained when the time derivative of the probability density vanishes. The solution to the FPK equation must satisfy the initial condition

$$\lim_{t\to\infty}p(x,t;y,s)=\delta(x-y) \tag{5.18}$$

where δ is the Dirac delta-function. It is possible to relate the drift and diffusion coefficients in the FPK equation directly to the parameters in, for instance, the stochastic dynamic equation that generates the Markov process

$$dX(t) = -\alpha X(t)dt + \sigma dL(t) \tag{5.19}$$

where α and σ are constants and L(t) is a unit Brownian motion described by Eq. (5.13). In this case, the coefficients of the FPK equation for the solution of the Markovian Process X(t) are evaluated as

$$\begin{aligned} A &= \lim_{\Delta t \to 0} \frac{1}{\Delta t} E\left[\Delta X \middle| X = x\right] = -\alpha x \\ B &= \lim_{\Delta t \to 0} \frac{1}{\Delta t} E\left[\Delta X^2 \middle| X = x\right] = \\ &= \lim_{\Delta t \to 0} \frac{1}{\Delta t} E\left[\alpha^2 x^2 \Delta t^2 - 2\alpha\sigma x \Delta t \Delta L(t) + \sigma^2 \Delta L^2(t)\right] = \sigma^2 \end{aligned} \tag{5.20}$$

The FPK equation is represented by

$$\frac{\partial}{\partial t} p_X(x,t|y,s) = -\frac{\partial}{\partial x}\left[-\alpha x p_X\right] + \frac{\sigma^2}{2}\frac{\partial^2 p_x}{\partial x^2} \tag{5.21}$$

The solution of the Langevin equation (Eq. 5.14) represents a Markov process, which implies that the joint probability density function of its components is described by an initial density function at time t_0 and the transition probability density function defining the conditional probability density function at time t given the values at time t_0. The solution to Eq. (5.19) expresses the Markov process X(t)

$$X(t) = x_0 e^{-\alpha t} + \int_0^t e^{-\alpha(t-s)} L(s) dt \tag{5.22}$$

5.5 Non-parametric Models

Let us now to extend the analysis to a second order equation of motion for a SDOF non-linear damping model

$$\ddot{x}(t) + D(E)\dot{x} + g(x) = W(t) \tag{5.23}$$

where D is the non-linear damping function with D(0,0) = 0, g(x) is a non-linear elastic force and W(t) is a white noise process with spectral density S_0,

$$\langle W(t)W(t+\tau)\rangle = 2\pi S_0\delta(t) \tag{5.24}$$

where the angle brackets denote expectation. This expression shows that the white noise is uncorrelated for any small finite time interval. This means that the future state of variables is independent of the past state being dependent only on the present state. This defines a Markov process.

If $U_x = \int_0^x g(\xi)d\xi$ is the potential energy function and D(E) is a function of the total energy

$$E(x,\dot{x}) = \frac{1}{2}\dot{x}^2 + U_x \tag{5.25}$$

The expression in Eq. (5.23) represents the force balance. Multiplying this equation by $\dot{x}(t)$ the energy balance equation is obtained

$$\frac{\partial E}{\partial t} = W(t)\dot{x} - D(E)\dot{x}^2(t) \tag{5.26}$$

where the first term on the right hand represents the energy introduced in the system, the second term corresponds to the energy dissipated.

The FPK equation for the Eq. (5.23) may be formulated according to

$$\frac{\partial p}{\partial t} + \dot{x}\frac{\partial p}{\partial x} + \frac{\partial}{\partial \dot{x}}\left[\left(-g(x) - D(E)\dot{x}\right)p\right] - \pi S_0\frac{\partial^2 p}{\partial \dot{x}^2} = 0 \tag{5.27}$$

The solution $p(x,\dot{x})$ of the joint stationary process $[x(t)\dot{x}(t)]$has been derived by Caughey (1964)

$$p(x,\dot{x}) = C\exp\left(-\frac{1}{\pi S_0}\int_0^E D(\xi)d\xi\right) \tag{5.28}$$

where C is a normalizing constant. The integral

$$d_1(E) = \int_0^E D(\xi)d\xi \tag{5.29}$$

designates the damping potential. In the special case of linear damping, D(E) = c, a constant, the solution of the FPK equation is

$$p(x,\dot{x}) = C\exp\left(-\frac{cE}{\pi S_0}\right) \tag{5.30}$$

From the general case represented by Eq. (5.23) there are some response distributions that can be developed. Let us now introduce two new variables (Roberts [1986], Iourtchenko, [2002]).

$$x = X\,sin(\omega_0 t + \varphi) \quad \text{and} \quad \dot{x} = \omega_0 X\cos(\omega_0 t + \varphi) \tag{5.31}$$

It can be seen that

$$X = \left(x^2 + \dot{x}^2/\omega_0^2\right)^{1/2}$$

$$\varphi = \arctan(\omega_0 x/\dot{x}) - \omega_0 t$$

In this transformation of variables, X is the amplitude envelope sequence and φ is the phase sequence. Then, Eq. (5.23) can be transformed into the following pair of equations

$$\dot{X} = \frac{1}{\omega_0}\left[-D(X\sin\theta, \omega_0 X\cos\theta)\right]\cos\theta + W(t)\cos\theta] \tag{5.32a)}$$

$$\dot{\varphi} = \frac{1}{X\omega_0}\left[D(X\sin\theta, \omega_0 X\cos\theta)\right]\sin\theta - W(t)\sin\theta] \tag{5.32b)}$$

Where $\theta = \omega_0 t + \varphi$. The corresponding Langevin stochastic differential equations for the amplitude X is

$$\dot{X} = -\frac{1}{\omega_0}d_1(X) + \frac{W_1(t)}{X} + W_2(t) \tag{5.33}$$

where $d_1(X)$ is averaged nonlinear damping function

$$d_1(X) = \frac{1}{2\pi}\int_0^{2\pi} D(X\sin\theta, \omega_0 X\cos\theta)\cos\theta d\theta \tag{5.34}$$

and

$$W_1(t) = \frac{\pi S_{ww}(\omega_0)}{2\omega_0^2} \tag{5.35}$$

S_{ww} is the spectral density. When the excitation is white noise then $S_{ww}(\omega_0)$ is S_0. $W_2(t)$ is white noise with intensity factor $2W_1(t)$.

It is obvious from Eq. (5.32) that the amplitude X(t) is uncoupled from the phase φ, i.e., the process X(t) is a one-dimensional Markov process with the transition density function $p(X, t|X_0, t_0)$ governed by the following FPK equation

$$\frac{\partial p}{\partial t} = \frac{\partial}{\partial X}\left\{\left[\frac{d_1(X)}{\omega_0} - \frac{W_1(t)}{X}\right]p(X,t)\right\} + W_2(t)\frac{\partial^2 p(X,t)}{\partial X^2} \tag{5.36}$$

If the random excitation is stationary, then the response will approach stationarity

$$\lim_{t\to\infty} p(X,t \mid X_0,t_0) = p(X) \tag{5.37}$$

and the stationary probability density w(X) of the amplitude process X(t) is governed by FPK equation

$$\frac{\partial}{\partial X}\left\{\left[-\frac{d_1(X)}{\omega_0} + \frac{W_1(t)}{X}\right]p(X)\right\} = W_2(t)\frac{\partial^2 p(X)}{\partial X^2} \tag{5.38}$$

which has the solution

$$p(X) = 2CX \exp(-F(X)) \tag{5.39}$$

where C is a normalizing constant and

$$F(X) = \frac{1}{\omega_0 W_1(t)}\int_0^X d_1(\xi)d\zeta \tag{5.40}$$

In the remaining part of this section, the non-parametric estimation of the system damping from the stochastic response based on the method describe above will be illustrated. In case of light damping, narrow band response to broad band excitation will result. This condition is primarily assumed when analysing the dynamic system described by Eq. (5.23). The slow variation of the energy that results following this condition forms the basis for the method of stochastic averaging. In the first step, a variable substitution is performed. The pair (X, φ) as described by Eq. (5.32) approaches a joint Markov process. The transition probability density function (p.d.f.) of the joint Markov process (X, φ) is governed by the FPK equation. It can be noticed that the amplitude X is uncoupled from the phase φ and the transition probability function of the amplitude X is governed by the FPK Eq. (5.36). By an accurate estimate of the p.d.f. p(X) from the response signal of the system excited by the broad band excitation, the function F(X) is calculated from Eq. (5.40).

$$F(X) = \ln(w(X)) - 2\ln(C) \tag{5.41}$$

and damping energy function $d_1(X)$ from Eq. (5.34)

$$\frac{d}{dX}G(X) = \frac{d_1(X)}{\omega_0 W_1(t)} \tag{5.42}$$

Finally, the damping in Eq. (5.23) is estimated from

$$H(X) = \int_0^{2\pi} \left[h(v\sin\theta) + vh'(X\sin\theta) \right] d\theta$$

as a solution to the Schlomilch's integral equation (Nayfeh, 1985).

The numerical simulation of Eq. (5.23) has been performed by using the Runge-Kunta method. For a linear viscous damping, D = 0.010 $\dot{x}$, the response and the amplitude square variation in time are illustrated in Fig. 5.4.

The estimation of the p.d.f p(X^2) from the system response is represented as a normalised logarithmic function and the corresponding linear interpolation function is shown as the function of amplitude square in Fig. 5.5. The fitted coefficients and goodness of fit statistics are shown in the caption below.

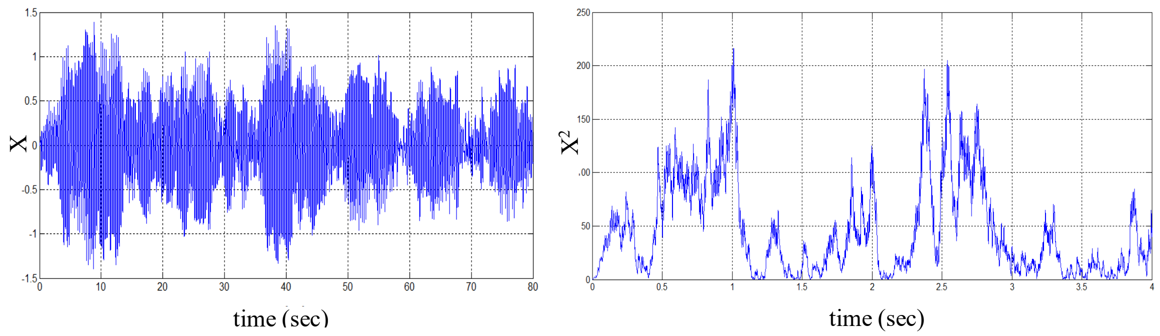

(a) (b)

Fig. 5.4 (a) Time response x(t) and (b) the square amplitude X^^{2}(t)

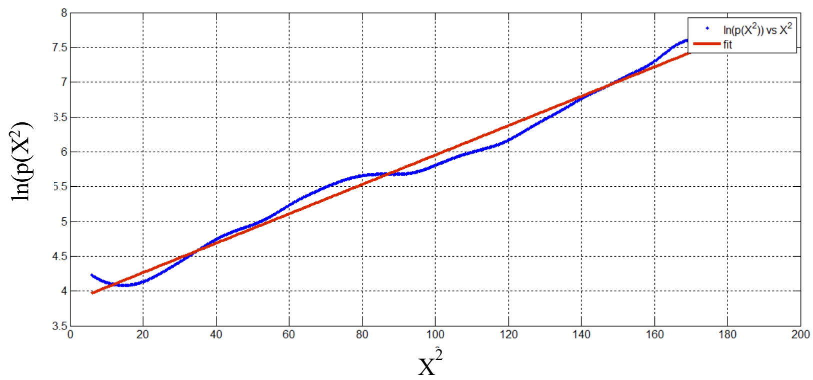

Coefficients with 95% Conf. limit p1 = 0.0211 (0.02093, 0.02127)

Goodness of fit: SSE: 11.23

R-square: 0.9876

RMSE: 0.1201

Fig. 5.5 Logarithmic p.d.f. of amplitude square and the linear fitting

The calculation of the damping value follows the above described steps

From F(X) = 0.0211X^2 and d1(X)= $\frac{0.0211}{2}X$

and the damping is estimated from the integral

$$H(X) = \int_0^{2\pi} \frac{0.02011}{2} v \sin\theta d\theta = 0.01055v$$

Similarly, the estimation of the damping characteristic for the simulation of Eq. (5.23) with damping 0.04 is illustrated in Fig. 5.6.

A summary over three linear damping estimates by fitting the logarithmic function of p.d.f of amplitude square and the corresponding interpolation function is shown in Fig. 5.7.

The procedure for identification of the damping characteristic from measured stationary response produces a very accurate estimate of damping characteristic for a linear case. In the next example the damping characteristic in Eq. (5.23) is represented by the dry friction damping D(E) = R sign($\dot{x}$). For three R values, 0.05; 0.1; and 0.2 the estimated results are presented in Fig. 5.8.

Coefficients (with 95% confidence limits):
p1 = 0.04104 (0.04072, 0.04136)
p2 = 3.183 (3.16, 3.205)
Goodness of fit: SSE: 17.9
R-square: 0.988

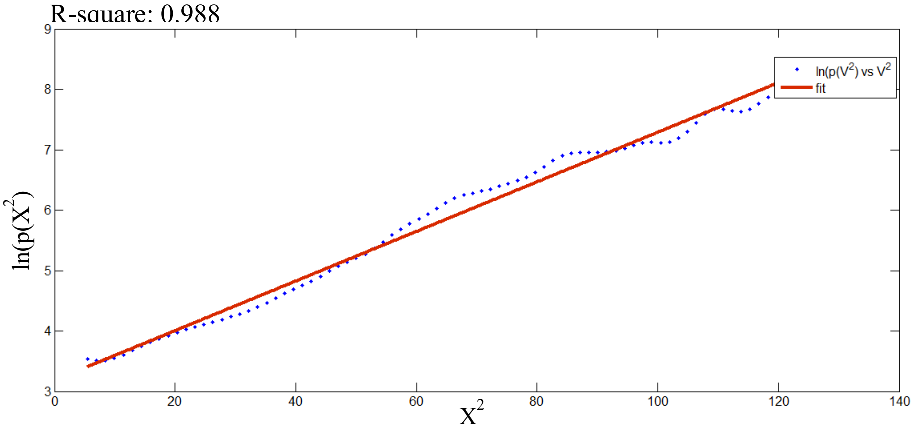

Fig. 5.6 Estimation of logarithmic p.d.f. of amplitude square for a simulation case with linear damping 0.04

ζth	0.01	0.02	0.04
ζest.	0.01055	0.02051	0.04104
Conf.	0.0104- 0.0106	0.02093, 0.02127	0.04072, 0.04136
Corr. Sq.	0.9876	0.988	0.988

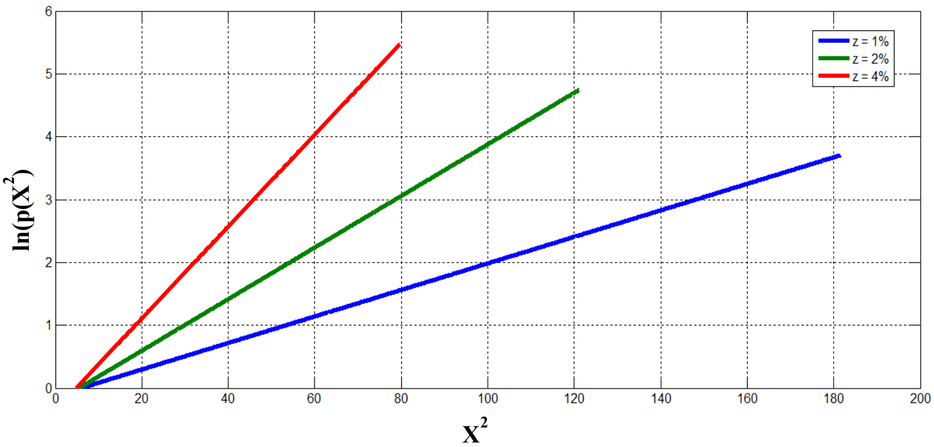

Fig. 5.7 Linear interpolation for damping 0.01, 0.02, 0.04

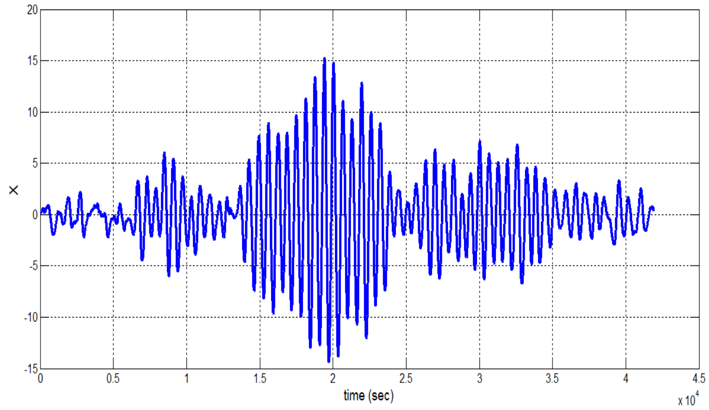

(a)

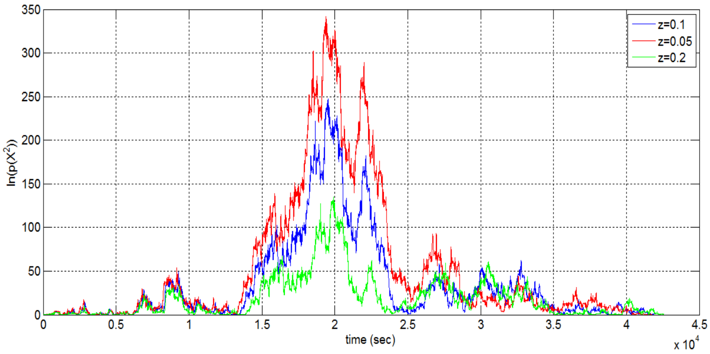

(b)

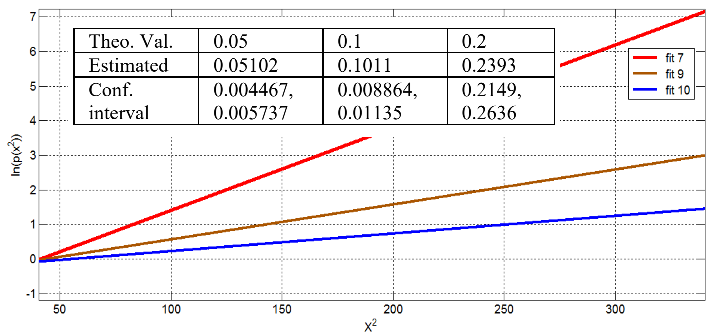

Theo. Val.	0.05	0.1	0.2
Estimated	0.05102	0.1011	0.2393
Conf. interval	0.004467, 0.005737	0.008864, 0.01135	0.2149, 0.2636

(c)

Fig. 5.8 (a) simulated system's time response; (b) amplitude square variation in time; (c) interpolation function of the logarithmic p.d.f. of square amplitude

From both the above examples the association between the logarithmic p.d.f. of the square amplitude and the damping estimate is apparent. Even for a dry friction damping case a good estimate of the damping characteristic can be noticed. Also, it can be observed that the higher the damping, the higher the fitting coefficient.

The operational damping identification is demonstrated from a signal recorded from a turning operation. The machining system's response during both stable and unstable processes is recorded and presented in Fig. 5.9 (a). The corresponding power density functions are illustrated in Fig. 5.9 (b).

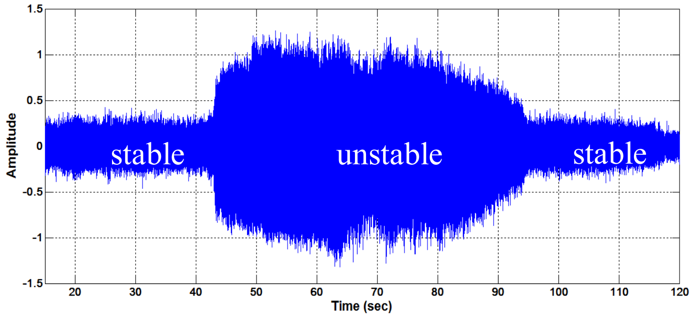

(a)

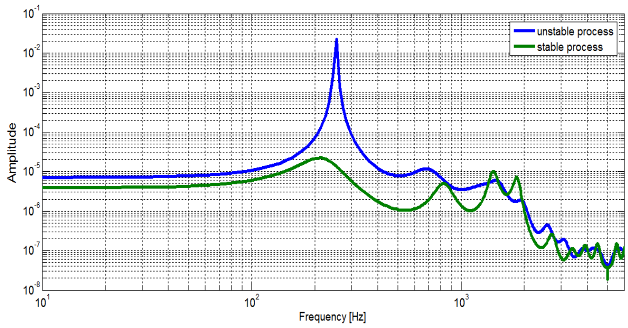

(b)

Fig. 5.9 (a) Time record of the machining system's response for stable and unstable processes; (b) PDF for stable and unstable machining processes, respectively

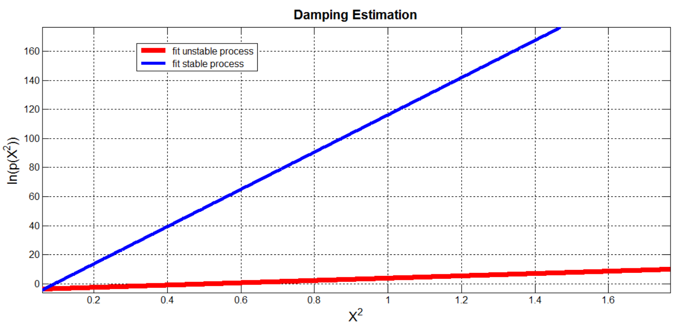

Process	stable	unstable
Est. damp	0.128	0.0079
Conf. Int.	0.106, 0.150	0.0078, 0.8106
R-square	0.653	0.9705
SSE	545	87.52

Fig. 5.10 Estimation of the damping characteristics from the interpolation function of the logarithmic p.d.f. of the square amplitude

It is important to recognise that in case of machining the input force is not measurable and therefore the variance of the excitation is not known. As a consequence, the damping estimates are not accurate. Only the relative ratio between them is reliable. Also, the accuracy of the estimation procedure is dependent on how well the input force excites the system's natural frequencies, in other words how well the white-noise excitation is approximated by the broad band excitation. In the stable process case, as is also revealed by the spectra in Fig. 5.9 (b), the response has a broad band of frequencies and therefore the estimation is poor. This compared to the unstable process where the response during self-excited vibration is periodic with the frequency close to one of the system's natural frequencies. Also, in this case, the damping is light, which helps to concentrate the energy in a narrow band.

The procedure based on the stochastic averaging method relates the damping characteristic to the measured probability density of the amplitude. The approach is of a non-parametric nature, which makes it convenient for testing hypotheses of damping mechanisms from measured random vibration data. However, as practical applications demonstrate, without knowledge about the input excitation variance it is impossible to correctly estimate the damping characteristic. Therefore, a much simpler classification criterion can be formulated.

At this point it is worth to consider the significance of the quantity $d_1(X)$. As represented in Eq. (5.40), the $d_1(X)$ term is the non-linear damping function averaged over one period. If $d_1(X) > 0$ for $X > 0$, then the system's response x(t) given by Eq. (5.23) is purely forced response to a random excitation; it is not possible for self-excited oscillations to occur. In the absence of random excitation, the steady-state response x(t) will vanish. If we assume that $d_1(X)$ has at least one nonzero root, then there exists an interval (X_1, X_2) such that $d_1(X) < 0$. This means that in the absence of random excitation, $W(t) = 0$ in Eq. (5.23), the self-excited oscillations are possible. It is now possible to derive a classification criterion for the response of Eq. (5.23) in terms of the statistical characteristics of the response (Dimentberg, 1988). For this purpose, it is convenient to replace X in Eq. (5.39) by

$$\bar{X} = X^2$$

Then the stationary solution to the FPK equation given by Eq. (5.39) becomes

$$w(\bar{X}) = C\exp(F(\sqrt{\bar{X}})) \tag{5.43}$$

From Eq. (5.43) we can further obtain

$$\frac{d}{d\bar{X}}\ln(w(\bar{X})) = -\frac{d_1(\sqrt{\bar{X}})}{2\omega_0\sqrt{\bar{X}}W_1} \tag{5.44}$$

From Eq. (5.44) it can be seen that if, and only if, $d_1(X) > 0$ then $w(\bar{X})$ is monotonically decreasing for every $\bar{X} > 0$. Then Eq. (5.44) provides the necessary and sufficient criteria for identification and classification of the response x(t) of the system; if an observed response signal x(t) has a monotonically decreasing $w(\bar{X})$ then it implies that x(t) represents the forced vibration response of the system to the broadband excitation. If on the other hand $w(\bar{X})$ is increasing then the system may be regarding as a self-excited type.

To verify this criterion for detection of self-excited systems, the response to random excitation of two different types of systems was simulated; one stable system with damping ratio, ξ_1 and natural frequency ω_0, and the other a Van der Pol oscillator with the same damping ratio and natural frequency. The damping function of the Van der Pol oscillator is

$$D(x,\dot{x}) = \xi(x^2 - \alpha)\dot{x}; \quad \xi,\alpha > 0 \tag{5.45}$$

The constant α was selected to obtain oscillations of amplitude X_0 in the absence of input excitation. The stationary probability density function for the Van der Pol oscillator is given by (Zhang, 1994)

$$p(x,\dot{x}) = C\exp\left(\alpha r(\omega_0^2 x^2 + \dot{x}^2)^2 - \frac{r}{8\omega_0^2}(\omega_0^2 x^2 + \dot{x}^2)^2\right) \tag{5.46}$$

where $r = \xi/S_0$, S_0 is the spectral density of the white noise excitation. Fig. 5.11 illustrates a typical representation of the probability density function of a Van der Pol oscillator.

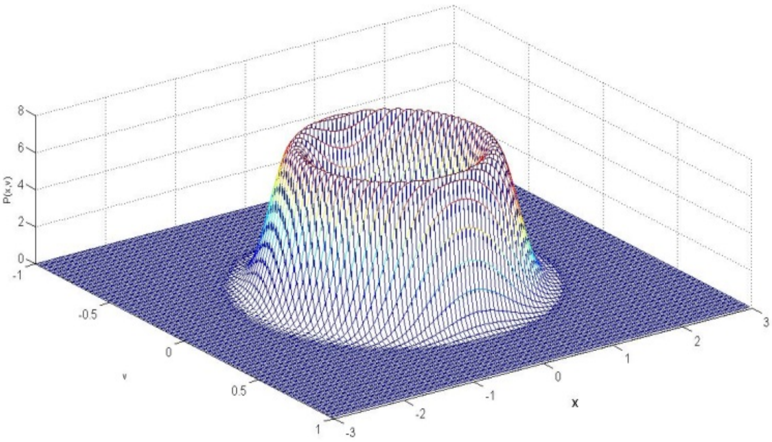

Fig. 5.11 P.d.f. of a Van der Pol oscillator

In the absence of random excitation all trajectories are "attracted" to the stable limit cycle (attractor). With zero mean white noise disturbance, the steady-state trajectories will fluctuate around the "attractor" (Zhang, 1994). The result of application of the classification criterion (5.44) in case of a stable system is presented in Fig. 5.12. It shows that in case of pure random excitation the probability of amplitude square monotonically decreases to zero.

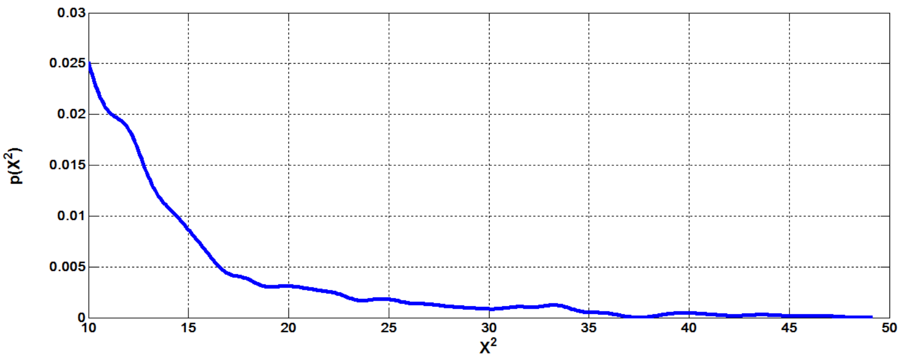

Fig. 5.12 Identification of the system's response for a stable case

Next, detection of self-excite oscillation is demonstrated in Fig. 5.13, where the application of the classification criterion (5.44) results in a deviation from monotonicity of the p.d.f. of square amplitude.

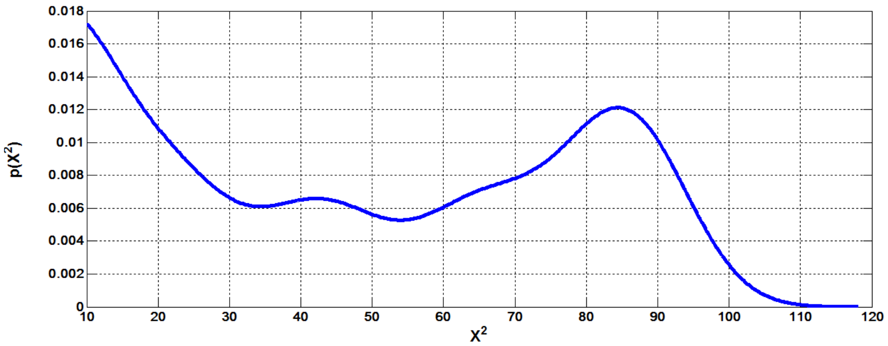

Fig. 5.13 Detection of self-exited oscillations

As illustrated in Fig. 5.13, the function ln($w(\overline{X})$) is monotonically increasing and thus correctly detecting a self-excited dynamic system. More importantly, in the case of machining system (Fig. 5.14) the criterion (5.44) accurately identifies the stable process.

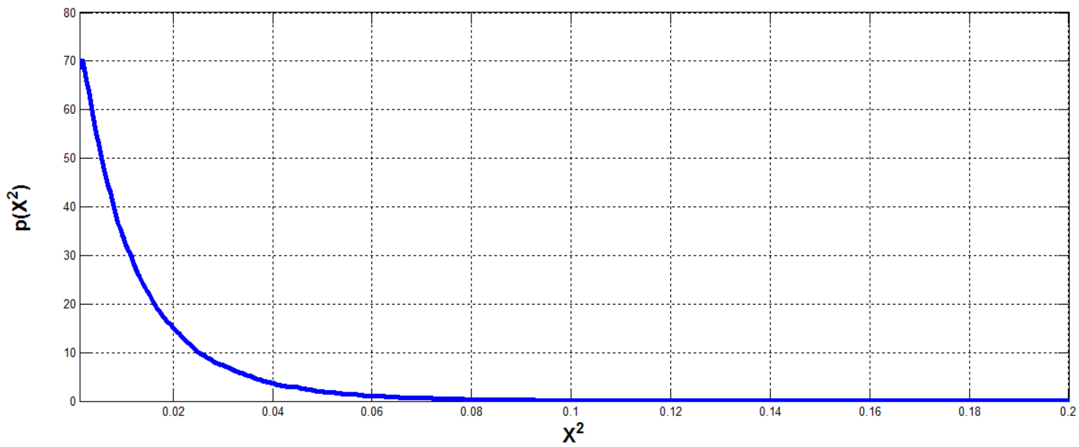

Fig. 5.14 Identification of stable machining system

5.6 Nonparametric Models Based on Energy Method

The problem of discrimination between random forced vibration and self-excited oscillations is a key issue in the evaluation of the system stability boundary during operational conditions. This is the boundary between forced vibration and self-excited vibration (chatter). The response of a dynamic system to a broadband random excitation will be a nonzero steady-state signal both in stable and in unstable states. In case of chatter vibration, the excitation persists even in the absence of the random excitation. The discrimination between self-excited and forced vibrations of a dynamical system in operational conditions is also important for selecting the type and strategy of control that may be implemented to reduce or cancel the vibration.

The nonparametric identification method presented in this section follows the approach developed by Roberts (1986), Krenk (1999) and Rüding (2001). The approach is implemented in three stages for generation of the response of a machining system using numerical simulation. At the first stage, a Gaussian white noise process is created. At second stage, the equation of motion is integrated with a suitably chosen time step, using a Runge-Kutta algorithm of 4th order that enables accurate response histories to be obtained. Finally, the response data are processed appropriately to estimate the system's parameters.

In Eq. (5.23) if it is assumed that the state space variables X and $\dot{X}$ enter the equation only through the total energy function E, then the damping is a function of the energy only. The total energy is given by

$$E = \frac{1}{2}\dot{X}^2 + U(X) \tag{5.47}$$

where

$$U(X) = \int_0^X u(\xi)d\xi$$

In Eq. (5.47) the right-hand side represents the sum of the kinetic energy (first term) and the potential energy (second term). With a change of variables, $X_1 = X$ and $X_2 = \dot{X}$, Eq. (5.23) is transformed into a set of two stochastic differential equations. Under the assumption of Gaussian white noise excitation, the state space vector (X_1, X_2) represents a Markov process and the probability density is the solution of FPK equation, Eq. (5.27) where $p(x_1, x_2; t)$ is the joint probability distribution of the state space vector (x_1, x_2). The initial conditions are given in the form: $p(x_1, x_2; t0) = \delta(x_1 - x_{10})\,\delta(x_2 - x_{20})$ for $x_1(t_0) = 0$ and $x_2(t_0) = x_{20}$. Different boundary conditions are possible such as reflective boundary, absorbing boundary and periodic boundary as discussed by Risken (1995).

The solution to Eq. (5.27) is given in the form described by Eq. (5.28). Equation (5.29) shows that the damping function D(E) can be obtained from the derivative of the damping potential $d_1(E)$. The damping potential is computed from Eq. (5.27) after the join probability $p(x_1, x_2)$ is evaluated. Because the probability density distribution of the energy envelope process, E(t), can be estimated from the system's response, it is required to relate the distribution p(E) to the distribution $p(x_1, x_2)$.

5.6.1 Stiffness Estimation

The estimation of system stiffness from the stochastic response obtained from Eq. (5.23) follows the Rüding approach (2001). The response X is calculated at zero level where the energy is kinetic energy and at extremes where the energy is potential energy. A nonlinear system with linear-cubic stiffness was used to generate a stochastic response. The damping ratio in the system is low, ξ = 0.1%. The results of stiffness identification are illustrated in Fig. 5.15. Each blue dot represents a sample ($1/2\,\dot{x}^2$, X_2). The values of the potential energy U(x), the target values, calculated from Eq. (5.46) are represented by the red line and the potential energy U(x) for an equivalent linear system is represented by the green dashed line. There are two important observations: (i) the points are centred on the target line, which represents the analytical expression, and (ii) the departure from linearity is apparent.

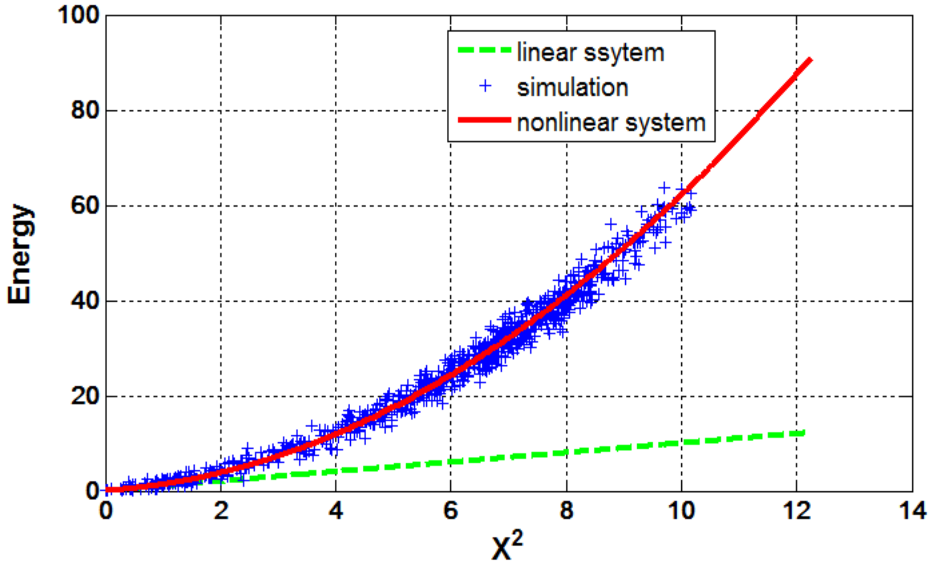

Fig. 5.15 Kinetic 1/2 and potential U(x) energy for a light damped system, 0.1% and linear-cubic stiffness

By increasing the damping to 1% the level of scatter around the target value increases as illustrated in Fig. 5.16. This is due to the variation of the energy from one period to another. As damping tends to zero, the energy will also vary infinitely slow, and the points will be virtually located on the target line. Therefore, the distance between a point and the line represents the energy variation during half of a period, i.e. the time between sampling a kinetic energy value and a potential energy value (or between a zero and an extreme value).

By examining the plots in Figs. 5.15 and 5.16, it is reasonable to accept that an estimate of U(x) can be extracted from the dot cloud. The procedure is based on dividing the energy plane in zones of equal energy. This approach is illustrated in Fig. 5.17. As the potential function U(x) is unknown at the beginning of the procedure, the potential energy is approximated to the linear value. After that, the samples (1/2 $\dot{x}^2$, x^2) are averaged in each zone and one average value is calculated for each zone, as illustrated by the green dots in Figure 5.17. The estimating procedure shows excellent results, but increasing deviations from the target is apparent at higher energy levels.

This is because of the smaller amount of samples at a higher energy level. Eliminating the samples above level 2 will considerably improve the estimation. The next step is to fit a polynomial to the estimates to compute the potential energy U(x). Then from Eq. (5.47) the stiffness function may be calculated.

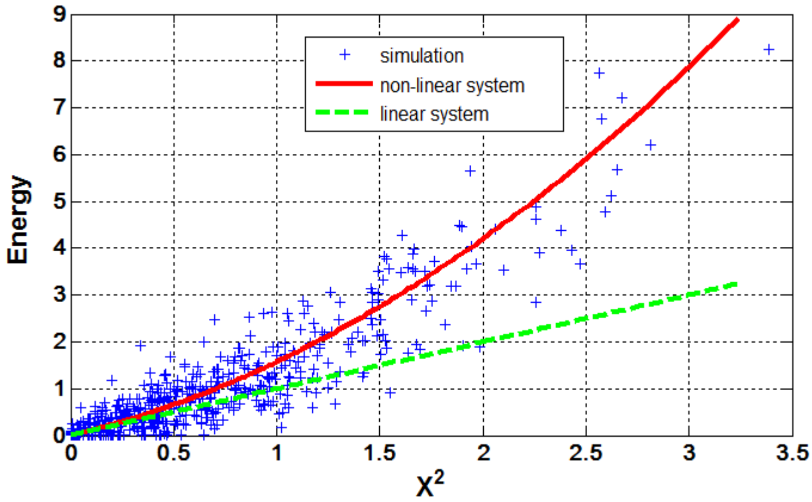

Fig. 5.16 Kinetic 1/2 and potential U(x) energy for a heavier damped system, 1%

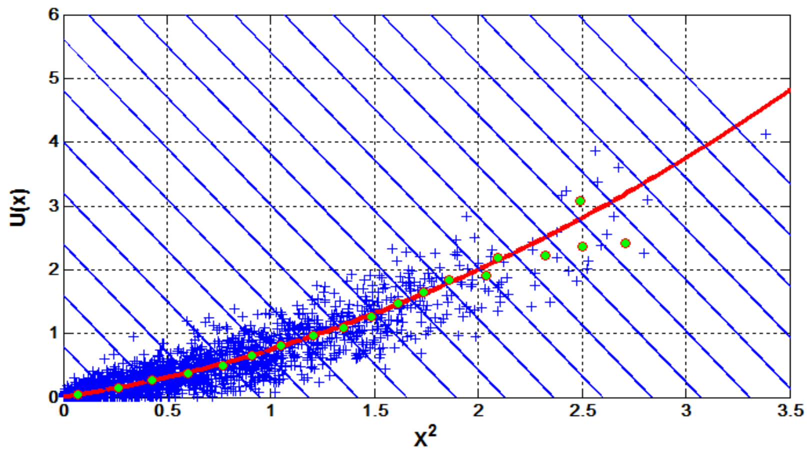

Fig. 5.17 Estimation of U(x) in zones of equal energy. The dots represent the average U(x) in each energy zone

5.6.2 Damping Estimation

Damping estimation is treated in two steps. The first step starts from the damping potential. The equation of motion is represented by Eqs. (5.23) and (5.27), and can be rewritten as

$$\frac{d_1(E)}{\pi S_0} = -\ln\left(\frac{p_{x,\dot{x}}(x,\dot{x})}{C}\right) \tag{5.48}$$

where $d_1(E)$ is the damping potential as described by Eq. (5.27).

By estimating the probability density function from the system's response, the damping potential can be calculated. This function, for a linear system, is represented in Fig. 5.18. By fitting a linear polynomial to the experimental data, the ratio between damping potential and excitation intensity, S_0 can be calculated.

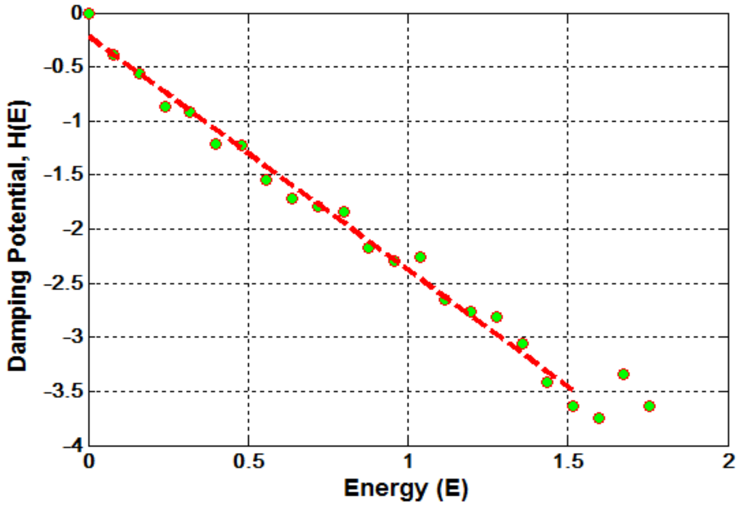

(a)

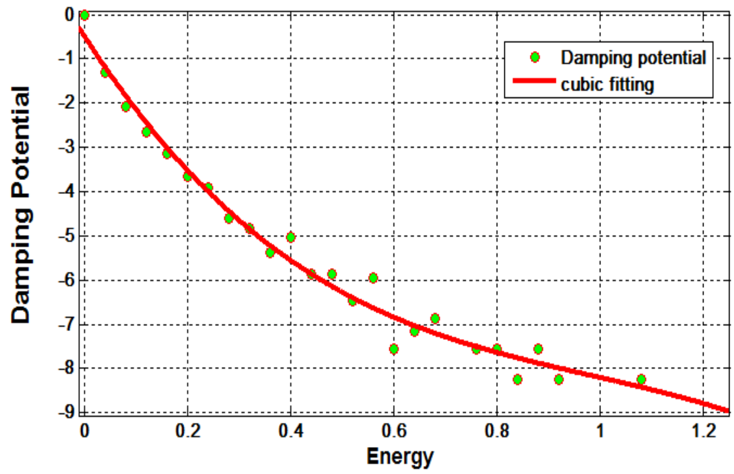

(b)

Fig. 5.18 Estimation of damping potential (a) linear system and linear polynomial fitting, (b) nonlinear damping system, dry friction, and cubic polynomial fitting

In the second step, the equivalent damping function, h_{eq}, in Eq. (5.27) is estimated from the covariance function at various energy levels according to

$$h_{eq} = \frac{4}{c(E)T(E)} \ln\left(-\frac{X_1}{X_2}\right) \tag{5.49}$$

where $c(E)$ is the participation factor in the covariance function, T(E) the natural period and X_1 and X_2 are the extreme values of the covariance function in the first period.

$$R_{\dot{x}}(\tau \mid E) = E \exp\left(-\tfrac{1}{2} h_{eq} \tau\right) \sum_{j=1}^{\infty} c_j(E)^2 \cos(j\omega\tau) \tag{5.50}$$

For a linear system the covariance functions at different energy levels are shown in Fig. 5.19. Having calculated $d_1(E)/S_0$ and h_{eq} the excitation intensity S_0 can be estimated. For each energy level the extreme values (shown in Fig. 5.19 at X_1 for potential energy, and at X_2 for kinetic energy) are extracted from the corresponding covariance functions and the equivalent damping computed according to Eq. (5.49). The calculated values are represented by dots in Fig. 5.20. As the system is linear the damping is independent of energy level and therefore constant. It can also be noticed in Fig. 5.19 that the natural period, and therefore the natural frequency, are constant for different energy levels. Each curve in Fig. 5.19 represents an energy level corresponding to the dots in Fig. 5.20.

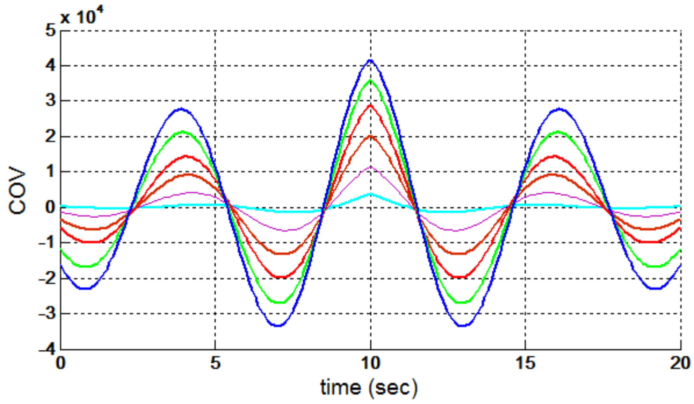

Fig. 5.19 Covariance function estimated at different energy levels

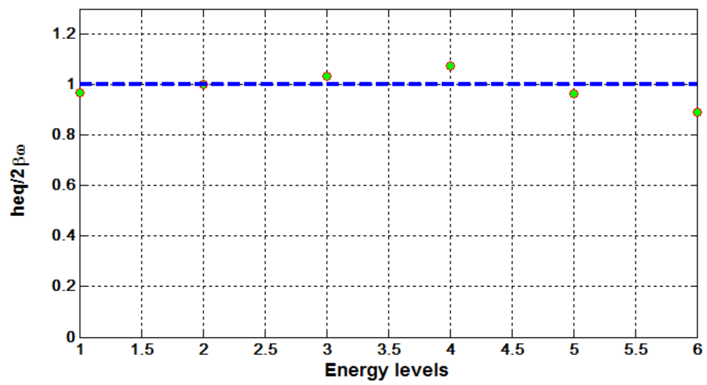

Fig. 5.20 Estimation of the equivalent damping function, heq, from measured autocovariance functions

After plotting the equivalent damping values, a line is fitted to represent the constant damping. As the energy level is increased, a larger deviation from the analytical value is apparent.

5.6.3 Identification of Machining System ODPs

The procedure developed above will be applied for the identification of the characteristics of the machining system. Steel bars (C < 0.20%) with a length of 1200 mm and an initial diameter of 42 mm were machined in longitudinal turning between tailstock and chuck at a cutting speed of v_c= 180 m/min, a feed rate of f_r = 0.3mm/rev and a variable depth of cut (0.5 – 3mm). Cemented carbide inserts with 1.2mm nose radius were used in all experiments. The vibration signals were measured by a pre-polarized microphone and sample at 12.8 kHz sampling rate. In Fig. 5.21 an example of stable machining is presented, while Fig. 5.22 illustrates an unstable machining process.

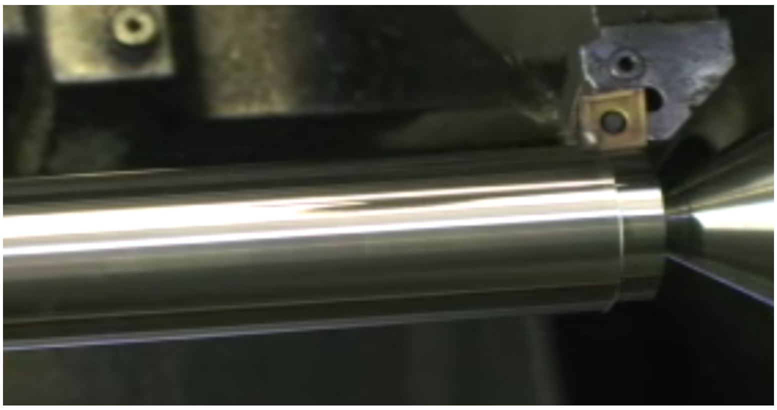

Fig.5.21 Stable machining (D = 38 mm)

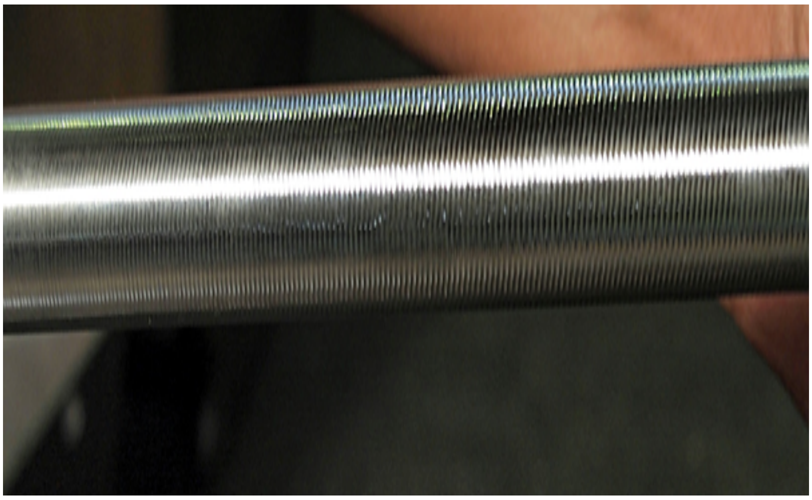

Fig. 5.22 Unstable machining, chatter

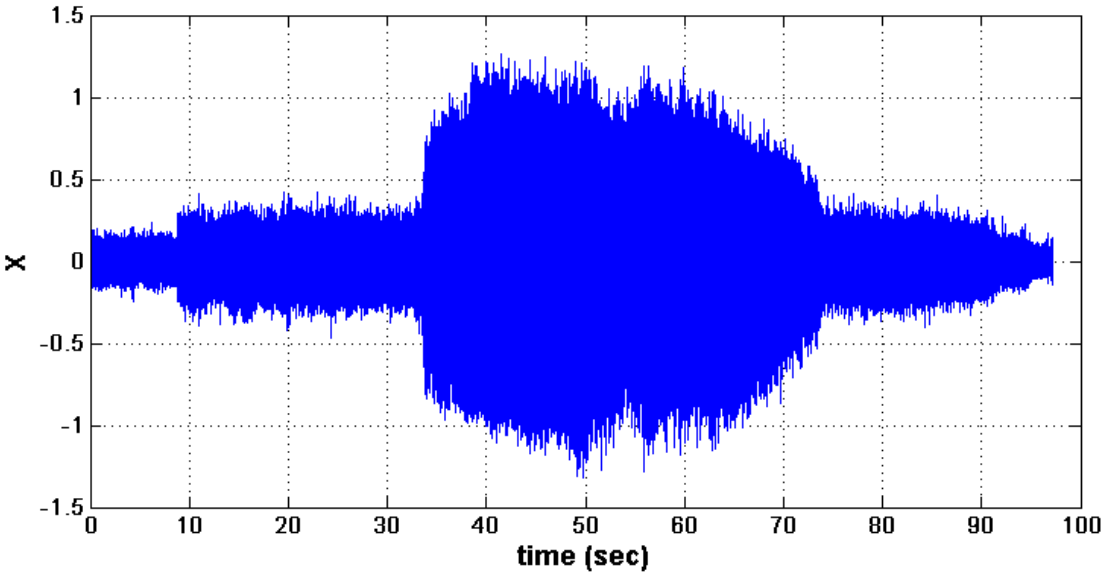

Fig.5.23 Unstable process, as the tool approaches the centre of the bar heavy vibration sets on (measured sound pressure)

Coming down to diameters below 34 mm, as the tool approaches the centre of the bar, chatter vibration is generated. Fig. 5.23 illustrates the time signal showing first a stable process, then the chatter in the middle of the bar, then as the tool approaches the chuck, the system recovers stability. In Fig. 5.24, the unstable and stable signals are represented in frequency domain.

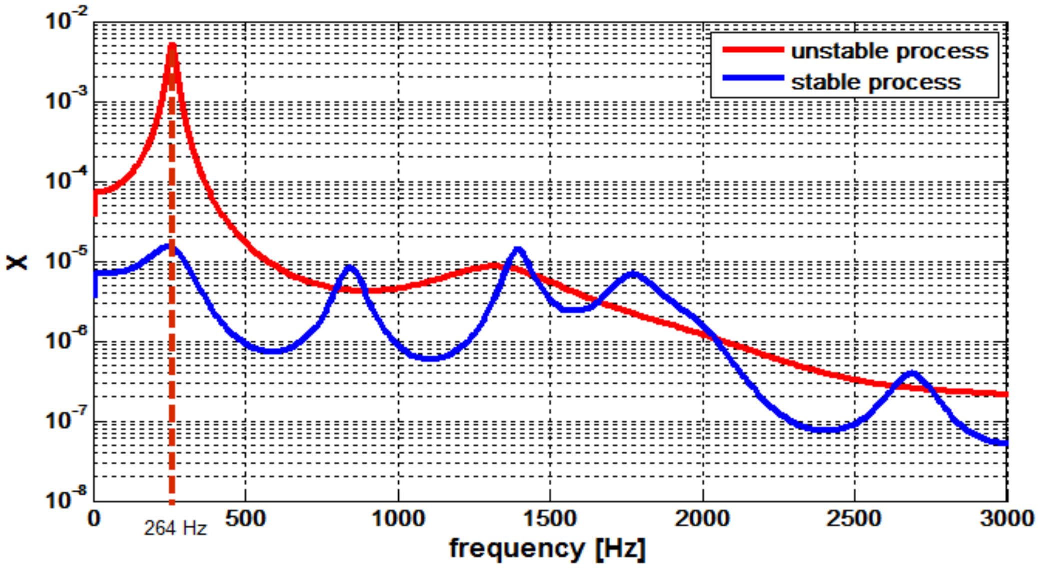

Fig. 5.24 The stable and unstable signals in frequency domain

5.6.4 Operational Stiffness Identification

Following the procedure described above, the overall stiffness of the machining system is estimated. For a stable process, Fig. 5.25 illustrates the potential function U(x). The function shows a soft nonlinear characteristic. After fitting to a quadratic polynomial function, the stiffness function can be extracted from Eq. (5.47). The blue line represents the theoretical linear system at the system's natural frequency.

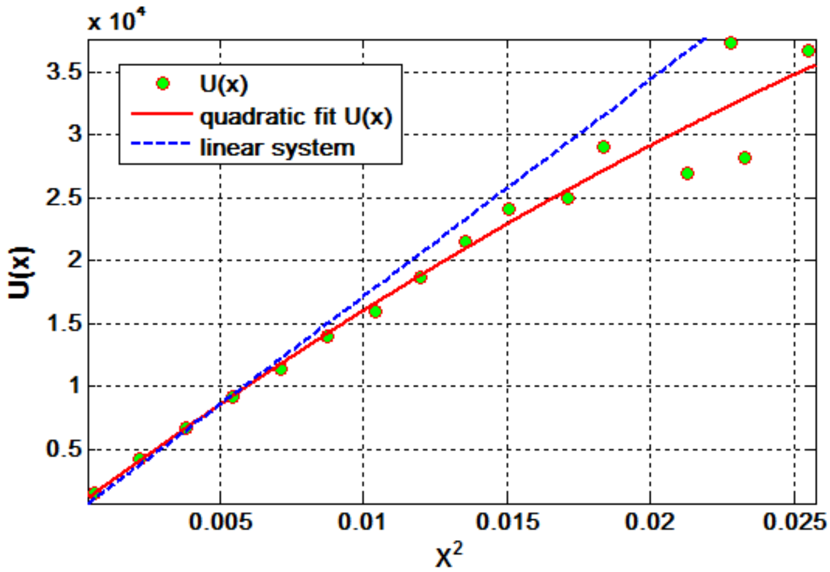

Fig. 5.25 Stiffness estimation - stable machining

The estimation of the overall stiffness of the machining system entering unstable behaviour is presented in Fig. 5.26. The potential function U(x) and consequently the stiffness function show a hard nonlinear behaviour which is characteristic for self-excited vibrations. The deviation from a nonlinear behaviour is apparent by comparing this to the linear characteristic shown by the blue dotted line. As these results show, if the stiffness of a machining system enters the inelastic range of the material, or the process becomes nonlinear, or a combination of both, and the degree-of-nonlinearity is large, using a linearization method for the nonlinear stiffness may yield large errors in response estimation.

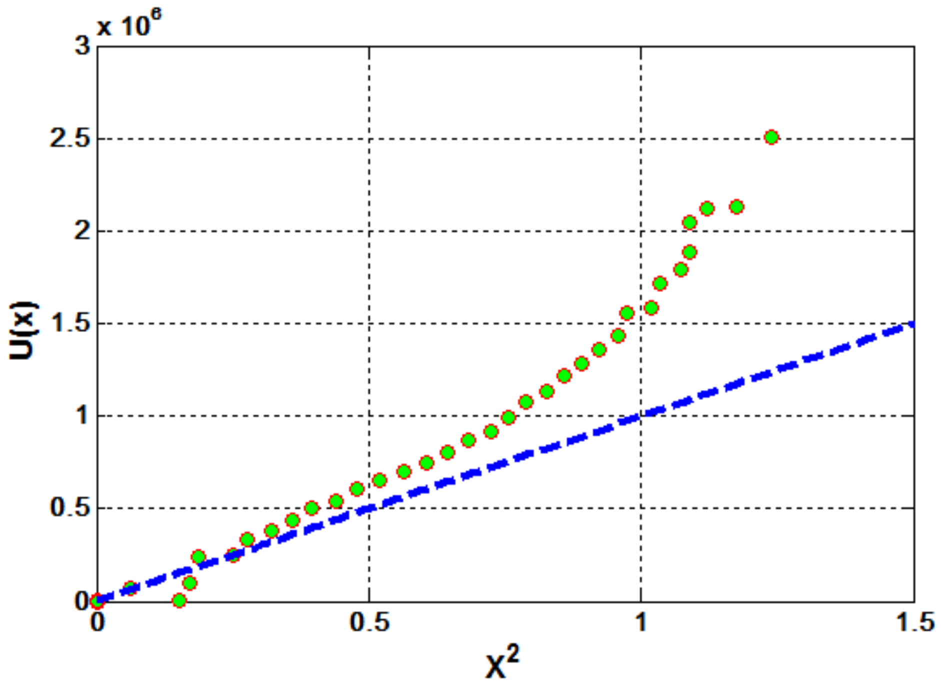

Fig. 5.26 Stiffness estimation - unstable machining

5.6.5 Operational Damping Identification

Following the approach described above, the damping potential and equivalent damping are estimated from the system's response both in stable and unstable conditions. However, the results are presented only for the unstable machining system.

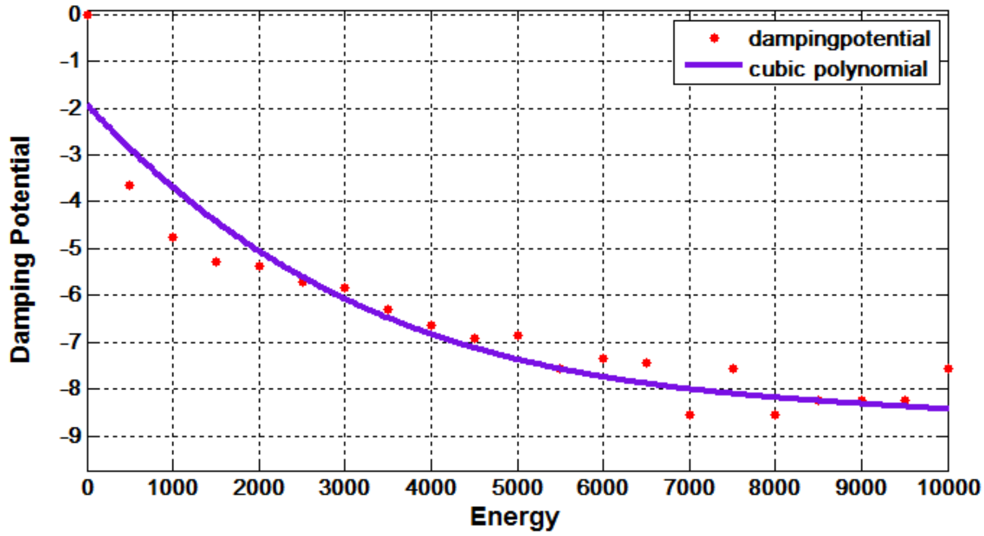

Fig. 5.27 Estimation and fitting of damping potential for unstable machining

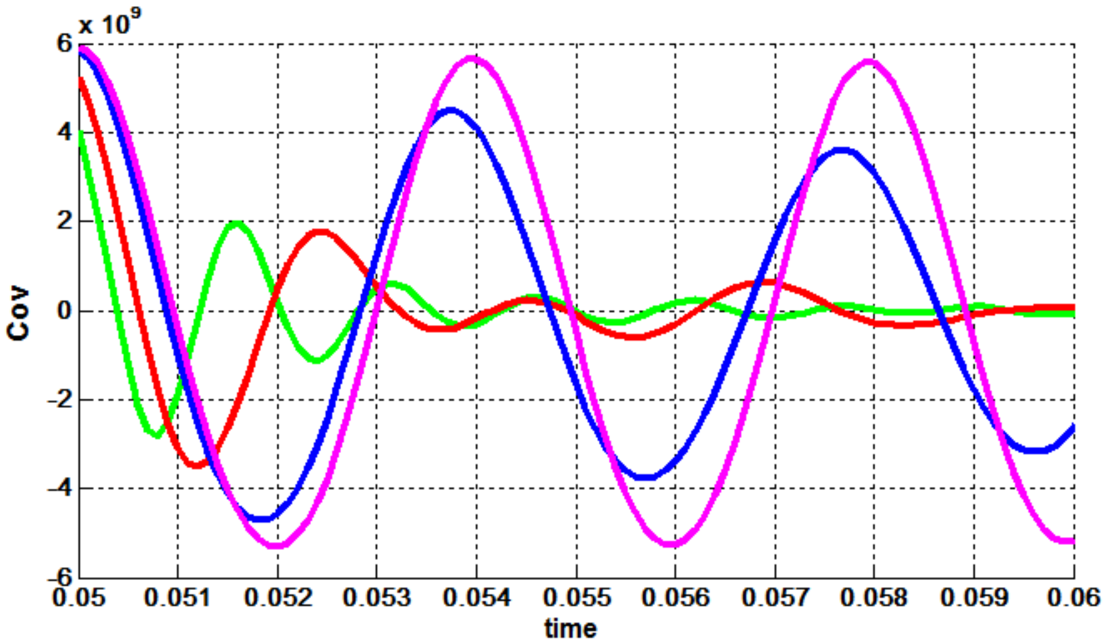

Fig. 5.28 Covariance function calculated for various energy levels

The estimation procedure starts with computation of the damping potential $d_1(E)$ from the experimental computation of the probability density function at different levels of energy. From Eq. (5.48), the function $d_1(E)$ is computed and then fitted to a polynomial. As in the case of stiffness, the damping in an unstable machining system shows a nonlinear behaviour and a cubic polynomial is then employed. In the second step, the covariance function is calculated for gradually increasing levels of energy. Some of these functions are represented in Fig. 5.28. It is worth noting that, as the stiffness is nonlinear, the natural period depends on the energy level. The same can be stated for the equivalent damping. A modified form of Eq. (5.49) is used to take into account the changes in the natural period. The total energy is calculated as a sum of the kinetic and potential energies. The kinetic energy is extracted from the derivative of the response while potential energy from an iterative procedure applied to the identified potential function U(x).

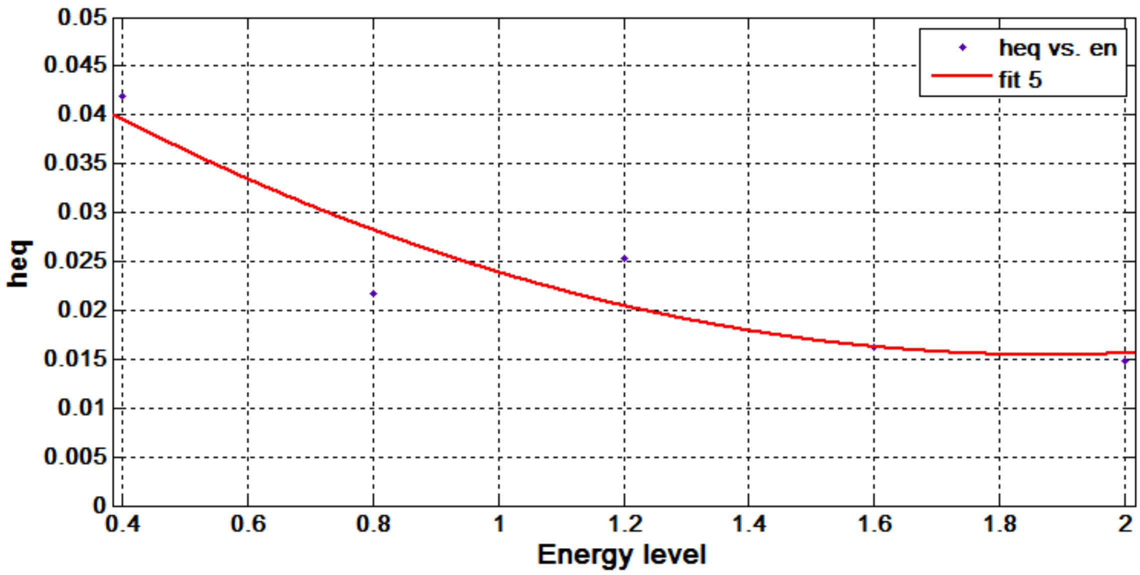

Fig. 5.29 Computation of equivalent damping function

5.7 Parametric Models for Machining System Identification

In section 5.5, non-parametric identification procedures have been used to estimate the ODPs from the response of the machining system in stable and unstable conditions. The main benefit of this approach is that the estimated dynamic parameters are extracted in operational conditions directly from the interaction between the elastic structure and the cutting process. Knowledge of ODP opens new opportunities for optimising the machining system. Strategies for improving, if necessary, the system may be straightforwardly implemented by comparing different solutions. Non-parametric identification has, however, the limitation that it requires long sample sequences. In addition, as the non-parametric models developed herein are based on SDOF system, special treatment of data is required. Another limitation is that this approach requires knowledge of the response probability distribution.

In this section, the identification technique based on parametric models is presented. Parametric models can be applied to any numbers of DOF and in their recursive implementation can take into account the nonlinear nature of the system. A parametric model is a special class of representation of a system, where the input in the model is driven by white noise processes and the model is described by rational system functions, including autoregressive (AR) (Burg, least square, Yule Walker, geometric lattice, instrumental variable), ARX (autoregressive with eXogeneous variables, iv4), moving average (MA), autoregressive-moving average (ARMA), Box Jenkins, Output Error models (Box [1970], Pamdit [1983], and Söderström [2001]). The process output of this class of models has a power spectral density (PSD) that is entirely described in terms of model parameters and the variance of the white noise process.

Parametric models described in this section have their origin in the Markov representation of stochastic processes. The problem of identifiability of a parametric autoregressive moving average (ARMA) process is discussed in the opening of this section and a complete solution is obtained by using the Markovian representation of the process.

5.7.1 Gauss-Markov Sequence

A sequence N(k) is called a purely random sequence if

$$p[N(k+1) \mid N(k)] = p[N(k+1)] \tag{5.51}$$

for all k, where f[N(k)] is the probability density of the sequence N(k), k=0,1,2, ..., n. Let X(k) be a random sequence generated by a linear difference equation

$$X(k+1) = a(k)X(k) + N(k) \tag{5.52}$$

where a(k) is a known deterministic sequence and N(k) is a random sequence. The conditional density of the random sequence

$$p[X(k+1) \mid X(k), X(k-1), \ldots, X(0)] = p[X(k+1) \mid X(k)] \tag{5.53}$$

In other words, the future state of the process X(k+1) depends only on the present state of the process X(k) and the random sequence N(k). Hence, X(k) is a Markov sequence. However, a sequence X(k+1) generated by a second order difference equation depends on present and past. For example, consider a second-order difference equation

$$\begin{aligned} &X(k+1) = a_1(k)X(k) + a_2(k)X(k-1) + N(k) \\ &\begin{cases} X(0) = c_1 \\ X(-1) = c_2 \end{cases} \end{aligned} \tag{5.54}$$

where $a_1(k)$ and $a_2(k)$ are known deterministic functions and N(k) is a random sequence.
Let

$$\begin{aligned} X_1(k) &= X(k) \\ X_2(k) &= X(k-1) \\ X(k) &= \begin{bmatrix} X_1(k) \\ X_2(k) \end{bmatrix} \end{aligned} \tag{5.55}$$

The second difference equation can now be expressed as a vector matrix equation

$$X(k+1) = \begin{bmatrix} a_1(k) & a_2(k) \\ 0 & 0 \end{bmatrix} X(k) + \begin{bmatrix} 1 \\ 0 \end{bmatrix} N(k) \tag{5.56}$$

X(k) is of dimension 2 and is a Markov vector sequence. In this way, a nth order difference equation can be reduced to a vector matrix equation of dimension n. Therefore, a sequence generated by a nth order linear difference equation is a Markov sequence. The ARMA model will generate a Markov vector sequence. It can be noticed that while the vector sequence is Markov, the components of the vector are not Markov. A Markov sequence is called a Gauss-Markov sequence if p[X(k)] and p[X(k+1)|X(k)] are Gaussian probability density functions for all k.

Let's now consider a general representation. When a discrete-time system is time-invariant, the state space representation of a system is given as (Akaike, 1974)

$$\begin{aligned} v_{n+1} &= Av_n + Bu_{n+1} \\ y_n &= Cv_n \end{aligned} \tag{5.57}$$

Where n denotes the time and u_n is a q x 1 vector of the input to the system, y_n is a r x 1 vector of the output and is v_n a r x 1 vector of the state. A, B and C are and C are respectively p x p, p x q and p x r matrices.

The Markovian representation is a stochastic analogue of (5.57) and is given by

$$\begin{aligned} v_{n+1} &= Av_n + Bz_{n+1} \\ y_n &= Cv_n + w_n \end{aligned} \tag{5.58}$$

where w_n is uncorrelated with v_n. In Eq. (5.58) z_{n+1} is the innovation of the input u_n at time n+1.

If the observations {yt} are from a stationary scalar ARMA(p, q) process then

$$y_t = \sum_{j=1}^{p} \phi_j y_{t-j} + z_t + \sum_{j=1}^{q} \theta_j z_{t-j} \tag{5.59}$$

Arranging the AR coefficients as a companion matrix ($\varphi_j = 0$ for $j > p$)

$$F = \begin{pmatrix} \phi_1 & \phi_2 & \cdots & \phi_{ds-1} & \phi_{ds} \\ 1 & 0 & \ldots & 0 & 0 \\ 0 & 1 & \ldots & 0 & 0 \\ \vdots & & \ddots & \vdots & \vdots \\ 0 & \cdots & 0 & 1 & 0 \end{pmatrix} \tag{5.60}$$

Then we can write ($\theta_j = 0$ for $j > q$)

$$\begin{aligned} &\overline{X}_t = F\overline{X}_{t-1} + \overline{V}z_t, \quad \overline{V} = (w_0, w_1, \ldots, w_q)' \\ &y_t = (1\theta_1 \ldots \theta_{ds-1})\overline{X}_t \end{aligned} \tag{5.61}$$

w_i's are the impulse response functions of the time-invariant linear system defined by (5.59) with the input z_n and the output y_n. This result shows that an ARMA process always has a Markovian representation.

5.7.2 Parametric ARMA Models

A serious limitation in practical validation of stability diagrams originates from the lack of a rigorous criterion to unambiguously detect the stability limit, i.e., impending chatter. In other words, formulation of a discrimination criterion to distinguish between forced and chatter vibrations will be much more useful from both a theoretical and, especially, a practical point of view. Many of the methods used to analyse, control and optimise machining systems are based on off-line procedures or test environments that do not represent the actual machining conditions.

The objective of the parametric modelling is to infer a model of the process from the recorded data. In other words, parametric modelling represents mapping from the data space to the model parametric space. The procedure by which a model is inferred from measured data is called identification. More precisely, parametric identification attempts to find the parameters in a linear model that will give the best fit to the data. The identification of a stationary time series as the output of a dynamic system whose input is white noise a(t), can be carried out in several ways. One way is to use the parsimonious parameterization, which is employing ARMA(p, q) representation.

Given a time series of data y_t, the ARMA model is a tool for analysing and predicting future values in this series. The model consists of two parts, an autoregressive (AR) part and a moving average (MA) part. The combined model is usually then referred to as the ARMA(p,q) model were p is the order of the autoregressive part and q is the order of the moving average part.

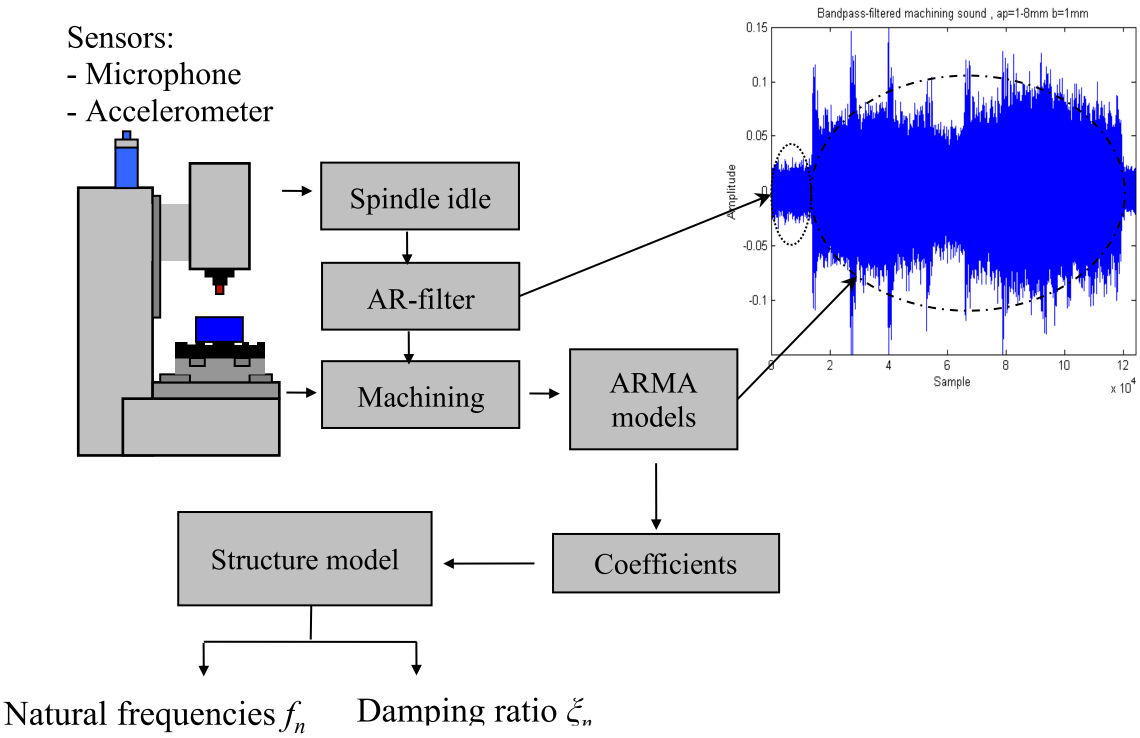

Fig. 5.30 ARMA model identification scheme (Archenti, 2008)

The model for ARMA process can be expressed as (Brockwell, 2002),

$$Y(z) = H(z)U(z) \tag{5.62}$$

where Y(z), U(z) and H(z) are the z-transforms (the z-transform is the discrete-time counterpart to the Laplace transform for continuous-time systems) of the output sequence, input sequence and the system impulse response (transfer function), respectively, and

$$H(z)=\frac{c_0+c_1z^{-1}+c_2z^{-2}+\ldots+c_qz^{-q}}{1-a_1-a_1z^{-1}-a_2z^{-2}\ldots a_pz^{-p}} \tag{5.63}$$

where the b_i and a_i coefficients of the polynomials of the MA part and AR part, respectively.

For a second order system with impulse response function given by equation

$$h(t)=Ae^{-\alpha t}\sin(\beta t+\phi) \tag{5.64}$$

the c_i and a_i parameters can be related to physical parameters, A (amplitude), α (damping), β (frequency)

$$H(z)=\frac{A\sin\phi+Ae^{-\alpha\Delta t}\sin(\beta\Delta t-\phi)z^{-1}}{1-2e^{-\alpha\Delta t}\cos(\beta\Delta t)z^{-1}+e^{-2\alpha\Delta t}z^{-2}} \tag{5.65}$$

where Δt is the sampling interval in seconds.

5.7.3 Power Spectral Density of ARMA Models

Estimation of the power spectral density (PSD) of sampled data containing stochastic components is traditionally performed with the help of FFT. There are however, a number of problems related to spectral analysis based on the Fourier approach.

The major limitation of FFT spectral analysis is the lack of ability to discriminate the spectral components of two signals with the frequency close to each other. This becomes a big problem when attempting to analyse short time series because the frequency resolution is approximately the inverse of the available data time length. Another drawback is the need for curve-fitting for modal parameter extraction.

The discrete-time counterpart of the Fourier transform is the discrete Fourier transform (DFT). The classical PSD based on DFT is given by Cooley (1965)

$$\phi_{yy}=\left|\frac{1}{N}\sum_{n=0}^{N-1}y_ne^{-j2\pi mn/N}\right|^2 \tag{5.66}$$

where N is the number of samples. The power spectrum for a process described by Eq. (5.66) is obtained by evaluating the impulse response function around the unit circle,

z^-1 = exp(-j2πfΔt)

Another problem with spectral analysis based on the Fourier approach is spectral leakage (Marple, 1987). The frequencies represented by lines in the spectrum, are harmonics of the fundamental frequency. Spectral leakage causes energy from distinct spectral features to leak into nearby frequency channels. This gives rise to false components in the frequency spectrum of the signal.

The power spectrum for a process described by Eq. (5.66) is obtained by evaluating the impulse response function around the unit circle, $z^{-1} = \exp(-j2\pi f\Delta t)$. Using only AR parameters, the PSD function is determined as follows, equation

$$\phi_{AR} = \frac{\sigma^2 \Delta t}{\left| 1 + \sum_{n=1}^{m} a_m e^{-j2\pi f n \Delta t} \right|^2} \tag{5.67}$$

The PSD can therefore be determined solely from a knowledge of the coefficient $a_1, a_2, \ldots, a_p$, and the variance, σ^2.

In the on-line identification procedure, the estimation of physical parameters, chatter frequency, ω_{ch} and damping ratio ξ can be used for control of dynamic stability. It is important to stress that in the context of stochastic modelling, the estimated physical parameters are meaningful only from a statistical point of view, i.e. they are properly significant within a certain confidence interval.

The transmutation process from the ARMA parameter domain to the ω_{ch} - ξ domain gives the advantage of robust chatter identification criteria. Theoretically, dynamic stability can be defined in terms of negative damping. A system is dynamically stable if the damping is positive and unstable when damping becomes negative. In machining, as we are interested in avoiding instabilities like chatter, when damping starts to decrease towards zero it is a proof that the system is approaching stability threshold. Therefore, monitoring damping in an on-line identification scheme can give a good indication of the dynamic state of the system.

The motion of an n degree-of-freedom system can be represented by a second-order differential system of equations

$$M\ddot{x}(t)+C\dot{x}(t)+Kx(t)=f(t) \tag{5.68}$$

If the model of an ARMA process is represented by Eq. (5.68) then the AR parameters are related to *M*, *C* and *K* through the characteristic equation of the form,

$$\begin{aligned}\sum_{t=0}^{2m} a_i \mu^{2m-i} &= \prod_{i=1}^{m}\left(\mu-\exp\left\{\xi_j \omega_{nj}\Delta t + i\omega_{nj}\sqrt{1-\xi_j^2}\,\Delta t\right\}\right)\times\ldots \\ \ldots\times&\prod_{i=1}^{m}\left(\mu-\exp\left\{-\xi_j \omega_{nj}\Delta t + i\omega_{nj}\sqrt{1-\xi_j^2}\,\Delta t\right\}\right)\end{aligned} \tag{5.69}$$

where $\xi_j\omega_{nj}$ and $\pm i\omega_{nj}\sqrt{i-\xi_j^2}$, j =1, … n are the eigenvalues of the system of Eq. (5.68).

The structural parameters ξ_i and ω_{nj}, j = 1, … 2*n*, may be determined from the AR parameters estimates equation

$$\begin{aligned}\xi_j\omega_{nj}\Delta t &= -\frac{1}{2\log\left(x_j x_j^*\right)} \\ \omega_{nj\sqrt{1-\xi_j^2}}\Delta t &= \tan^{-1}\left|\frac{x_j - x_j^*}{x_j + x_j^*}\right|\end{aligned} \tag{5.70}$$

5.7.4 Operational Dynamic Parameters (ODP)

In machining, real-time systems for detecting self-excited vibrations are based on vibration amplitude monitoring. However, the vibration amplitude criterion is not consistent with the nature of the vibration source. A high amplitude vibration can be the result of a stable system working close to resonance, or in condition of tougher cutting parameters. Likewise, self-excited vibrations need a very low energy level to be excited and are therefore difficult to detect before they are fully developed. A nonconservative mechanical system with positive damping is said to be dynamically stable, whereas one with negative damping is said to be unstable. This gives a robust criterion for discrimination between forced and self-excited vibrations, which is not related to the vibration amplitude criteria.

The concept of ODP is introduced due to the fact that the machining system is a closed-loop system between the cutting process dynamics and the machine tool elastic structure. The structure damping of the machine tool elastic structure and the dynamic cutting process damping cannot be separated from a response measure point of view. ODPs include the contribution of the structural vibration modes and process vibration modes generated during a machining system operation. The ODPs are the operational damping ratio (ODR) and operational frequency (OF). The ODR, ξ_{op}, is the overall damping of the machine tool structure ξ_{mod} (modal damping) and the dynamic cutting process ξ_{cp} (process damping)

$$\xi_{op} = \xi_{\mathrm{mod}} + \xi_{cp} \tag{5.71}$$

ξ_{op} is used in this study as the index of the chatter stability boundary.

In Eq. (5.68), M, C and K represent n x n mass, damping and stiffness matrices respectively; f(t) is a vector of external excitation. Matrices C and K contain both structural and process damping and stiffness respectively. $\mathbf{x}(t), \dot{\mathbf{x}}(t), \ddot{\mathbf{x}}(t)$ are n ϕx 1 vectors of displacement, velocity and acceleration of the n degrees of freedom. The eigenvalue problem associated with Eq. (5.68) is given by

$$\left(\lambda_i^2\mathbf{M} + \lambda_i\mathbf{C} + \mathbf{K}\right)\mathbf{\Phi_i} = 0, i = 1, 2, \ldots, 2n \tag{5.72}$$

where λ_i and ϕ_i are the eigenvalues and eigenvectors respectively.

Let $x_j(k\Delta T)$, k = 0, 1,2 … be the discrete samples of the displacement of the j-mass. ΔT is the sampling interval. Then the observations $x_j(k\Delta T)$ can be represented by an ARMA model

$$\sum_{i=0}^{p} a_i x(t-i) = \sum_{i=0}^{q} c_i e(t-i),\ a_0 = 1 \tag{5.73}$$

Model parameter estimation for a given model structure seeks the parameter vector θ(t) [a_1, a_2 … a_p, c_1, c_2, … c_q] and the residual variance $\sigma e^2(t)$ at every time t = 1, 2, … n.

The characteristic equation of (5.74) can be written

$$\sum_{i=0}^{p} a_y x(t-i) = \prod_{i=1}^{n} (\mu - \mu_j)(\mu - \mu_j^*) \tag{5.74}$$

where

$$\mu_{j1,2} = \exp(-(\omega_{op})_j (\xi_{op})_j \Delta T \pm i(\omega_{op})_j \sqrt{1-\xi_j^2}\Delta T) \tag{5.75}$$

From equation (5.75), the ODP, operational damping, $(\xi_{op})_j$ and frequency $(\omega_{op})_j$ are calculated at each time t and for each eigenvalue.

$$(\xi_{op})_j = \frac{\ln(\mu_j \mu_j^*)}{\sqrt{\ln(\mu_j \mu_j^*)^2 - 4\left[\tan^{-1}\left(\frac{\mu_j - \mu_j^*}{\mu_j + \mu_j^*}\right)\right]^2}} \tag{5.76}$$

$$(\omega_{op})_j = -\frac{1}{2\Delta T}\sqrt{\ln(\mu_j \mu_j^*)^2 - 4\left[\tan^{-1}\left(\frac{\mu_j - \mu_j^*}{\mu_j + \mu_j^*}\right)\right]^2} \tag{5.77}$$

5.7.5 Stability Analysis

A series of experiments were carried out with the scope of demonstrating the identification procedure based on a parametric model approach. Both off-line and on-line identification methods were used to find modal parameters describing the static and dynamic stability of the system.

Figure 5.31 displays the experimental set-up of the test and data acquisition system. The experiments were carried out in a conventional turning machine equipped with a chuck, revolver and tailstock. To acquire data for machining analysis, the acoustic signal from the machining process was recorded. Experimental modal analysis was used for analysing the interaction between machine tool elastic structure and workpiece. For further investigation of the chuck-workpice-tailstock system, an FEM model was developed. Natural frequencies and mode shapes were computed and used for analysis.

A long slender workpiece of steel was used (length 585 mm), and prepared with a series of tapered segments (diameter 43 – 49 mm). For robustness and sensitivity analysis purpose, three different workpieces all with the same material properties and geometries were used, Table 5.1.

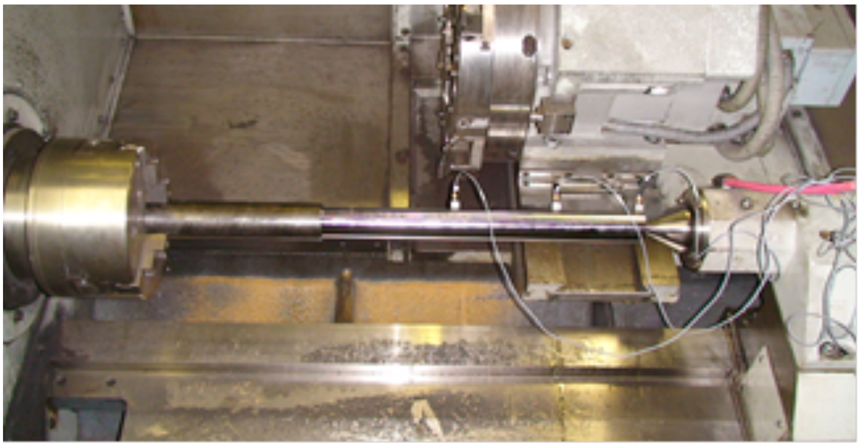

(a)

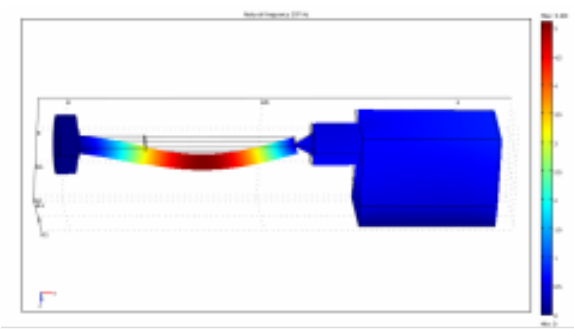

(b)

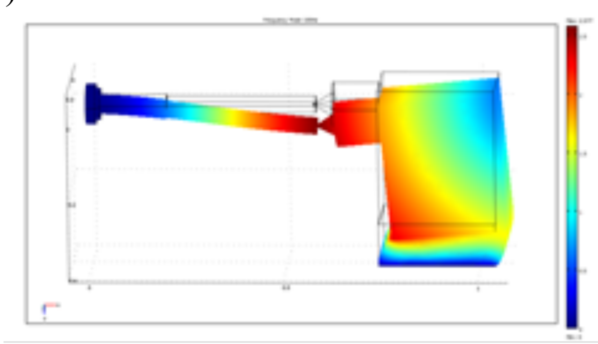

(c)

Fig. 5.31 a) Experimental set-up (b) unstable state only the workpiece frequency mode is excited (c). In stable state, several modes shapes are excited

Workpiece	**Tool, Insert Sandvik**	**Feed[mm/rev]**	**Cutting speed[m/min]**
Steel 42CrMoS4, C = 0.38%	CNMG120412-PM	0.25	150
Length 585, Ø43-49 [mm]	Grade 4025		155
			161

Table 5.1 Experimental conditions

From Experimental Modal Analysis (EMA), the following modal parameters were obtained

Natural frequency [Hz]	**Damping ratio [%]**
26.35	0.15
59.76	0.21
114.35	0.23
198.21	0.26
311.14	0.11

5.7.6 ARMA Model-based Off-line Identification

The suitable order for the models was chosen after a number of trials, both on stable and unstable processes, in order to find the optimum order for each of the time series. The reliability of the identification approach is reflected by either plotting the residual curves for each model or by evaluating the standard deviation for each parameter. The ARMA parameters, estimated from the appropriate models along with their standard deviations are calculated and the ODPs are then extracted in Table 5.2.

	Stable region	Unstable region
Roots	0.1148±0.8124i	0.2875±0.8856i
Frequency [Hz]	256	270
Damping ratio [%]	5.1	0.011

Table 5.2 ODPs for stable and unstable process, respectively

5.7.7 Parametric Modelling for a Milling Operation

The tests were performed in full immersion (slotting) with an end tool holder, see Fig. 5.32 (b). A tool holder type R390-020A20-11M with three inserts and diameter D = 20mm was selected. The overhang of the toll holder was l = 60 mm, i.e., three times the diameter. At this ratio l/D the risk of tool holder chatter is reduced. The tool holder is designed for three inserts. Inserts for steel type R390- 11 T3 12E-PM 1030 were employed. The nose radius was 1.2 mm. The tool diameter selected was larger enough not to influence the process dynamics by generating chatter.

Workpieces with dimensions 70 x 70 x 70 mm were adapted to the pallet system size and pre-prepared for machining, see Fig. 5.32 (a). Three slots were machined at every height level on the workpiece.

Chemical Composition Element of workpiece material	min/max
C	<=0.20
Mn	(1.00 - 1.60) 773)
P	<=0.050
S	<=0.050
Cr	<=0.30
Cu	<=0.40
N	<=0.009

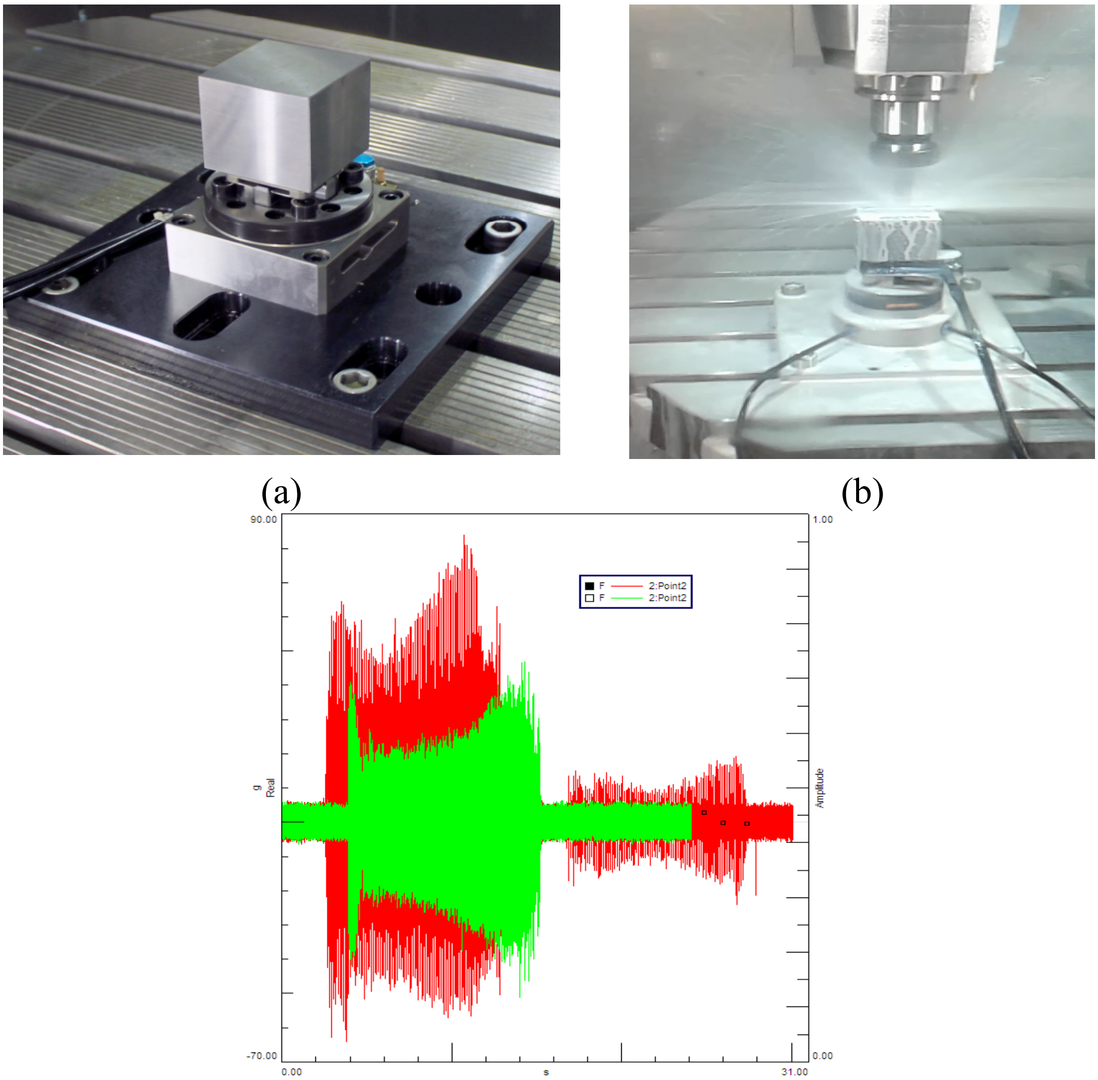

(a) (b) (c)

Fig. 5.32 Workpiece clamped on a pallet system (a), full immersion (slotting) (b), comparison between vibration measured at the top of the workpiece and at the bottom of the workpiece. Red curve: vibration amplitude at the top, Green curve: vibration amplitude at the bottom (c)

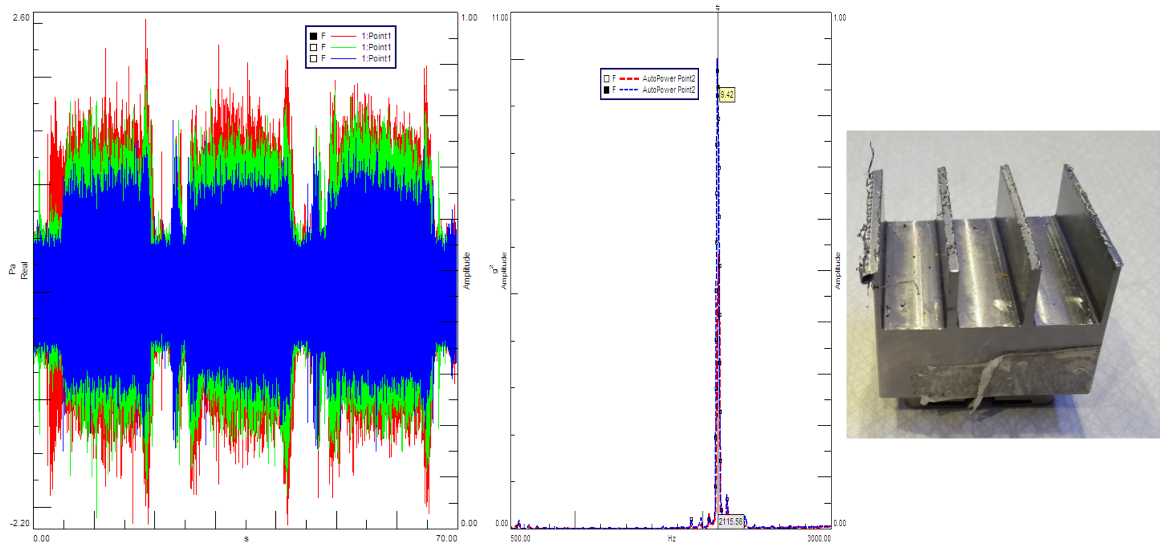

Fig. 5.33 Increasing the axial depth of cut until reaching the stability threshold. Left: time records with various axial depth of cut; blue - 1mm, green – 1.5 mm; red - 2 mm; Right: Frequency domain auto-spectrum; Red curve – 2mm and Blue curve - 2.5 mm

The first mode of vibration of the pallet system is a bending mode, which means that for the same magnitude of the dynamic force, the vibration amplitude at the top of the workpiece will be higher than at the bottom. For the second mode of vibration, which is a torsion mode, the vibration amplitude at the extremities of the workpiece is larger than at the centre. In Fig. 5.32 (c), the vibration amplitude was measured during machining at the top of the workpiece (red curve) and during machining at the bottom of the workpiece (green curve).

5.7.8 Evaluation of the Operational Modal Parameters

The EMA was used to determine the modal parameters in off – operation conditions. This means that the machine tool mechanical structure was separated from the cutting process. In order to assess the interaction between the machine tool structure and the cutting process, the stochastic parametric modelling was employed. The structure is assumed to be excited by a random force and the output signal measured is identified and modelled by parametric models, so called ARMA models. As the interest in this report is to evaluate and compare pallet systems, the analysis will refer only to the interaction between pallet system's structure and cutting process. At higher excitation levels, not only is the pallet system brought into vibration but even the cutting tool holder (see Fig. 5.34). Also, in the waterfall diagram, the tooth passing frequency can be identified.

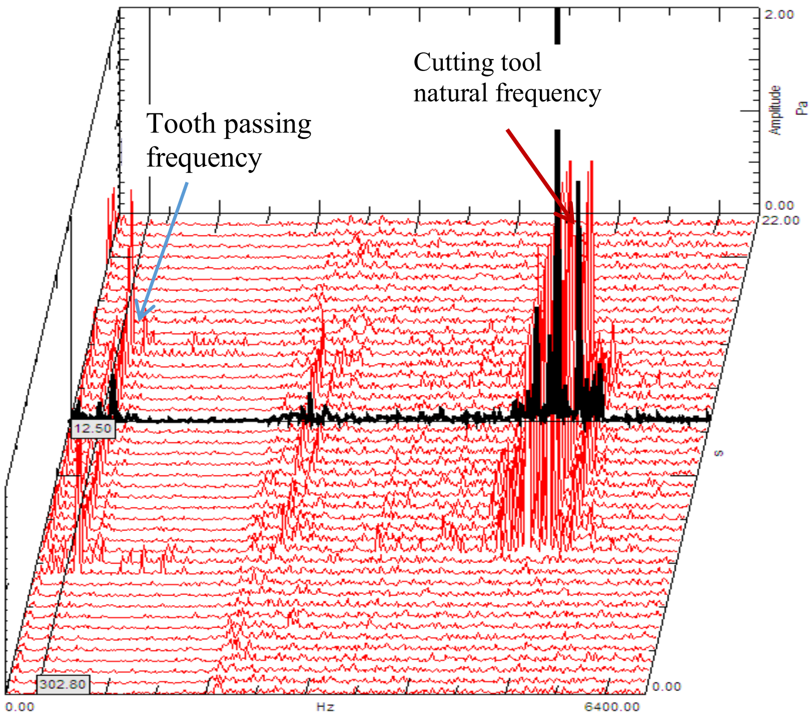

Fig. 5.34 Waterfall diagram at feed rate fr = 0.12 mm/tooth and axial depth of cut doc_{ax} = 2.5 mm

The procedure for evaluation of the ODP is:

1. Identify the output signals: acoustic noise, acceleration in x-, y- and z-directions
2. Build ARMA synthetic models
3. Transform ARMA models to physical models
4. Estimate frequency and damping ratios from physical models.

An example is illustrated below. The time record from machining with Macro pallet system with depth of cut, doc_{ax} = 2.8mm, cutting speed, v_c = 270 m/min and feed rate, f^r = 0.14 mm/tooth is represented in Fig. 5.35.

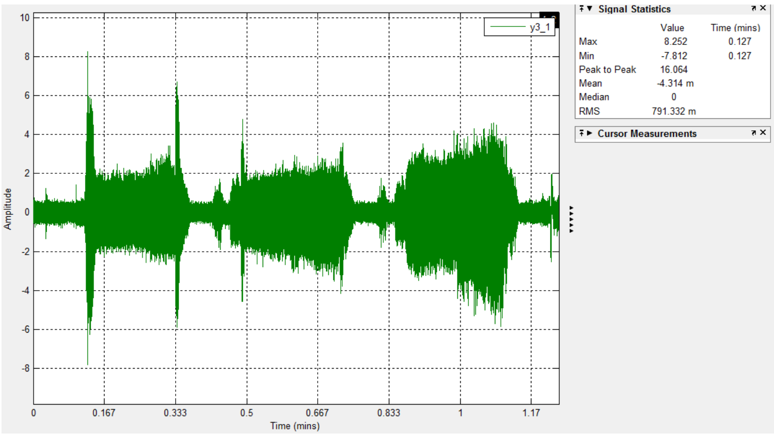

Fig. 5.35 Time record of the machining on pallet system

The acoustic signal represented in Fig. 5.34 is then identified by an ARMA model. An ARMA model is a parametric model consisting in an AR part and an MA part:

Discrete-time ARMA model: $A(z)y(t) = C(z)e(t)$

AR part

Output signal

MA part

Input noise

<u>Parameterization:</u>

Polynomial orders: AR na=12 MA nc=11

$A(z) = 1 - 0.8087\ (+/- 0.2946)\ z^{-1} - 0.1551\ (+/- 0.444)\ z^{-2} + 0.01815\ (+/- 0.2205)\ z^{-3} + 0.1578\ (+/- 0.07877)\ z^{-4} + 0.01117\ (+/- 0.09527)\ z^{-5} + 0.2581\ (+/- 0.07606)\ z^{-6} - 0.06554\ (+/- 0.08284)\ z^{-7} - 0.461\ (+/- 0.07969)\ z^{-8} + 0.4674\ (+/- 0.1457)\ z^{-9} - 0.1881\ (+/- 0.2604)\ z^{-10} - 0.04093\ (+/- 0.2113)\ z^{-11} + 0.1853\ (+/- 0.08648)\ z^{-12}$

$C(z) = 1 - 0.4828\ (+/- 0.2952)\ z^{-1} - 0.1279\ (+/- 0.3529)\ z^{-2} + 0.1373\ (+/- 0.1566)\ z^{-3} - 0.04195\ (+/- 0.0483)\ z^{-4} + 0.01585\ (+/- 0.05173)\ z^{-5} + 0.1642\ (+/- 0.05134)$ z^-6 $+ 0.1326\ (+/- 0.04548)\ z^{-7} - 0.4016\ (+/- 0.05148)\ z^{-8} + 0.3727\ (+/0.1616)$ z^-9 $+ 0.07662\ (+/- 0.2277)$ z^-10 $- 0.07114\ (+/- 0.1135)\ z^{-11}$

Fit to estimation data: 23.97% (prediction focus)

FPE: 0.1948, MSE: 0.191

In the present case, the model was identified by an AR of order 12 and an MA of order 11. The ARMA power spectrum is illustrated in Fig. 5.36.

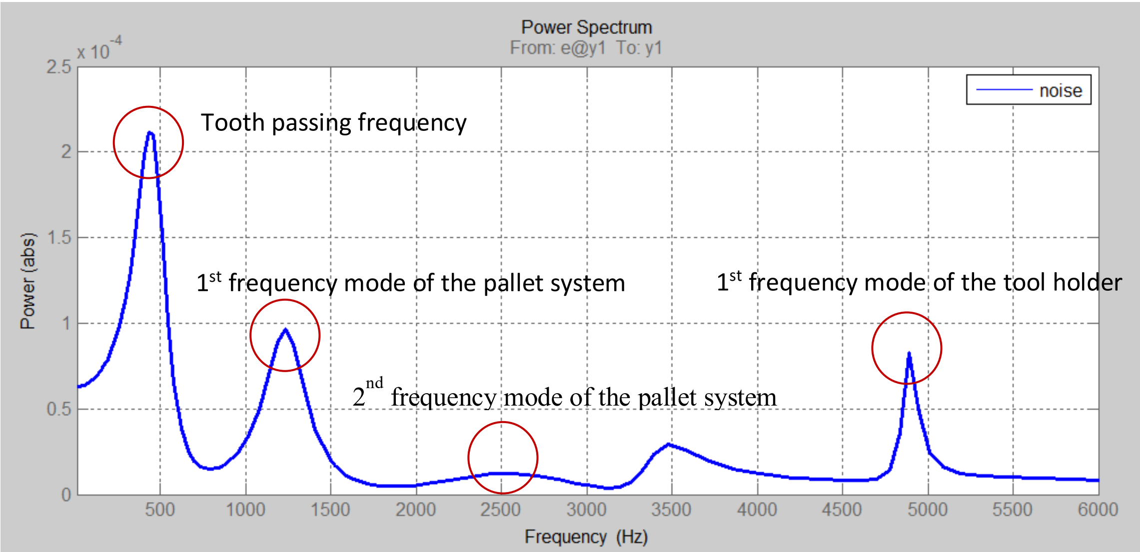

Fig. 5.36 ARMA Power spectrum of the output signal

From the ARMA parameters, the physical model can be built. The operational frequencies and damping are then estimated. The damping and frequency values are statistical estimates of the interaction between mechanical structure and process. The intermittent cutting force exciting the structure at tooth passing frequency generate a forced vibration. The closer the tooth passing frequency to the structure frequency modes, the higher are the amplitude of vibration. Also, as the excitation is the cutting force, it is proportional to the depth of cut and the chip thickness. The higher one of these parameters is, the higher the amplitude of vibration.

In a machining process on the pallet system with doc_{ax} = 1 to 3 mm, feed rate fr = 0.14 mm/tooth, cutting speed vc = 270 m/min, the dominant dynamic source of excitation is the tooth passing frequency. This is illustrated in Fig. 5.37, where the tooth passing frequency is indicated. The ODPs are presented in Table 5.3.

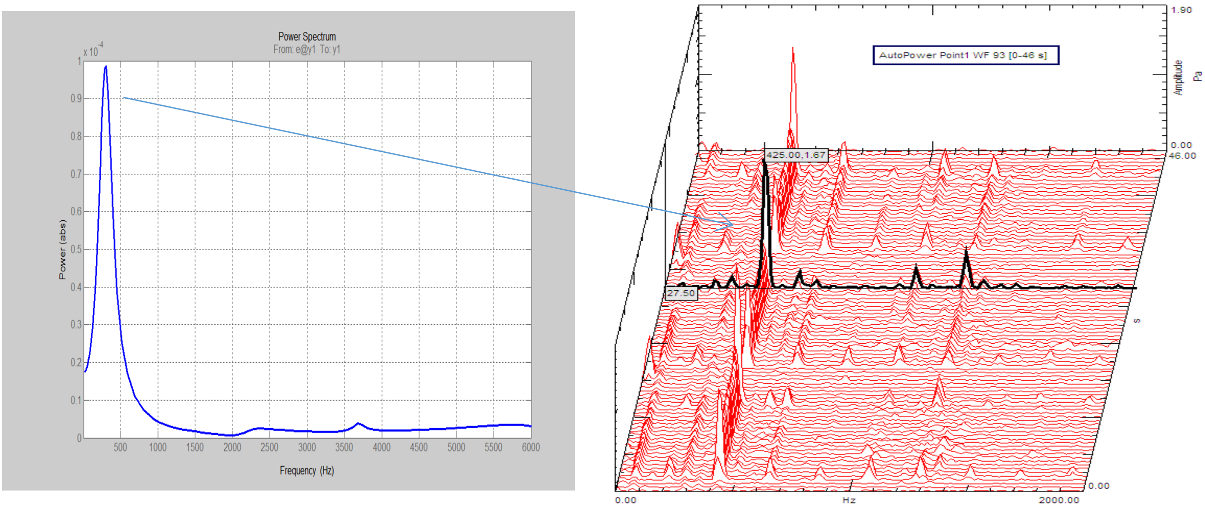

Fig. 5.37 ARMA power spectrum for a machining with doc_{ax} = 3 mm, fr = 0.14 mm/tooth, vc = 270 m/min (left) and waterfall plot (right)

	Frequency (Hz)	**Damping (%)**
Mode 1 (tooth passing)	380	NA
Mode 2 (2nd pallet system)	2224	0.9
Mode 3 (3rd pallet system)	3676	1.6
Mode 4 (tool holder)	4916	0.72

Table 5.3 ODPs in stable machining (non-filtered signal)

Since the tooth passing frequency is outside the first mode range, the forced vibration caused by the excitation at this frequency is controlled by the static stiffness of the structural system. In addition, as the modal damping is defined only in the region around the resonance, this damping cannot be calculated for the excitation force at tooth passing frequency. In stable machining on pallet system, the only excitation that exists is at the tooth passing frequency.

In order to evaluate the operational modal parameters of the pallet system, the signal is filtered to eliminate the tooth passing frequency. The signal processing leads to the estimation of a new spectral function represented in Fig. 5.38. The diagram now reveals the first frequency mode of the pallet system. In Table 5.4 the modal parameters are calculated. Parameters were calculated for a machining operation on pallet system with doc_{ax} = 3 mm and the feed rate fr = 0.14 mm/tooth. The cutting speed is vc = 270 m/min. In this case the material removal took place on the top of the workpiece.

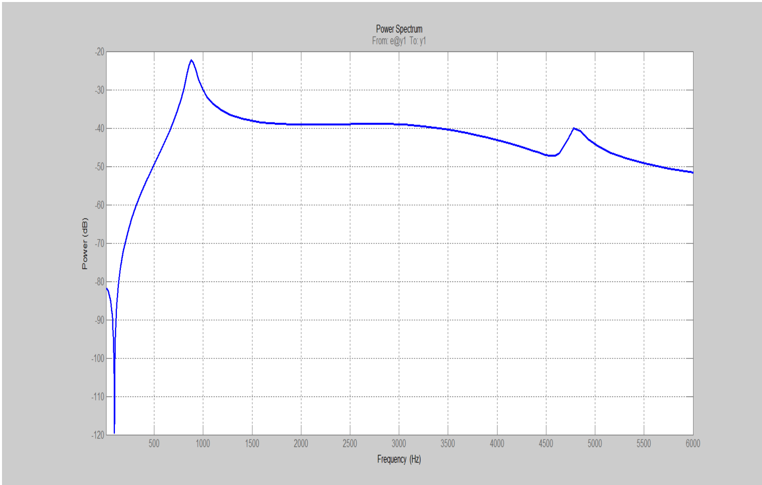

Fig. 5.38 ARMA spectrum of the signal after removing the tooth passing frequency

	Frequency (Hz)	Damping (%)
Mode 1 (1^{st} pallet system mode)	1079	4.78
Mode 2 (tool holder mode)	4778	1.77

Table 5.4 ODPs for machining at top of the workpiece

By continuing the material removing process, as the tool cuts down on the workpiece, the vibration at the first mode is decreasing. However, the vibration at the tool frequency increases mainly due to tool wear. This situation is shown in Fig. 5.39 where the ARMA power spectrum recorded from machining at top level is compared to the machining at the bottom level of the workpiece. While the damping at the first mode of the pallet is twice at the bottom than at the top of the workpiece, the damping at the tool mode is reducing drastically. One of the reasons is machining at a relatively high cutting speed, 270 m/min, which caused thermal damage of the cutting teeth. The tool wear was measured after 14min. machining.

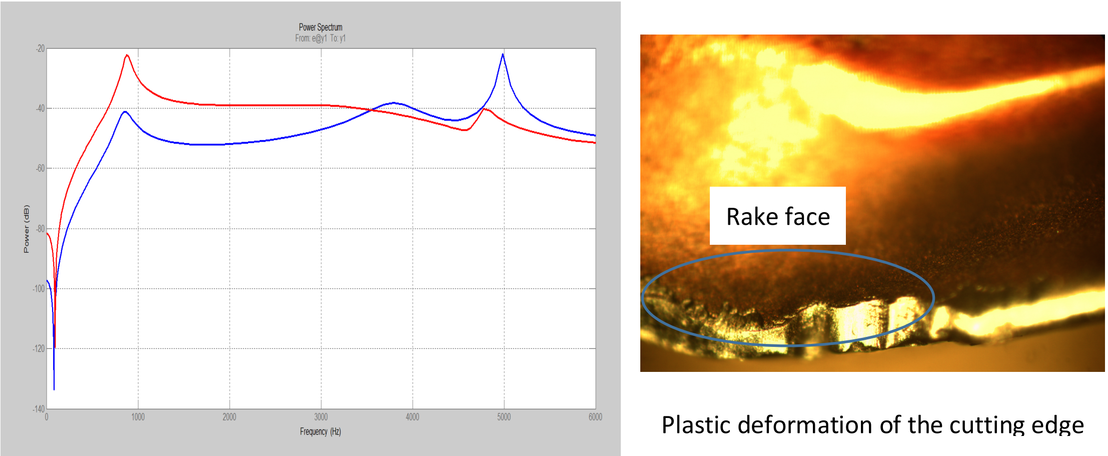

Fig. 5.39 Left - Comparison between ARMA power spectrum at top of the workpiece (red line) and that at the bottom level (blue line). Right – plastic deformation on the cutting edge

	Frequency (Hz)	**Damping (%)**
Mode 1 (1st pallet system mode)	1072	8.67
Mode 2 (tool holder mode)	4985	0.54

Table 5.5 ODP parameters at the bottom of workpiece after 14 min machining

When increasing the depth of cut above the stability threshold, chatter occurs at the pallet system first mode. Fig. 5.40 illustrates the ARMA power spectrum of the signal recorded during machining with feed rate, fr = 0.14 mm/tooth, cutting sped, vc = 286 m/min and depth of cut, doc_{ax} = 3.5 mm.

The depth of cut exceeds the value corresponding to the stability threshold and high vibration is generated in the form of chatter. This can be clearly observed in Fig. 5.40 and in Table 5.6 where the instability at the first frequency mode is proved by the very low damping. It can be noticed from the auto-spectrum that a very large energy is concentrated at the first mode. The energy is about three orders of magnitude higher than in stable machining.

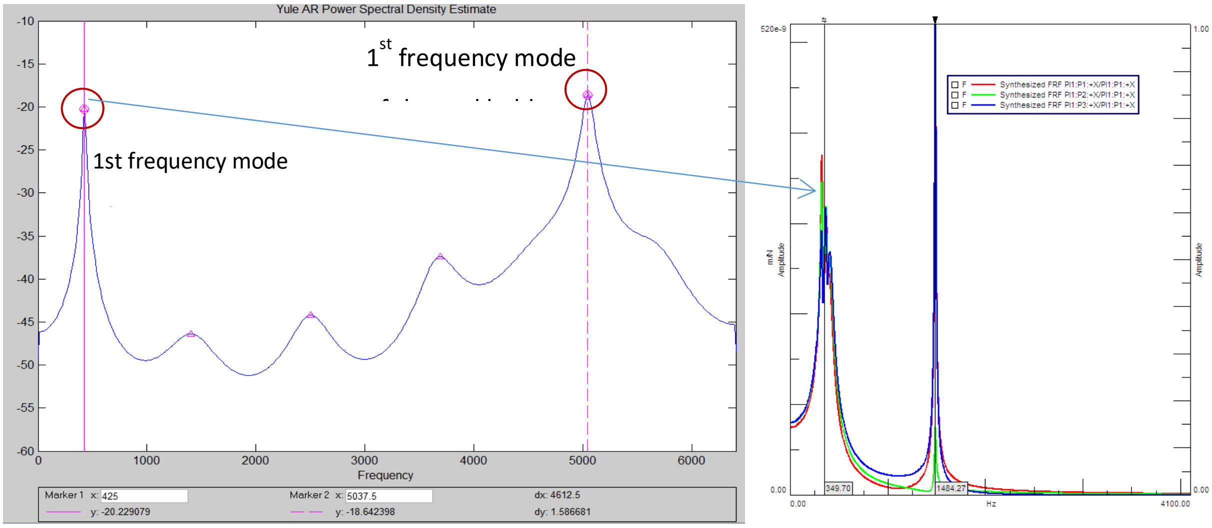

Fig. 5.40 Auto-spectrum for unstable cutting conditions

As illustrated in Fig. 5.40 the dominant frequency modes present are the first mode of the pallet system and the frequency mode of the tool holder. In Table 5.7 the operational damping ration is very close to zero, which describes a genuine unstable process.

	Frequency (Hz)	Damping (%)
Mode 1 (pallet system)	429	0.01
Mode 2 (tool holder)	5078	0.03

Table 5.6 Operational dynamic parameters for unstable cutting conditions

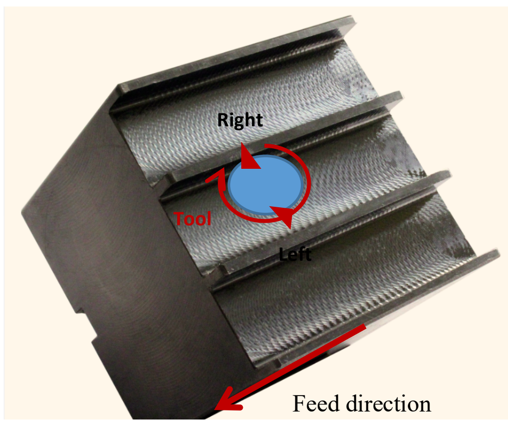

Fig. 5.41 Chatter generation in slot milling; full immersion operation, chatter marks

5.7.9 Real-time Identification of Machining Systems

By real time identification we define procedures for on-line monitoring of the process and to infer a model at the same time as the data is collected. The model is updated at each time instant new data becomes available.

A batch method gives only an average behaviour and cannot monitor time-varying systems. If the model, however, is needed to constantly monitor and control a system during operational conditions, as for instance a machining system under cutting action, it is necessary to identify the model at the same time as new data is acquired (Goethals, 2004). This way the model is recursively updated at each time instant the new data sample becomes available. By 'recursive' term it is understood that at time t the algorithm produces a model by processing the data acquired at time t in a fixed (t-independent) and finite number of arithmetic operations making use of prior information condensed into a fixed (t-independent) and finite memory space.

The reason for using real time identification is that the dynamics of machining systems change in time. In order to detect the onset of chatter and transition from forced vibration to self-excited vibration, close tracking of the system is required.

Recursive identification methods have the following general features (Ljung, 1983):

- they are the main part of adaptive systems where action is taken based on the most recent model;
- they do not occupy much memory space, since not all data are stored;
- they can track time-varying parameters; and
- they can be used as a first step in a fault detection algorithm to find out if the system characteristics have changed significantly.

There are two main drawbacks to recursive identification:

- the model structure has to be selected before starting the recursive identification; and

- the accuracy of recursive methods is not as good as that of off-line methods.

Some well-known recursive methods are (Ljung, 1981):

- recursive prediction-error methods (RPEM);
- recursive pseudolinear regression methods (RPLR); and
- recursive instrumental-variable methods (RIV).

The model-based identification method used in this chapter is based on the recursive prediction-error method (RPEM) (Söderström, 2001). The model structure is based on a parametric process where the input to the model is driven by white noise processes and the model is described by a rational system function and represented by the recursive autoregressive moving average (RARMA) model structure. The process output of this model has the power spectral density (PSD) that is entirely described in terms of model parameters and the variance of the white noise process.

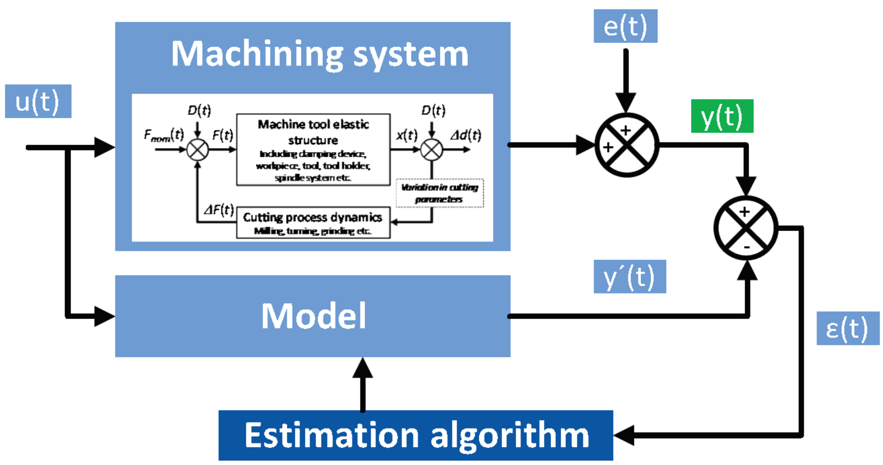

Fig. 5.42 Recursive model-based identification. The algorithm is used to estimate the mathematical model that represents the real operational machining system

Let, as before, $y_j(k\Delta T)$, k = 0, 1, 2 …n be the discrete samples of the measurement response of the displacement of the j-mass for a dynamic system represented by Eq. (5.68). ΔT is the sampling interval. Then the observations $y_j(k\Delta T)$ can be represented by an ARMA model described by Eq. (5.62). The measurement equation is then of the form

$$Y_i = H(k\Delta t, X_j; \Theta) + e_k \qquad (5.78)$$

The RARMA method is designed to minimize the criterion

$V(\theta) = \bar{E}\, f(t, \theta, \varepsilon(t,\theta))$

where $\varepsilon(t,\theta)$ is the prediction error associated with the parameter q, and $\bar{E}$ is the expectation operator.

$$\varepsilon(t,\theta) = y(t) - \hat{y}(t,\theta)$$

where $\hat{y}(t,\theta)$ is the prediction of y(t) and

$$\bar{E}f(t) = \lim_{N\to\infty} \frac{1}{N} \sum_{t=1}^{N} Ef(t)$$

This is done by recursively adjusting the estimates in the negative gradient direction modified by multiplication with a strictly positive define matrix R^{-1}. The purpose of RARMA is to recursively identify the parameters Θ in Eq. (5.79) from the response measurements in the time domain. The recursive algorithm follows the steps

$$\begin{aligned}
\hat{\Theta}_k &= \hat{\Theta}_{k-1} + \mu_k R_k^{-1} \psi_{k;\Theta_{k-1}} \varepsilon_{k;\Theta_{k-1}} \\
\varepsilon_{k;\Theta} &= y_k - \hat{y}_{k;\Theta} \\
R_k &= R_{k-1} + \mu_k \left[\psi_{k;\Theta_{k-1}} \psi^T_{k;\Theta_{k-1}} - R_{k-1} \right]
\end{aligned} \qquad (5.79)$$

where Ψ_k is the gradient of y.

$\psi(t,\theta) = \left[-\frac{d}{d\theta} \varepsilon(t,\theta \right]^T$ which is a column vector, and γ is the gain.

5.7.10 Model Structure Selection and Model Validation

The selection of an appropriate model (from a set of candidate models) to represent an observed system involves traditionally a series of iterative steps. The two major steps in this series are (Hannan, 1979):

- model order selection; and
- checking the selected order validity.

This procedure is normally referred to as the model order selection and validation procedure and the primary objective, both regarding batch ARMA modelling or recursive ARMA modelling, is the choice and validation of AR(p)-order and MA(q)-order.

5.7.11 Model Structure Selection

Once a set of data has been acquired and the removal of DC level, linear trend (corrupting the AR spectra estimates) and seasonal components has been done (assuming stationary properties), appropriate values for the order p and q have to be chosen (Burnham, 2002). Two common and well-known criteria for choosing model order are proven by Akaike, Burnham (2011).

The first criterion, the final prediction error (FPE), selects the model order so that the average error variance for on-step prediction is minimized (Akaike, 1969). The second criterion, Akaike (1973) information criterion (AIC), uses the maximum likelihood approach. A model with a lower value of FPE and AIC is considered to be a better model. By increasing the model order, the sum of squares of the residual will decrease, and a better fit is achieved. In many practical situations, however, it is not advantageous from an identification point of view to choose large p and q random. A high model order will take longer to compute than a model with low order. This time constraint is not crucial for batch identification as the modelling is normally performed off-line.

In real-time recursive schemes for chatter detection, where time-varying processes are tracked, the computation time becomes crucial. If for instance a vibratory process is tracked in time, the choice of model order is a trade-off between increased resolution and decreased variance. In such a system, filtering of data might be helpful when signals vary around a large signal level, improving computational accuracy by removing frequency bands of no interest. This leads to a reduction of spectral components and models of lower order can be used for identification. A high order model will generally result in a small estimated noise variance. However, the mean squared error of the forecast will depend not only on the noise variance of

the fitted model but also on estimation errors of the model parameters. These will be larger for high-order models.
Further, as the vibratory process is assumed to be underdamped, complex conjugate pairs of roots are expected to be obtained from the response characteristic equation. Since the characteristic equation is determined by the AR coefficients, an even order p=2n, of the AR components should be assumed in order to not force real roots. The choice of model order for MA component should be done q=2n-1 (Pandit, 1983).

5.7.12 Model Validation

Once a model has been chosen as a candidate to represent a system it must be checked against a validation criterion. There is no standard method to do this, however, one way is to confront the candidate model with as much information about the true system as possible. This includes a priori knowledge, experimental data and experience of using the model (Bohlin, 1991). From this perspective, some useful techniques that can be used for discarding models are discussed in Ljung (2006).

5.7.13 On-line Identification – Turning Case

A turning experiment demonstrates the recursive identification of ODPs. The longitudinal turning operation was carried out in a conventional turning machine with cutting conditions specified in Fig. 5.43. To acquire data for machining analysis, the sound from the machining process was recorded. A long slender workpiece of steel was used. The suitable order of the models was chosen after a number of trials (based on AIC), both on stable and unstable processes, in order to find the optimum order for each of the time series. The ARMA(3,2) model parameters, estimated from the appropriate models along with their standard deviations are depicted for stable and unstable machining, respectively, in Table 5.7. As can be noticed, the RARMA-ODP algorithm identifies two dominant operational frequencies and related damping ratios.

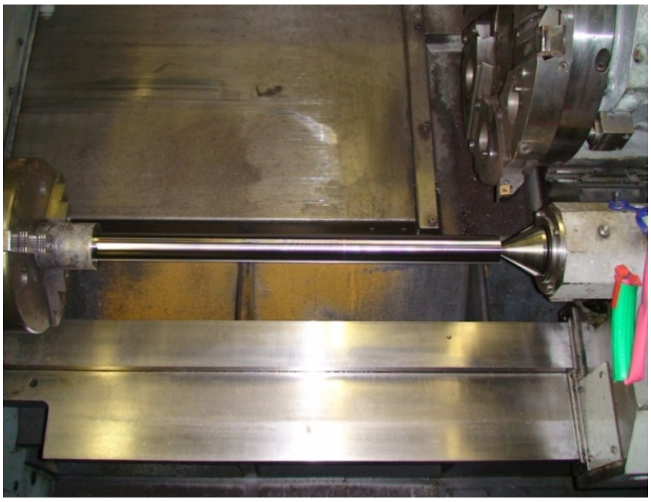

Cutting conditions

Material	Steel grade 0.35-0.40% C, HBS 262.
Workpiece	Length: 585mm Diameter: 45mm
Insert	Sandvik CNMG 120412
Feed	0.25 mm/rev
Cutting speed	150, 155, 160 m/min

Fig. 5.43 Experimental set up for identification of chatter in turning

AR parameters			**MA parameters**	
Stable machining				
a_1	a_2	a_3	b_1	b_2
-0.5029 ±0.0107	0.2472 ±0.0794	-0.5619 ±0.0645	-0.7519 ±0.0127	0.09649 ±0.0121
Unstable machining				
a_1	a_2	a_3	b_1	b_2
-0.3947 ±0.0273	0.4593 ±0.0181	-0.9344 ±0.0262	-0.5464 ±0.0720	0.4476 ±0.0716

Table 5.7 ODP parameters in stable and unstable machining

Figure 5.44 illustrates the results from on-line modelling of the first and second identified modes during the machining of the slender bar. As the cutting tool approaches the middle section of the bar, the system's stiffness and damping reach very low values. The machining system becomes unstable. As the tool approaches the chuck, the system is gradually recovering its stable conditions.

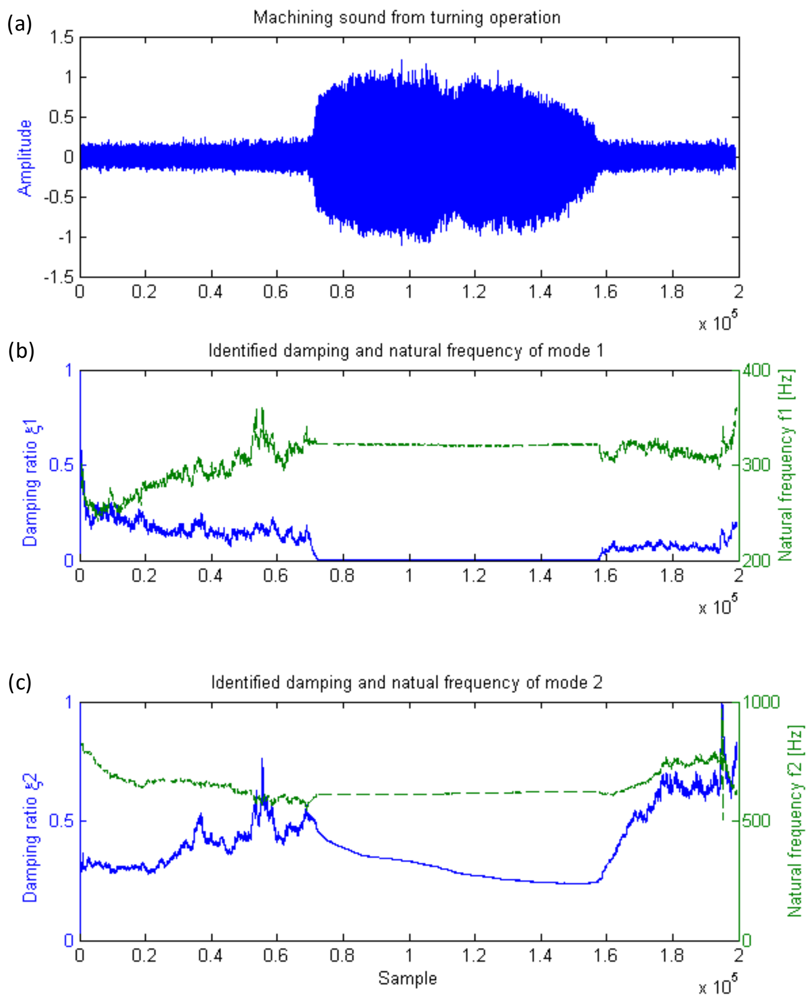

Fig. 5.44 In - process identification and modelling of damping and natural frequency in turning. Sound pressure level measured by a microphone (a), Identified first natural frequency and damping ratio (b), Identified second natural frequency and damping ratio (c)

The sound pressure level was acquired by a microphone. When chatter is completely developed, its frequency stabilizes at f_1 = 290 Hz for the first mode, Fig. 5.44 (b). With increased chatter intensity a significant drop in the damping ratio is apparent, see Table 5.6 and Fig. 5.44 (b). In Fig. 5.44 (c), the ODPs for the second mode are tracked.

5.7.14 Discussions and Conclusions

In this chapter the subject of statistical dynamics has been discussed for the analysis of stability of machining systems. Markov process representation in continuous and discrete representation is used in this study for system parameter identification. In continuous form the Markov process leads to a FKP equation, which is described by a partial differential equation whose solution has been demonstrated can be used as a criterion for stability analysis of systems of random ex citation. In the discrete case the Markov process has been showed to be generated by an ARMA process. An ARMA process can also be used to formulate a parameter based criteria for dynamic stability of machining processes. In sections 5.5 and 5.6 this criterion was used for recursive and batch identification.

The parameter estimation through statistical methods is subjected to estimation errors. In estimating of unknown parameters, errors are likely to arise and it may be appropriate to estimate the interval in which the parameter will lie. Some basic techniques for interval estimation can be found. The major limitation with time-domain approaches is the lack of a reliable model order determination mechanism.

Comparing batch and recursive estimation methods, recursive methods usually have lower accuracy due to limited time to compute models. Another issue concerning recursive estimation methods accuracy is the fact that model order and model structure has to be chosen before identifying the system characteristics. This selection is traditionally done by using some well-known criterion. Choosing model order according to such criterion can in some cases lead to high model orders (depending on degrees of freedom etc.). This can result in unnecessarily large data effecting the computation time. Unfortunately, in industrial applications, no prior knowledge of the number of freedom of the system to perform the analysis is known. In such situations the choice of the sampling frequency becomes critical.

Furthermore, to reduce bias a more flexible model structure (many parameters) is needed whilst reduced variance requires decreasing the number of parameters. Thus, the selection of a model order is determined by two conditions: flexibility; and parsimony (a parameterization is parsimonious if it has as few parameters as possible).

To summarise, there are several benefits arising from employing stochastic models for analysis of dynamics of machining systems:

- RARMA models are characterised by high frequency resolution and objective assessment of component significance. This is in contrast to non-parametric models, such as FFT technique, where the frequency resolution is approximately the inverse of the available data time length.
- Estimation of ARMA model parameters can be implemented in recursive schemes and used for real-time identification of the dynamics of the join system: machine tool elastic structure – cutting process.
- Parsimony – relative short data lengths and few parameters in the model can describe the system behaviour and consequently may be implemented in fast algorithms.

References

Akaike H. (1969) *Fitting autoregressive models for prediction*. Ann. Inst. Stat, Math; 21: 243-347.

Akaike H. (1973) *Information theory and an extension of the maximum likelihood principle*. Akademiai Kiado, Budapest, p. 267-281.

Akaike H, Markovian (1974) *Representation of Stochastic Processes and Its Application to the Analysis of Autoregressive Moving Average Processes*. Annals of the Institute of Statistical Mathematics; 26-3.

Altintas Y, Budak, E. (1995) *Analytical prediction of stability lobes in milling*. CIRP Annals, Manufacturing Technology; 44-1:357-362.

Archenti A. (2008) *Model-based investigation of machining systems characteristics*. KTH Royal Institute of Technology, Licentiate thesis.

Archenti A, Nicolescu C M. (2009) *Model-based identification of manufacturing processes operational dynamic parameters*. In: International conference NewTech, p. 11-18; Galati; Vol. 30/8; ISSN 1221-4566.

Archenti A, Nicolescu C M. (2010) *Recursive Estimation of Operational Dynamic Parameters in Milling Using Acoustic Signal*. CIRP 2nd International Conference on Process Machine Interactions, Vol. 1, Vancouver, BC, Canada.

Archenti A. (2011) *A Computational Framework for Control of Machining System Capability: From Formulation to Implementation*. Doctoral Thesis, KTH Royal Institute of Technology, Stockholm, ISBN: 978-91-7501-162-2.

Beck C, Roepstorff G. (1987) *From Dynamical Systems to the Langevin Equation*. Physica 145A. p. 1-14.

Blankenship G, Papanicolaou G C. (1978) *Stability and control of stochastic systems with wide-band noise disturbances*. I. SIAM J. Appl. Math.; 34-3:437–476.

Bohlin T. (1991) *Interactive system identification: prospects and pitfalls*. Berlin, Germany: Springer-Verlag.

Box G E P, Jenkins G M. (1970) *Time Series Analysis*.

Brecher C, Esser C M, Witt S. (2009) *Interaction of manufacturing process and machine tool*. Annals of the CIRP; 58-1: 588-608.

Brockwell P J, Davis R A. (2002) *Introduction to time series and forecasting*. 2nd ed. USA: Springer Science Business Media Inc.

Budak E, Tunc L T. (2010) *Identification and modeling of process damping in turning and milling using a new approach*. CIRP Annals, Manufacturing Technology; 59-1: 403–408.

Burnham K P, Anderson D R (2002) *Model Selection and Multimodel Inference: A Practical Information-Theoretic Approach*. 2nd ed. Springer-Verlag. ISBN 0-387-95364-7.

Burnham K P, Anderson D R, Huyvaert K P. (2011) *AIC model selection and multimodel inference in behavioral ecology*. Behavioral Ecology and Sociobiology; 65: 23–35.

Cai G Q, Lin Y K. (1996) *Exact and approximate solutions for randomly excited MDOF non-linear systems*. International Journal of Non-Linear Mechanics; 31-5: 647-655.

Caughey T K. (1986) *On the response of non-linear oscillators to* *stochastic excitation*. Probabilistic Engineering Mechanics; 1-1.

Chua A L, Haselwandter C A, Baggio C, Vvedensky D D. (2005 Nov. 8) *Langevin equations for fluctuating surfaces*. Phys Rev E Stat Nonlin Soft Matter Phys. 72(5 Pt 1):051103.

Cooley J W, Tukey J W. (1965) *An algorithm for the machine calculation of complex Fourier series*. Math. Comput.; 19: 297–301.

Crandall S H. (1963) *Perturbation Techniques for Random Vibration of Nonlinear Systems*. The Journal of the Acoustical Society of America; 35-1: 1700-1705.

Dimentberg M F. (1988) *Statistical Dynamics of Nonlinear and Time-Varying Systems*. John Wiley & Sons Inc.

Dimentberg M F, Iourtchenko D V. (2004) *Random Vibrations with Impacts: A Review*. Nonlinear Dynamics; 36: 229–254.

Ghasemi F, Sahimi M, Peinke J, Friedrich R, Jafari G R, Tabar M R. (2007) *Markov analysis and Kramers-Moyal expansion of nonstationary stochastic processes with application to the fluctuations in the oil price*. Phys Rev E Stat Nonlin Soft Matter Phys. Jun; 75(6 Pt 1):060102.

Goethals I, Mevel L, Benveniste I A, De Mo B. (2004) *Recursive output only subspace identification for in-flight flutter monitoring*. In: Proceedings of the 22nd International Modal Analysis Conference (IMAC-XXII), Dearborn, Michigan.

Gradišek J, Friedrich R, Govecar E, Grabec I (2002) *Analysis of data from periodically forced stochastic processes*. Physics letters A. p. 234-238.

Hannan E J, Quinn B G. (1979) *The Determination of the order of an autoregression*. Journal of the Royal Statistical Society, Series B; 41: 190–195.

Harrison R F, Hammond J K. (1986) *Approximate, time domain, non-stationary analysis of stochastically excited, non-linear systems with particular reference to the motion of vehicles on rough ground*. Journal of Sound and Vibration; 105-3: 361-371.

Insperger T, Stepan G. (2002) *Semi-discretization method for delayed systems*. International Journal for Numerical Methods in Engineering; 55: 503–518.

Iourtchenko D V, Dimentberg M F. (2002) *In-Service Identification of Non-Linear Damping From Measured Random Vibration*. Journal of Sound and Vibration; 255-3: 549-554.

Kazakov I E. (1954) *Aproximate Methods for the Statistical Analysis of Noninear Systems*. Trudy VVIA 394.

Kazakov I E. (1955) *Aproximate Probability of Operational Precision of Essentially Nonlinear Feedback Control Systems*. Automation and Remote Control; 17: 423-450.

Krenk S, Roberts J B. (1999) *Local similarity in nonlinear random vibration*. J. Appl. Mech.; 6-1: 225-235.

Ljung L. (2006) *System Identification: Theory for the User*. Prentince-Hal Inc, Englewood, New Jersey.

Ljung L. (1981) *Analysis of a general recursive prediction error identification algorithm*. Automatica; 17-1:89-99.

Ljung L, Söderström T. (1983) *Theory and practice of recursive identification*. Cambridge, Massachusetts, London, England, The MIT Pres.

Manning J E. (1975) *Response Spectra for Nonlinear Oscillations*. Journal of Engineering for Industry, ASME; 97: 1223-1226.

Marple S L Jr. (1987) *Digital spectral analysis with applications*. Englewood, New Jersey, Prentice-Hall Inc.

Mohanty N. (1986) *Random Signals estimation and Identification*. Van Nostrand Reinhold.

Nayfeh v. (1985) *Problems in perturbation*. New York, Wiley.

Nicolescu C M. (1996) *On-Line identification and control of dynamic characteristics of slender workpieces in turning*. Journal of materials processing technology; 58: 374-378.

Nogouchi T. (1985) *The responses of a building on sliding pads to two earthquake models*. Journal of Sound and Vibration; 103-3: 437-442.

Pandit S M, Wu S M. (1983) *Time series and system analysis with application*. Wiley.

Polidori D C, Beck J, Papadimitriou C. (2000) *A new stationary PDF approximation for non-linear oscillators*. International Journal of Non-Linear Mechanics, Vol. 35.

Quintana G, Ciurana J. (2011) *Chatter in machining processes: A review*, International Journal of Machine Tools & Manufacture; 51: 363–376.

Rahman M, Ito Y. (8 Sep. 1986) *Detection of the onset of chatter vibration*. Journal of Sound and Vibration;109-2: 193–205.

Risken H. (1996) *The Fokker-Planck Equation*. Springer-Verlag.

Rivin E I. (2002) *Machine-tool vibration*, 5th ed. C.M. Harris and A.G. Piersol (eds), N.Y., USA, MacGraw-Hill.

Roberts J B, Spanost P D. (1986) *Stochastic averaging: An approximate method of solving random vibration problems*. Int. J. Nonlinear Mechanics; 21-2: 111-134.

Roy R, Spanost P D. (1989) *Wiener-Hermite functional representation of nonlinear stochastic systems*. Structural Safety; 6-2: 187-202.

Rüding F, Krenk S. (2001) *Non-parametric system identification from nonlinear stochastic response*. Probabilistic Engineering Mechanics; 16: 233-243.

Sawaragi Y. (1962) *Statistical Studies on Nonlinear Control Systems*. Osaka, Nippon Print and Pub. Co.

Sun Jian-Qiao. (2006) *Stochastic Dynamics and Control*. Elsevier.

Svetlitsky V A. (2003) *Statistical Dynamics and Reliability Theory for Mechanical Structures*. Springer.

Söderström T, Stoica P. (2001) *System identification*. Uppsala, 2001

Tarantola A. (2005) *Inverse Problem Theory and Model Parameters Estimation*. Philadelphia, SIAM.

Taylor F W. (1907) *On the art of cutting materials*. Transaction of ASME; 28.

Tlusty J M, Spacek (1954) *Self-excited vibrations in machine tools*. Publication of the Czech Academy of Sciences, Prague.

Tlusty J, Ismail F. (1983) *Special aspects of chatter in milling*. ASME J. of Eng. for Industry; 105: 24-32.

Tobias S A. (1965) *Machine Tools Vibrations*. Blackie, London.

Van Kampen N G. (1981) Stochastic Processes in Physics and Chemistry. (North-Holland Personal Library).

Wenjing Ding. (2010) *Self-Excited Vibration, Theory, Paradigms, and Research Methods*. Springer.

Zhang W, Zhang G H. (1994) *Modeling and analysis of nonlinear damping mechanisms in vibrating systems*. Int. J. Mech. Sci.; 36-9.

Chapter 6 Milling Dynamics: Forced Vibration, Self-excited Vibration, and Period-*n* Bifurcations

6.1 Introduction

This chapter investigates the three possible milling response types: forced vibration, self-excited vibration, and period-*n* bifurcations [1-45]. In milling, a rotating tool with defined cutting edges is moved relative to a workpiece in order to remove material and obtain the desired workpiece geometry and dimensions. The tool is typically mounted in a holder which is attached to the spindle. The spindle provides the tool's rotational speed, torque, and power. Multiple axes are then used to manipulate the tool-holder-spindle relative to the workpiece. As the tool rotates relative to the workpiece, the instantaneous chip thickness varies periodically. This gives a periodic forcing function which excites the structural dynamics of the tool-holder-spindle-machine and workpiece. The forcing function exhibits, in general, content at the tooth passing frequency (i.e., the product of the spindle speed and number of cutter teeth) and its integer multiples (or harmonics).

The cutting force causes deflections of the tool and/or workpiece. These vibrations are imprinted on the workpiece surface as a wavy profile and produce time-delayed surface regeneration, which occurs from tooth to tooth. This provides a feedback mechanism because the instantaneous chip thickness depends not only on the process geometry, but also on both the current vibration and the surface left by the previous tooth (one tooth period, or time from one tooth to the next, earlier). The variable chip thickness governs the cutting force which, in turn, affects subsequent tool vibrations. The result is the possibility for the three response types.

Forced vibration, or stable machining conditions, is the desired response because the force level, vibration level, and surface roughness are lower than for the other two options. When stable machining conditions are selected, an additional consideration for high quality part manufacture is surface location error, or part geometric errors that occur due to forced vibrations. Surface location error has been modeled and predicted for stable milling conditions by several authors [46-61]. In these publications, the difference between the machined surface location and the commanded location is measured and/or predicted to determine the influence of (stable) machining conditions on the error.

Due to the time-delayed surface regeneration, various bifurcations (i.e., the appearance of a qualitatively different solution as a control parameter is varied) are exhibited. These bifurcations include: 1) secondary Hopf instability (traditional chatter described by self-excited vibration); and 2) period-n motions (e.g., a period-2, flip, or period doubling bifurcation). Operating under secondary Hopf bifurcation conditions is avoided due to the large tool and/or workpiece motions and cutting forces and, subsequently, poor workpiece surface finish, reduced part accuracy, and potential damage to the workpiece-tool-spindle system. Period-n bifurcations are not as common in practice, but are also generally avoided due to increased surface roughness.

The outline for this chapter follows. To begin, a milling time domain simulation is described. The simulation is then used for a selected dynamic system to generate a stability map that separates stable and unstable spindle speed-axial depth of cut combinations by applying a periodic sampling-based stability metric. The metric is then extended to incorporate subharmonic sampling and the stability map is updated to individually identify stable, secondary Hopf, and period-n bifurcation zones. To augment the stability map, bifurcation diagrams are then presented to display the specific stability behavior versus spindle speed for a fixed axial depth of cut. To add insight to the bifurcation diagrams, Poincaré maps are included, as well as the supporting time dependent displacements. Finally, surface location error results are presented for both stable and period-2 behaviors. Experimental results are included to validate the time domain simulation predictions for both the Poincaré maps and surface location error analysis.

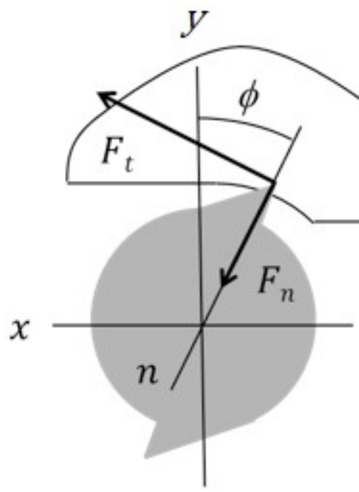

Fig. 6.1 Cutting force geometry. The normal and tangential direction cutting forces, F_n and F_t, are displayed. The fixed x (feed) and y directions, as well as the rotating normal direction, n, are also shown. The angle ϕ defines the tooth angle. The tool feed is to the right for the clockwise tool rotation and the axial depth is in the z direction.

6.2 Time Domain Simulation

Time domain simulation enables the numerical solution of the time-delay equations of motion for milling in small time steps [59]. It is well-suited to incorporating the inherent complexities of milling dynamics, including the nonlinearity that occurs if the tooth leaves the cut due to large amplitude vibrations and complicated tool geometries (incorporating runout, or different radii, of the cutter teeth, non-proportional teeth spacing, and variable helix). The simulation is based on the regenerative force, dynamic deflection model described by Smith and Tlusty [26]. As opposed to analytical stability maps that provide a global picture of the stability behavior, time domain simulation provides information regarding the local cutting force and vibration behavior for the selected cutting conditions. The simulation used in this study proceeds as follows (see Fig. 6.1):

1. the instantaneous chip thickness, $h(t)$, is determined using the vibration of the current and previous teeth at the selected tooth angle

2. the cutting force components in the tangential (t) and normal (n) directions are calculated using:

$$F_t(t) = k_{tc}bh(t) + k_{te}b,$$
$$F_n(t) = k_{nc}bh(t) + k_{ne}b, \text{ ------(6.1)}$$

   where b is the axial depth of cut and the cutting force coefficients are identified by the subscripts t or n for direction and c or e for cutting or edge effect.
3. the force components are used to find the new displacements by numerical solution of the differential equations of motion in the x and y directions:

$$m_x\ddot{x} + c_x\dot{x} + k_x x = F_t(t)\cos\phi + F_n(t)\sin\phi,$$
$$m_y\ddot{y} + c_y\dot{y} + k_y y = F_t(t)\sin\phi - F_n(t)\cos\phi, \text{ ------(6.2)}$$

   where m is the modal mass, c is the modal viscous damping coefficient, and k and the modal stiffness. The subscripts identify the direction and multiple degrees of freedom in each direction can be accommodated.
4. the tool rotation angle is incremented and the process is repeated.

The instantaneous chip thickness depends on the nominal, tooth angle-dependent chip thickness, the current vibration in the direction normal to the surface, and the vibration of previous teeth at the same angle. The chip thickness can be expressed using the circular tooth path approximation as:

$$h(t) = f_t\sin\phi + n(t-\tau) - n(t), \text{ ------(6.3)}$$

where f_t is the commanded feed per tooth, ϕ is the tooth angle, n is the normal direction (see Fig. 6.1), and τ is the tooth period and represents the time delay. The tooth period is defined as:

$$\tau = \frac{60}{\Omega N_t} \text{ (sec), ------(6.4)}$$

where Ω is the spindle speed in rpm and N_t is the number of teeth. The vibration in the direction of the surface normal for the current tooth depends on the x and y vibrations as well as the tooth angle according to:

$$n = x \sin \phi - y \cos \phi \text{ ------(6.5)}$$

For the simulation, the strategy is to divide the angle of the cut into a discrete number of steps. At each small time step, Δt, the cutter angle is incremented by the corresponding small angle, $\Delta\phi$. This approach enables convenient computation of the chip thickness for each simulation step because: 1) the possible teeth orientations are predefined; and 2) the surface created by the previous teeth at each angle may be stored. The cutter rotation:

$$\Delta\phi = \frac{360}{SR} \text{ (deg) ------(6.6)}$$

depends on the selection of the number of steps per revolution, SR. The corresponding time step is:

$$\Delta t = \frac{60}{SR\Omega} \text{ (sec). ------(6.7)}$$

A vector of angles is defined to represent the potential orientations of the teeth as the cutter is rotated through one revolution of the circular tool path, ϕ = $[0,\ \Delta\phi,\ 2\Delta\phi,\ 3\Delta\phi,\ \dots\ ,\ (SR-1)\Delta\phi]$. The locations of the teeth within the cut are then defined by referencing entries in this vector.

In order to accommodate the helix angle for the tool's cutting edges, the tool may be sectioned into a number of axial slices. Each slice is treated as an individual straight tooth endmill with radius r, where the thickness of each slice is a small fraction, Δb, of the axial depth of cut, b. Each slice incorporates a distance delay:

$$r\chi = \Delta b \tan\gamma \text{ ------(6.8)}$$

relative to the prior slice (nearer the cutter free end), which becomes the angular delay between slices:

$$\chi = \frac{\Delta b \tan\gamma}{r} = \frac{2\Delta b \tan\gamma}{d} \quad \text{(rad) ------(6.9)}$$

for the rotating endmill, where d is the endmill diameter and γ is the helix angle. In order to ensure that the angles for each axial slice match the predefined tooth angles, the delay angle between slices is:

$$\chi = \Delta\phi. \text{ ------(6.10)}$$

This places a constraint on the Δb value. By substituting $\Delta\phi$ for χ and rearranging, the required slice width is:

$$\Delta b = \frac{d(\Delta\phi)}{2\tan\gamma}\ . \text{ ------(6.11)}$$

Once the x and y direction displacements are determined (Eq. 6.2), the final spatial trajectory for each tooth is determined by summing these vibration-induced displacements with the nominal cycloidal motion of the teeth due to the combined translation and rotation. This final spatial trajectory is finally used to define the machined surface and, subsequently, to predict the SLE and surface roughness. The nominal cycloidal motion components in the x and y directions are defined in Eqs. 6.12 and 6.13, where i is the time step index and Δf is the linear feed per time step (see Eq. 6.14).

$$x_{nom} = r \sin \phi + i\Delta f \text{ ------(6.12)}$$

$$y_{nom} = r \cos \phi \text{ ------(6.13)}$$

$$\Delta f = \frac{f_t N_t}{SR} \text{ ------(6.14)}$$

This simple description can be extended to include:

1. multiple tool modes – the x and y forces are used to calculate the acceleration, velocity, and displacement for each tool mode (represented by the modal parameters) and the results are summed in each direction
2. flexible workpiece – the x and y forces are also used to determine the workpiece deflections, again by numerical integration, and the relative tool-workpiece vibration is used to calculate the instantaneous chip thickness
3. runout of the cutter teeth – the chip thickness is updated by the runout of the current tooth
4. unequal teeth spacing – the tooth angle vector is modified to account for the actual tooth pitch.

Using this time domain simulation approach [59], the forces, displacements, and velocities are calculated. These results are then used to generate stability maps, bifurcation diagrams, and Poincaré maps.

6.3 Stability Maps

Stability maps, or stability lobe diagrams, identify the limiting axial depth of cut (vertical axis) as a function of spindle speed (horizontal axis).

Traditionally, this limit is represented as a single contour which separates stable (forced vibration only) from unstable (secondary Hopf or period-n bifurcations) parameter combinations. In milling, the forcing frequency is defined by the tooth period, which depends on the spindle speed and number of teeth; see Eq. 6.4. Therefore, to evaluate the process performance, the output signals (force and vibration) from the time domain simulation were sampled at the tooth period. This provided once-per-tooth sampling. If the once-per-tooth sampled points repeat, the response is periodic with the forcing function and the process is stable. If they do not repeat, the response exhibits either secondary Hopf or period-n bifurcations and is considered unstable.

To construct a stability map using the time domain simulation results, a separate simulation was completed at each position in the selected grid of spindle speed and axial depth values. To automatically establish the stability limit using the predicted time domain signals, the following stability metric was implemented [62]:

$$M1 = \frac{\sum_{i=2}^{N} |x_{s1}(i) - x_{s1}(i-1)|}{N}, \text{ ------(6.15)}$$

where x_{s1} is the vector of once-per-tooth sampled x displacements and N is the length of the x_{s1} vector. Other variables, such as y displacement or cutting force could be selected as well. With this stability metric, the absolute value of the differences in successive sampled points is summed and then normalized. The sampled points repeat for a stable cut, so the $M1$ value is ideally zero. For unstable cuts, on the other hand, $M1 > 0$ and grows over time, due to the asynchronous motion in secondary Hopf instability and jumps from one fixed point to the next in period-n bifurcations.

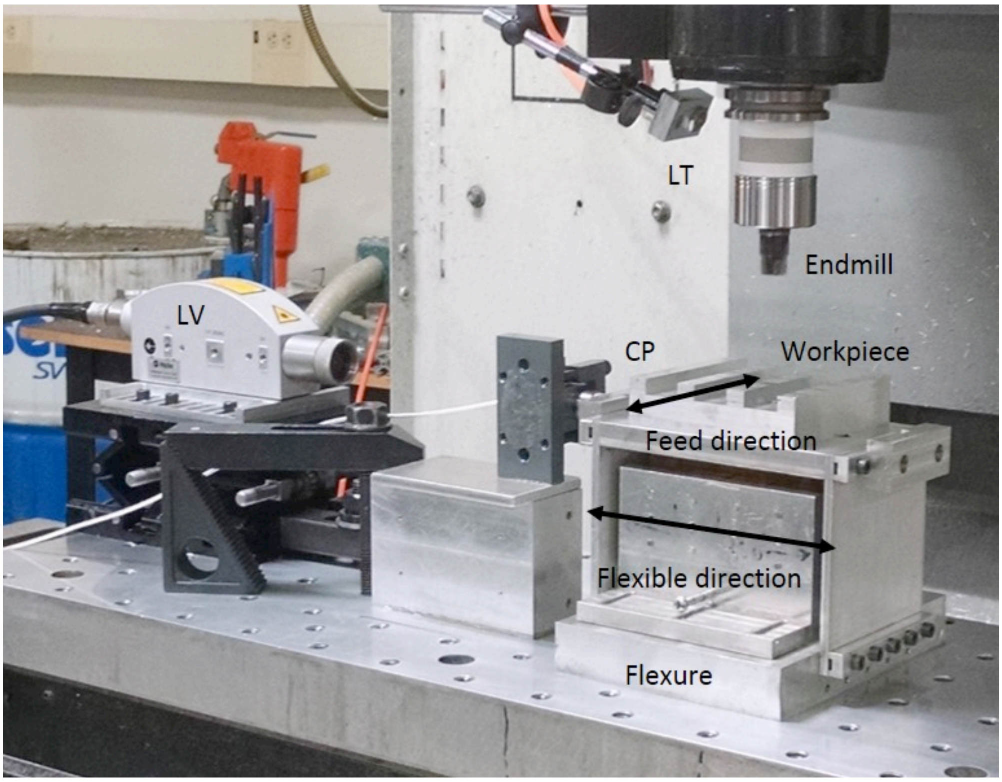

Fig. 6.2 Flexure-based experimental setup with laser vibrometer (LV), laser tachometer (LT), and capacitance probe (CP). The feed direction and the flexible direction for the single degree of freedom flexure are also identified. The setup was located on a Haas TM-1 CNC milling machine.

The flexure-based setup displayed in Fig. 6.2 was used to define a physical system for simulation and testing [63-64]. The setup included a parallelogram leaf-type flexure with an aluminum workpiece mounted on top. The in-process vibration data was collected using a Polytec OFV-5000 laser vibrometer (velocity) and Lion Precision DMT20 capacitance probe (displacement). Both were aligned with the flexible direction for the single degree of freedom flexure. Note that the feed direction was perpendicular to this flexible direction. Once-per-tooth sampling for stability identification was accomplished using a laser tachometer and reflective target attached to the rotating tool holder. The flexure dynamics were identified by modal testing: 125.8 Hz natural frequency, 0.0136 viscous damping ratio, and 1.75×10^6 N/m stiffness in the flexible direction. The dynamics for the 19.1 mm diameter, 0 deg helix angle tool (one insert) were symmetric: 1188 Hz natural frequency, 0.095 viscous damping ratio, and 4.24×10^7 N/m stiffness. The 6061-T6 aluminum alloy cutting force coefficients were: k_{tc} = 770×10^6 N/m^2, k_{nc} = 368×10^6 N/m^2, k_{te} = 22×10^3 N/m, and k_{ne} = 22×10^3 N/m. The experimental up milling cutting conditions were: 5 mm axial depth, 2 mm radial depth, 0.35 mm/tooth, and variable spindle speed. Spindle speed values were selected to span from forced vibration, self-excited vibration, and period-n conditions while holding all other parameters constant.

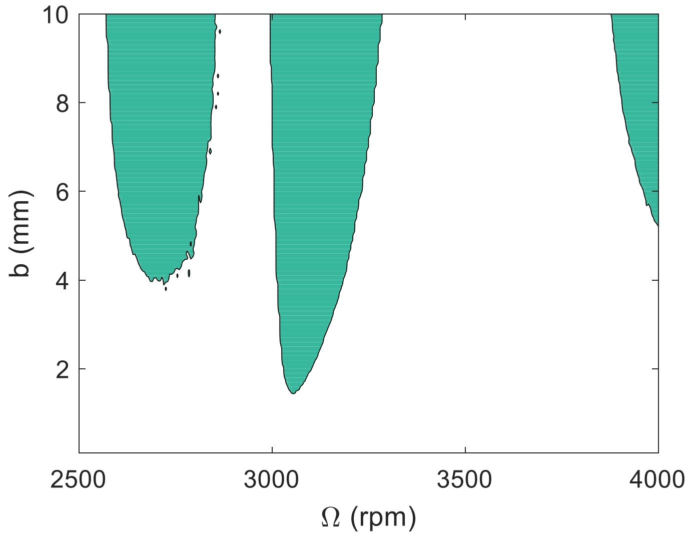

Fig. 6.3 Simulated stability map for selected dynamic system with a 2 mm radial depth and 0.35 mm/tooth feed per tooth ($M1 = 1$ μm contour).

The stability map for up milling with a 2 mm radial depth and 0.35 mm/tooth feed per tooth is displayed in Fig. 6.3. To construct the map, the Eq. 6.15 stability metric was applied to the time domain simulation x direction workpiece displacements; this was the flexible direction for the flexure (the feed was in the y direction, which corresponded to the flexure's stiff direction). The resolution for the time domain simulations was 5 rpm in spindle speed and 0.1 mm in axial depth. The initial transients were removed and the $M1$ value for each simulation was calculated from the final 25% of each time record. An arbitrarily small value of $M1$ = 1 μm was selected to differentiate between stable and unstable parameter combinations; this contour is shown in Fig. 6.3 and identifies the stability limit. Both stable (no color) and unstable (shaded) zones are observed. As noted, the stable area identifies the spindle speed-axial depth combinations where only forced vibration is observed. The unstable are may be either secondary Hopf or period-n bifurcations.

The $M1$ stability metric defined in Eq. 6.15 and applied in Fig. 6.3 does not separately identify secondary Hopf and period-*n* bifurcations. However, using subharmonic sampling at $n\tau$ (n = 2, 3, 4, …), the corresponding period-*n* bifurcations can be established [65]. For example, when sampling at 2τ, the stability metric becomes "blind" to period-2 bifurcations, or behavior that repeats every other tooth period rather than each period as in forced vibration. By sampling at every other tooth passage (2τ), the period-2 behavior appears as synchronous motion (stable). The same is true for period-3 bifurcations if the sampling interval is 3τ, and so on. This subharmonic sampling can be applied to add detail to the Fig. 6.3 stability map. To do so, the $M1$ metric is augmented to enable sampling at other integer tooth periods. Generically, the metric can be expressed as shown in Eq. 16, where the integer n = 1, 2, 3, … defines the sampling period (i.e., $n\tau$).

$$Mn = \frac{\sum_{i=2}^{N} |x_{sn}(i) - x_{sn}(i-1)|}{N} \quad \text{------(6.16)}$$

The subharmonic sampling approach was implemented to construct a stability map that individually identifies each bifurcation type. The metrics $M1$ through $M7$, which represent τ through 7τ integer sampling periods, are used to isolate the stable zone as well as the different bifurcation types: period-2, -3, -4, -5, -6, -7, and secondary Hopf.

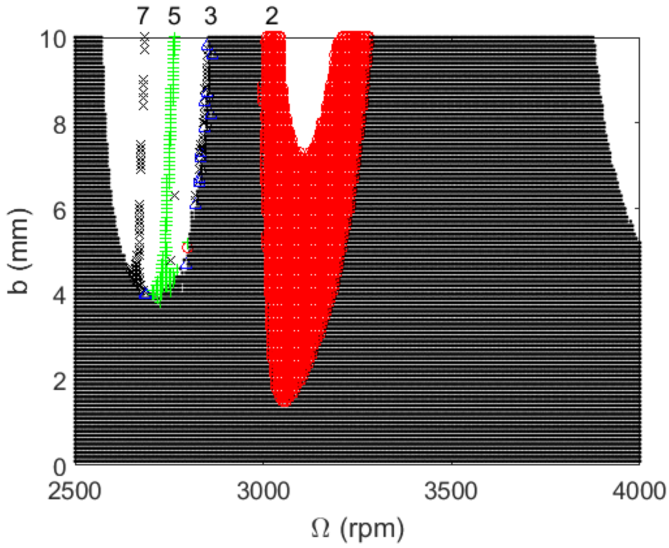

Fig. 6.4 New stability map. Period-2 (circle), period-3 (triangle), period-5 (+), period-7 (×), and secondary Hopf (open space) bifurcations are identified. The dots indicate stable (forced vibration) behavior.

The logic used to construct the stability map follows:

```
if M1 ≤ 1 μm
        plot a dot (stable)
elseif M2 ≤ 1 μm
        plot a circle (period-2)
elseif M3 ≤ 1 μm
        plot a triangle (period-3)
elseif M4 ≤ 1 μm and M2 > 1 μm
        plot a square (period-4, excludes period-2)
elseif M5 ≤ 1 μm
        plot a + (period-5)
elseif M6 ≤ 1 μm and M2 > 1 μm and M3 > 1 μm
        plot a diamond (period-6, excludes period-2 and period-3)
elseif M7 ≤ 1 μm
        plot an × (period-7)
else
        do nothing (secondary Hopf or high order period-n)
end
```

The result is displayed in Fig. 6.4. The stable zone is the dark area filled with dots and the various instabilities are indicated by the symbols. The open space represents secondary Hopf bifurcation. The period-*n* bifurcation zones are also identified by the numerals at the top of the figure (i.e., periods-2, 3, 5, and 7).

6.4 Bifurcation Diagrams

In the bifurcation diagrams developed for this study, the once-per-tooth sampled displacement, x_s (vertical axis), was plotted against the spindle speed (horizontal axis). The transition in behavior from stable to period-*n* or secondary Hopf bifurcations is then directly observed. A stable cut appears as a single point (i.e., the sampled points repeat when only forced vibration is present). A period-2 bifurcation, on the other hand, appears as a pair of points offset from each other in the vertical direction. This represents the two solutions, or fixed points, that appear due to the behavior that repeats every other tooth period. A secondary Hopf bifurcation is seen as a vertical distribution of points; this represents the range of once-per-tooth sampled displacements that occur due to the quasi-periodic, asynchronous behavior.

Returning to Fig. 6.4, it is seen that the stability behavior changes with spindle speed at an axial depth of b = 10 mm. Starting at the left end of the stability map, stable conditions are observed at 2500 rpm (dots). This changes to secondary Hopf instability (open area) at 2753 rpm. Zones of period-7, 5, and 3 occur prior to a return to stable conditions at 2858 rpm. The corresponding bifurcation diagram for this axial depth over the spindle speed range from 2500 rpm to 2900 rpm is provided in Fig. 6.5, where the spindle speed resolution is 1 rpm.

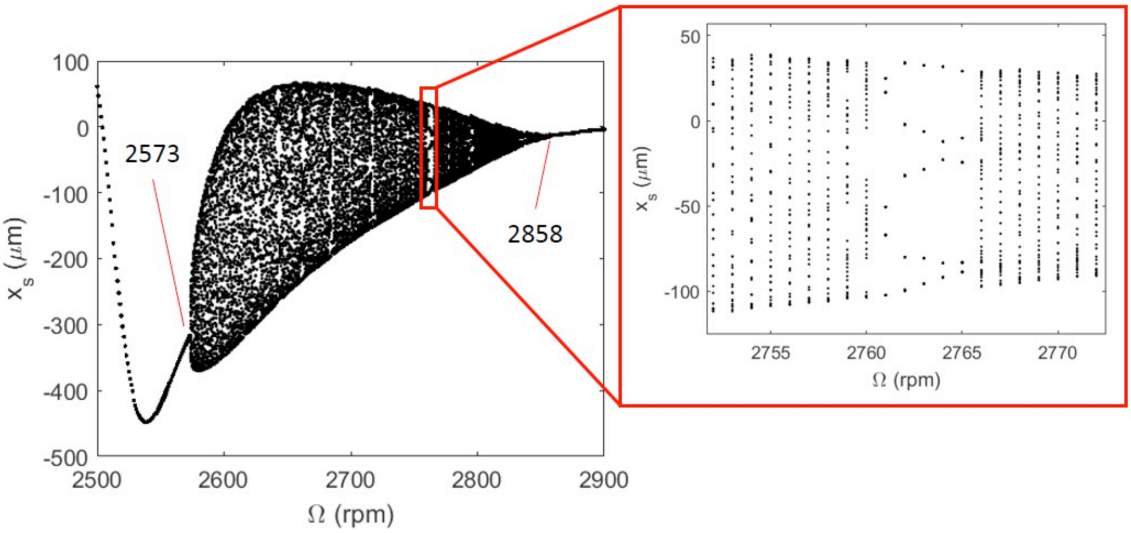

Fig. 6.5 Bifurcation diagram for a 10 mm axial depth of cut and spindle speeds from 2500 rpm to 2900 rpm. The vertical axis is the once-per-tooth sampled workpiece displacements and the horizontal axis is the spindle speed. The inset shows the period-5 bifurcation range between 2761 rpm and 2765 rpm identified in Fig. 6.4.

A second bifurcation diagram is displayed in Fig. 6.6. The axial depth is again 10 mm, but the spindle speed range is 2900 rpm to 3400 rpm. This new spindle speed range spans the period-2 zone shown in Fig. 6.4. It is seen that stable behavior persists from 2900 rpm to 2998 rpm (a single point at each spindle speed). Period-2 instability then occurs between 2998 rpm and 3047 rpm (two points). Combined period-2 and secondary Hopf conditions are observed between 3047 rpm and 3104 rpm (two separate lines of points). The spindle speed range between 3104 rpm and 3145 rpm is characterized by secondary Hopf instability before transitioning back to the combined behavior between 3145 and 3200 rpm. Period-2 bifurcations occur from the range from 3200 rpm to 3282 rpm. Stable cutting then persists between 3282 rpm and the right hand side of the diagram at 3400 rpm.

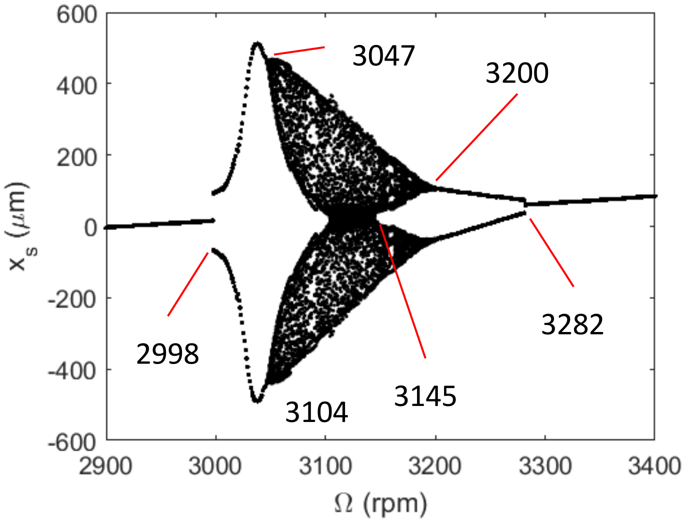

Fig. 6.6 Bifurcation diagram for a 10 mm axial depth of cut and spindle speeds from 2900 rpm to 3400 rpm. Stable, period-2, combined period-2 and secondary Hopf, and secondary Hopf behavior is observed.

6.5 Poincaré Maps

Poincaré maps were constructed using both experiments and simulations. For the experiments, the displacement and velocity of the flexible workpiece (Fig. 6.2) were recorded using a capacitance probe and laser vibrometer and then sampled once-per-tooth period using a laser tachometer. In simulation, the displacement and velocity were predicted, but the same sampling strategy was applied. By plotting the displacement versus velocity, the phase space trajectory could be observed in both cases. The once-per-tooth period samples were then superimposed and used to interrogate the milling process behavior.

For stable cuts, the motion is periodic with the tooth period, so the sampled points repeat and a single grouping of points is observed. When secondary Hopf instability occurs, the motion is quasi-periodic with tool rotation because the chatter frequency is (generally) incommensurate with the tooth passing frequency. In this case, the once-per-tooth sampled points do not repeat and they form an elliptical distribution. For a period-2 bifurcation, the motion repeats only once every other cycle (i.e., it is a sub-harmonic of the forcing frequency). In this case, the once-per-tooth sampled points alternate between two solutions. For period-n bifurcations, the sampled points appear at n distinct locations in the Poincaré map.

The time domain simulation result for an up milling operation with an axial depth of 5 mm, radial depth of 2 mm, 0.35 mm/tooth feed, and spindle speed of 3180 rpm is displayed in Fig. 6.7. Both the x (flexible direction) displacement and the once-per-tooth sampled points are included. It is seen that, after the initial transients attenuate, two solutions occur that alternate from one tooth passage to the next. This represents a period-2 bifurcation. Note this spindle speed-axial depth combination appears within the period-2 zone in Fig. 6.4.

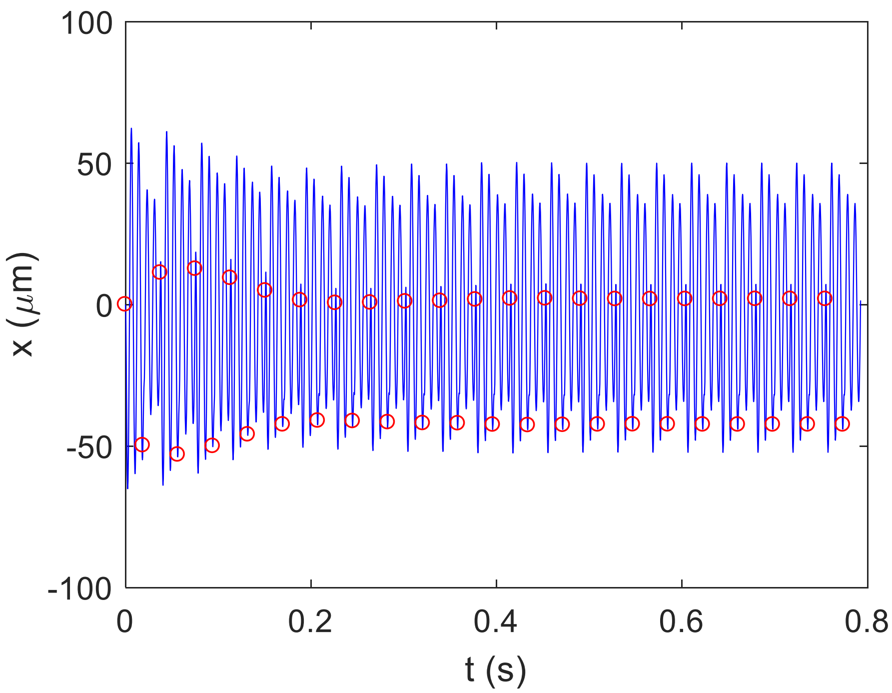

Fig. 6.7 Simulated x displacement for 3180 rpm, 5 mm axial depth, 2 mm radial depth, and 0.35 mm feed per tooth. The continuous signal (line) and once-per-tooth sampled points (circles) show period-2 behavior.

The simulated and experimental Poincaré maps for $\{\Omega, b\}$ = {3180 rpm, 5 mm} are provided in Fig. 6.8. Two fixed points appear for the period-2 bifurcation condition. The simulation (left) and experiment (right) agree.

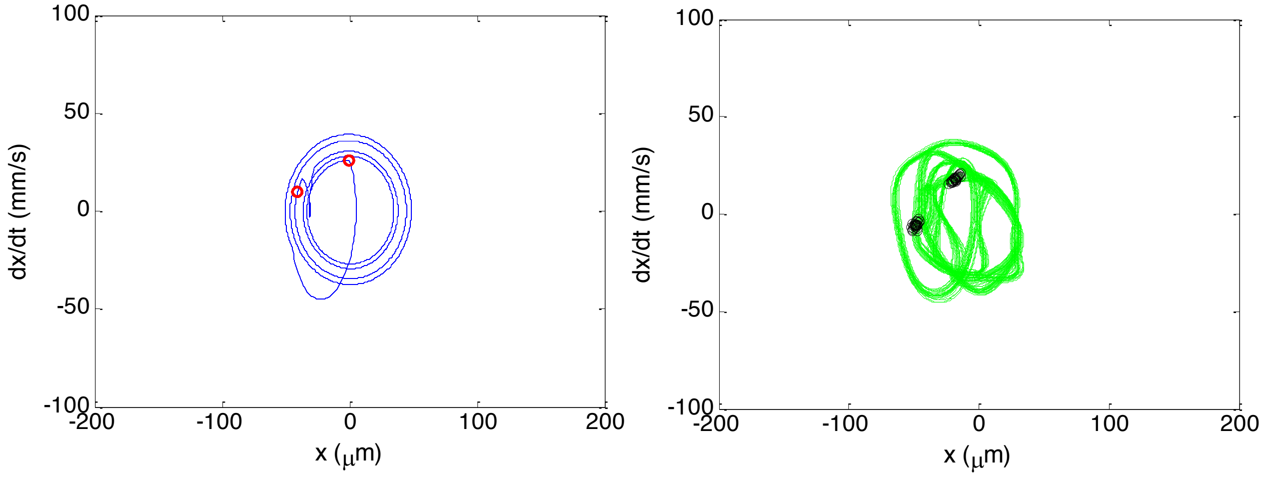

Fig. 6.8 Predicted (left) and measured (right) Poincaré maps for 3180 rpm. Period-2 behavior is seen. Note that x indicates the flexible direction for the flexure. The feed direction was y for the experiments.

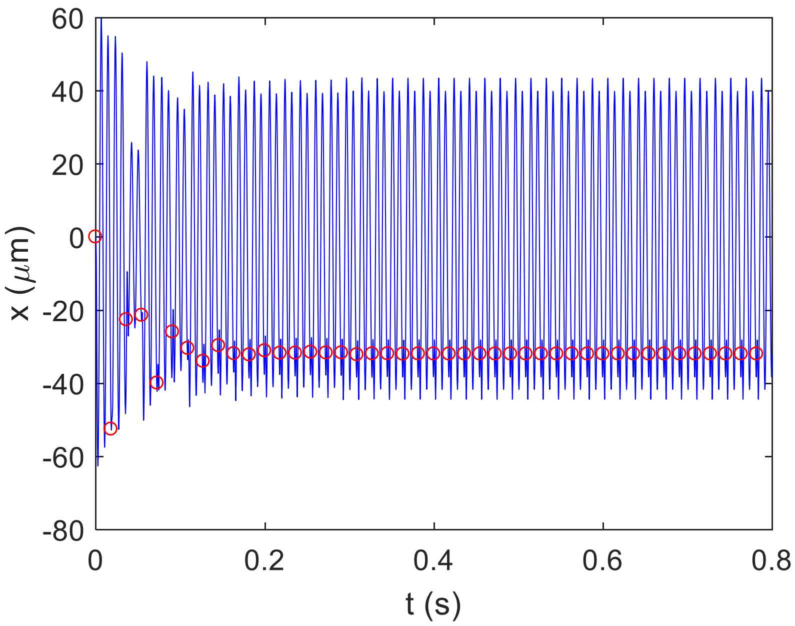

Fig. 6.9 Simulated x displacement for 3300 rpm, 5 mm axial depth, 2 mm radial depth, and 0.35 mm feed per tooth. The cut is stable.

The spindle speed was next increased to 3300 rpm with all other parameters remaining constant. The time domain simulation results are displayed in Fig. 6.9 and the corresponding Poincaré maps in Fig. 6.10. For this spindle speed, stable behavior is obtained (see Fig. 6.4). The simulation and experiment again agree.

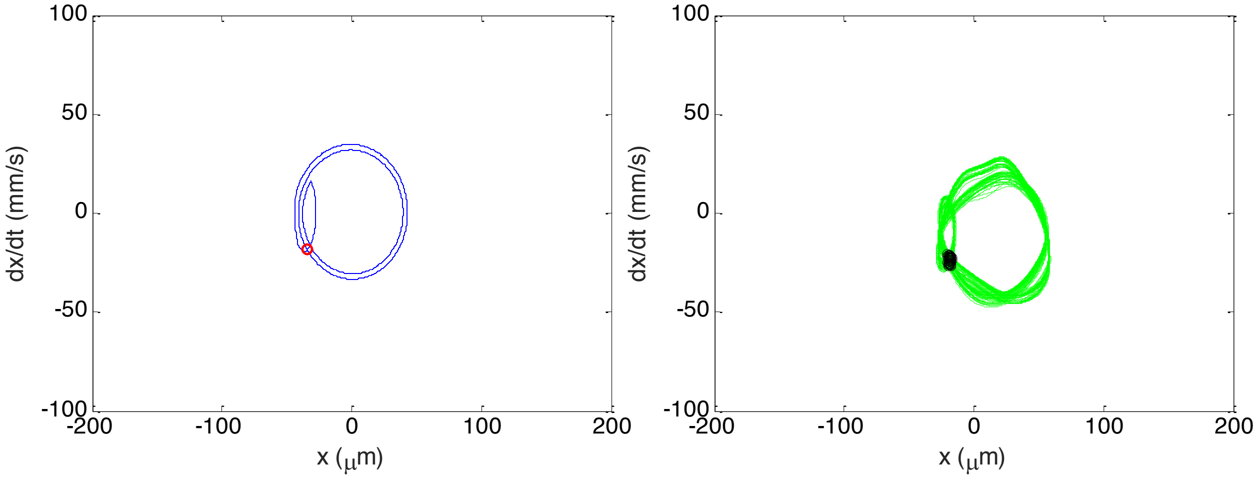

Fig. 6.10 Predicted (left) and measured (right) Poincaré maps for 3300 rpm. Stable behavior is seen.

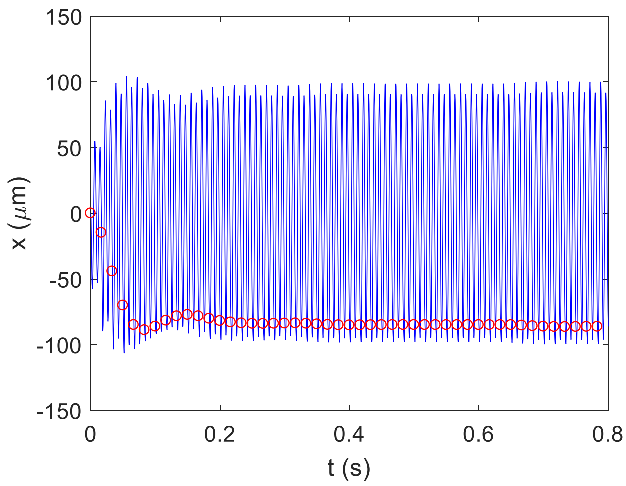

Fig. 6.11 Simulated *x* displacement for 3600 rpm, 5 mm axial depth, 2 mm radial depth, and 0.35 mm feed per tooth. The cut is stable.

The final spindle speed was 3600 rpm. The time domain simulation results are displayed in Fig. 6.11 and the corresponding Poincaré maps in Fig. 6.12. For this spindle speed, stable behavior is again obtained (see Fig. 6.4), but the forced vibration response is larger than Figs. 6.9 and 6.10 because the first harmonic of the tooth passing frequency (3600/60·2 = 120 Hz) is close to the flexure's natural frequency (125.8 Hz). The simulation and experiment again agree.

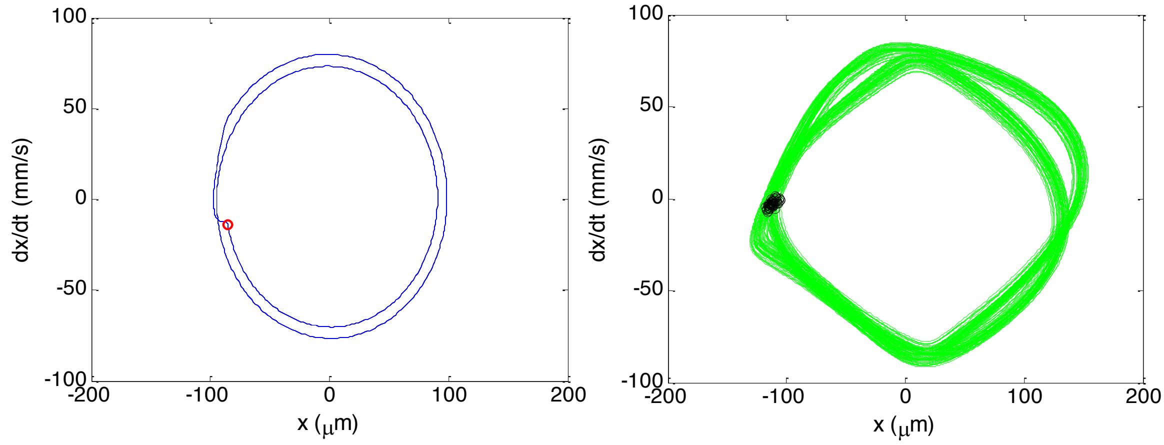

Fig. 6.12 Predicted (left) and measured (right) Poincaré maps for 3600 rpm. Stable behavior is seen with increased amplitude relative to 3300 rpm (Fig. 6.10).

6.6 Surface Location Errors

The process dynamics can impose significant limitations on milling efficiency due to secondary Hopf bifurcations that lead to large forces, displacements, and poor surface quality. However, productivity can also be limited by forced vibrations which cause surface location error (SLE), or workpiece geometric inaccuracies that result from dynamic displacements of the tool during stable milling. In order to explore the variation in SLE with spindle speed, the workpiece geometry shown in Fig. 6.13 was selected. The initial ribs were machined directly on the flexure so it was ensured that the part was aligned with the machine axes. Low axial and radial depths were selected to minimize vibration levels and the same conditions were used to machine each rib. Prior to beginning the SLE experiments, a test workpiece was machined and the four ribs were measured on a coordinate measuring machine, or CMM, to evaluate the repeatability of the starting rib dimensions (Zeiss Prismo). The mean value was 9.82 mm with a standard deviation of 2.8 μm.

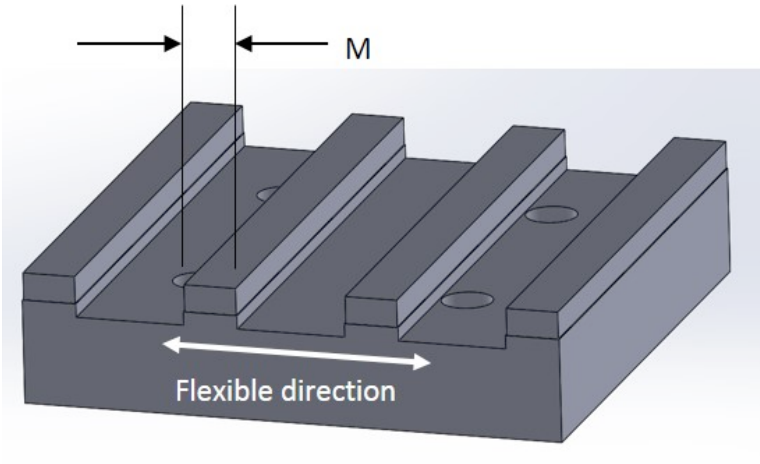

Fig. 6.13 The SLE workpiece included four ribs that were initially machined to the same dimensions. The 5 mm axial depth, 2 mm radial depth cuts were then performed on one edge at a different spindle speed for each rib. The SLE was calculated as the difference between the commanded and measured, M, rib widths. The flexible direction for the flexure (Fig. 6.2) is identified.

Based on Figs. 6.3 and 6.4, the 11 spindle speeds in Table 6.1 were used to machine 11 ribs (three total workpieces). As shown, this enabled SLE for both period-2 and stable behavior to be evaluated. Other than spindle speed, all other machining conditions were identical between the tests (up milling, 5 mm axial depth, 2 mm radial depth, and 0.35 mm/tooth feed).

Spindle speed (rpm)	Behavior
3180	Period-2
3190	Period-2
3200	Period-2
3210	Period-2
3270	Stable
3300	Stable
3330	Stable
3360	Stable
3400	Stable
3500	Stable
3600	Stable

Table 6.1 Spindle speeds and bifurcation behavior for experiments.

A comparison between the simulated and experimental SLE results is presented in Fig. 6.14 and Table 6.2. Four tests were completed under period-2 conditions and seven were performed under stable conditions. Good agreement is observed between prediction and measurement. The average error between prediction and measurement is 0.5 μm for all tests.

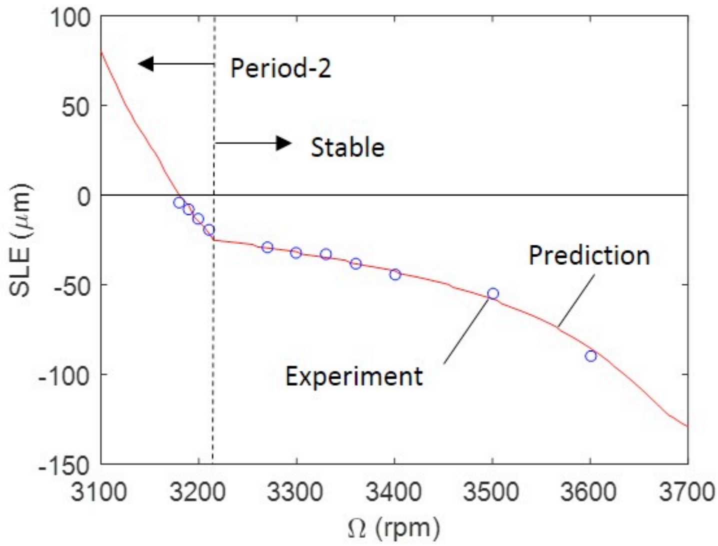

Fig. 6.14 SLE prediction from simulation (line) and experimental results (circles). The four period-2 bifurcation tests are identified.

Spindle speed (rpm)	Behavior	Measured SLE (μm)	Predicted SLE (μm)	Error (μm)
3180	Period-2	-4	0	-4
3190	Period-2	-8	-6	-2
3200	Period-2	-13	-15	+2
3210	Period-2	-19	-21	+2
3270	Stable	-29	-30	+1
3300	Stable	-32	-32	0
3330	Stable	-33	-35	+2
3360	Stable	-38	-38	0
3400	Stable	-44	-42	-2
3500	Stable	-55	-58	+3
3600	Stable	-90	-85	-5

Table 6.2 Comparison of measured and predicted SLE results for rib cutting tests.

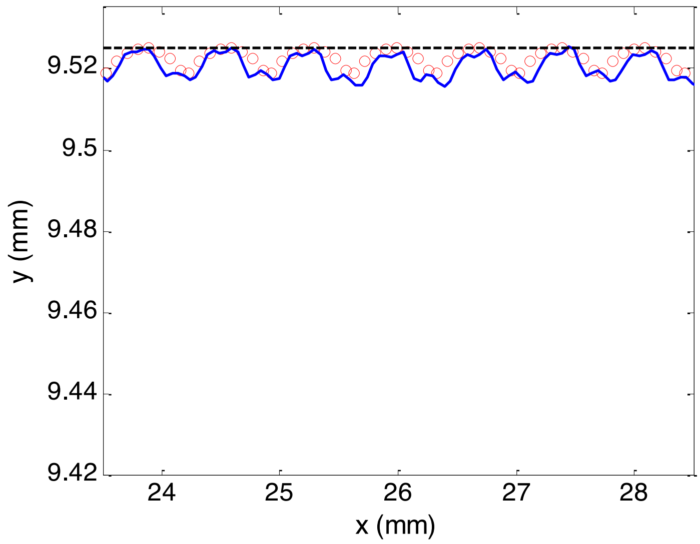

Fig. 6.15 Commanded surface (dashed line), CMM scan (solid line), and simulation result (circles) for 3180 rpm (period-2). These results correspond to Figs. 6.7 and 6.8.

Figures 6.15-6.17 provide a direct comparison between the time domain simulation and the CMM surface points obtained by continuous scanning

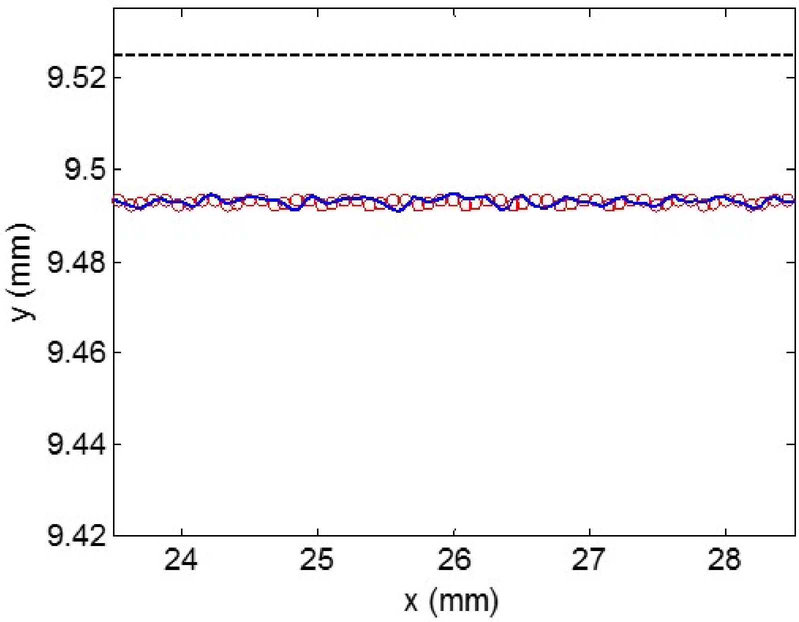

Fig. 6.16 Commanded surface (dashed line), CMM scan (solid line), and simulation result (circles) for 3300 rpm (stable). These results correspond to Figs. 6.9 and 6.10.

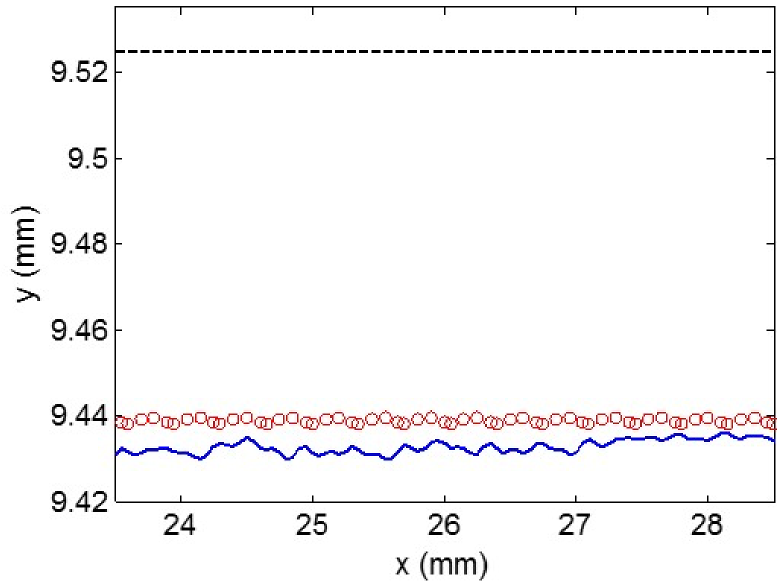

Fig. 6.17 Commanded surface (dashed line), CMM scan (solid line), and simulation result (circles) for 3600 rpm (stable). These results correspond to Figs. 6.11 and 6.12.

along the machined surface. In these figures the commanded surface is identified by the dashed line, the solid line is the CMM data, and the circles are the simulation results. The SLE is the difference between the commanded and actual surface and, again, good agreement is observed between simulation and measurement.

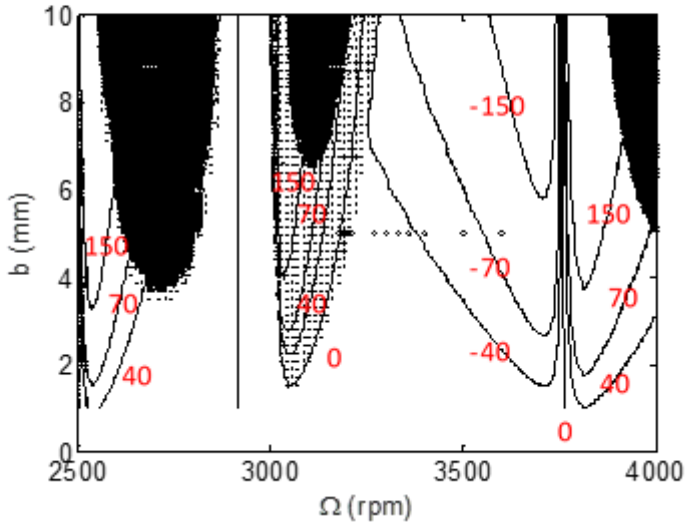

Fig. 6.18 Combined stability and SLE map for rib cutting process dynamics. The secondary Hopf instability is represented by the dark zone, the period-2 behavior is identified by the dotted zone, and the SLE is given by the contours (lines of constant SLE) with numerical labels (SLE in μm).

The stability and SLE information is combined in Fig. 6.18. In this figure, the dark area represents secondary Hopf instability, the dotted area identifies the period-2 bifurcations, and the contour lines give the SLE as a function of spindle speed (horizontal axis) and axial depth of cut (vertical axis). Zero SLE is seen near the traditional best speed of 3774 rpm (125.8·60/2). However, a steep gradient for small changes in spindle speed is also seen near this speed (i.e., the zero SLE contour is vertical). A zero SLE contour is also observed within the period-2 zone. Interestingly, the SLE gradient is not as steep within the period-2 zone as it is near the best speed at 3774 rpm.

6.7 Conclusions

This chapter explored the three possible milling response types: forced vibration, self-excited vibration, and period-*n* bifurcations, using both time domain simulation and experiment. Stability maps, bifurcation diagrams, and Poincaré maps were used to visualize the milling behavior. Experiments were used to validate the predictions. It was shown that all three behavior types are possible with changes in spindle speed and axial depth of cut. It was also demonstrated that, even for stable conditions, surface location error can limit milling productivity due to part geometric errors introduced by the forced vibration response.

References

[1] Arnold R N. (1946) *The mechanism of tool vibration in the cutting of steel*. In: Proceedings of the Institute of Mechanical Engineers: 154.

[2] Doi S, Kato S. (1956) *Chatter vibration of lathe tools*. Transactions of the ASME; 78: 1127-1134.

[3] Tobias S A, Fishwick W. (1958) *The chatter of lathe tools under orthogonal cutting conditions*. Transactions of the ASME; 80: 1079-1088.

[4] Tlusty J, Polacek M. (1963) *The stability of machine tools against self-excited vibrations in machining*. In: Proceedings of the ASME International Research in Production Engineering Conference, Pittsburgh, PA: 465-474.
[5] Tobias S A. (1965) *Machine Tool Vibration*. Wiley, New York, NY.
[6] Merritt H E. (1965) *Theory of self-excited machine-tool chatter*. ASME Journal of Engineering for Industry; 87: 447-454.
[7] Shridar R, Hohn R E, Long G W. (1968) *A general formulation of the milling process equation*. ASME Journal of Engineering for Industry; 90: 317-324.
[8] Hohn R E, Shridar R, Long G W. (1968) *A stability algorithm for a special case of the milling process*. ASME Journal of Engineering for Industry; 90: 326-329.
[9] Shridar R, Hohn R E, Long G W. (1968) *A stability algorithm for the general milling process*. ASME Journal of Engineering for Industry; 90: 330-334.
[10] Hanna N H, Tobias S A. (1974) *A theory of nonlinear regenerative chatter*. ASME Journal of Engineering of Industry; 96: 247-255.
[11] Tlusty J, Ismail F. (1981) *Basic non-linearity in machining chatter*. Annals of the CIRP; 30: 299-304.
[12] Tlusty J, Ismail F. (1983) *Special aspects of chatter in milling*. ASME Journal of Vibration, Stress and Reliability in Design; 105: 24-32.
[13] Tlusty J. (1985) *Machining dynamics*. In: Handbook of High-speed Machining Technology (Ed. R I King), Chapman and Hall, New York, NY: 48-153.
[14] Tlusty J. (1986) *Dynamics of high-speed milling*. ASME Journal of Engineering for Industry; 108: 59-67.
[15] Minis I, Yanusevsky R. (1993) *A new theoretical approach for prediction of chatter in milling*. ASME Journal of Engineering for Industry; 115: 1-8.

[16] Altintas Y, Budak E. (1995) *Analytical prediction of stability lobes in milling*. Annals of the CIRP; 44-1: 357-362.
[17] Davies M A, Dutterer B S, Pratt J R, Schaut A J. (1998) *On the dynamics of high-speed milling with long, slender endmills*. Annals of the CIRP; 47-1: 55-60.
[18] Moon F C, Kalmár-Nagy T. (2001) *Nonlinear models for complex dynamics in cutting materials*. Philosophical Transactions of the Royal Society London A; 359: 695-711.
[19] Davies M A, Pratt J R, Dutterer B S, Burns T J. (2000) *The stability of low radial immersion milling*. Annals of the CIRP; 49-1: 37-40.
[20] Moon F C. (1994) *Chaotic dynamics and fractals in material removal processes*. In: Nonlinearity and Chaos in Engineering Dynamics (Ed. J Thompson and S Bishop), Wiley: 25-37.
[21] Bukkapatnam S, Lakhtakia A, Kumara S. (1995) *Analysis of sensor signals shows turning on a lathe exhibits low-dimensional chaos*. Physics Review E; 52: 2375-2387.
[22] Stépán G, Kalmár-Nagy T. (1997) *Nonlinear regenerative machine tool vibrations*. In: Proceedings of the 1997 ASME Design Engineering Technical conference on Vibration and Noise, Sacramento, CA. DETC 97/VIB-4021, 1-11.
[23] Nayfey A, Chin C, Pratt J. (1998) *Applications of perturbation methods to tool chatter dynamics*. In: Dynamics and Chaos in Manufacturing Processes (Ed. F C Moon), Wiley: 193-213.
[24] Minis I, Berger B S. (1998) *Modelling, analysis, and characterization of machining dynamics*. In: Dynamics and Chaos in Manufacturing Processes (Ed. F C Moon), Wiley: 125-163.
[25] Moon F C, Johnson M. (1998) *Nonlinear dynamics and chaos in manufacturing processes*. In: Dynamics and Chaos in Manufacturing Processes (Ed. F C Moon), Wiley: 3-32.

[26] Smith K S, Tlusty J. (1991) *An overview of modeling and simulation of the milling process*. Journal of Engineering for Industry; 113: 169-175.
[27] Campomanes M L, Altintas Y. (2003) *An improved time domain simulation for dynamic milling at small radial immersions*. Journal of Manufacturing Science and Engineering; 125-3: 416-422.
[28] Zhao M X, Balachandran B. (2001) *Dynamics and stability of milling process*. International Journal of Solids and Structures; 38: 2233-2248.
[29] Davies M A, Pratt J R, Dutterer B, Burns T J. (2002) *Stability prediction for low radial immersion milling*. Journal of Manufacturing Science and Engineering; 124: 217-225.
[30] Mann B P, Insperger T, Bayly P V, Stépán G. (2003) *Stability of up-milling and down-milling, Part 2: Experimental verification*. International Journal of Machine Tools and Manufacture; 43-1: 35-40.
[31] Mann B P, Insperger T, Bayly P V, Stépán G. (2003) *Stability of up-milling and down-milling, Part 1: Alternative analytical methods*. International Journal of Machine Tools and Manufacture; 43-1: 25-34.
[32] Insperger T, Stépán G, Bayly P V, Mann B P. (2003) *Multiple chatter frequencies in milling processes*. Journal of Sound and Vibration; 262: 333-345.
[33] Insperger T, Stépán G. (2004) *Vibration frequencies in high-speed milling processes or A positive answer to Davies, Pratt, Dutterer, and Burns*. Journal of Manufacturing Science and Engineering; 126-3: 481-487.
[34] Mann B P, Bayly P V, Davies M A, Halley J E. (2004) *Limit cycles, bifurcations, and accuracy of the milling process*. Journal of Sound and Vibration; 277: 31-48.
[35] Merdol S D, Altintas Y. (2004) *Multi frequency solution of chatter stability for low immersion milling*. Journal of Manufacturing Science and Engineering; 126: 459-466.

[36] Govekar E, Gradišek J, Kalveram M, Insperger T, Weinert K, Stepan G, Grabec I. (2005) *On stability and dynamics of milling at small radial immersion*. Annals of the CIRP; 54-1: 357-362.

[37] Gradišek J, Kalveram M, Insperger T, Weinert K, Stépán G, Govekar E, Grabec I. (2005) *On stability prediction for milling*. International Journal of Machine Tools and Manufacture; 45-7~8: 769-781.

[38] Mann B P, Garg N K, Young K A, Helvey A M. (2005) *Milling bifurcations from structural asymmetry and nonlinear regeneration*. Nonlinear Dynamics; 42-4: 319-337.

[39] Stépán G, Szalai R, Mann B P, Bayly P V, Insperger T, Gradisek J, Govekar E. (2005) *Nonlinear dynamics of high-speed milling – Analyses, numerics, and experiments*. Journal of Vibration and Acoustics; 127: 197-203.

[40] Zatarain M, Muñoa J, Peigné G, Insperger T. (2006) *Analysis of the influence of mill helix angle on chatter stability*. Annals of the CIRP; 55-1: 365-368.

[41] Insperger T, Munoa J, Zatarain M A, Peigné G. (June 2006) *Unstable islands in the stability chart of milling processes due to the helix angle*. In: CIRP 2nd International Conference on High Performance Cutting, Vancouver, Canada: 12-13.

[42] Patel B R, Mann B P, Young K A. (2008) *Uncharted islands of chatter instability in milling*. International Journal of Machine Tools and Manufacture; 48-1: 124-134.

[43] Moradi H, Vossoughi G, Movahhedy M. (2014) *Bifurcation analysis of nonlinear milling process with tool wear and process damping: Sub-harmonic resonance under regenerative chatter*. International Journal of Mechanical Sciences; 85: 1-19.

[44] Honeycutt A, Schmitz T. (2015) *The extended milling bifurcation diagram*. Procedia Manufacturing; 1: 466-476.

[45] Honeycutt A, Schmitz T. (2016) *A numerical and experimental investigation of period-n bifurcations in milling*. Journal of Manufacturing Science and Engineering; 139-1: 011003.
[46] Kline W, DeVor R, Shareef I. (1982) *The prediction of surface accuracy in end milling*. Journal of Engineering for Industry; 104: 272-278.
[47] Kline W, DeVor R, Lindberg J. (1982) *The prediction of cutting forces in end milling with application to cornering cuts*. International Journal of Machine Tool Design Research; 22: 7-22.
[48] Tlusty J. (1985) *Effect of end milling deflections on accuracy*. in: Handbook of High Speed Machining Technology (Ed. R I King), Chapman and Hall, New York: 140-153.
[49] Sutherland J, DeVor R. (1986) *An improved method for cutting force and surface error prediction in flexible end milling systems*. Journal of Engineering for Industry; 108: 269-279.
[50] Montgomery D, Altintas Y. (1991) *Mechanism of cutting force and surface generation in dynamic milling*. Journal of Engineering for Industry; 113-2: 160-168.
[51] Altintas Y, Montgomery D, Budak E. (1992) *Dynamic peripheral milling of flexible structures*. Journal of Engineering for Industry; 114-2: 137-145.
[52] Tarng Y, Liao C, Li H. (1994) *A mechanistic model for prediction of the dynamics of cutting forces in helical end milling*. International Journal of Modeling and Simulation; 14-2: 92-97.
[53] Schmitz T, Ziegert J. (1999) *Examination of surface location error due to phasing of cutter vibrations*. Precision Engineering; 23-1: 51–62.
[54] Altintas Y (2000) *Manufacturing Automation*. Cambridge University Press, Cambridge, UK.
[55] Mann B P, Bayly P V, Davies MA, Halley J E. (2004) *Limit cycles, bifurcations, and accuracy of the milling process*. Journal of Sound and Vibration; 277: 31-48.

[56] Schmitz T, Couey J, Marsh E, Mauntler N, Hughes D. (2007) *Runout effects in milling: Surface finish, surface location error, and stability*. International Journal of Machine Tools and Manufacture; 47-5: 841-851.
[57] Yun W-S, Ko J, Cho D-W, Ehmann K. (2002) *Development of a virtual machining system, Part 2: prediction and analysis of a machined surface error*. International Journal of Machine Tools and Manufacture; 42: 1607-1615.
[58] Schmitz T, Mann B. (2006) *Closed-form solutions for surface location error in milling*. International Journal of Machine Tools and Manufacture; 46-12~13: 1369-1377.
[59] Schmitz T, Smith K S. (2009) *Machining Dynamics: Frequency Response to Improved Productivity*. Springer, New York, NY.
[60] Dombovari Z, Stépán G. (2015) *On the bistable zone of milling processes*. Philosophical Transactions of the Royal Society A; 373: 20140409.
[61] Bachrathy D, Munoa J, Stépán, G. (2016) *Experimental validation of appropriate axial immersions for helical mills*. The International Journal of Advanced Manufacturing Technology; 84: 1295-1302.
[62] Honeycutt A, Schmitz T. (2016) *A new metric for automated stability identification in time domain milling simulation*. Journal of Manufacturing Science and Engineering; 138-7: 074501 (7 pages).
[63] Mann B P, Insperger T, Bayly P V, Stépán G. (2003) *Stability of up-milling and down-milling, Part 2: Experimental verification*. International Journal of Machine Tools and Manufacture; 43-1: 35-40.
[64] Ransom T, Honeycutt A, Schmitz T. (2016) *A new tunable dynamics platform for milling experiments*. Precision Engineering; 44: 252-256.
[65] Honeycutt A, Schmitz T. (2017) *Milling stability interrogation by subharmonic sampling*. Journal of Manufacturing Science and Engineering; 139-4: 041009 (9 pages).

Chapter 7 Quick Notes for Rigidity and Damping Capacity of Main Spindle Supported by Rolling Bearing

7.1 Introduction

With the increase of challenging research into the applicability of the stability chart to the higher-speed range, we can observe the obvious disagreement of the theoretical stability chart with that obtained by the experiment as already shown in Figs. 3.5 and 3.6. In short, it was suggested that such behavior are caused by the speed-dependence of the spindle dynamics, and furthermore gyroscopic and centrifugal effects in both the front and rear bearings in the main spindle system. It is however regrettable that the validity of these suggestions is not verified as yet.

Paraphrasing, such a disagreement is derived considerably from the inadequate determination of the parameters in the "*Structural Equation*" in the chatter theory and not acceptable to contrive the remedy for the chatter suppression. Of note, people in chatter concerns are not familiar to the knowledge so far obtained in the sphere of the "*Machine Tool Joint*", although the main spindle system is one of the leading machine tool joints.

In general, the main spindle system can be facilitated with the rolling bearing when its rotating speed is higher, and thus a facing problem is to what extent we have the engineering data for the rigidity and damping of the rolling bearing, which are available for the higher rotational speed.

In this context, we must be aware that the available data are for the speed less than 2,000 rev/min, and that even the rolling bearing manufacturer has not arranged and systematized yet any engineering data with respect to the rigidity and damping capacity while rotating the main spindle more than 2,000 rev/min, and up to 40,000 rev/min. This is because of too much difficulty in measuring the corresponding data as will be discussed later. Of course, we need to have such data to advance the chatter theory and contrive the innovative remedy for chatter suppression hereafter, and thus some quick notes will be stated in the following to give a clue for conducting a forerunning research.

7.2 Fundamentals of Main Spindle Supported by Rolling Bearing

In discussing the main spindle of rolling bearing type, we must first be aware of the three leading design attributes, i.e. "*Higher-accuracy Machining*", "*Higher-speed Machining*", and "*Heavy Machining Capability*", which should be actualized in the main spindle. In general, in accordance with the design specifications, we design the main spindle in consideration of (1) only one attribute, (2) combination of two of three attributes, or (3) all the three attributes simultaneously. Obviously, we must understand that the chatter behavior depends considerably upon the characteristic features given by the design specifications. Figs 7.1 (a), (b) and (c) show thus the typical structural configurations with respect to each leading attribute.

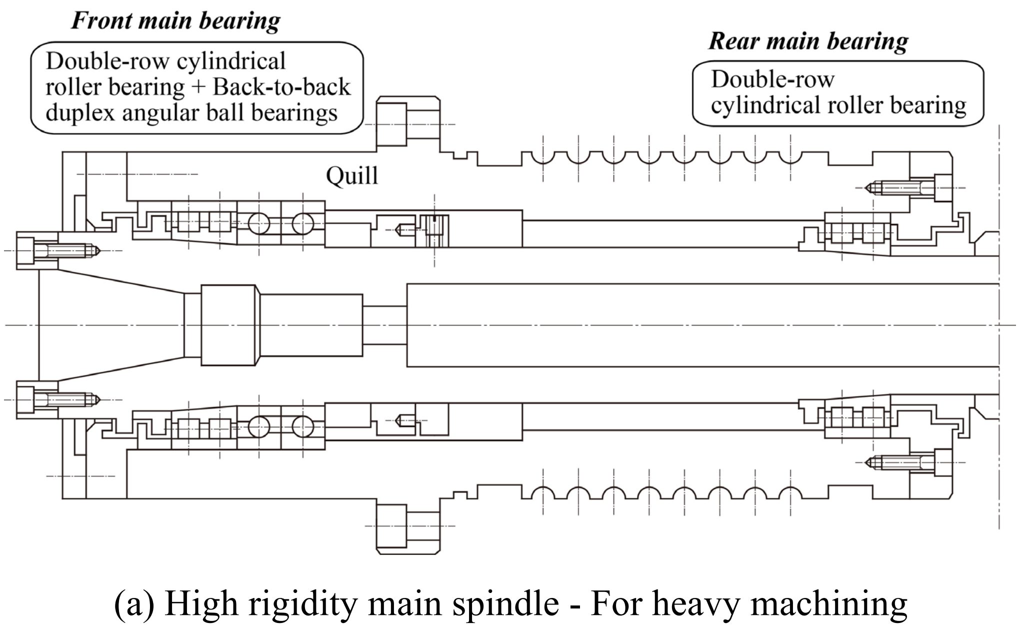

(a) High rigidity main spindle - For heavy machining

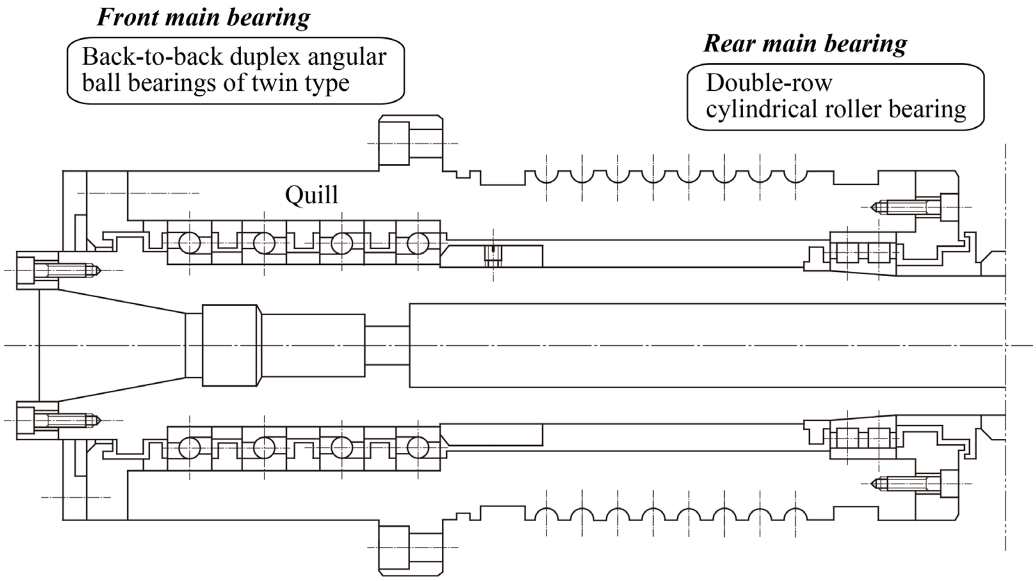

(b) For higher-speed machining

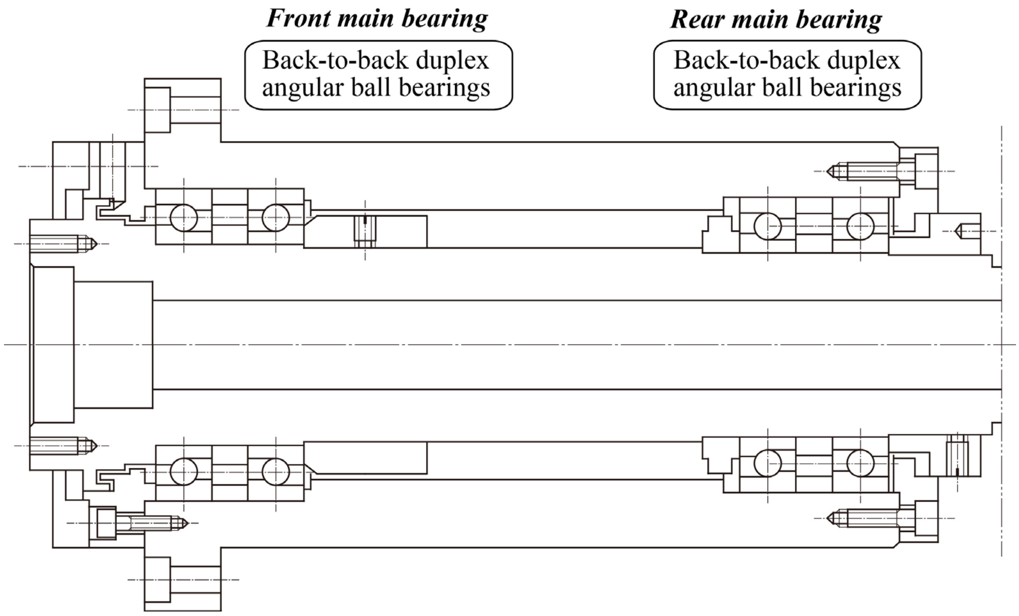

(c) For higher-accuracy machining

Fig. 7.1 Different features in structural configurations of main spindle depending upon weighing design attribute

As can be seen from these, there are considerable differences in the kinds of bearing, arrangement of bearings, mechanism of pre-load, and so on, depending upon the design requirements. In this context, we must furthermore be aware of the following.

(1) As a rule of the machine tool joint, the rigidity and damping in the main spindle are in reciprocal relation.

(2) The leading three design attributes are in reciprocal relation one another; however, to respond properly the machining requirement of the user, we often consider simultaneously three or two of these as mentioned beforehand. Obviously, it is very difficult to optimize the structural configuration of the main spindle in such a case, and thus we can realize the preferable one, even which results in very complicated spindle configuration.

(3) Although the main spindle of two-point supporting type has been prevailed, in certain cases, we used to design the main spindle of three-point supporting type to reinforce furthermore the rigidity.

(4) We can estimate the design qualification of each machine tool manufacturer by the integrated rate of the three leading attributes, and as reported elsewhere, German and Japanese manufacturers can manage the design with utmost integrated rate, i.e. structural configuration simultaneously integrated three attributes.

Importantly, both the main spindles for heavy machining and higher-speed machining are at burning issue from the viewpoint of the chatter. Apart from the main spindle for heavy machining, the main spindle for higher-speed machining appears not to be related to the chatter; however, such a main spindle can facilitate the large chip removable rate per unit time, i.e. another type of heavy machining, which is applicable to machining of the aircraft component made of Al alloy and concerns.

In discussing the discrepancy between the theoretical stability charts and experimental one while machining either with lower-speed or with higher-speed, it is thus reasonable that such discrepancies are derived from the dynamics of the main spindle; however, it is too much difficult to detail what is the determinant. Paraphrasing, we must exploit the correlation between the structural configuration of the main spindle and its influencing magnitude to the chatter, and a recommendable research is to estimate both the rigidity and damping capacity distribution diagrams within a main spindle system (see Fig. 3.9).

Of course, such a research is very valuable; however, in this context, we may assert first the urgent necessity of the measurement of the rigidity and damping of the main spindle while rotating the higher-speed more than 2,000 rev/min in consideration of the details of the design attributes shown in Table 7.1. Table 7.1 summarizes in detail the design attributes of the main spindle, and as can be seen, we can obtain the suitable structural configuration as per the machining requirement by the preferable combination of these attributes.

Main spindle system as a whole	Maximum allowable torque of main spindle Reduction of thermal deformation Adjustment mechanism for unbalance Lubrication system including remedies for oil in sump Remedies for oil tight - Oil sheal, labyrinth, and so on
Bearing	Kinds and arrangement of main bearings - Front + rear Thrust supporting and its adjustment method Diameter of front main bearing Pre-loading mechanism Assembly and disintegration methods of main bearing
Main spindle	Dimensional specifications and rigidity of spindle nose Kinds of tapered hole and size Diameter of through-hole Tapered hole, or reference for adapter mounting at rear end Material and finishing method (in general, alloy steel)
Driving system of main spindle - Main motor and driving method	Built-in motor Direct drive by main motor Separate mounting motor - Gear driving, belt driving and so on Floating driving method Gear train method - Direct mounting of gear by key way, spline, polygon and so on Kinds of gear - Spur gear, helical gear, double helical gear

Table 7.1 Leading attributes to be considered in design of main spindle system

On the basis of the basic knowledge mentioned above, we must discuss another fatal issues in the main spindle as follows.

Thrust supporting at front main bearing and chuck mounting at spindle nose

In the main spindle, a crucial issue in the design is thrust (axial load) supporting including the pre-loading mechanism, and in general, the front main bearing can facilitate such a function together with maintaining the allowable rigidity and damping capacity. Paraphrasing, the machine-attachment-tool-work system can be characterized by the front main bearing, which plays the role of quasi-fixation point, to a large extent.

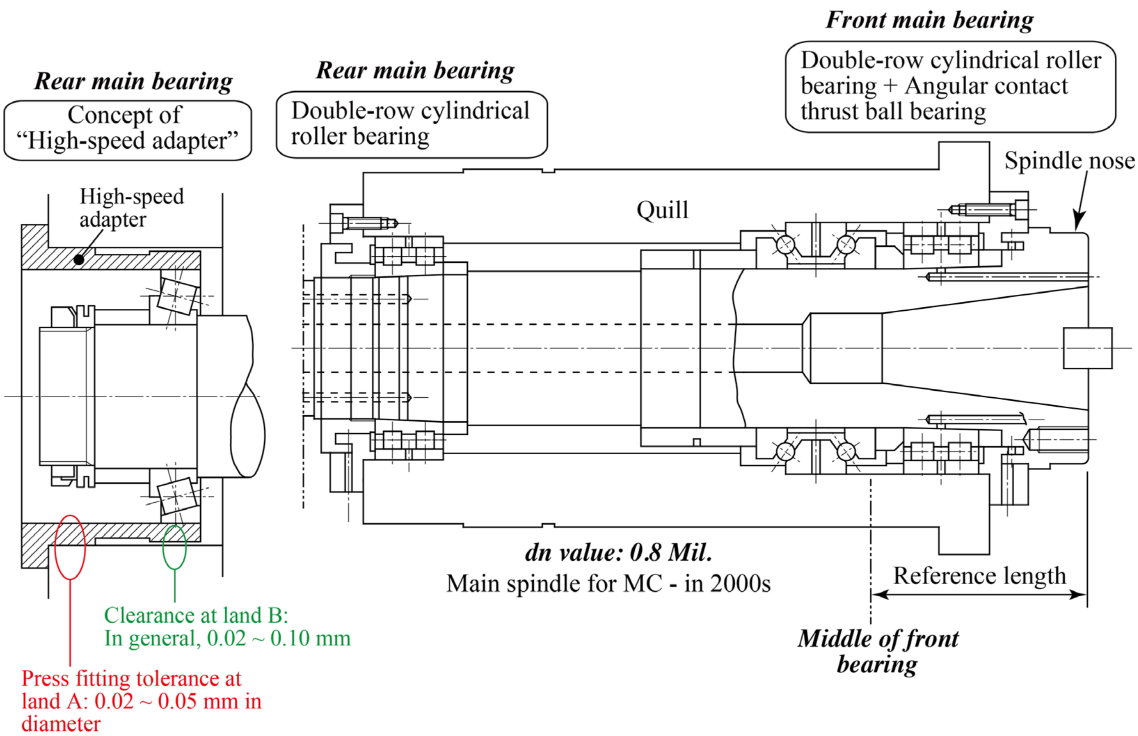

Fig. 7.2 Further crucial issue in main spindle from viewpoint of chatter

For the sake of further convenience, Fig. 7.2 shows another structural configuration of the front main bearing, and as will be clear from it, we must be aware of the considerable influence of the front bearing to the chatter. Importantly, the chatter behavior depends upon the reference length shown also in Fig. 7.2 to certain extent together with mounting method of the chuck at the spindle nose. In this context, we must remind again that the jaw traveling mechanism in the jaw chuck affects considerably the magnitude of mingling parametric vibration within the regenerative chatter as already suggested by M. Doi (see Figs. 1.8 and 1.9). In addition, Feng (2003) suggested the better applicability of the jaw traveling mechanism of wedge bar type to the higher-speed main spindle, although not verifying its validity to satisfactory level.

<u>Relieving mechanism of thermal elongation of main spindle at rear bearing</u>

In general, the rear main bearing cannot support any thrust, so that the thermal elongation of the main spindle can be in free. Otherwise, as reported elsewhere and will be shown later, the temperature rise of the main spindle varies the pre-load, fitting tolerance between the bearing and the quill, and so on to a large extent, resulting in the considerable influences on the chatter. We must thus pay the special attention to the structural configuration of the rear main bearing.

Of special note, a noteworthy contrivance is also shown in the left of Fig. 7.2, which is for the tapered roller bearing and called "*High-speed Adapter*". The tapered roller bearing is often employed in the main spindle, because of its simplicity in load supporting, although the temperature rise is larger than those of other kinds of the rolling bearing, and thus Timken contrived, as well known, the high-speed adapter. More specifically, the thermal deformation of the outer ring is quicker in radial direction than that in axial direction, and thus small clearance at the land B can be facilitated the release of the dynamic constrain of the outer ring, resulting in the reduction of heat generation.

To this end, it emphasizes that a suitable setting of mathematical model is at issue in the chatter analysis. Paraphrasing, to what extent we must replace the structural configuration of the main spindle with a model. Fig. 7.3 shows a grinding wheel spindle, which is similar configuration to that for higher-accuracy machining because the grinding machine is, in general, for finish machining. In fact, we cannot see a large differing feature in the bearing arrangement in Fig. 7.3 as compared with that shown in Fig. 7.1 (c). More specifically, both the front and rear bearings are with "Back-to-Back" arrangement for Fig. 7.1(c) and "Back-to-Face" arrangement for the grinding wheel spindle. Thus, we need not to consider such an arrangement difference when producing the mathematical model; however, in the analysis of thermal deformation, we must consider its meaningful influences.

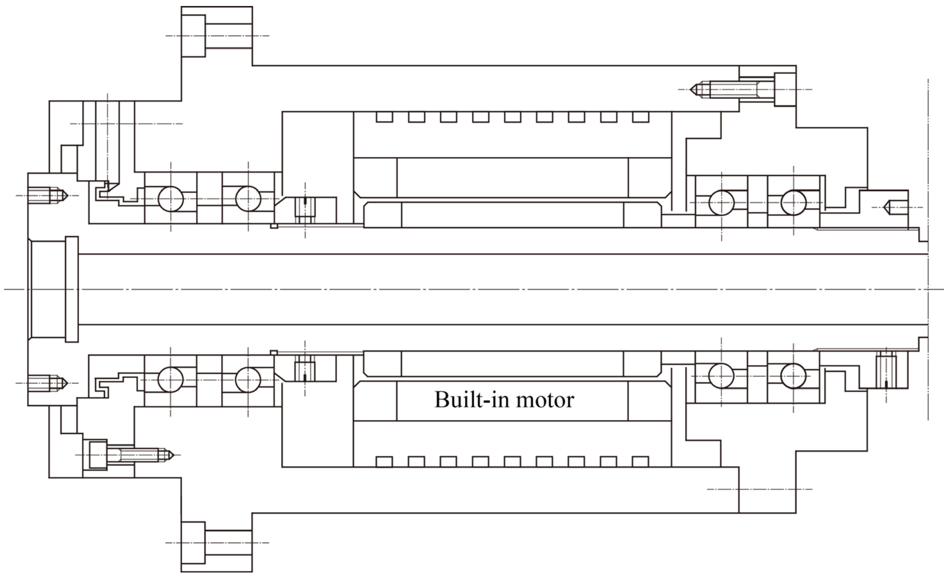

Fig. 7.3 Grinding wheel spindle of built-in motor type

We learn also the same story in the case of the angular contact thrust ball bearing shown in Fig. 7.2. With the advance of the due technology, we can use such a new bearing without the distance collar (spacer) together with the improved raceway finish and concerns to reduce the friction as shown in Fig. 7.4. Obviously, we can expect the large effect on the reduction of the heat generation, whereas we may not expect the sufficient increases in both the rigidity and the damping capacity to suppress the chatter.

As will be clear from the above, the new angular contact thrust ball bearing is compact, because of having no distance collar, and thus capable of replacing the application sphere of the cross-ball bearing. For example, the cross-roller bearing has prevailed in table supporting of the quinaxial-controlled MC of trunnion type.

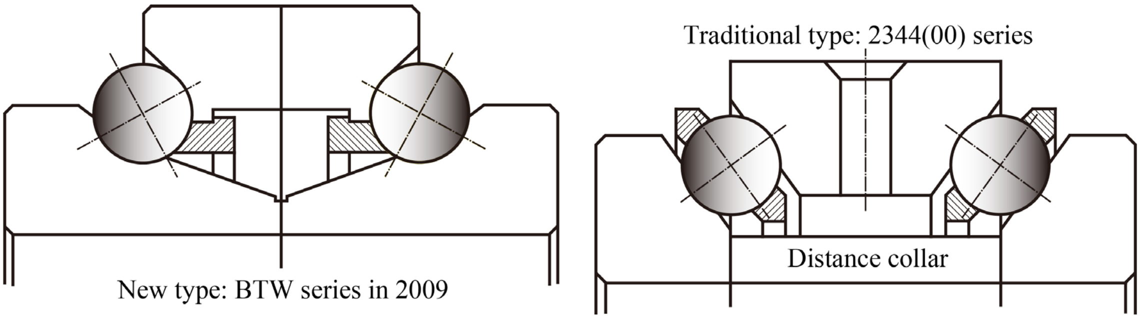

Fig. 7.4 Improvement in angular contact thrust ball bearing – SKF-brand

Of special note, we must take into consideration of the influence of the built-in-motor, which is shown in Fig. 7.3, in the analyses of the chatter and thermal deformation, and as can be readily seen, the spindle configuration should be modeled by weighing the essential features of the chatter.

7.3 Difficulties in Measuring Rigidity and Damping Capacity of Rolling Bearing While Rotating Main Spindle

Reportedly, damping in the rolling bearing may be caused by the following factors.

(1) Deformations of rolling elements and rings.
(2) Deformation in ring fits.
(3) Friction of rolling elements against rings especially arising the change of inclination angle of the shaft.
(4) Friction of rolling elements against the cage.
(5) In the tapered roller bearing, the friction between the roller ends and the ribs of inner ring, resulting in the appearance of peculiar behavior.

Obviously, these factors are also related closely to the rigidity, it is thus recommendable to produce both the “Rigidity Distribution Diagram” and the “Damping Capacity Distribution Diagram” within the machine-attachment-tool-work system as already mentioned above.

Admitting the importance for producing such distribution diagrams, the facing problem is however the too much difficulty in the measurement of both the rigidity and damping capacity in the main spindle system while rotating higher-speed as exemplified by the test rig shown in Fig. 2.17 (Ito, 2008).

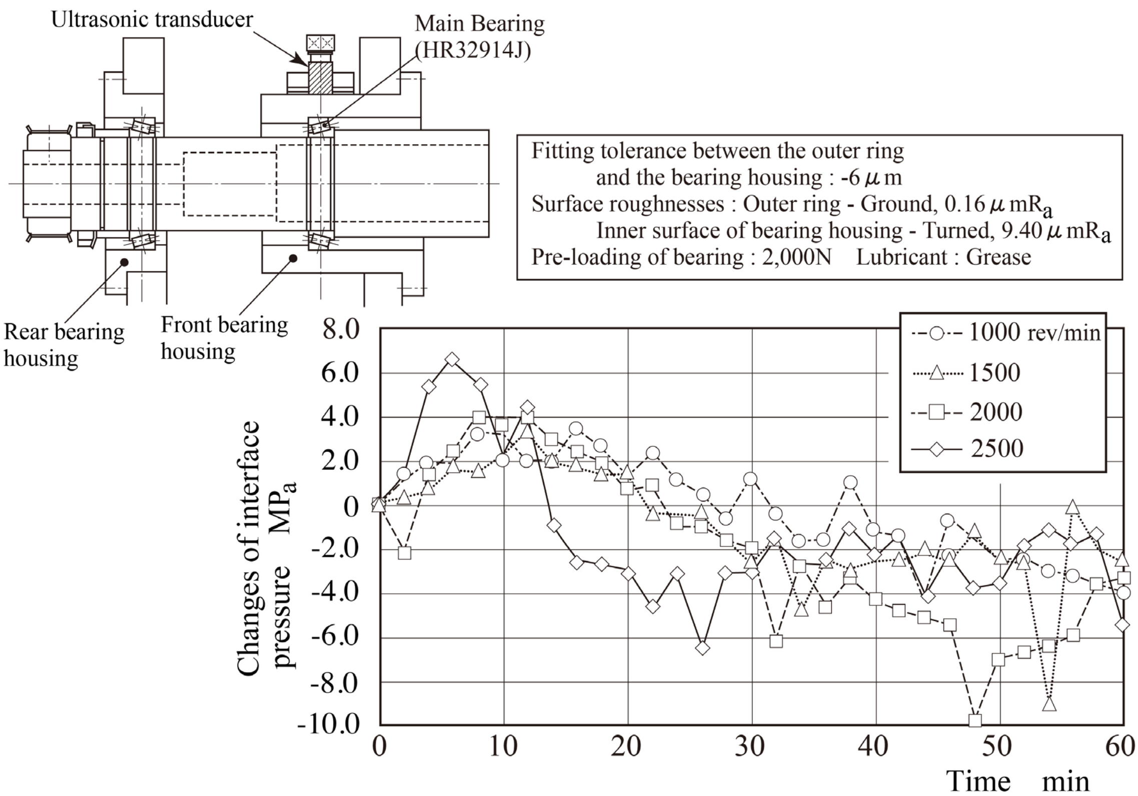

Fig. 7.5 Variations of interface pressure with running time

A root cause of further difficulty lies in the changes of the dynamic characteristics of the main spindle system with the laps of time after starting the rotation. In fact, a crux is the variation of both the fitting tolerances between the outer race and the housing, and between the shaft and the inner race. More specifically, Inaba et al (1995, 2000) measured the changes of the interface pressure between the quill and the outer ring of the bearing by using the test rig shown in Fig. 7.5, where the ultrasonic transducer of focus type (Oscillating frequency: 5 MHz, incident area at joint: 5 mm) detects the interface pressure.

It is very interesting that the interface pressure varies obviously with the running time, showing a peak value immediately after starting the run and gradually decreasing value with the running time as also shown in Fig. 7.5. This behavior can be interpreted as an obvious evidence to demonstrate a considerable difference in fitting tolerance between the still and running conditions. In short, the main spindle system varies its dynamic characteristics by running, and thus we can suggest the considerable change in the stability charts between in still stand and in cutting.

7.4 Concluding Remarks

As will be clear from the above, people in chatter concerns are not familiar to the fundamental knowledge about the machine tool joint so far accumulated; however, they must recognize that the main spindle-attachment-tool-work system is one of the machine tool joints, and that to what extent the knowledge so far obtained are available. In fact, at burning issue is to measure the rigidity and damping capacity of the main spindle system while rotating more than 2,000 rev/min, and in the preferable case, we must estimate the "*Rigidity Distribution Diagram*" and "*Damping Capacity Distribution Diagram*" within the main spindle system. More specifically, we must also measure both the dynamic joint stiffness, for example, between the chuck and the spindle nose of main spindle, and between the tool shank and the tapered hole in the main spindle.

To this end, it is worth suggesting that we must identify roughly the structural configuration of the main spindle, which is beneficial to interpret the characteristic features in the stability chart for higher-speed cutting. In short, the more clarification the structural configuration of the main spindle, the more accurate is the chatter analysis; however, from the practical application point of view, at facing issue is how far and to what extent we must replace the actual structural configuration with the simplified model.

In this context, people in chatter concern might assert that the structural expression can represent satisfactorily the characteristic feature of the spindle configuration even when rotating with higher-speed, provided that we can measure the equivalent mass, damping coefficient and spring constant while spindle rotating. In contrast, *we must eye why we differentiate the structural configuration of the main spindle in accordance with its design specifications as shown in Fig. 7.1. We have so far paid any attention to such differences; however, we could observe the differing chatter pattern when machining the work by MC with spindle for heavy-cutting from that machining by MC with spindle for higher-speed (see Figs. 7.1 a and b).*

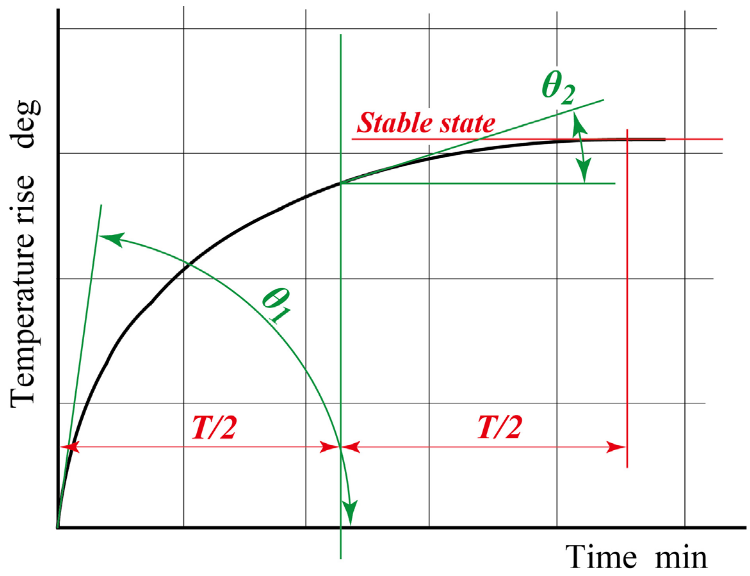

Fig. 7.6 Generalized warm-up characteristics of main spindle and estimation factors for structural configuration in main spindle

To enhance the chatter theory, intuitively, we need to deploy such a new vision, and it is thus recommendable that we must eye the effective use of the "*Thermal Stability Chart*" shown in Fig. 7.6 to estimate roughly the structural configuration of the main spindle. More specifically, the thermal stability chart reveals indirectly the characteristic feature in the structural configuration of main spindle, and thus we must measure the temperature rise and its rising rate every certain time interval as schematically shown in Fig. 7.4 while maintaining the rotational speed in constant. Of course, it is better to change the rotational speed in various steps.

References

Feng P F. (2003) *Berechnungsmodell zur Ermittlung von Spannkräften bei Backenfuttern*. Dr. Dissertation of Technische Universität Berlin.

Inaba C et al. (1995) *In-Process Measurement of Contact Pattern Variations in Rotating Main Bearing of Machine Tools Using Ultrasonic Waves Method*. Trans. of JSME (C); 61-588: 3375-3381.

Inaba C et al. (2000) *Estimation of Contact Pressure between Bearing and Bearing Housing by Means of Ultrasonic Waves*. Trans. of JSME (C); 66-645:1674-1680.

Ito Y. (2008) *Modular Design for Machine Tools*. McGraw-Hill, New York.

Chapter 8 Thought-provoking Quick Notes for Characteristic Factors in Metal Grinding

In the block diagram shown in Fig.1.19, the regenerative effect ($1/(1-e^{-T_wS})$), ($1/(1-e^{-T_sS})$) and the ratio of the vibration amplitudes to the amplitudes of generated waviness in the workpiece surface g mean pure geometrical relationships. The other transfer functions have deep relationships with grinding wheels, which are affected by truing and dressing operations, and are varying with the progress of grinding operations.

Grinding wheels consist of abrasive grains, binders and pores, and these constructions are determined in industrial standards. In these standards, however, the grains geometries and the distributions of binders from micro-viewpoint are not prescribed and these distributions are standardized statistically. And then even if the specification is same, two grinding wheels with same characteristics do not exist. From such a viewpoint, the transfer functions consisting of Fig. 1.19 have to be evaluated as functions of the surface conditions of grinding wheels. In this chapter, considering the relationships between these transfer functions and grinding wheels, the characteristics of grinding wheel surfaces affecting the chatter vibrations are described.

8.1 Contact Compliance of Grinding Wheel to Workpiece

Contact compliance of grinding wheel $1/K_{con}$ shown in Fig.1.19 is a parameter meaning the elasticity of grinding wheel at contact area to the workpiece. Since metal workpieces are harder than grinding wheels, their elastic deformations can be negligible, and then K_{con} means the deformations of only grinding wheels at contact area to the workpiece.

K_{con} have been discussed experimentally so far (Snoys,1968) (Hoshi,1983). A measured example of K_{con} is shown in Fig. 8.1 (Fukuda,1974). According to this example, the approaching amount between the grinding wheel and the workpiece increases with the pushing force, i.e. normal force, and tends to hard spring characteristics. Therefore, this character

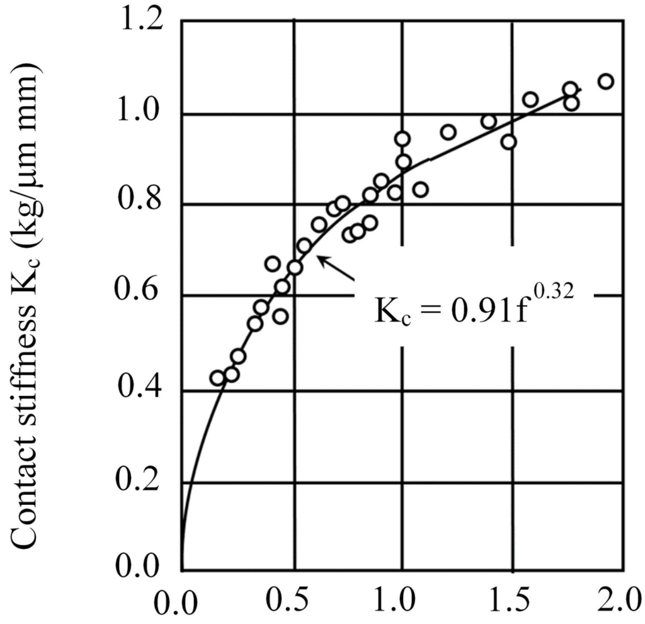

Fig. 8.1 A measured example of contact stiffness of grinding wheel (by Fukuda)

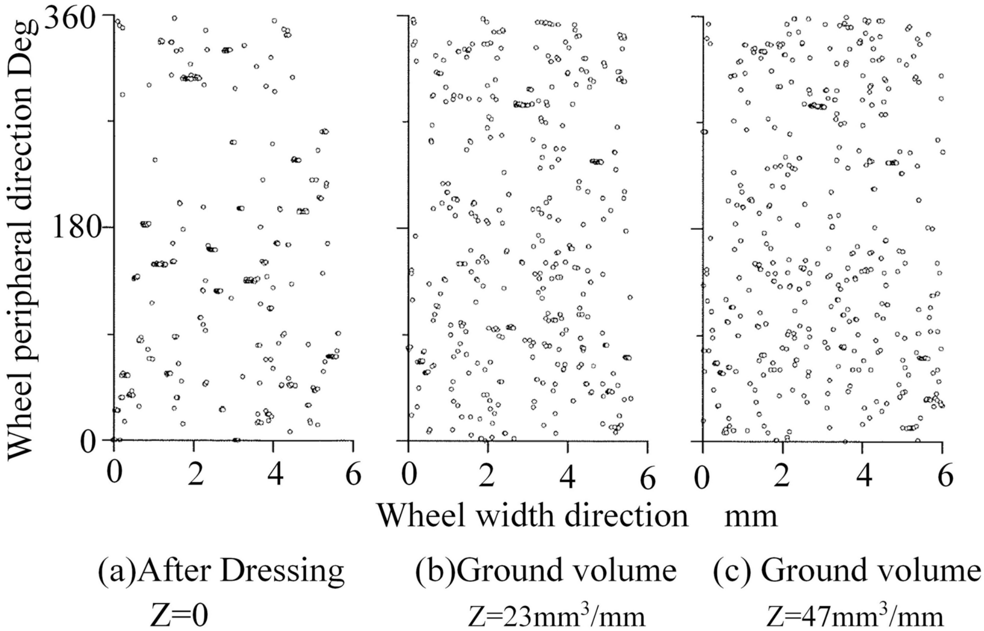

Fig. 8.2 Measured cutting edge distributions in grinding wheel surface (by Izumi)

can be explained by Hertz contact theory depending on the assumption that both the grinding wheel and the workpiece are uniform bodies from

macro-viewpoint.
Grinding wheel consists of abrasive grain, binder and pore. In the surface of grinding wheel, since cutting edges distribute as shown in Fig. 8.2 (Izumi, 2002), their contact model shown in Fig. 8.3 was assumed (Brown, 1971). In this model, it is considered that the deformation in contact area consists of two deformations between the grains and the workpiece and between the grinding wheel and the workpiece. In this case, Hertz contact theory is also applied and the experimental results of the deformation in contact area are explained in macro-viewpoint.

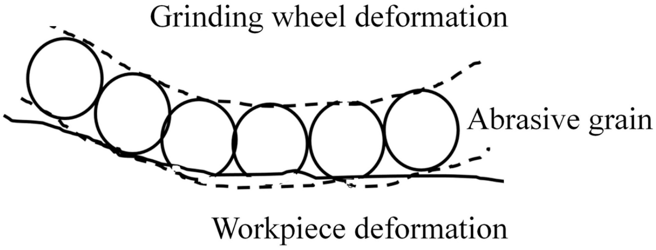

Fig. 8.3 Grinding wheel contact model to workpiece (by Brown)

Taking into account discontinuous grains as shown in Fig. 8.2, some approaches to explain the dynamic phenomena in contact area have been proposed. Yamada et al (2003) tried to explain the static phenomena by assuming that rigid grains are suspended by the binder with linear spring characteristics (Yamada,2003). By this assumption, the static stiffness of binders connecting grains can be obtained as shown in Fig. 8.4. From this trial, it is clarified that the static stiffness k connecting grains is independent from the grinding wheel geometry and determined only by the grain size. Furthermore, it is shown that the amount k is inverse proportion to grain size as;

$$K = 470 / \# \qquad \text{------} \quad (8.1)$$

where, # is grain size.

This tendency can be understood under the assumption as follows. Supposing that the binder is a simple beam, its stiffness increases with the increase of grain size. However, since the grain distribution is assumed to be body centered cubic in this model, the constant shown in Eq. (8.1) varies by the model arrangement [1]. And then, this shows only the qualitative tendency.

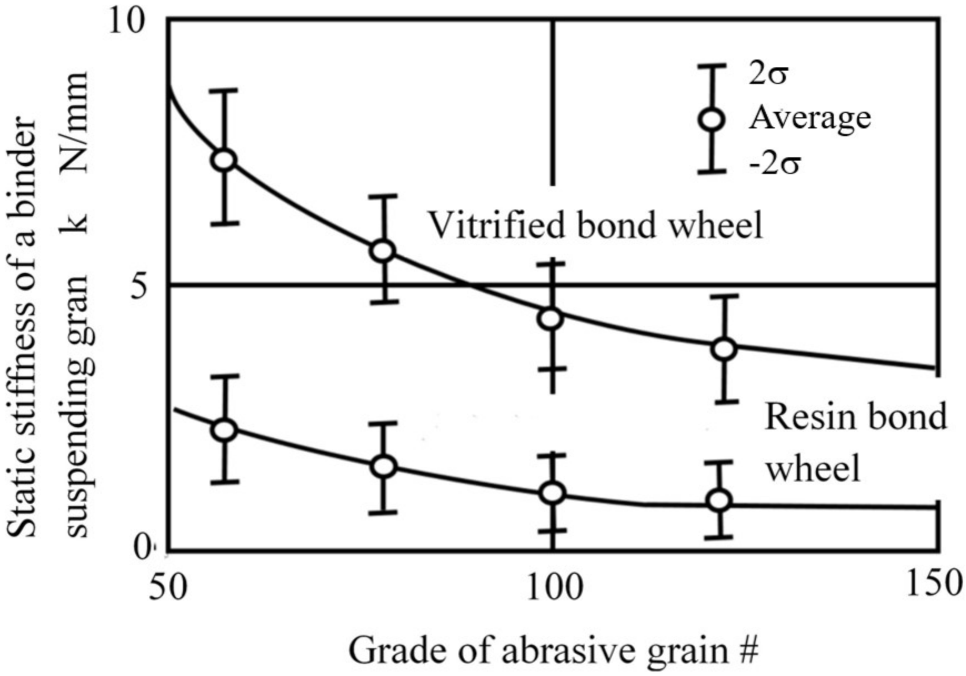

Fig. 8.4 Static stiffness of a binder suspending grains (by Yamada)

According to this model, one grain suspended binders with stiffness k contacts to the workpiece at first contact as shown in Fig. 8.5. With increasing the normal force, the number of grains contacting to the workpiece increases. Since these springs have parallel distribution, the contact stiffness K_{con} increases with the increase of the number of contact grains. By this discussion, hard spring characteristics from macro-viewpoint shown in Fig. 8.1 experimentally obtained can be explained.

In the same experiment, it is confirmed that the experimental relationship between the normal force and the approaching deformation varies with the contact direction. Hence, it is experimentally clear that grinding wheels have some anisotropic characteristics. However, no theoretical models of

[1] Yamada et al calculated the static stiffness of binder connecting abrasive grans under an assumption that the grains are connected in body centered cubic mode. Another type of grain model is also proposed in the following paper;
Salem S H, Russell J K. (August 1980) *Applying finite element method in the solution of the elastic problems in grinding wheels*. International Conference on Manufacturing Engineering, Melbourne. p.150.

the grinding wheel, which can explain such phenomena, has been proposed yet.

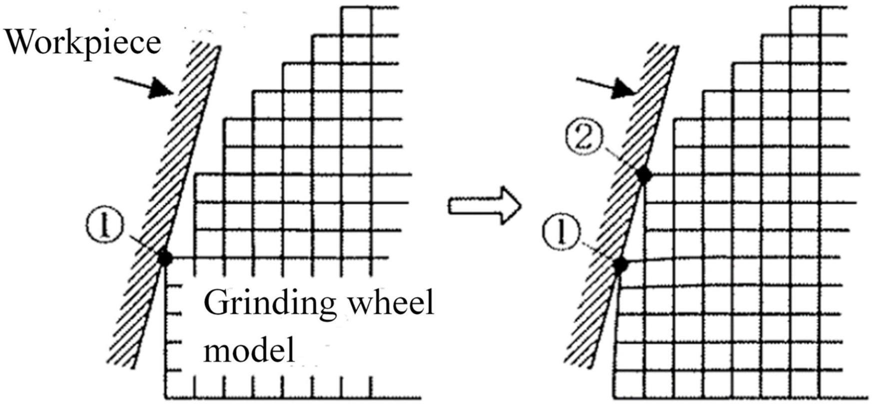

(a) First contact (b) Second contact

Fig. 8.5 Grain contact to workpiece (by Yamada)

8.2 Grinding Stiffness

Grinding forces in metal grinding can be divided into the normal force and the tangential force as shown in Fig. 8.6. In these forces, since the normal force has deeply related with static and dynamic phenomena, experimental discussions on F_n are carried out. The relationship between the normal grinding force and the actual depth of cut u is shown as;

$$K_g = F_n / u \qquad (N / \mu m) \quad ----- \quad (8.2)$$

Since this ratio has the same unit with stiffness, it is called as "*Grinding Stiffness*". It is known that it can be a function of grinding condition as follows;

$$K_g = F_n / u$$
$$= \kappa\, b\, v / (V+v) \qquad ----- \quad (8.3)$$

where, κ is specific grinding force, b is grinding width, v is workpiece speed and V is grinding wheel speed.

In short, this K_g means the "*Grindability*".

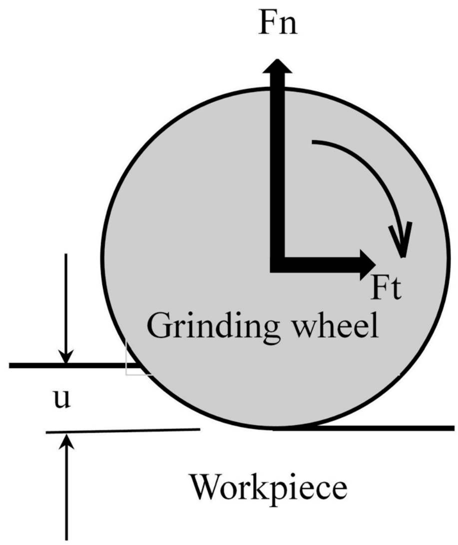

Fig. 8.6 Normal and tangential components of grinding force

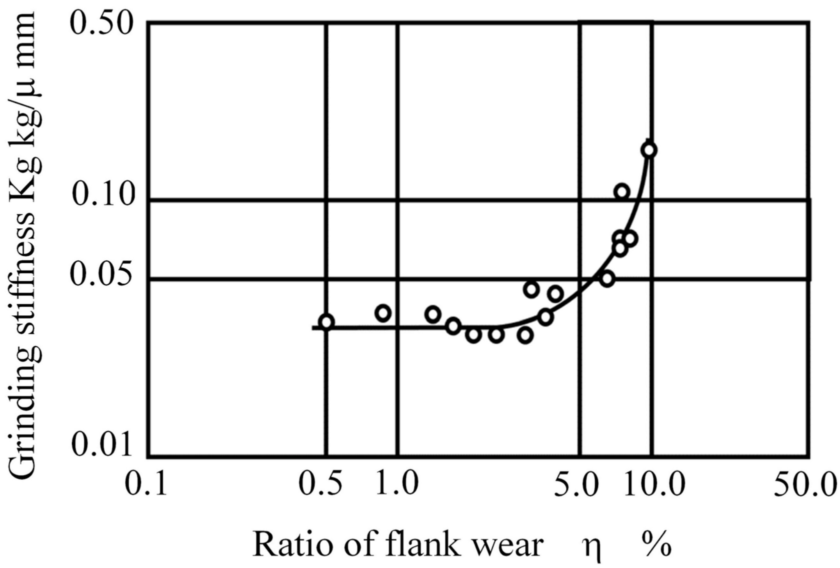

Fig. 8.7 Relationship between grinding stiffness and ratio of flank wear (by Inasaki)

In grinding the metal with a grinding wheel just after dressing, K_g is almost proportion to the actual depth of cut. This amount has a tendency to increase with the increase of the grade of grinding wheel hardness. On the other hand, it is known that the ratio of flank wear η becomes a certain amount, K_g increases rapidly as shown in Fig. 8.7 independent from the grade of the grinding wheel hardness experimentally (Yoshikawa, 1962 and

Inasaki, 1970). Furthermore, the non-linear soft-spring characteristics also appears. It is known that with increasing the ratio of flank wear, grazing takes place in the surface of grinding wheel and then normal grinding cannot be continued. This is the reason that rapid increase of K_g shown in Fig. 8.7. However, the physical effect of flank wear on K_g and the quantitative discussion on the amount of η and its effect have not been conducted yet.

8.3 Unbalance of Grain Distributions in Grinding Wheels

After combining abrasive grains and binder, grinding wheels are fabricated by pressing and sintering. Therefore, the unbalance of the abrasive grains distribution in grinding wheel cannot be avoided. Since the grinding wheel with unbalanced grain distribution has not even elastic modulus, the unbalance of grain distribution and cutting edges can be evaluated by measuring the elastic modulus [2]. Fig. 8.8 shows a measured example of the elastic modulus E of a vitrified-bond grinding wheel WA46 (Umino, 1983). This figure shows that E is small at the point 1 and is large at the point 5. This means the unbalance of grade of hardness in this grinding wheel, and consequently the dynamic characteristics are not even in this grinding wheel.

After balancing this grinding wheel carefully, carrying out dressing, large acceleration synchronizing with grinding wheel rotation is monitored. This acceleration is large at the position where the elastic modulus is large. This experimental results show that the place where elastic modulus is large, the grade of hardness is large and the density of abrasive grain distribution is high. The density of cutting edge distribution after dressing is shown in Fig. 8.9. This figure shows that the cutting edge density is high at the position 5 where elastic modulus is high. And at the position 1, the cutting edge density is low. This result means that at the position 1, the cutting edge density is small and the grade of hardness is also small. Then the wheel

[2] It is reported that both the grain distribution and the grade of hardness of the grinding wheel can be evaluated by measuring the lastic modulus of grinding wheel as exemplified by the following papers. In these papers, the elastic modulus is evaluated by the use of ultrasonic pulse.
Umino K, Shinzaki N. (1979) *Study on Grading of Grinding Wheels by Ultrasonic Pulse Method (Part 1 and Part 2)*. Precision Engineering; 36-8: 538, and 36-9: 608.

wear tends to proceed fast at the point 1, and it causes uneven grinding wheel wear. Consequently, the variation of elastic modulus in the grinding wheel is the cause of uneven grinding forces synchronizing with grinding wheel rotation, and the forced chatter vibration synchronizing with grinding wheel rotation takes place.

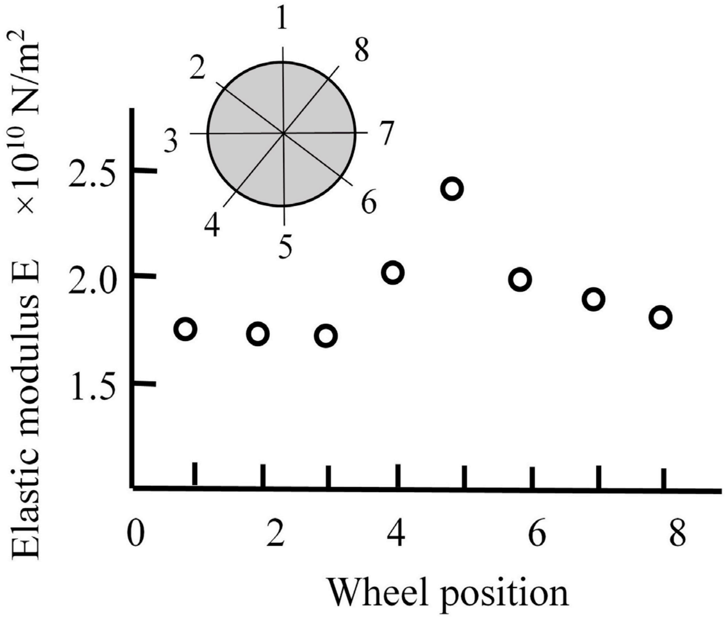

Fig. 8.8 Distribution of wheel grade of hardness (by Umino)

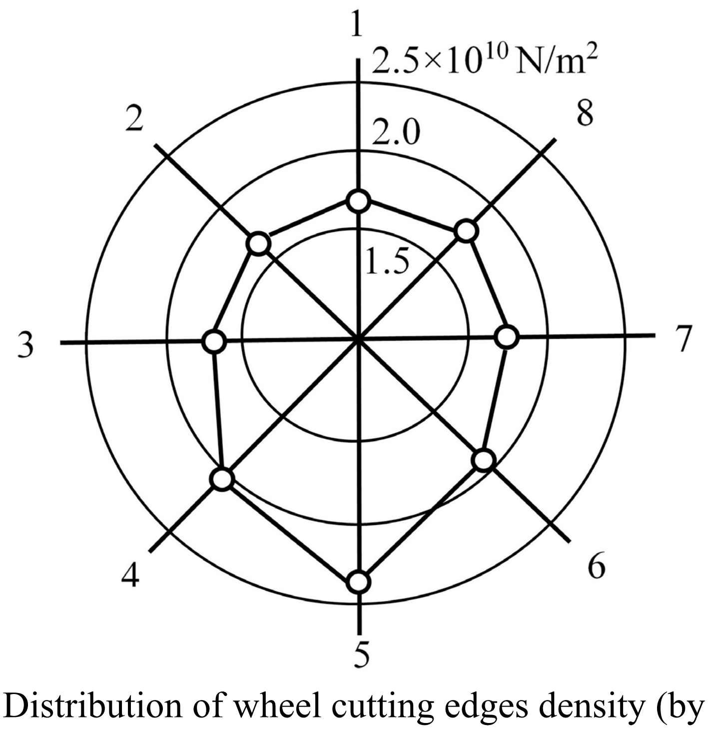

Fig. 8.9 Distribution of wheel cutting edges density (by Umino)

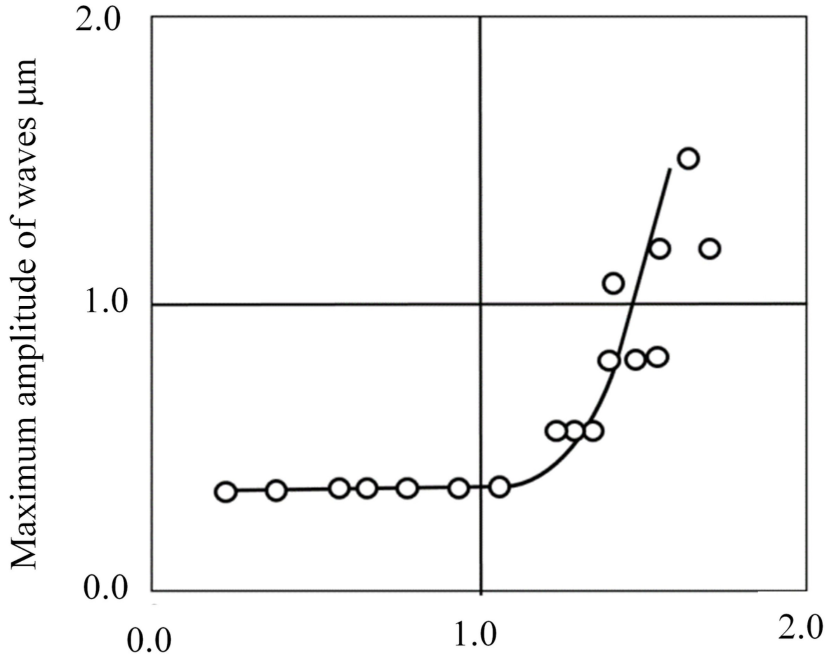

Fig. 8.10 Maximum waviness amplitude in grinding wheel (by Inasaki)

Inasaki et al investigated on the waviness generated in the grinding wheel surface and its effect on the chatter vibration in spark-out grinding process experimentally (Inasaki, 1968). In this study, it is shown that the amplitude of waviness rapidly increases at the cumulative metal removal becomes a certain amount as shown in Fig. 8.10. The number of generated waviness is;

$$n = f(N/60) \qquad \text{-----} \ (8.4)$$

Since this number depends on the grinding wheel rotating cycle N, this vibration is due to the grinding wheel run-out and/or uneven grinding wheel wear depending on the uneven grade of hardness or distribution of abrasive grains.

These phenomena described above means that the wear compliance K_a shown in Fig.1.19 varies by synchronizing with the grinding wheel rotating cycle.

Some trials to fabricate even and balanced grinding wheels started. At present, however, any production methods of the balanced grinding wheel have not been proposed.

8.4 Grinding Damping

Grinding damping is a parameter induced from a geometrical analysis of regenerative effect as shown in Fig.1.18 (Ohno, 1969 and Lee,1982). This analysis is carried out under the condition that the grinding force is proportional to the removed volume of ground workpiece per unit time. As the analyzed result, it is clarified that the radial component of grinding force $P_n(s)$ has a term proportional to the relative vibrating speed as shown in Eq. (1.18).

Grinding damping C_g shown in Fig. 1.19 is described in Eq. (1.20), it is proportional to the length of arc contact L_c;

$$L_c = \sqrt{\frac{2Rr}{R+r}u_0(t)} \qquad \text{----- (8.5)}$$

Therefore, with increasing the depth of cut u, the effect of C_g is increasing, and consequently the chatter does not occur. On the other hand, the chatter tends to take place when u is small, for example, in spark-out process. This tendency cannot be observed in metal cutting, and importantly is a representative characteristic in grinding operation. This effect has been understood that the grinding wheel contacts to the workpiece at a surface, which consists of the length of arc contact and grinding width, and this surface suppresses the vibration in its normal direction. However, the actual contact surface is not flat as shown in Fig. 8.2, but some plural points are contacting to the workpiece. From such a viewpoint, grinding damping C_g may be induced from the damping effect of binders. However, any discussions on the damping effect of binder have not been carried out so far.

8.5 Effects of Parameters Being Current Issues on Chatter

In order to describe the effects of previously shown parameters on chatter, both the stability limits for types I and II shown in Fig.1.19 are reproduced herein. Characteristic equations for types I and II are described respectively as;

$$1 + \{G_m(s) / k_m + 1 / k_{con}\}\{C_g s + kg\ (a\text{-}e^{-Tws})\} = 0$$
$$G_m(s) / k_m + 1/K_g = 1 / K_a\ (1\text{-}e^{-Tss})$$

From these equations, asymptotic stability limits for both the type can be obtained as follows;

$$\mathrm{Re}\{1 / (K_m(s) / G_m + C_g s)\} = -1/(2K_g) \qquad \text{----- (8.6)}$$
$$\mathrm{Re}\{G_m(s) / K_m + 1/K_g\} = -1 / (2K_a) \qquad \text{----- (8.7)}$$

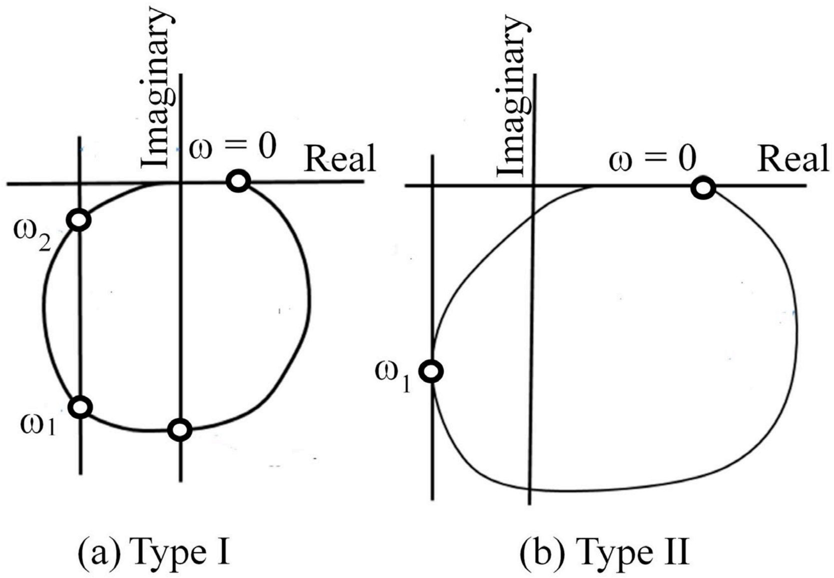

Fig. 8.11 Stability limits in Type I and II chatter vibrations

Figures 8.11 (a) and (b) illustrate the meanings of these expressions. More specifically, in Fig. 8.11(a), when the left hand side of Eq. (8.6) coincides to right hand side of it, chatters take place under frequency ω_1 or ω_2. In case of type II shown in Fig. 8.11(b), as well.

Since these characteristic equations and stability limits consist of the parameters K_{con}, K_g, K_a and C_g mentioned above, the stability limits are affected by these parameters. Supposing that the machining speed V is 10 times faster than previous amounts, the effects of these parameters on chatter vibration will be discussed in the following.

On the effect of contact stiffness K_{con}, it is experimentally shown that its magnitude varies depending on the contact direction to the workpiece as described in Section 8.1. For example, in case of that grinding wheel diameters are 100 to 300 mm, the grinding spindle have to be rotated in N = 28,000 to 84,000 rev/min, i.e. 480 to 1,440 rev/sec, i.e. Hz, and these are within similar area of natural frequencies of grinding machine constructions. Considering that K_{con} varies with grinding wheel direction, it induces the forced vibration synchronizing with spindle rotation. From such a viewpoint, the effect of K_{con} is very important to discuss the forced vibrations.

The grinding stiffness K_g shown in Eq. (8.3) is a function of specific grinding force κ, and so far investigated experimentally, and thus qualitative amounts are obtained. It is known that this amount varies with grinding wheel speed V, workpiece speed v, depth of cut u, wheel diameter D, workpiece diameter d, successive cutting-point spacing a, and cutting edge density n, and duly some experimental expressions were proposed. In these parameters, a and n vary with the surface condition of the grinding wheel. As shown in Fig. 8.2, the cutting edge distribution in grinding surface varies randomly in grinding process. Furthermore, since the cutting edge distribution is not uniform, K_g is also the vibration source as similar as K_{con}.

The wear stiffness of the grinding wheel K_a is a parameter concerning type II chatter as shown in Eq. (8.7) and Fig. 8.11(b). In case of that it is constant, the stability limit based on the chatter due to the regenerative effect of the waviness on the grinding wheel surfaces can be induced. However, considering the unevenness in the cutting edge distribution as shown in Fig. 8.9, and the sudden increase of the amplitude in grinding wheel waviness as shown in Fig. 8.10, the stability limit for type II cannot be explained only by Fig. 8.11(b).

In order to explain the stability for type II chatter developing relatively long time as shown in Fig. 1.17, the wear process of grinding wheel and its effect on the chatter of regenerative type have to be discussed.

References

Snoys R, Wang I C. (1968) *Analysis of the static and dynamic stiffness of the grinding wheel surface*. Preprint of the 9th MTDR Conference, p.1133.

Hoshi T, Koumoto Y. (1983) *Mechanism of vibration in plunge-cut cylindrical grinding*. JSPE; 49-12: 1680.
Fukuda R, Tokiwa T. (1974) *A study on the contact stiffness between grinding wheel and workpiece*. JSPE; 40-10: 809.
Izumi M, Lee H S, Inoue S. (2002) *Development of an instrument for grain cutting edges in a grinding wheel profile*. JSGE; 46-2: 189.
Brown R H, Saito K, Shaw M C. (1971) *Local Elastic Deflections in Grinding*. Annals of the CIRP; XVIV: 105.
Yamada T, et al. (2003) *Study on elasticity of grinding wheels (Modeling and calcutating the stiffness of grinding wheels)*. JSME; 69-683: 1933.
Yoshikawa H. (1962) *Criterion of between–dressing tool life of grinding wheel*. JSPE; 28-5: 286.
Inasaki I, Yonetsu S. (1970) *Experiments on the grinding stiffness*. JSPE; 36-3: 207.
Umino K, Tooe S, Shinozaki N. (1983) *Study on irregularity of wheel grade (1st report) Irregularity of wheel grade and grinding phenomenon*. JSPE; 49-6: 741.
Inasaki I, Yonetsu S. (1968) *Surface waves generated on the grinding wheel*. Bulletin of JSME; 11-47: 922.
Ohno S. (1969) *Study on self-excite vibration in cylindrical grinding*. JSME; 35-276: 1806.
Lee H S, Furukawa Y. (1982) *On the dynamic grinding process under vibrating condition*. JSPE; 48-5: 603.